ACOUSTIC LINER FEASIBILITY PROGRAM

Contract NAS 9-8852

DESIGN GUIDE

Prepared for

NATIONAL AERONAUTICS AND SPACE ADMINISTRATION
Manned Spacecraft Center
Houston, Texas

Report 8852-DG

19 April 1970

AEROJET LIQUID ROCKET COMPANY
A DIVISION OF AEROJET-GENERAL
SACRAMENTO, CALIFORNIA

ACOUSTIC LINER FEASIBILITY PROGRAM

Contract NAS 9-8852

DESIGN GUIDE

Prepared for

NATIONAL AERONAUTICS AND SPACE ADMINISTRATION
Manned Spacecraft Center
Houston, Texas

Report 8852-DG

19 April 1970

FOREWORD

This report is submitted in compliance with the requirements of Contract NAS-8852, Article XII, Paragraph G of the contract schedule.

The purpose of this report is to provide guidelines for the design of Helmholtz resonator acoustic liner arrays for rocket combustion chambers.

The work was conducted by the Thrust Chamber Engineering Section of the Liquid Rocket Company, Aerojet-General Corporation, Sacramento, California. The program was under the direction of Dr. C. B. McGough, program manager; J. M. McBride, project manager, and R. A. Hewitt, project engineer.

The contract was funded by the National Aeronautics and Space Administrations Manned Spacecraft Center, Houston, Texas. The NASA project engineer for the program is Mr. C. E. Mayhew.

ACKNOWLEDGEMENTS

Special acknowledgement is given to H. V. Kiser for his contribution in the reduction of acoustic liner design theory to design criteria, to Mr. R. W. Michel for development of heat transfer analytical models and trade off studies, to Mr. H. O. Davis for the materials studies, to Mr. P. J. Krusi for structural analysis and to Mr. W. J. Nord for organizing and editing the material contained in this report.

Report 8852-DG

ACOUSTIC LINER FEASIBILITY PROGRAM DESIGN GUIDE

TABLE OF CONTENTS

APPENDIXES

TABLE LIST

FIGURE LIST

FIGURE LIST (cont.)

FIGURE LIST (cont.)

NOMENCLATURE

A, a	Constants
A_f	Area of flow, or acoustic liner face surface, ft^2
A_i, A_o	Inner and outer heat transfer areas
A_o	Area of acoustic liner orifice cross section, ft^2
A_r	Area of resonator
A_t	Area of combustion chamber throat, or cross sectional area of tube, $in.^2$
$A_{\nu n}$	Pressure sensitive coefficient
A-50	AeroZINE 50 fuel
a	Thermal expansion coefficient, in./in.-°F
b	Slot base width
Btu	British thermal unit
C	Viscosity constant for gases
c	Speed of sound, ft/sec
c_r	Resonator gas speed of sound
c*	Characteristic exhaust velocity, ft/sec
c_c	Chamber gas speed of sound
c_1, c_2	Constants
c_t	Thermal conductivity of material
C_p	Specific heat at constant pressure, Btu/lbm-°F
C_s	Stagnation chamber gas speed of sound, ft/sec
d	Diameter, or depth
D_c	Chamber diameter, in.
d_o	Acoustic liner orifice diameter, ft
d_t	Tube outer diameter
e_1	Fracture elongation
e	Base of natural logarithm
E_1	Electrical voltage
E_t	Youngs modulus of elasticity, psi
F_{ty}	0.2% offset yield strength at maximum temperature of cycle

NOMENCLATURE (cont.)

°F	Degrees Fahrenheit
F_o	Force function, lbf
ffc	Fuel film cooling
Ft	Feet
f(x)	Function of x
f	Frequency, sec
f_o	Acoustic liner resonant frequency without mean gas flow, sec^{-1}
G	Resonator geometry factor, $G = \sqrt{\ell_e/(L\sigma)}$
g	Gravitational constant, 32 ft/sec^2
G_1	Structural geometric factor, G ~ 1.0 to 1.25
gm/cm^3	Grams per cubic centimeter
H_{pq}	Normalizing factor in Eigenfunction expansion
H_2O	Water
h	Height of slot aperture
h_g	Gas-side heat transfer coefficient
h_{fusion}	Heat of fusion, Btu/lbm
ID	Inside diameter
Inj	Injector
I	Electrical current
I_{sp}	Specific impulse, lb-sec/lbm
i	$\sqrt{-1}$, indicates an imaginary number
in.	Inch
$in.^3$	Cubic inch
J	Bessel function of the first kind of order
j	$\sqrt{-1}$, indicates an imaginary number
ksi	Thousands of pounds per square inch
k	Thermal conductivity, Btu/in.-sec-°F
k_1	Spring constant, lbf/ft
L	Backing distance of acoustic liner cavity, ft

NOMENCLATURE (cont.)

L_2	Half the structural wall thickness
L_Q	Length of quarter wave tube, ft
L*	Chamber characteristic length, in.
ℓ	Length
ℓ_e	Effective length of orifice, ft
lb	Pound
lbf	Pounds force
lbm	Pounds mass
M_c	Mean chamber Mach number at entrance to nozzle
MR	Mixture ratio
m	Mass, lbm-sec^2/ft
N	Average cyclic life
N_c	Number of channels
N_p	Number of passes
N_{St}	Stanton number
N_t	Number of tubes
n	Pressure interaction index of Crocco theory
N_2O_4	Nitrogen tetroxide
OD	Outside diameter
O/F	Oxidizer to fuel ratio, mixture ratio
Q	Measure of absorption coefficient bandwidth, $Q = 2\pi f_o \ell_e / c\sigma\bar{\theta}$
P	Pressure, lb/in.^{2}
p'	Perturbation in acoustic pressure
P_c	Chamber pressure, psia
P_i	Incident acoustic pressure
P_r	Reflected acoustic pressure
p_r	Reference acoustic pressure (0.0002 dynes/cm^2), rms
P_i	Local injector acoustic pressure oscillation, psi
$P_{\nu h}$	Axial dependent factor of perturbation pressure

NOMENCLATURE (cont.)

psi	Pounds per square inch
q/A	Heat flux, Btu/in.^{2}-sec
°R	Degrees Rankine
1R	First radial acoustic mode of chamber
R	Radial dependent factor of perturbation pressure
R_{BO}	Burnout heat flux ratio
R'	First derivative of R
R_s	Acoustic resonator surface area resistance
R''	Second derivative of R
R_t	Total acoustic resistance
$R_{\nu h}$	Same as R except ν and h identify acoustic mode
r	Radial distance from centerline of chamber, ft
r_1	Damping constant, lb-sec/ft^5
r_c	Radius of chamber, ft
S	Spacing, in.
$S_{\nu h}, \nu$	Separation constants
sec	Second
S_u	Ultimate tensile strength, psi
SPL	Sound pressure level in decibels, db, defined by equation SPL = 20 $\log_{10}$ (p'/p)
SWT	Standing wave tube
T_c	Chamber gas temperature
T_∞	Mainstream temperature
T_r	Recovery temperature, or resonator gas temperature
T_o	Core gas temperature
T_s	Suddenly imposed surface temperature
T	Temperature
T_2	Temperature of gas in acoustic liner cavity, °R
T_{wL}	Liquid wall temperature
T_B	Bulk temperature, °F

NOMENCLATURE (cont.)

T_{wg}	Gas-side wall temperature
T_w	Wall temperature
1T	First tangential acoustic mode of the chamber
2T	Second tangential acoustic mode of the chamber
t	Time, sec
t_o	Acoustic liner orifice thickness, ft
t_e	Acoustic liner orifice effective thickness
U	Axial dependent factor of perturbation axial velocity
u	Mean chamber gas velocity, or velocity in x direction, ft/sec
$\bar{u}$	Nondimensionalized mean chamber gas velocity, u/c_s, or steady state velocity in the x direction
u'	Nondimensional axial perturbation of gas velocity
V	Volume of acoustic liner cavity, ft^3
V_l	Velocity, ft/sec
V_o	Volume of acoustic liner orifice, ft^3
$\bar{v}$	Steady state velocity in y direction
w	Width
W_f	Fuel flow rate, lb/sec
W_o	Oxidizer flow rate, lb/sec
$\dot{w}_t$	Total propellant flow rate, lbm/sec
X	Acoustic reactance
X_v	Acoustic reactance ratio based on velocity perturbation
X_Q	Acoustic reactance ratio based on volume flow rate perturbation
X_m	Aperture acoustic reactance due to its mass
X_s	Cavity acoustic reactance due to its spring stiffness
x	Distance in x direction, ft, or flow direction
$\dot{x}$	Velocity in x direction, ft/sec
$\ddot{x}$	Acceleration, ft/sec^2
Y_r	Nondimensional Holmholtz resonator admittance
$Y_{n\tau}$	Nondimensional intrinsic combustion admittance

NOMENCLATURE (cont.)

Y_ν	Bessel function of the second order of
Z	Axial length, in.
Z	Acoustic impedance
$A,B,D,E,A_{\nu h}$	Constants determined by boundary conditions

Greek Symbols

α	Absorption coefficient
α_1	Thermal diffusivity, $in.^2/sec$
β	Biot number = $h L_2/K$
γ	Ratio of specific heats
Δ	Amount difference
Δ_{nl}	Nonlinear SPL correction factor, ft
δ	Effective aperture length correction ($\delta = \ell_e - t$)
δ	Damping rate, db/sec
δ	Boundary layer thickness
$\partial/\partial x$	Partial differentiation with respect to x
ε_t	Strain, in. per in.
λ	Wave length, $\lambda = c/f$
θ	Angular distance around perimeter of chamber, radian
$\overline{\theta}$	Acoustic resistance ratio
μ_c	Chamber gas viscosity
μ	Gas viscosity, lb/sec-ft
μ_1	Poisson's ratio
μ_r	Resonator gas viscosity
ρ_a	Empirically determined acoustic cavity gas density
π	Ratio of circumference to diameter of circle (3.1416)
ρ	Gas density, $lbm\text{-}sec^2/ft^4$
ρ_d	Design density for acoustic cavity gas
ρ_r	Resonator gas density
ρ_1	Density, $lb/in.^3$

NOMENCLATURE (cont.)

ρ_c	Chamber gas density
$\overline{\rho}$	Nondimensional mean chamber gas density, ρ/ρ_s
ρ'	Nondimensional perturbation of gas density
ρ_s	Stagnation chamber gas density, $lbm\text{-}ft^4/sec^2$
$\dot{\Sigma}$	Summation
σ_x	Meridional stress
σ	Ratio of acoustic liner orifice area to injector face area
σ_ψ	Hoop stress
σ_1	Calculated stress, psi
τ	Sensitive time lag of combustion, sec
τ_1	Shear stress, psi
Φ	Modified acoustic resistance ratio
ϕ	Heat flux
ϕ_{BO}	Burnout heat flux
ψ	Modified acoustic reactance ratio
$\overline{\chi}$	Acoustic reactance ratio of acoustic liner orifices
ω	Angular frequency, $2\pi f$, sec^{-1}
ω_d	Angular frequency with damping, sec^{-1}
ω_n	Undamped natural frequency, sec^{-1}
Ω	Nondimensional angular frequency, $\omega r_c/c$
H	Angular dependent factor of perturbation pressure
H''	Second derivative of H
H_ν	Same as H except ν identifies tangential component of acoustic mode
∇	Del operator
$>$	Greater than
$<$	Less than

I. INTRODUCTION

This report is intended for use by design engineers in the design of combustion stability control devices. An effort is made in Section II to familiarize the design engineer with the common types of combustion instability. The content of this report is limited to consideration of high frequency or acoustic modes of combustion instability. A brief discussion of various theories used to correlate storable liquid rocket injector design parameters with high frequency combustion instability is included in order to allow the designer to determine if combustion control devices are needed.

Chapter III contains a discussion of four methods of analyzing acoustic liner performance along with ways of estimating the liner's cavity gas environment.

Review of the state of the art evaluation of heat transfer analytical models, materials and structural considerations is included in Chapter IV. The results of the "Acoustic Liner for an Ablative Chamber Feasibility Study" program for which a program plan is shown in Figure 1 plus previous experience were used to compile this document.

The Phase I portion of the program consisted of a literature search, formulation of analytical models, performing trade off studies, determining problem areas, establishing design criteria, and selecting designs for fabrication. This includes heat transfer, materials, and structural evaluations relating to acoustic liner design.

The Phase II or development portion of the program was planned to provide data for verification of the analytical models and the assumed environmental properties.

The Phase III of the program was performed to verify the analysis, design and development efforts of Phase I and II.

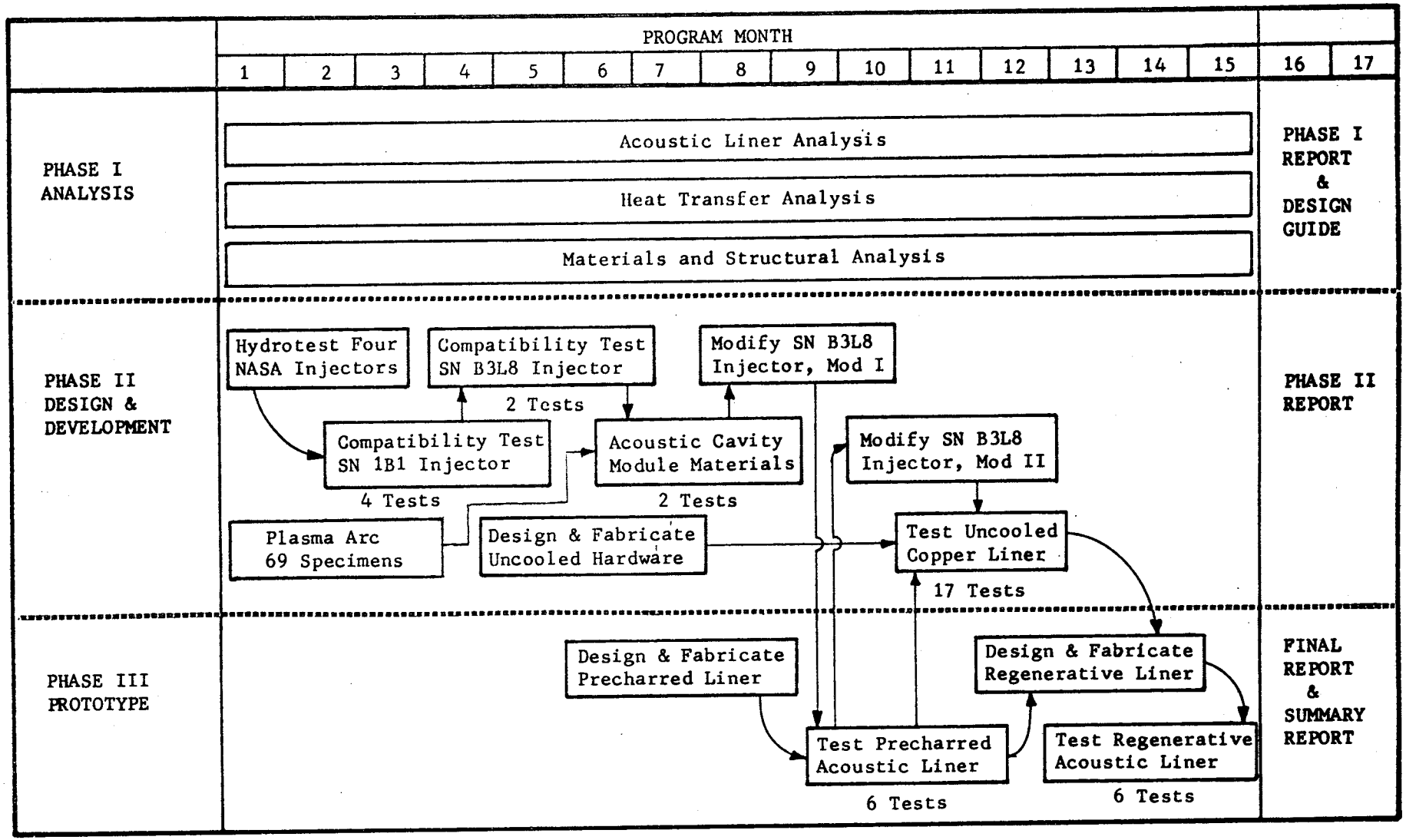

Figure 1. ALFP Program Plan

I, Introduction (cont.)

The content of this design guide will attempt to answer basic design questions relating to three major topics: (1) acoustic damping, (2) heat transfer, and (3) materials and structures. Obviously the three topics cannot be completely covered in a program of this scope, however, certain basic questions are answered and general design practices identified which will aid significantly in the design of a successful acoustic liner.

Some of the basic questions considered relevent but not limited to the design of acoustic liners for ablative chambers using Lunar Module (LM) development hardware and operating conditions are as follows:

ACOUSTICS

1. When is an acoustic damper required?
2. What frequency (s) should be design for?
3. Should more than one damper geometry (tune) be used?
4. Where should the damper (s) be located? (also with baffles)
5. What size should the damper be?
6. What cavity gas properties should be estimated?
7. What range of gas properties are possible?
8. What effect does start and shutdown transients have?
9. What is the orifice impedance as a function of flow through?
10. What is the orifice impedance as a function of flow past?
11. What is the orifice impedance as a function of SPL?
12. What is the effect of the damper presence on the chamber modes?
13. What is the best criterion for an optimized damper design?
    (a) Absorption coefficient, (b) modified absorption coefficient,
    (c) maximum damping, (d) maximum admittance.
14. What are the best aperture configurations? (Slots, teardrop, slant, contoured)
15. What is the acoustic mass of the aperture gas? (ℓ_e, A_o)

I, Introduction (cont.)

HEAT TRANSFER

1. When is cooling required?
2. What are the requirements of the cooling mechanisms?
3. What amount of cooling is required?
4. What are the boundary conditions expected?
5. What are the probable sources of thermal failure?

MATERIALS AND STRUCTURES

1. What are the strength requirements?
2. What is the thermal environment?
3. What is the chemical environment?
4. What are the durability requirements?
5. What are the duration requirements?
6. What are the effects of apertures and cavities?
7. What are the possible sources of structural failure?

II. COMBUSTION STABILITY BACKGROUND

A. INTRODUCTION

This Section will attempt to familiarize the design engineer with the three basic types of liquid propellant combustion instabilities. The emphasis is on the high frequency or "Acoustic" type of combustion instability, which is primary reason for designing acoustic liners.

Acoustic modes of a cylindrical chamber are defined, discussed and sufficient references provided to enable the design engineer to estimate the acoustic mode frequencies of a conventional rocket chamber. Also a method for calcuating annular chamber acoustic mode frequencies is given.

A basic description of the liquid propellant combustion stability feedback mechanism is given. The emphasis is placed on the Crocco combustion stability model which postulates a combustion sensitive time lag (τ) which corresponds to a combustion sensitive frequency, (f_s), and is related as follows:

$$f_s = \frac{1}{2\tau}$$

This and other theories and correlations for estimating sensitive combustion frequencies are cited in Reference 1.

B. THE NATURE OF COMBUSTION INSTABILITY

It is well known that the processes occurring within a liquid rocket combustion chamber are never entirely smooth. Even when the mean operating conditions are constant, fluctuations around these mean values occur in all of the quantities that characterize the flow. The nature of the fluctuations can vary widely from one combustor to another and in a single combustor

II, B, The Nature of Combustion Instability (cont.)

for different operating conditions. If the fluctuations are random and of small amplitude, this unsteadiness is referred to as "combustion noise". With random fluctuations of large amplitude, the operation of the rocket is said to be "rough", and the functioning of the system of which the rocket is a part may be impaired.

Much more serious than rough operation is the problem of combustion instability, also termed unstable combustion, oscillatory combustion, or resonant combustion. Whereas rough combustion refers to random fluctuations, combustion instability consists of organized oscillations that are maintained and amplified by the combustion process itself. The various types of combustion instability can be classified roughly into three categories: low frequency, intermediate frequency, and high frequency. However, the classification is not based simply on frequency alone. Just as electrical and mechanical systems respond to specific frequencies depending on the type of coupling, so also liquid rocket systems exhibit representative frequency and amplitude patterns.

The basic coupling mechanisms for the three general types of combustion instability found in liquid propellant rocket engines are illustrated in Figure 2. For the low frequency ("chugging") type, interaction between the propellant feed system and the combustion chamber places the frequency generally less than 200 Hertz. The coupling is effected by the oscillating propellant feed rates. In the case of intermediate frequency combustion instability (sometimes referred to as entropy wave instability), the injector characteristics (especially the internal injector manifolding and orifice impedances) account for part of the interaction, with the mean gas flow and pressure wave propagation in the combustion chamber completing the process. Typical frequencies are in the several hundred Hertz range.

In this report, attention will be focused on the third type of combustion instability, namely, high frequency instability. This type depends

Type	Characteristic coupling
1. Chugging (low frequency)	(1) feed system (2) combustion chamber

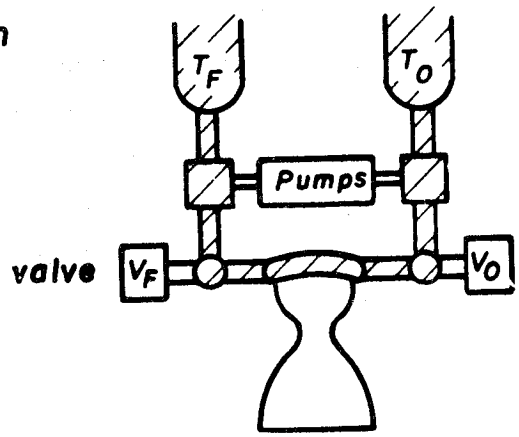

2. Entropy wave

(1) injector (mixture ratio)

(2) chamber ; u_g , gas velocity ; u_w , wave velocity

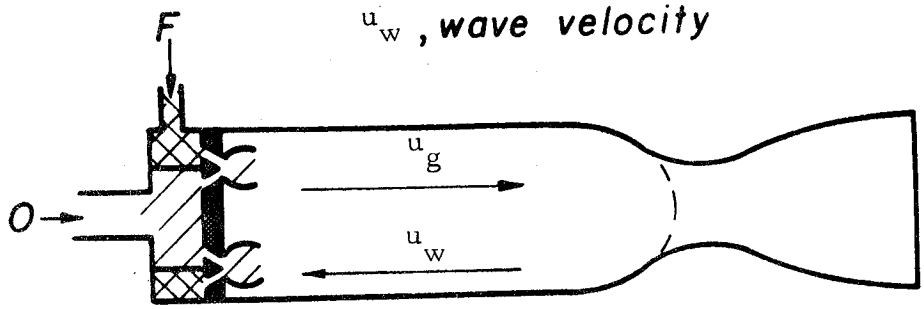

3. Hi - frequency

(1) combustion process

(2) chamber geometry (wave travel time)

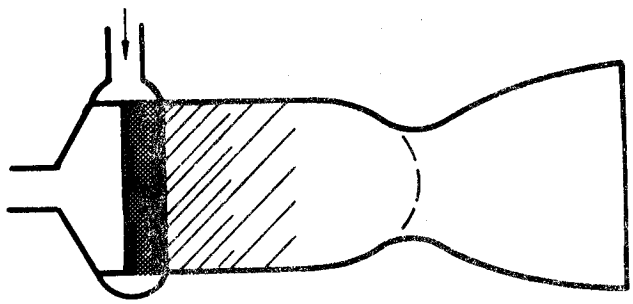

Figure 2. Liquid Propellant Combustion Instability

II, B, The Nature of Combustion Instability (cont.)

upon a coupling between the combustion processes and flow oscillations in the combustion chamber. Such coupling requires no input from the feed system, although it is possible for the feed system to have an effect when the combustion chamber is large and acoustic frequencies are reduced to several hundred cycles per second. Normally, the frequencies to be expected are in the thousand Hertz range for most current engines.

The combustion chamber geometry is an important factor in high frequency combustion instability because the possible frequencies depend on the internal geometry. Since it is effectively closed at one end by the injector and has a choked-flow exhaust nozzle at the other end, the chamber acts acoustically much as a double closed-end cavity. For instances, for purely longitudinal modes, an approximate point of effective reflection in the nozzle can be determined theoretically; between that point and the injector face standing patterns of acoustic waves can be established. Similarly in the transverse plane, tangential modes of the spinning or standing types as well as radial modes may be established. Frequencies correspond approximately to those of the acoustic modes, either the fundamental or higher harmonics. Modes containing combinations of tangential, radial and longitudinal oscillations may also exist, each characterized by its own frequency as calculated by formulas shown in Table I. Pressure and velocity patterns for several transverse modes are illustrated in Figure 3. Annular chamber mode frequencies can be calculated using Table II and Figure 3. However, despite the similarity of the modes and the closeness of frequencies, the continuous generation of gases produces effects that do not exist in a closed chamber. In a closed chamber, the only source of damping originates from the friction on the walls. This source of damping is also of course active in the combustion chamber, but it plays a very modest role compared to other, more powerful sources of damping. Indeed, the very existence of the nozzle produces damping in the case of pure or combined longitudinal modes because the reflection of waves from the convergent (subsonic) portion of the nozzle departs from that of the ideal closed end.

TABLE I

$s_{\nu\eta}$ FOR A CYLINDRICAL CHAMBER

For transverse modes the frequency of oscillation is given by:

$$f_T^* = \frac{s_{\nu\eta}\, C_o^* \times 12}{2\,\pi\, r_c^*}$$

Mode	ν	η	$s_{\nu\eta}$
1st radial	0	1	3.8317
2nd radial	0	2	7.0156
3rd radial	0	3	10.1734
1st tangential	1	1	1.8413
2nd tangential	2	1	3.0543
3rd tangential	3	1	4.2012
4th tangential	4	1	5.3175
5th tangential	5	1	6.4154
6th tangential	6	1	7.5013
1T, 1R combined	1	2	5.3313
2T, 1R combined	2	2	6.7060
3T, 1R combined	3	2	8.0151
4T, 1R combined	4	2	9.2825
1T, 2R combined	1	3	8.5263

For a longitudinal mode the frequency can be estimated by:

$$f_L^* = \frac{C_o^* \times 12}{2\,(L_c^* + 2/3\, L_N^*)}\,(1 - M_m^{\,2})$$

where: L_N^* = length of nozzle in inches

M_m = average Mach number in nozzle-chamber combination

$*$ = dimensional values

For combined transverse and longitudinal mode the frequency can be estimated by

$$f_{T+L}^* = \sqrt{f_L^{*2} + f_T^{*2}}$$

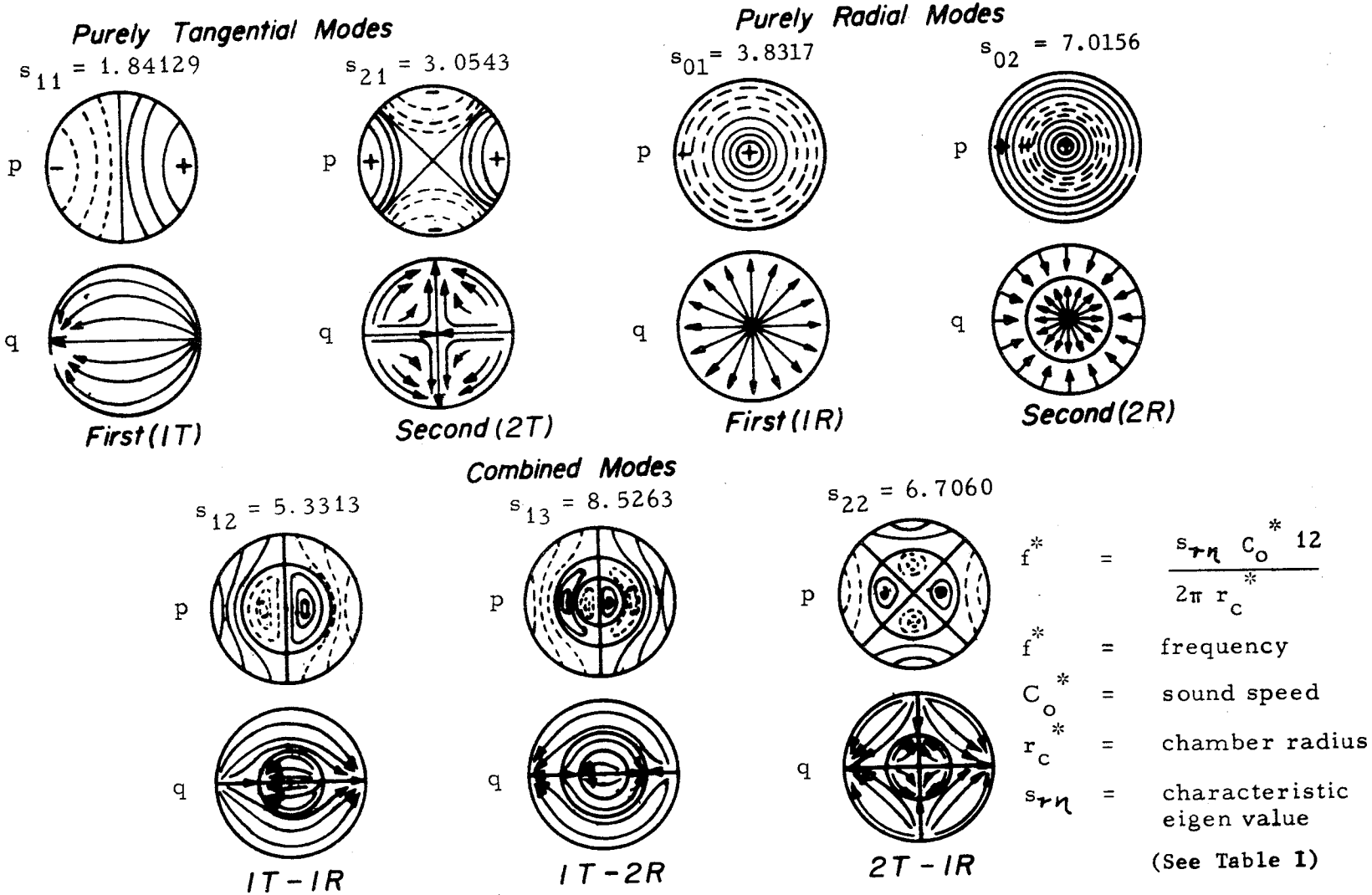

Figure 3. Pressure, p, and Velocity, q, Characteristics of Several Transverse Modes

TABLE II

BESSEL FUNCTION VALUE $(s_{\nu\eta})_{ann}$ FOR TANGENTIAL MODES IN ANNULAR CHAMBERS

Annular Chamber Geometry (Radius) Inner / (Radius) Outer		Tangential Modes 1T	2T	3T	4T	5T	6T
0.910	$(s_{\nu\eta})_{ann}$ =	1.04802	2.09602	3.14401	4.19197	5.23989	6.28778
0.833		1.092	2.1846	3.27672	4.368	5.4588	6.5496
0.667		1.209	2.412	3.61	4.80	5.98	7.14
0.500		1.35	2.68	3.98	5.18	6.34	7.45
0.400		1.41	2.85	4.10	5.27	6.40	7.5
0.333		1.54	2.91	4.17	5.31	6.42	7.5
0.286		1.60	2.99	4.18	5.31	6.42	7.5
0.250		1.64	3.00	4.18	5.31	6.42	7.5
0.222		1.67	3.02	4.18	5.31	6.42	7.5
0.200		1.70	3.025	4.18	5.31	6.42	7.5

NOTE: 1. Figure 4 gives the frequency ratio viz. $\frac{(s_{\nu\eta})_{annular}}{(s_{\nu\eta})_{cylindrical}}$ for different chamber geometries.

2. Calculation of annular chamber tangential frequencies

$$\left[f^* = \frac{C_o^* \, (s_{\nu\eta})_{annular}^{12}}{2\pi \, r_c^*} \right]$$

Reference: Bridge and Angrist, "Math. of Computation, 16, 78," April 1962.

* = dimensional values.

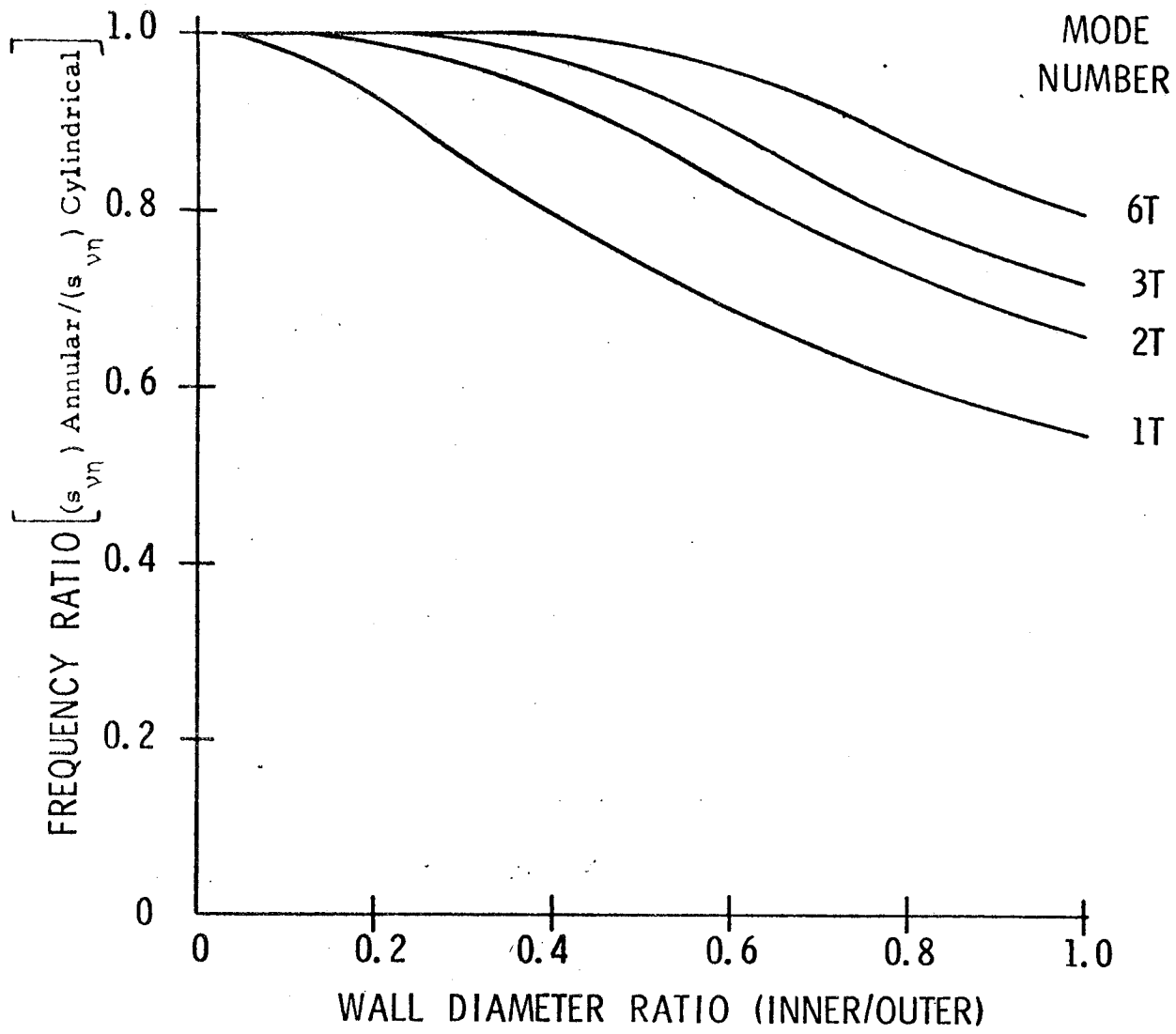

Figure 4. Tangential Mode Acoustic Frequencies for Annular Chambers

II, B, The Nature of Combustion Instability (cont.)

The most important source of damping, however, is related to the process of gas generation itself, and consists of two parts of approximately equal importance. The most obvious comes from the fact that, from the conditions of the steady propellant injection flow (steady, of course, only if the feed system perturbations are disregarded) the combustion gases must have acquired, at the moment of generation, the perturbed momentum corresponding to the oscillatory flow. The acquisition of this momentum demands a certain work which must be absorbed from the system. The fact that momentum exchanges due to the drag of the droplets can take place prior to the moment of generation can only add additional damping.

The other, more subtle source of damping comes from the fact that at the moment of generation the volume of the propellant must change from its practically negligible liquid volume, to the full volume of the burned gases. To this change of volume corresponds a certain "pumping work" proportional to the local instantaneous pressure. Hence, more work must be absorbed from the system when the pressure is higher, and less when it is lower, thus providing an effective damping mechanism.

The significance of the preceding discussion is that, from the point of view of instability, each combustion system is characterized by certain well-defined proper frequencies at which the gases can oscillate in well-defined modes, and by certain damping mechanisms which absorb energy from the oscillating system. It is clear that self-sustained oscillations can exist (and instability appear) only if the combustion process is able to generate, at any one of the proper frequencies, enough feedback combustion energy (in excess of the stead-state conditions) to restore continually the amount which is being lost.

Suppose, for a moment, that the amount of combustion feedback energy is independent of frequency. Then the only important factor in the balance

II, B, The Nature of Combustion Instability (cont.)

would be the energy damping corresponding to each mode, that (or those) mode(s) becoming unstable which correspond(s) to the lowest level of damping. Experience shows that this is not the case, and that, for a given injector, the selection of the unstable mode is rather governed by its proper frequency than by its damping level. This has been shown to be the case both for longitudinal and for transverse forms of instability. In both it has been possible to observe the switch from one unstable mode to another (for instance from the fundamental to the second mode) when the geometrical (or other) conditions are gradually changed. It is not our purpose to discuss here the details of the transition from one mode to the other (it does not take place suddenly), but rather to point out that the transition occurs in such a way as to maintain the oscillation frequency within a well-defined narrow range.

The only logical interpretation of this observation is that not only the combustion feedback energy must depend on frequency, but that actually only in a narrow range around one, well defined, frequency (determined in a complicated way by the various geometrical, physical and chemical conditions on which the combustion process depends), can the combustion feedback energy reach a level sufficient to balance the damping.

The empirically observed existence for a given combustion system of one narrow frequency range in which instability can appear can be interpreted by stating that, among the features characterizing the response of a given combustion system to oscillatory conditions, one can single out a "characteristic time" simply proportional to the reciprocal of frequency, such that only when its ratio to the oscillation period is around a certain value, maximum feedback can be generated and, possibly, instability produced.

This behavior has similarities to that of a resonant system, which is able to oscillate at certain natural frequencies with amplitudes that depend on the value of the frequency of the exciting forces compared to those of the

II, B, The Nature of Combustion Instability (cont.)

natural frequencies. In the combustion instability problem also the exciting force due to the unsteady combustion processes is characterized by its own frequency (or its characteristic time), and maximum amplitudes are to be expected where there is coincidence with one of the proper frequencies. However, there is an important difference, residing in the fact that the exciting force is not independently applied from the outside, but is produced (in a sort of feedback loop) by the oscillations themselves, with the result that considerations of stability appear and take fundamental importance, and that the eventual oscillatory situation is determined by nonlinear effects. Nevertheless the terms "resonance" and "resonant" are often applied also to this case.

It appears that the knowledge of the characteristic time associated with a particular combustion system would be of primary importance in the design of new rockets, since it determines in which mode instability is able to appear. Such a knowledge could, for instance, allow the choice of the chamber and injector geometry in such a way that all of the proper frequencies would be too high to become unstable. Unfortunately, even assuming the characteristic time to be known, the choice of the propellant combination, as well as the chamber and basic injection system geometry, has always been fixed in the past during the early stages of development programs based on other stringent requirements of size, weight and performance, and there is very little chance that even in the future the designers may base their designs only on stability requirements. Therefore, a more sophisticated approach to the problem of stability is necessary, in which the second condition for appearance of instability, that of the energy balance, is also taken into consideration. In other words, even if it is impossible to avoid having some of the proper frequencies fall in the range where they may become unstable for the given combustion system one should make sure that for the corresponding modes the combustion feedback is not sufficient to balance the damping.

II, B, The Nature of Combustion Instability (cont.)

Clearly there are two ways in which this balance can be improved in favor of stability: one is the depression of the combustion feedback, the other the increase of the damping. Of the two solutions, the second has been favored in recent times because it is better understood and hence easily controlled. Such damping devices as baffles, quarter wave tubes, or acoustic liners have been introduced, with the cost of more or less profound design complications, and have been very effective in producing substantial levels of damping, due to the dissipation caused by the devices. At the same time these devices also entail a change of the proper frequencies, and, in view of the previous discussion, this change can also have an effect on the balance.

On the other hand, the solution of depressing the combustion feedback has not been used in any consistent and systematic fashion, but only by looking for injector designs which, fortuitously or nearly so, result in the most stable operation on the test stand.

It may be added that a third, and the most effective solution, clearly consists in applying simultaneously the two solutions above, by (1) using an injector which is as stable as possible, and (2) adding a certain amount of extra damping to attain whatever safety margin is required.

The difficulty with a systematic application of the second (or the third) solution has been that the behavior of the combustion systems under oscillatory conditions is still very incompletely understood, so that it is impossible today, starting from the fundamental consideration of the basic physico-chemical processes involved, not only to predict the value of the characteristic time or the magnitude of the energy feedback, but often even the very direction in which these quantities are affected by a change in design.

However, a less fundamental approach exists, which may still help the designer considerably, that is based upon the idea of establishing empirical

II, B, The Nature of Combustion Instability (cont.)

correlations between the characteristic time and the energy feedback on one side and, on the other side, a certain number of appropriate combinations of parameters characterizing the injector geometry, the propellant mixture and the operating conditions. The feasibility of such an approach is offered by the sensitive time lag concept, introduced by Crocco in 1951 (Ref 2). Although originally formulated with the sole intent of gaining an insight into the essential features of the high frequency instability phenomenon, the sensitive time lag combustion model was later found to predict reasonably accurately the quantitative behavior of the system in quite a few cases. In fact, this was beyond the expectations of such a heuristic approach.

This is indeed the primary advantage of the sensitive time lag concept, that the complexity of the actual combustion process can be avoided through the use of a very small number of lumped parameters. This is not to say that phenomena, such as droplet breakup, vaporization, mixing, chemical reactions, etc., are not important in determining stability and performance characteristics, but rather that, lacking such specific knowledge, the general nature of the coupling between the chamber conditions and the combustion process may still be described.

According to the Crocco model, the dynamic aspects of the injection-combustion process that are of significance in high frequency instability are characterized by a time lag, which is sensitive to the local, instantaneous values of pressure, temperature, gas velocity, etc. The degree of sensitivity is measured by one or more interaction indices. The sensitive time lag, then, plays the role of the above discussed characteristic time, while the interaction indices, properly combined, hold the key to the magnitude of the energy feedback. Thus, the occurrence of high frequency combustion instability is seen to result from the matching of the sensitive combustion time lag with one of the proper frequencies of the combustion chamber,

II, B, The Nature of Combustion Instability (cont.)

provided that the degree of sensitivity of the combustion is sufficiently large to offset the damping effects present in the chamber. The stability conditions can then be expressed only in terms of the time lag and the interaction indices, and the ways to stabilization are easily discussed.

C. SENSITIVE FREQUENCY ESTIMATES

The best general answer to the question "when is acoustic damping required" is "always". This is not to say that some rocket engines do not run stably, only that those that do, have some prominent stabilizing mechanism. Some rocket engines are stable until perturbated by natural engine noises, pressure perturbations or small explosions. Some rocket engines are almost never stable and are called spontaneously unstable.

The degree of stability or instability is best correlated to the frequency (s) of the instabilities relative to the fundamental transverse mode of the chamber. If only a first tangential mode instability occurs (or is anticipated) it is likely that the system can be stabilized with relative ease by incorporating a three bladed baffle or a relatively small resonator array. If the hardware is in the design stage the design engineer can only use previous experience in the form of a correlation like that shown in Figure 5, to predict stability. This "sensitive frequency" correlation is valid for propellants combinations in which the fuel has the lowest vapor pressure and is classified as "storable". In order to understand the use of this correlation it is useful to consider two example rocket engines with the same thrust, chamber pressure, and throat size as follows:

Rocket Engine "A" has a contraction ratio of 1.14 and a chamber Mach number of 0.50 while rocket engine "B" has a contraction ratio of 11.86 and a Mach number of 0.05. If both engines are assumed to have chamber pressures of 125 psia, total lengths of 8.0 in. and throat diameters of 3.0 in.

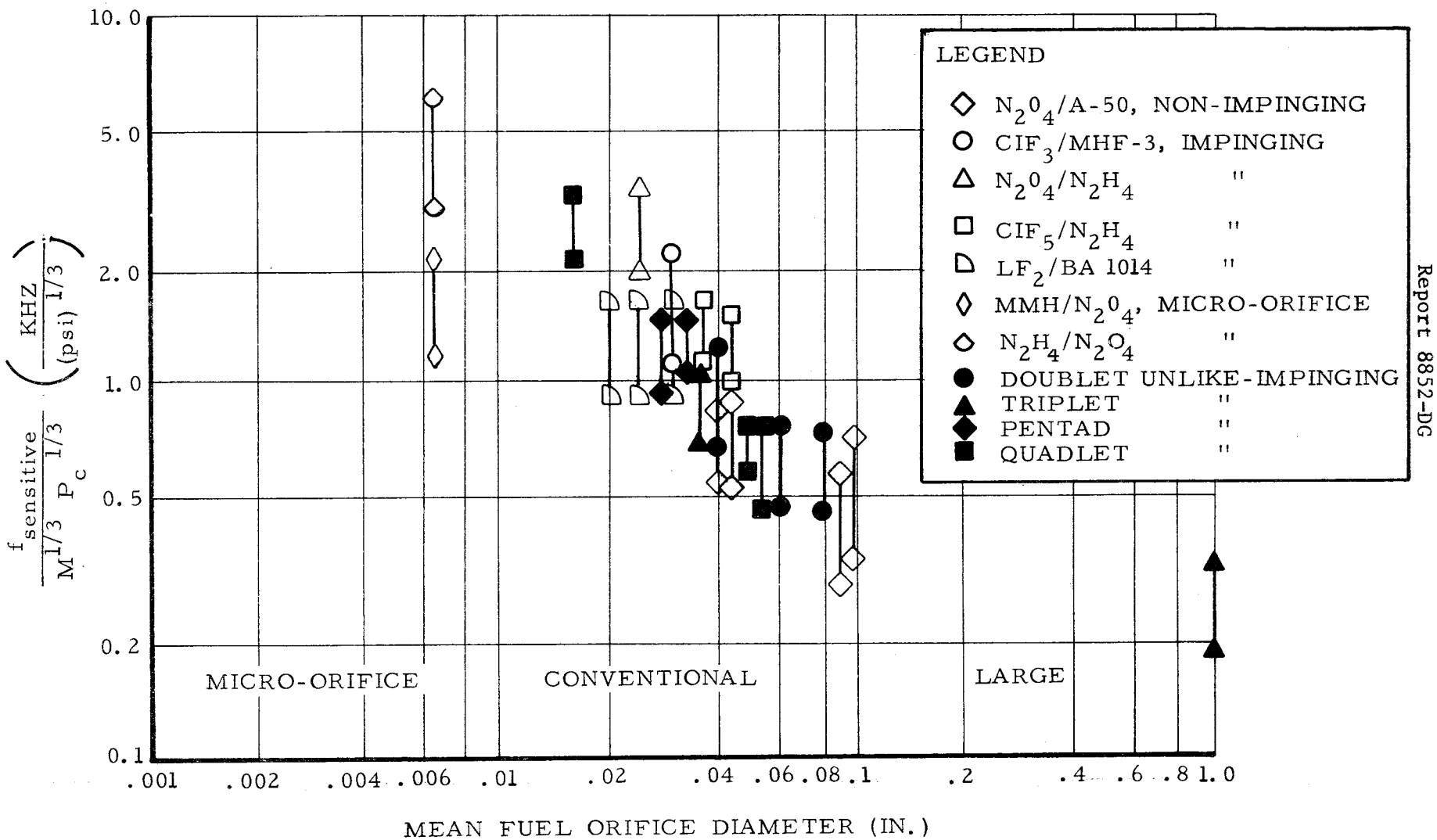

Figure 5. Sensitive Frequency Correlation

II, C, Sensitive Frequency Estimates (cont.)

all that remains to be evaluated is the fuel orifice size. The fuel orifice sizes selected should, for a fair comparison, be chosen to yield approximately the same theoretical performance. This means the low Mach number chamber will require smaller fuel orifices due to the poorer vaporization rates associated with low Mach number chamber gases. However, to make this comparison simple we will arbitrarily assume that both injectors have fuel orifice diameters of 0.030 in.

Using the two contraction ratios and the throat diameter we can calculate the injector diameters: rocket engine "A" is 3.2 in. and rocket engine "B" is 10.3 in. The first tangential mode frequency for each chamber can then be estimated as follows assuming an effective speed of sound of 3500 ft/sec.

Rocket engine "A" $f_{1T} = \frac{c\, S_{nh}}{\pi\, D_c} = \frac{(3500)(1.84)}{(3.14)(3.2/12)} = 7700 \text{ cps} = 7.7 \text{ khz}$

Rocket engine "B" $f_{1T} = \frac{(3500)(1.84)}{(3.14(10.3/12)} = 2400 \text{ cps} = 2.4 \text{ khz}$

To use Figure 5 we must calculate the value of the correlation parameter as follows:

Rocket engine "A" $\frac{f_{1T}}{M^{1/2}\, P_c^{1/3}} = \frac{7.7 \text{ khz}}{(0.5)^{1/3}\ (125)^{1/3}} = \frac{7.7}{(0.794)(5)} = 1.94$

Rocket engine "B" $\frac{f_{1T}}{M^{1/2}\, P_c^{1/3}} = \frac{2.4}{(0.5)^{1/2}\ (125)} = \frac{2.4}{(0.368)(5)} = 1.3$

II, C, Sensitive Frequency Estimates (cont.)

Now by going to Figure 5 we find that the first tangential mode of rocket engine "A" is slightly above the mean data curve which implies it will be probably stable, whereas rocket engine "B" falls right in the midst of the mean data curve which indicates the first tangential mode will be unstable. It can be seen by scrutinizing the various types of fuel data used in Figure 5 that hydrazine (N_2H_4) is unstable at higher frequencies that monomethyl hydrazine (MMH). Therefore it can be seen that MMH could be used in rocket engine "B" to improve its combustion stability potential, or if N_2H_4 were used it is possible that the engine could experience both the first and second tangential modes.

Due to the rather large range of frequency that injector elements are sensitive to it is difficult to predict exactly what orifice size is required to be safely stable without being excessively large. As previously stated it is best to assume that damping devices will be needed and make provision for them in the original design effort. Provision should be made for each and every mode that appears to be reasonably possible. Many rocket engines have experienced combustion instability in modes above the third tangential. Even if higher modes have not been previously experienced some provision should be made for at least one mode higher than those observed since the eventual damping of one mode often results in the next higher mode occurring.

In the example of the two rocket engine designs it should be clear that the smaller injector orifices tend to be unstable at higher frequencies than large orifices. This means they are more prone to support combustion instability since there are an infinite number of acoustic modes above the fundamental mode. There is no possibility that an injector element will have stable combustion if its sensitive frequency falls between two acoustic modes; it is more probable that it can be unstable to all acoustic modes from the

II, C, Sensitive Frequency Estimates (cont.)

fundamental through the higher of two modes that the sensitive frequency is thought to fall between.

D. ACOUSTIC MODE FREQUENCY DEPRESSION

Using the formulas on Table I to calculate acoustic mode frequencies for a given chamber geometry without an acoustic liner present is not sufficient for estimating the frequencies with a resonator or baffle present. Experimental evidence obtained during the Gemini Stability Improvement Program (GEMSIP, Ref 3) indicated very clearly that the presence of baffles depressed the frequency of the first tangential (1T) acoustic mode from 1900 cps to as low as 1200 cps.

Ambient acoustic tests and analyses verified that this mode frequency depression does occur. A similar frequency depression occurs using acoustic liners in the chamber wall. The frequency depression is most clearly seen in the first tangential mode in conventional chambers with large baffles or acoustic liners. However, this frequency depression is not generally observed experimentally due to the fact that depressed first tangential may be damped appreciably along with being decreased in frequency, to the point of not having a significant amplitude. Also the first tangential mode combined with the first longitudinal mode (1T + 1L) tends to be depressed in frequency just enough to be confused with the unlined chambers first tangential mode.

Calculated results for acoustic mode frequency depression as a function of resonator geometry and cavity gas temperatures are given in Table I.

III. ACOUSTIC LINER DESIGN CONSIDERATIONS

A. ACOUSTIC LINER DESIGN EXPERIENCE AND LITERATURE

The acoustic liner analyses discussed in Appendix I are limited to resonators (Helmholtz resonators), and their influence on the combustion stability of a rocket engine. Knowledge of many other factors such as: system frequency response, combustion energy release profile, chamber gas velocity profile, chamber gas static pressure profile, acoustic mode profiles and amplitude, the use of film cooling (in front of the resonators or from behind), nozzle admittance, and baffles effects are necessary to optimize a particular liner design. These and other more obvious resonator geometry factors are related to the acoustic damping capability of a mechanical stabilizing device.

At present there are three mechanical stabilizing devices: baffles, the quarter-wave tubes and the Helmholtz resonators. Baffles have been the most common stabilizing device for high performance rocket engines but are being presently augmented by Helmholtz resonator arrays in the injector face or chamber wall. Quarter-wave tube resonators have been used during the development of at least two systems and are presently being used on the LMA rocket engine to augment a three-blade baffle.

The application of Helmholtz resonators has been limited to technology hardware and to date no operational engine uses them. However, Helmholtz resonators offer many geometric advantages under certain conditions thus making them worth consideration in future engines.

1. Summary of AGC Testing Experience

Aerojet-General Corporation (AGC) experience with the use of Helmholtz resonators as a means of damping combustion instabilities dates back to 1964 with the design and fabrication of an acoustic liner for the M-1 gas

III,A, Acoustic Liner Design Experience and Literature (cont.)

generator. During the succeeding six years approximately 50 different acoustic liners have been designed and used at Aerojet to stabilize combustion for fourteen different rocket engine programs with varying success. A summary of these programs is shown in Table III. Of the fifteen programs listed, the nine most recent, high performing rocket engine programs are the most significant since they are representative of the accumulation of the best acoustic liner design knowledge at Aerojet to date.

2. Literature Search

A literature survey was made to obtain a more general background in the field of using acoustic resonators to damp rocket engine combustion instabilities. Hundreds of documents were surveyed. Forty were selected and summarized in an annotated bibliography, because of their direct concern with the subject originality, and clear presentation. Documents describing 25 acoustic liner programs are shown in Table IV.

The primary sources for well documented technical information of this nature are:

a. Technical meetings (ICRPG, CPIA, AIAA)

b. Technical journals (JASA, AIAA, ARS)

c. Government agencies (NASA, AFRPL, AFSOR, AMRL, DDC)

d. Private industry (AGC, BAC, NAA, PWA)

e. Text books (Beranek, Ingard, Morse, Rayleigh, Wood)

f. College or University theses (McAuliffe, Reardon, Sirignano)

There are sources of information other than those listed above; however, it can be assumed that the sources referenced contain all the best aspects of the others.

TABLE III

SUMMARY OF AEROJET ACOUSTIC LINER EXPERIENCE

No.	Program	Date Initiated	Chamber Dia., Inches	Chamber Length, Inches	Chamber P_c, psia	F, lb_f	Propellants	M.R.	No. of Injectors Tested	No. of Acoustic Liners
1	M-1 GGA	1964	8.125	20	1145	120,000 (hp)	LO_2/LH_2	0.80	4	1
2	METRE	1965	8.0	14	5-200	240-9000 lb_f	A-50/N_2O_4		1	2
3	HSIP	1966	11.91	20	100	8000	A-50/N_2O_4	2.0	2	2
4	Solid Rocket	1966	8	60	300-2500	--	Solid Propellant		4	10
5	PBPSΔV	1967	4	9	300	2800	N_2H_4/N_2O_4	1.1	2	1
6	IFAR	1967	4	9	300	2800	N_2H_4/N_2O_4	1.1	1	6
7	Fluorine TCA	1968	9.45	19	100	7000	LF_2/BA1014	1.9	1	3
8	SPARTAN	1968	2.7	3	500	1600	MMH A-50/ N_2O_4		1	2
9	S.P.S. I.O.S.	1968	17	24	100	20,000	A-50/N_2O_4	1.6	1	2
10	PBPS-N_2H_4	1968	3.25	5	300	2800	N_2H_4/N_2O_4		1	1
11	ITIP	1969	11.91	20	100	8000	A-50/N_2O_4	2.0	3	14
12	MIST	1969	1.7 x 2	4	--	--	A-50/N_2O_4	--	1	1
13	Liner Feasibility	1969	7.8	11	120	3500 vac	A-50/N_2O_4	1.6	1	4
14	Excitation Chamber	1969	3x 13	17	100	1000	A-50/N_2O_4	1.6	1	4

TABLE IV

SUMMARY OF INDUSTRY WIDE ACOUSTIC LINER EXPERIENCE

Source	Contract No.	Date	Chamber: Diameter Dc	Chamber: Length Lc	Chamber: Contraction Ratio	Chamber: Pressure Pc	Thrust F	Propellants: Oxid	Propellants: Fuel	Propellants: MR	Liner Cooling Method	Remarks
PWA FR-960	NAS 8-11038	Apr 64	10"	12	3.32	300	15K	LO_2	LH_2	4.	None	RL10A-1 engine
PWA FR-1279	PWA Applied Research	Mar 65	5"	--	--	300	3K	N_2O_4	A-50	1.6	None	
PWA FR-1279	AF 04(611)-9575C	Mar 65	10"	--	--	300	15K	N_2O_4	A-50	1.6	Uncooled and Regen H_2O	RL10 chamber only
CPIA No. 95	NASA Lewis	Nov 65	10.78"	18	1.89	100 or 300	20K	N_2O_4	A-50	1.6	Uncooled and Ablative	
PWA FR-1922	NAS 8-11038	Jul 66	10"	12"	3.32	300	15K	LO_2	LH_2	5.	Uncooled	ϵ = 1.3, RL10A-1
CPIA No. 118	NASA Lewis	Oct 66	10.78"	18"	1.89	300	20K	LO_2	LH_2	5.	Uncooled	
PWA FR-2168	AF 04(611)-11387	Nov 66	11.95"	17.23"	2.4	100	5K	N_2O_4	A-50	2.0	Uncooled	HSIP Injector, ϵ = 1.0
PWA FR-2522	AF 04(611)-11387	Aug 67	11.95"	17.23"	4.8	200	5K	N_2O_4	A-50	2.0	Film Cooled or Ablative	HSIP Injector, ϵ = 1.0
PWA FR-2522	AF 04(611)-11387	Aug 67	11.95"	17.23"	22.8	800	5K	N_2O_4	A-50	2.0	Film Cooled	HSIP Injector. ϵ = 1.0
CPIA No. 162	NASA Lewis	Oct 67	10.78"	18"	1.89	300	20K	LO_2	LH_2	5.0	Uncooled	
CPIA No. 162	AFRPL	Oct 67	12.8"	--	1.56	300	35K	N_2O_4	A-50	--	Uncooled	ϵ = 3.0
CPIA No. 162	AFRPL	Oct 67	12.8"	--	3.2	600	35K	N_2O_4	A-50	--	Uncooled	ϵ = 6.0
CPIA No. 162	NAS 3-4195,-6296	Oct 67	10"	12.35	2.8	100	5K	FLOX	Hydro-carbons	--	Uncooled	Methane, Propane, Butene
NASA TN D-4210	NASA-MSFC	Nov 67	3.73	12."	4.5	1031	3690	LO_2	RP-1	2.0	Uncooled or Regen	
AFRPL-TR-67-272	AF 04(611)-07402	Nov 67	--	--	>3.0	900	5K	--	--	--	Ablative	Thiokol Annular Engine
NASA TN D-4442	NASA Lewis	Mar 68	10.78"	30.5"	1.6	100	6.7K	N_2O_4	A-50	1.6 & 2.0	Uncooled	
CPIA No. 183	Rocketdyne	Oct 68	--	--	--	--	--	Solid	Propellant		Uncooled	T-burner
CPIA No. 183	Rocketdyne Research	Oct 68	--	--	--	--	3K	FLOX	Hydro-carbon		Uncooled	CH_4 and C_2H_6
CPIA No. 183	Rocketdyne Research	Oct 68	3"	3"	4.9	125	300	N_2O_4	MMH	1.6	Uncooled	
CPIA No. 183	NAS 9-9866	Oct 68	8"	11"	2.8	120	3.5K	N_2O_4	A-50	1.6	Interregen	LM"A" Rocketdyne
CPIA No. 183	NASA-MSFC	Oct 68	1.6"	--	1.6	96	100	N_2O_4	MMH	1.6	Interregen	C-1 Thiokol
Rocketdyne R-7792	NAS 8-21345	Mar 69	39"	35"	1.25	1000	1.5M	LO_2	RP-1	2.35	Uncooled	F-1 Engine
NASA TM X-1845	NASA Lewis	Aug 69	10.78	28.4	1.9	300	20K	N_2O_4	N_2H_4	3.0	Uncooled and H_2O Regen	= 1.3
Rocketdyne	R-7908 NAS 9-7498	Aug 69	8"	11"	2.8	120	3.5K	N_2O_4	A-50	1.6	Interregen	LM "A" Program
NASA TMS-1845	NASA-Lewis	Aug 69	10.78"	28"	1.9	300	20K	N_2O_4	A-50	3.0	Regen	Gas Source
Rocketdyne	R-7800-3 NAS 8-14	Oct 69	18.46"	20"	1.6	725	230K	LO_2	H_2	5.0	Interregen	J-2 Program

III, Acoustic Liner Design Considerations (cont.)

B. ACOUSTIC LINER DESIGN STUDY

1. General Guide Lines

An acoustic liner trade-off study can be made with any one of the several analyses described in Appendix I of this report. No single analysis has been proven conclusively to be superior to date. Experimental results have shown only that resonator designs can be altered in the direction indicated by simple theory (i.e., classical theory as described in Appendix I.A.), and be made to work successfully in most applications.

The primary criteria for designing acoustic liners are to tune them for the frequency of instability. The number of resonators required to assure stable combustion has not been determined; however, general guidelines are presented. The classical theory can be used to tune liners without flow effects or high sound pressure levels. Simple modifications can be made to adjust for flow effects. The effect of sound level is difficult to design for, since the level is variable, from 1 to 200% of the mean chamber pressure. However, since high amplitude instabilities are so destructive, it is safest to assume sound levels of 100% of chamber pressure. Such an assumption results in excessive nonlinear aperture resistance requiring that the liner design be made with an emphasis on decreasing the geometric resistance of the liner. The resonator acoustic resistance is decreased by: decreasing the thickness of the aperture, increasing the aperture diameter, and increasing the total amount of aperture area. The resonator gases contribute to decreasing the resistance only by extreme changes in their properties since the various property changes with chemical composition and temperature tend to cancel each other out.

III,B, Acoustic Liner Design Study (cont.)

2. Initial Design Estimate

The P&W absorption coefficient approach (Ref 4) can be used to make design and tradeoff studies. A simplification of this approach is included in Appendix I. The simplification involves the treatment of the nonlinear resistance term which is assumed to be constant and can result in a maximum error in the absorption coefficient of $\pm$ 10%. A reasonable relationship between the desired open area ratio, the aperture diameter and the number of apertures can be obtained from Figure 6. Then the liner face thickness should be selected with as thin an aperture as is structurally or thermally feasible in order to obtain the largest possible bandwidth. Having established reasonable values of all geometric parameters except the liner backing distance, an estimate of the cavity gas speed of sound is required in order to solve for the backing distance.

3. Cavity Gas Properties

Cavity gas speed of sound is a complex function of many variables such as cooling method, injector compatibility, liner design, and propellants used, but experimental results tend to show the minimum initial temperature observed is due simply to adiabatic compression of whatever gases are present in the liner at startup which can be estimated from Figure 7 for sea level testing. If no appreciable mean gas flow through the liner occurs, the liner remains relatively cool, usually one-quarter of the chamber stagnation temperature. However, if the liner design allows mean gas flow in upstream orifices and out downstream orifices, the temperature can quickly exceed one-half the chamber stagnation temperature. The liner cavity gas density is determined approximately by simply taking the inverse of the ratio of chamber gas temperature to liner cavity gas temperature times the density of the chamber gas as follows:

$$\rho_{liner} = \rho_{chamber} \left(T_{chamber}/T_{liner}\right)$$

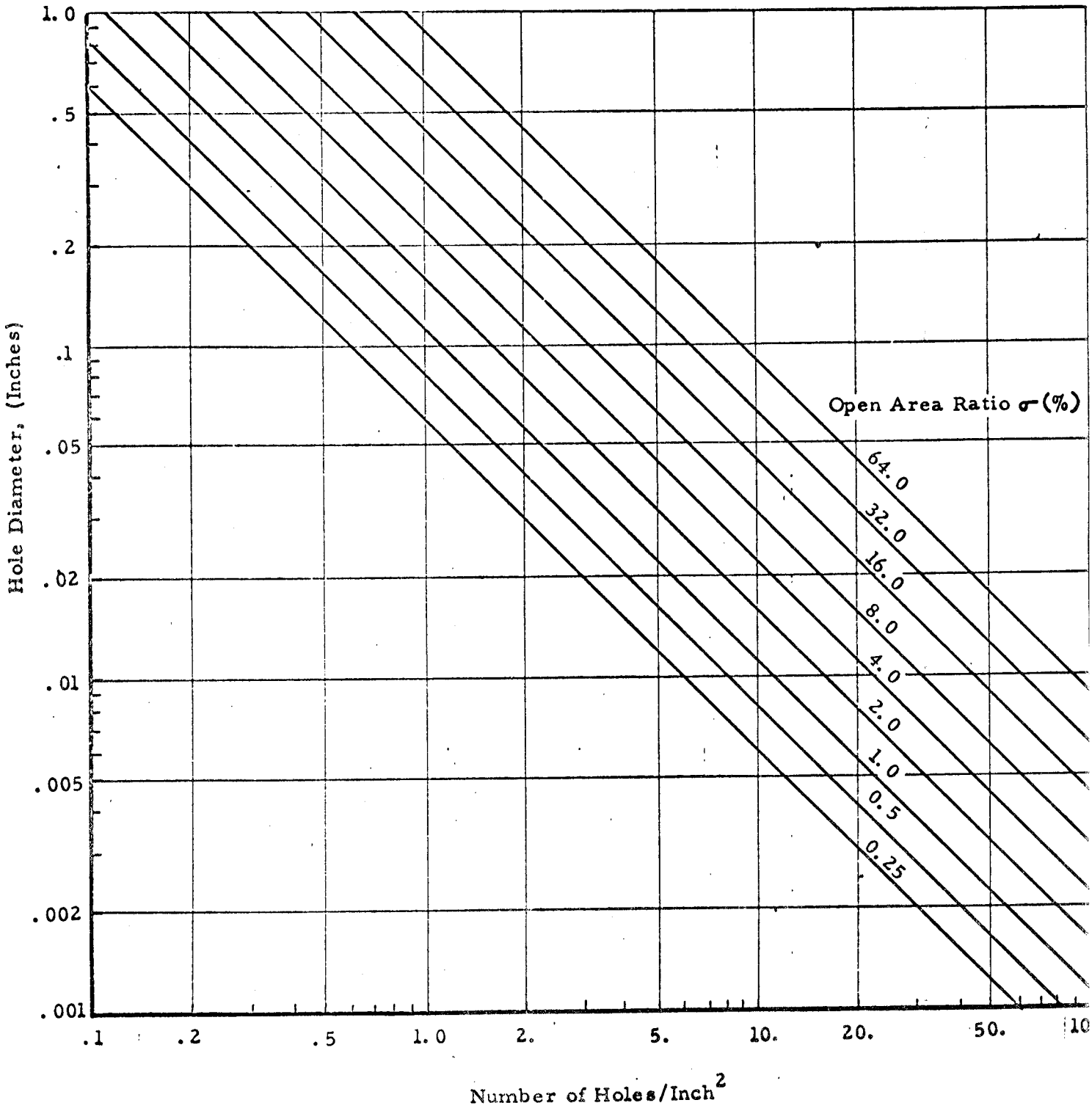

Figure 6. Acoustic Liner Array Hole Diameter vs Number of Holes per Square Inch for Various Open Area Ratios

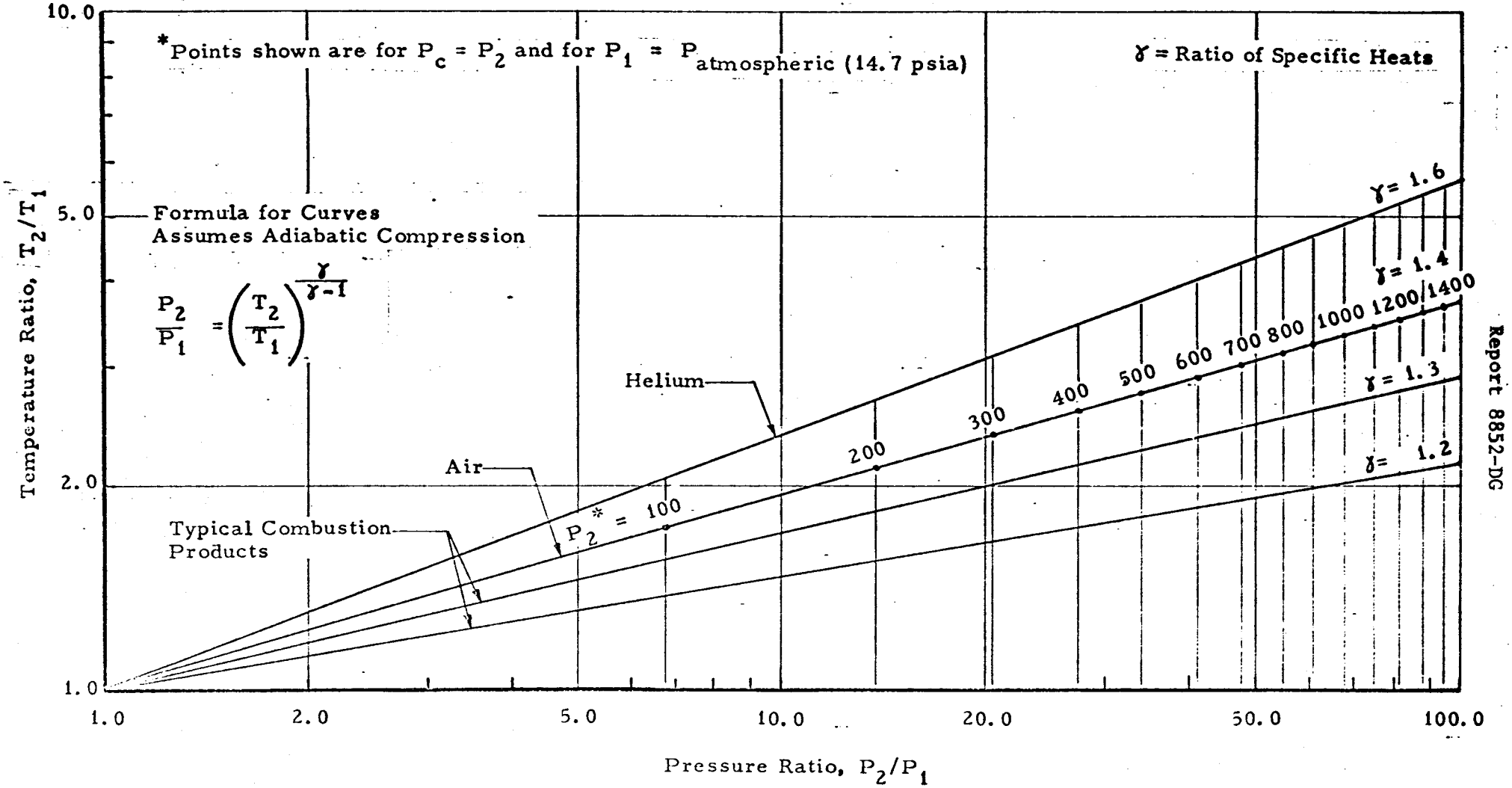

Figure 7. Acoustic Cavity Gas Temperature Ratios Versus Pressure Ratios for Various Ratios of Specific Heats

III,B, Acoustic Liner Design Study (cont.)

Similarly, the liner cavity gas speed of sound is:

$$C_{liner} = C_{chamber} \sqrt{T_{liner}/T_{chamber}}$$

assuming the chemical composition is the same.

As estimate of the liner cavity gas viscosity is slightly more difficult due to the need for a constant, which is a function of the gas composition (or rather molecular bond). The formula relating the chamber gas viscosity to liner cavity gas viscosity is as follows (based on Sutherland formula Ref 5):

$$\mu_{liner}/\mu_{chamber} = \left[\frac{.555 + C/T_c}{.555\ T_L/T_c + C/T_c}\right] \left[\frac{T_L}{T_c}\right]^{3/2}$$

where C is defined in Figure 8 for several common gases, along with a graph of viscosity ratios versus temperature ratios for different C/T_c ratios. Typical liner cavity gas viscosities are less than half that of the chamber gas.

4. Absorption Coefficient Design Parameters

Having assumed the cavity gas properties it is necessary to establish the tentative liner geometry, and then to estimate a reasonable backing distance such that it does not exceed one tenth of a wavelength of the frequency being considered in the cavity gas, or that it is not so short that the cavity cannot be reasonably classified as a spring volume when compared to the aperture mass volume. These two restrictions are purely analytical in nature; however, they must be kept in mind if these design methods are to be correct. Successful resonators, similar to quarter-wave tubes, can be designed though they do not obey these criteria, but they are not being considered here.

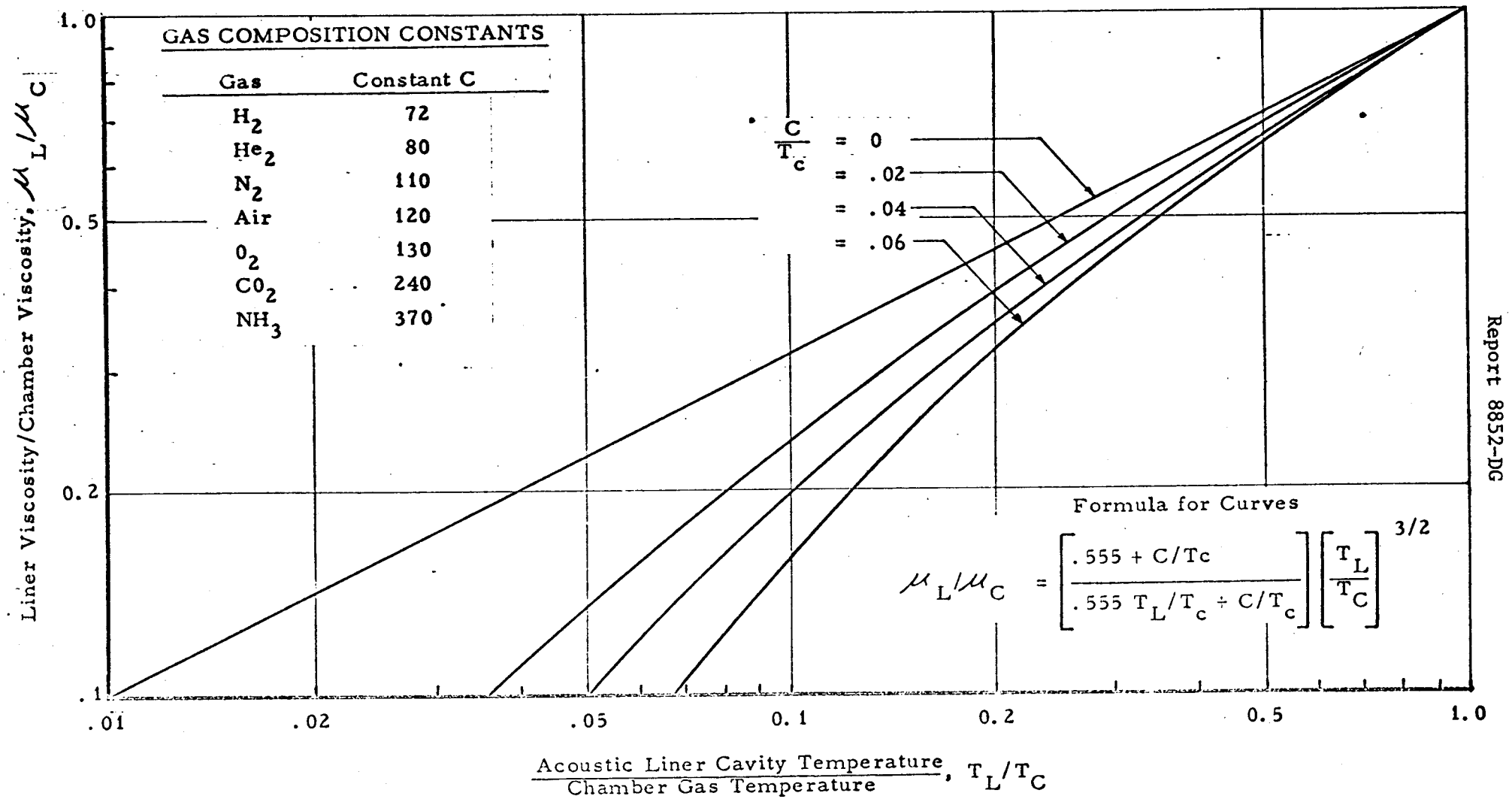

Figure 8. Acoustic Cavity Temperature Ratio vs Viscosity Ratio for Various Gas Composition Constants to Chamber Gas Temperature Ratios

III,B, Acoustic Liner Design Study (cont.)

A quality factor for the liner can now be estimated which is inversely related to the resonators absorption coefficient bandwidth as follows:

$$Q = \frac{2\pi f_o t_e}{c\sigma}\left(\frac{f}{f_R} - \frac{f_R}{f}\right) = \sqrt{\frac{t_e}{L\sigma}}\left(\frac{f}{f_R} - \frac{f_R}{f}\right) = G\left(\frac{f}{f_R} - \frac{f_R}{f}\right)$$

Plotting absorption coefficient versus the frequency ratio f/f_R for various values of Q in Figure 9 shows the effect on bandwidth. The curves shown in Figure 9 are based on the assumption that the liner acoustic resistance ratio, θ, is unity which is the optimum condition (see Appendix A). Similar plots of absorption coefficient versus the resonant frequency ratio f/f_R are made for various values of acoustic resistance ratio for a constant value of the liner geometric "Q" coefficient G as shown in Figure 10.

If the geometric coefficient G is allowed to vary, then the reactance term X also varies. Thus, a plot of acoustic resistance versus absorption coefficient can be generated for various X or G's, as shown in Figure 11 for a frequency equal to half or twice the resonate frequency. In Figure 11 it is apparent that the optimum absorption off resonance occurs above an acoustic resistance ratio of unity when the value of G is greater than zero (which it physically has to be). A typical value of G would be between 1.0 and 5. This implies from Figure 11 that the maximum absorption would occur at a resistance ratio of around 2.0 for a frequency that is a factor of 2 above or below resonance. This result suggests that an acoustic resistance ratio above unity is desirable if accurate tuning is not possible.

5. Acoustic Liner Size Requirements

None of the considerations made so far have suggested how much liner is necessary. Nor have they helped to determine where the acoustic modes are after the resonator is added to the chamber wall. Both of these

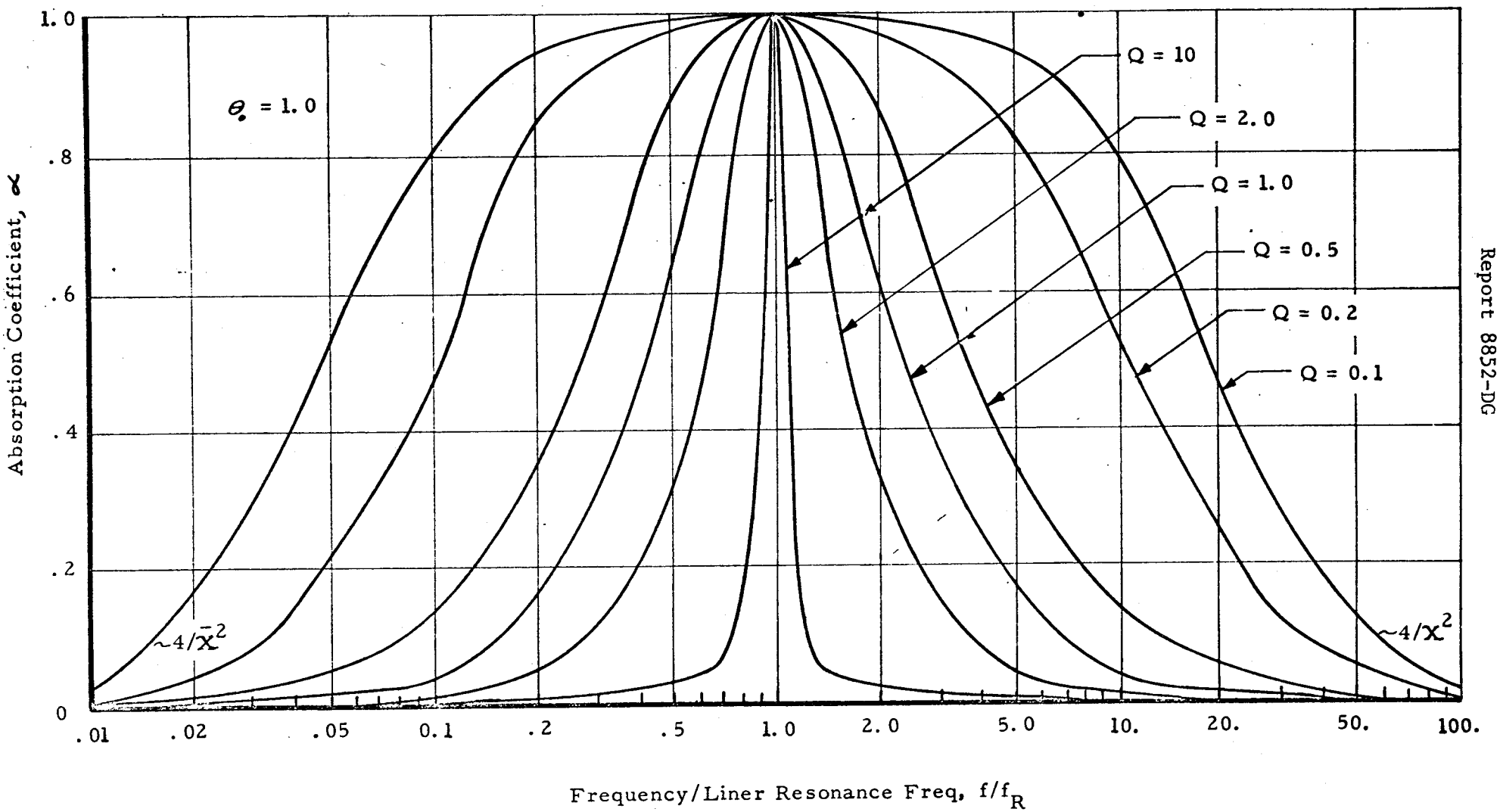

Figure 9. Absorption Coefficient vs Frequency Ratio for Various Quality Factors

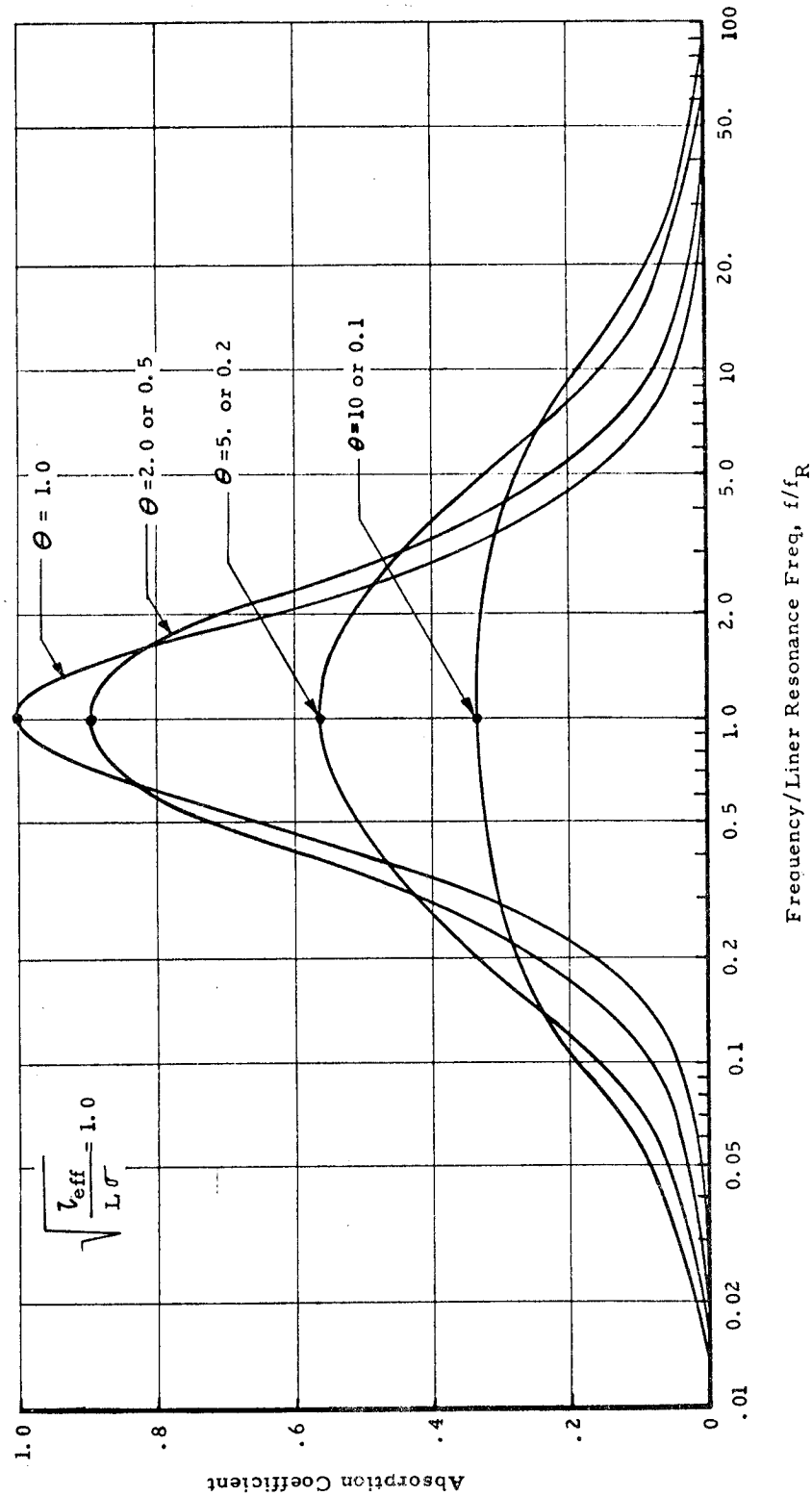

Figure 10. Absorption Coefficient vs Resistance

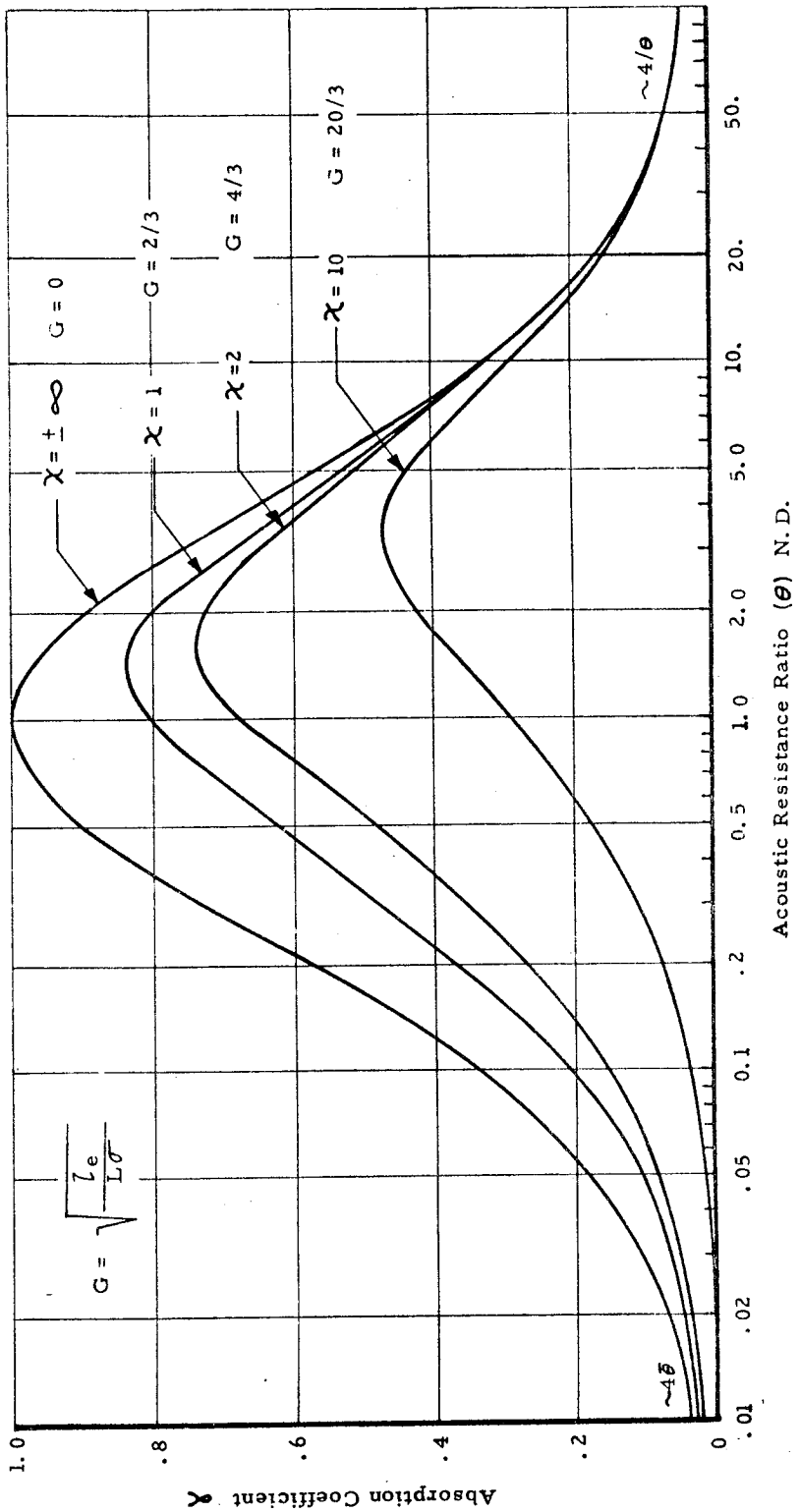

Figure 11. Absorption Coefficient vs Reactance

III,B, Acoustic Liner Design Study (cont.)

factors are taken into account in the systems approach to designing liners. Using the injector face acoustic resonator (IFAR) systems analysis for the evaluation of a LMA chamber acoustic liner design resulted in two significant facts that are clear. First, the systems pure transverse acoustic mode resonances generally move down in frequency as size of the liner increases and, second, the damping increases as the mode frequency moves into the resonance of the resonator as shown in Table V. This moving of modes as the size of the resonator increases occurs to some extent regardless of whether the resonator is tuned far above or below the mode of interest.

Table V shows IFAR data obtained for various sizes of resonators which are all tuned to about 4550 cps and their effect on the first tangential mode at about 3300 cps and the second tangential mode at 5300 cps. Comparison of the data in Table V and in Figure 12 tends to indicate that a relatively small resonator (aperture area equal to 2% of the injector face area as for resonator G in Figure 12) tuned very closely (within 5%) is very effective or that a moderate size resonator (aperature area equal to about 4% of the face area as for resonator D in Figure 12) tuned within 20% of the mode frequency is functionally adequate, but that a large size resonator (aperature area equal to 10% of the injector face area) off-tuned by about 35% is functionally inadequate. This is verified by some experimental evidence that aperature areas equal to 18% of the injector face are required to stabilize some injectors (Ref J-2). Of these three possible size and tune situations, only the latter two can be seriously considered, since the precise tuning required for the first is very difficult. Therefore, the absolute minimum resonator aperture area that can be expected analytically to produce a significant stabilizing influence is equal to about 4% of the injector face area. This assumes that the tune is within 20% of the mode frequency. Larger resonator aperture areas always appear to help, but tuning accuracy is more important. Therefore, it is wiser to design two or three separately tuned resonators each

III,B, Acoustic Liner Design Study (cont.)

TABLE V

EFFECT OF LINER SIZE ON ACOUSTIC MODES*

Damper Configuration				First and Second Tangential Acoustic Mode		
Designation (letter)	Orifice Area ($in.^2$)	Cavity Volume ($in.^3$)	Resonator Frequency (cps)	Mode Frequency (cps)	Index n (N.D.)	Time Lag (N.D.)
No Resonator						
A	0	0	0	3275=1T 5275=2T	0.341 0.350	2.53 1.1
1T Resonator						
B	0.63	3.93	2886	3325=1T	0.464	1.35
C	1.26	7.86	3022	3350=1T	0.572	1.37
D	1.89	11.79	3042	2750=1T	1.11	2.57
E	2.51	15.8	3045	2650=1T	1.09	2.62
F	5.03	31.6	3102	2450=1T	0.99	2.60
2T Resonator						
G	1.26	3.5	4505	3225=1T 4350=2T	0.399 1.60	1.60 1.85
H	2.51	7.075	4555	3175=1T 4125=2T	0.441 1.36	1.63 1.79
I	5.03	14.15	4635	3050=1T 3850=2T	0.490 1.125	1.77 1.76

*Design Constants:

Resonator speed of sound	2605 ft/sec
Chamber speed of sound	3600 ft/sec
Orifice thickness (1T)	0.3 inches
Orifice diameter (1T)	1.875 inches

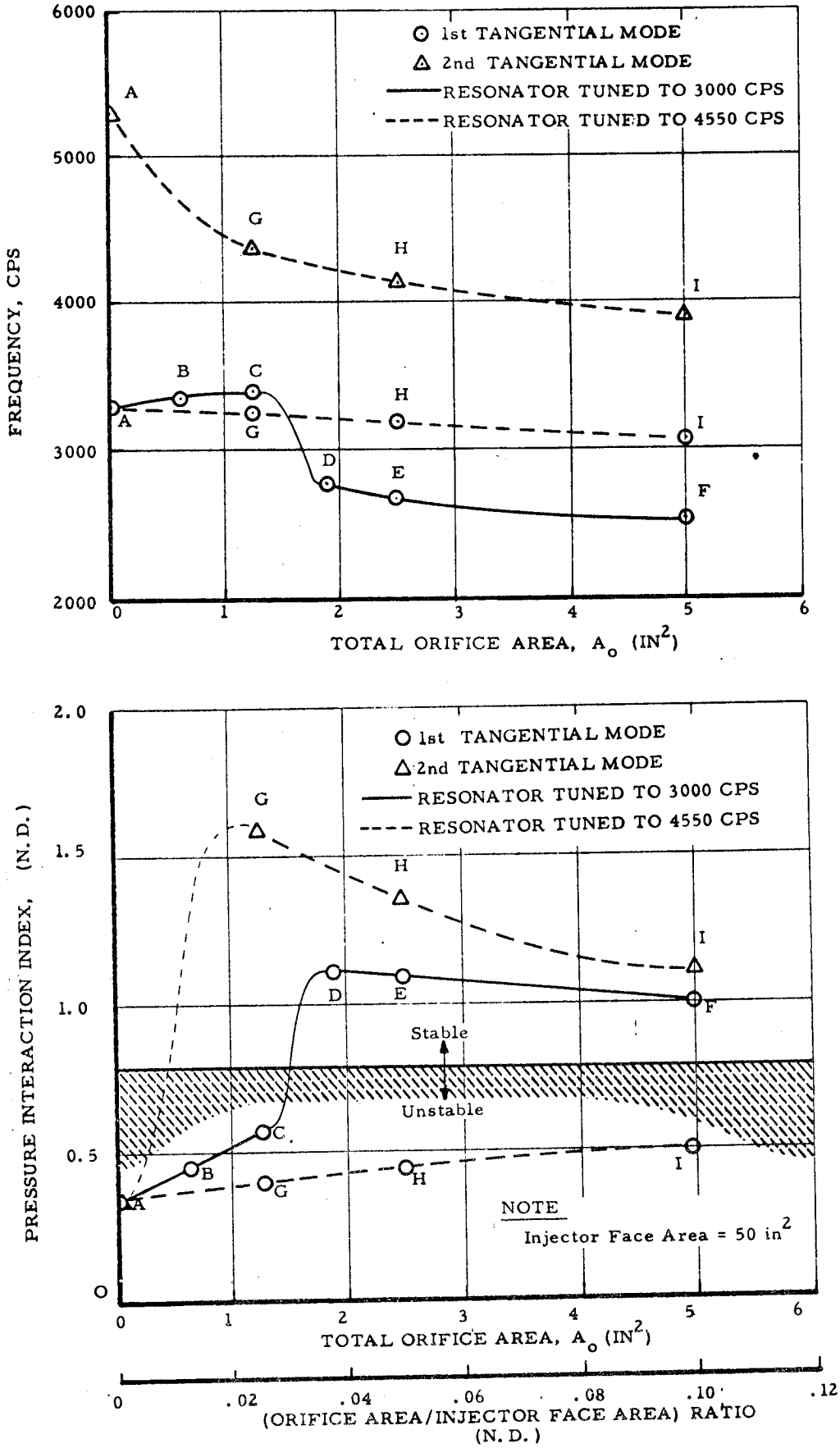

Figure 12. Effect of Acoustic Liner Size and Tune on Acoustic Mode Frequencies and Pressure Interaction Indices

III,B, Acoustic Liner Design Study (cont.)

with aperture areas of 4% of the injector face than it is to double or triple the size of a single resonator design. Although there may be enough variation in the cavity gas speed of sound to provide the necessary variation in tune frequency.

C. ACOUSTIC LINER PROBLEM AREAS

Acoustic damper problems fall into two general categories: (1) those problems associated with the determining of the gaseous environment imposed on the resonator by combustion, and (2) those problems due to geometry and physical limitations of the system. The first category makes designing Helmholtz resonators difficult due to presence of unknowns, due to transient variations, and due to uncontrollable and/or hostile conditions. The second category causes problems in the design of a liner due generally to limitations in the number, size, location, tune, and absorption coefficient frequency bandwidth of the resonators.

1. Gaseous Environment

The gaseous environmental parameters affecting acoustic liner design consist primarily of the following: (1) cavity gas temperatures, (2) cavity gas composition, (3) mean gas flow past the liner aperture, (4) mean gas flow through the liner aperture, and (5) the sound pressure level of the resonant combustion.

The first two parameters, cavity gas temperature and composition (MR), are not always measured or are measured only indirectly and not necessarily as a function of time. Generally, the first two parameters are transients and can vary by a factor of two, even during steady state operation. This result implies that the speed of sound used to tune the resonator design

III,C, Acoustic Liner Problem Areas (cont.)

will vary by a factor equal to the square root of two, or about ± 40%. However, the error is not generally that great due to the compromise between temperature and MR, generally found as shown in Figure 13. Note that for a typical rocket liner the speed of sound is almost constant as the mixture ratio and temperature change.

Unless some means of stabilizing the cavity gas temperature and composition or speed of sound is used, some other allowance must be made for "off tuned" resonators. Multiple resonator frequency tunes and geometries and very large amounts of resonators can suffice also.

The last three parameters all have the effect of increasing the resonant frequency of the resonator and decreasing the resonant absorption with increasing gas velocity or sound pressure level. The resonance frequency can be increased as much as 63% above the nonflow condition for thin apertures with about 300 ft/sec gas velocity past the aperture, or about 15 ft/sec gas velocity through the aperture, or about 15 ft/sec oscillatory (S.P.L.) gas velocity in the aperture. Such resonant frequency changes are nearly impossible to measure in a hot firing rocket engine. The amount of frequency shift is also a function of the aperture L/D (as shown in Appendix A, Figure A-3) and contour. If the maximum resonant frequency shift is assumed, then the accompanying increase in the aperture's acoustic resistance becomes so great that the resonator would be theoretically unacceptable in any tradeoff study due to poor absorption.

2. Geometry and Physical Limitations

Geometrical and physical limitations are imposed by system requirements such as dimensional envelopes, or thermal envelopes, or chemical compatibility, or material strength. For example, the minimum aperture thickness of an ablative liner may be determined by erosion rate and structural

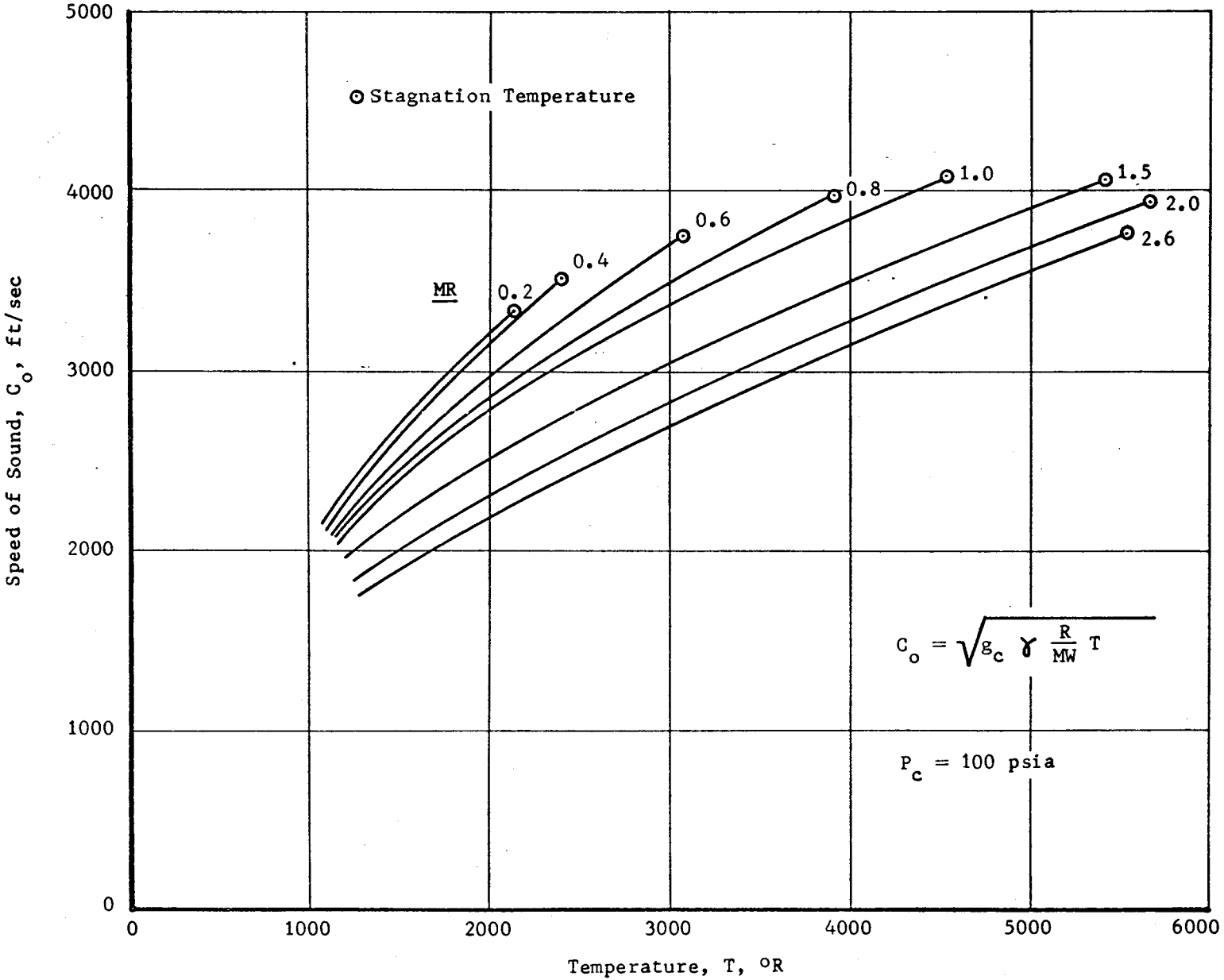

Figure 13. Acoustic Liner Cavity Gas Speed of Sound vs Cavity Temperature for Various Mixture Ratios

III,C, Acoustic Liner Problem Areas (cont.)

integrity, whereas the minimum aperture thickness of a regenerative liner may be determined by the hydraulic passage widths as dictated by heat transfer and hydraulic pressure drop considerations as well as structural integrity. Whatever the reason for determining the minimum aperture thickness, the fact is that the thickness will generally exceed about 0.2 inches for the LMA system. This represents a problem in that it limits the liner admittance or absorption coefficient bandwidth that can be obtained. Usually, the conservative approach used in any structural design results in a thicker aperture and, therefore, a less conservative design from an acoustic damping point of view.

Similarly, the aperture diameter is determined by material properties or fabrication limitations. Ideally, an acoustic resonator would consist of an infinite number of infinitely small diameter apertures that are infinitely thin. The number of apertures is easy to compromise since acoustic damping is not directly affected; however, the aperture diameter should be minimized since the effective thickness of the aperture is proportional to the aperture diameter for resonators exposed to low sound levels and no mean gas flow velocities through or past the aperture. However, in rocket engine applications with high sound levels and mean gas flow velocities, the aperture diameter is not as critical a parameter in determining the effective thickness of the aperture.

Physical limitations require that silica ablative liners have aperture diameters exceeding 0.15 inch to prevent plugging due to molten silica flow solidifying in the aperture. Regenerative acoustic liners with nominal percent open areas ($\sim$10%) require aperture diameters greatly exceeding 0.10 inches due to fabrication considerations which require each aperture to have a surrounding metal thickness of about 0.05 inches, thereby making the hydraulic flow channel aperture diameter 0.20 inches. This results in apertures so closely spaced that coolant cannot easily flow behind apertures. Hydraulically speaking, the optimum aperture diameter for a regeneratively cooled liner is

III,C, Acoustic Liner Problem Areas (cont.)

the maximum that can be uniformly spaced around the circumference of chamber with a minimum of two aperture hydraulic diameters between aperture centers. This does not significantly compromise the acoustic damping capability of the resonator since diameter is a second order parameter for normal rocket engine environments. Analytical restrictions simply require that all dimensions of the individual resonators be less than one-tenth of a wavelength of the frequency being damped.

The resonator backing distance is usually limited by the combination of the dimensional and thermal envelopes imposed by other system requirements. The outer chamber envelope is the limiting dimension of the resonator cavity and then the thermal envelope further limits it by imposing a need for some finite amount of insulation thickness in order to reduce the chamber's outer skin temperature. The optimum resonator cavity backing distance (or volume) is the maximum that can be tuned. Since tuning requires, for a constant open area, that the product of the aperture thickness and the cavity backing distance be a constant, then minimizing the aperture thickness requires a maximizing of the cavity backing distance. Backing distance is generally not a problem due to the fact that the aperture thickness is usually so thick that the backing distance is of the same order of size.

D. ACOUSTIC LINER DESIGN CRITERIA

Helmholtz resonator design criteria have three major objectives: (1) to optimize the acoustic damping, (2) to be compatible with the other system requirements, and (3) to be economically feasible to fabricate. The first objective is approximated by considering all the analytical methods of optimizing the design parameters, and comparing each with previous experimental results. The second objective is equally intangible but is usually conservatively selected to insure reliability of the liner design with respect to heat transfer and structural considerations. The third objective is initially

III,D, Acoustic Liner Design Criteria (cont.)

ignored in a thorough preliminary analysis but must be foremost in the final trade-off considerations. A design that is technically feasible may require an excessive development effort in order to establish the reliability of the fabrication method desired.

The Helmholtz resonator design criteria for optimizing the acoustic damping capability of a volume limited acoustic liner are as follows:

(1) Locate the resonators near the region of maximum oscillatory pressure amplitude.

(2) Locate the resonators near the region of maximum combustion.

(3) Locate the resonators in regions with low gas velocities past the resonator orifice (less than 500 ft/sec) or low gas velocities through the orifice (less than 25 ft/sec).

(4) Size the liner such that the total orifice area exceeds 4% of the injector face area for each acoustic mode to be damped.

(5) Tune the resonators to a frequency ($f_R = \frac{C}{2\pi}\sqrt{\frac{Ao}{V\ell_e}}$) approximately 10 percent higher than the frequency to be damped, to allow for warming up during the start transient.

(6) Size the aperture such that its thickness to diameter ratio is less than 1.0, to minimize acoustic resistance due to geometry.

(7) Isolate each axial row of resonator apertures to prevent gas flow in at upstream apertures and out at downstream apertures.

III,D, Acoustic Liner Design Criteria (cont.)

(8) Maximize the resonators absorption coefficient bandwidth by minimizing the geometric parameter $\left[\ell_e / (L\sigma) \right]^{1/2} = G$ which means maximizing the resonator backing distance and open area ratio while minimizing the orifice thickness.

(9) Assume that the resonator cavity gases are of the same composition as chamber wall boundary layer gases (usually low mixture ratio).

(10) Assume that the cavity gas temperature is about one-fourth of the chamber gas stagnation temperature and correct the gas properties accordingly.

(11) Assume that a single resonator geometry can be effective from 70% to 140% of its nominally tuned frequency (assuming G = 2.0).

The last three resonator design criteria assumptions are based on the premise that the first eight have been approximately satisfied and should be used only if more meaningful experimental data are not available.

IV. DESIGN MECHANICS

A. INTRODUCTION

The specific objective of Phase I of the ALFP program was to establish the design criteria necessary to demonstrate the integrity, durability and damping capacity of an acoustic liner over a 600-sec Lunar Module Ascent Rocket Engine (LM-A) duty cycle including multiple starts. Preliminary to this extensive analysis were literature searches required in the areas of heat transfer, materials, and structures in order to identify problem areas and to suggest possibilities for trade-off.

In all technical areas the starting point for analysis was the review of previous Aerojet experience and of the applicable technical literature. A search for improved materials includes contacting vendors for additional information; the investigation of the possible use of graphite, quartz, and zirconia in addition to silica-phenolics, and the establishment of screening methods. Structural analysis also includes the modification of computer programs for finite-element analysis to handle the special geometry of resonator modules.

Two general categories of problems are identified, namely areas where conflicting requirements might inhibit the execution of a successful design and lack of adequate data until some hot firing unlined testing is completed.

For chambers with ablative liners the primary concern is for a material with an adequately low regression rate under the thermal environment so that the resonator will be intact at the end of the duty cycle. For regeneratively cooled liners the problem is in providing adequate channels for cooling without intruding on the space required for the resonator apertures. Final answers to both questions depended upon a knowledge of the injector chamber compatibility and the heat flux immediately aft of the apertures.

IV, A, Introduction (cont.)

Trade-offs were analyzed in light of the requirements for experimental chambers to be tested during Phase II or development phase of the program and for the design of flight weight prototype chambers to be demonstrated during the Phase III or prototype portion of the program.

In the area of heat transfer consideration was given to four methods for utilizing regenerative cooling, both with and without film cooling. The flow requirements were established for a transpiration-cooled chamber, but these were so high as to offer no significant advantage over film cooling. Parameter studies of film cooling and barrier cooling were made in conjunction with designs for ablative resonator liners.

Material trade-offs included the effects of precharring, type of reinforcement, resin and filler content, and density in the behavior of ablatives. Consideration was also given to the use of composite systems and to coatings. The method of wrapping the tape material to form the acoustic liner or chamber wall is found to be a very important consideration.

Specific structural trade-offs generally cannot be outlined in advance of the initial design configurations. General admonitions are offered concerning resonator support and allowance for the effect of thermal expansion.

System trade offs are most important and also dependent on many predetermined mission requirements. For this sample design evaluation it will be assumed that the LMA system design limitations are imposed, since they are highly restrictive.

IV, Design Mechanics (cont.)

B. OVERALL ROCKET ENGINE SYSTEM CONSIDERATIONS

1. System Problem Areas

System problems stemming from the presence of an acoustic resonator assembly located in the combustion chamber wall fortunately appear to be limited in number. However, in the absence of an engine operating schedule for a general design situation, all discussions in the field of system problems must be considered tentative.

Based on the results of this program the ablative acoustic liner is feasible for application with low pressure ($\sim$ 120 psia) engines and will require the minimum of system compromise over a engine without a liner. The program also showed that a regeneratively cooled acoustic liner integrated with a ablative chamber is entirely feasible with minimal additional system pressure drop ($\sim$ 5 psi) and weight penalty.

Use of a regeneratively cooled resonator assembly requires the recognition of problems associated with engine restart in space. Short duration firings and or short coast periods, due to inadequate temperature buildup in chamber components, may create a condition preventing elimination of residual fuel in injector - resonator circuitry. The residual fuel may be frozen creating a flow blockage on the following engine restart. Or the time between firings may be too short to permit complete fuel expulsion resulting in an unknown ignition-start transient condition during the following engine burn.

Either a regeneratively cooled chamber or an acoustic liner section may be limited in the restart capability of the engine because of the danger of fuel (coolant) detonation on contact with the hot wall surfaces.

IV, B, Overall Rocket Engine System Considerations (cont.)

The usual recourse is to allow sufficient coast time for the section to cool to a safe temperature level, normally below the fuel saturation temperature, before engine restart. Again, a thermal model of the entire engine system is required for analysis. Parenthetically it may be noted that lessening the heat soakback problem probably will worsen the restart condition by increasing the danger of detonations on the next engine restart.

Liquid flow into resonator cavities may occur in at least three instances: on startup prior to injector manifold filling, by one or both propellants dribbling into the chamber; on shutdown as the manifolds empty; or during firing, especially with liquid film-cooled units. The first two conditions are, of course, intensified in a gravity environment for other than vertical firings. Whether such liquid flow into the cavities may prove damaging to the hardware or detrimental to the damping characteristics of the liner has not been demonstrated. The potential exists, however, for fuel detonation or combustion to take place within the cavities, as well as for an incompatible oxidizer-rich atmosphere to occur.

2. System Trade-Off Studies

Several materials and fabrication techniques are considered for use in both the non-regenerative and regeneratively cooled acoustic resonator concepts. One means of attempting to objectively compare the different features of various cooling methods is to develop a rating system that would assist the selection process as illustrated by Tables VI, VII, and VIII. Ratings 1 (excellent) through 5 (poor) in descending order of merit were selected as the rating indicators. A normal ablative chamber, without an acoustic resonator, was used as standard in the rating system.

TABLE VI

DESIGN AND FABRICATION CONSIDERATIONS

(600 sec Multiple Restart Duty Cycle)

ACOUSTIC LINER TYPE	Design Data Avail.	Simplicity	Flexibility	Dim. Envelope	Thermal Envelope	Mat'l Availability	State of the Art	Weight	Reproducibility	Cost
A. STANDARD ABL. CHAMBER (W/O RESONATOR)	2	1	1	1	1	1	1	1	1	1
B. NON-REGEN COOLED										
1. Ablative (Carbonized Assy)	2	1	1	3	2	1	1	2	2	2
a. Rosette Wrap	3	3	1	3	2	1	1	2	2	3
b. Flat Wrap	2	2	1	3	2	1	1	2	2	2
c. Molded	1	2	1	3	2	1	1	2	2	1
2. Transpiration (Platelet)	1	5	4	2	1	1	3	3	1	4
3. Refractory	2	1	3	2	3	1	3	3	2	5
C. REGEN COOLED										
1. Concentric Cylinders (Electroformed)	1	5	2	2	1	1	3	2	2	3
2. Grooved Cylinder (Copper Brazed)	1	4	2	2	1	1	1	3	1	2
3. Drilled Cylinder (Copper)	1	3	3	2	1	1	1	4	1	2
4. Platelet Cylinder	1	5	4	2	1	1	1	5	2	2
5. Tubular	1	5	4	2	1	1	1	3	2	4

Rating - 1 thru 5 with 1 best

TABLE VII

ACOUSTIC LINER FUNCTIONAL REQUIREMENTS

(600 sec, Multiple Restart Duty Cycle)

	TYPE	Chemical Compatibility	Restart Capability	Strength	Reliability	Durability	Hydraulic Press. Drop.	Performance	Thermal Shock	Dynamic Press (Bomb)	Fatigue
A.	STANDARD ABL. CHAMBER (W/O RESONATOR)	1	1	1	1	1	1	1	1	1	1
B.	NON-REGEN COOLED (w/Acoustic Resonator)										
	1. Ablative (Carbonized Assy)	1	1	2	2	3	1	1	1	1	1
	a. Rosette Wrap	1	1	2	2	2	1	1	1	1	1
	b. Flat Wrap	1	1	2	2	3	1	1	1	1	1
	c. Molded	1	1	2	2	3	1	1	1	1	1
	2. Transpiration (Platelet)	1	1	1	3	1	2	1	1	1	2
	3. Refractory	1	4	3	1	3	1	1	3	1	1
C.	REGEN. COOLED										
	1. Concentric Cylinders (Electroformed)	1	1	1	3	1+	3	1	1	1	2
	2. Grooved Cylinder (Copper-Brazed)	1	1	1	3	1+	3	1	1	1	2
	3. Drilled Cylinder (Copper)	1	1	1	3	1+	3	1	1	1	2
	4. Platelet Cylinder	1	1	1	4	1+	3	1	1	1	2
	5. Tubular	1	1	1	3	1+	3	1	1	1	3

Rating - 1 thru 5 with 1 best

TABLE VIII

SYSTEM OPERATIONAL REQUIREMENTS*

(600 sec Multiple Restart Duty Cycle)

ACOUSTIC RESONATOR TYPE	Repeatability (Start)	Reliability (Start)	Simplicity	Weight	Pressure Drop	Space Envelope	Restart Capability
A. STANDARD ABL. CHAMBER (W/O RESONATOR)	1	2	1	1	1	1	2
B. NON-REGEN COOLED							
1. Ablative (Carbonized Assy)	1	2	1	1	1	3	3
a. Rosette Wrap	1	2	1	1	1	3	3
b. Flat Wrap	1	2	1	1	1	3	3
c. Molded	1	2	1	1	1	2	3
2. Transpiration (Platelet)	2	2	4	3	4	2	1
3. Refractory	3	5	1	2	1	2	4
C. REGEN. COOLED							
1. Concentric Cylinders (Electroformed)	1	1	4	3	3	1	1
2. Grooved Cylinder (Copper Brazed)	2	3	1	3	3	2	2
3. Drilled Cylinder (Copper)	2	3	1	3	3	2	2
4. Platelet Cylinder	1	2	2	2	4	1	1
5. Tubular	1	1	2	2	2	2	1

*Due to presence of, but not including resonator assy

Rating - 1 thru 5 with 1 best

IV, B, Overall Rocket Engine System Considerations (cont.)

State-of-the-art and fabrication costs probably influenced the selection to a greater extent than indicated in the tables. Electroforming the regeneratively cooled resonator assembly presented some very attractive features, primarily in the area of optimizing resonator assembly design details. However it maybe rejected at present due to lack of experience for this particular application and an unknown cost factor.

The three sample concepts based on copper cylinders show in Figures 14b, c, and d are quite similar and the selection of one over another would have to be based on design and fabrication details.

IV, Design Mechanics (cont.)

C. HEAT TRANSFER

1. Heat Transfer Design Analysis

The concerns of the heat transfer design analysis is (1) to develop methods for describing the heat transfer coefficient downstream of resonator apertures, since the apertures are expected to trip the boundary layer and cause increased heat transfer, and (2) to investigate the heat transfer within the resonator orifice and cavity itself. These are relatively unstudied areas, at least as applied to rocket thrust chambers. There are frequent related cases in the technical literature, however: flow over slots, flow over forward and backward facing steps, free jet boundaries, wakes, vortex flow, etc. The largest portion of the present study is devoted to the gas-side condition, that being considered the most critical with respect to cooling requirements.

The following sections review previous experience, discuss two methods of dealing with the gas-side heat transfer, and dwell lightly on orifice and cavity heat transfer.

a. Review of Previous Experience

There does not appear to be any previous analytical experience that deals directly with flow over and in a circular hole which has a large closed volume at its end. There are numerous related studies that are indirectly applicable. Fox (Ref 6) showed that a shear layer similar to that for a free jet boundary exists for flow over a rectangular slot. Charwat (Refs 7 and 8) found that the boundary layer separating at the leading edge of the cavity subsequently reattaches either at the recompression corner or at the base, depending on depth-to-width ratio, oncoming boundary layer

IV, C, Heat Transfer (cont.)

thickness, and the relative heights of the forward and rear steps; for narrow slots, the boundary layer was found to "bridge" the gap. Larson (Ref 9) measured the heat transfer for both laminar and turbulent flow over rectangular slots. Roshko (Ref 10) studied the pressure, velocity, and skin friction for the flow over rectangular slots. Seban et al. (Ref 11) studied the heat transfer in separated and reattached flows downstream of a backward facing step and found a maximum local heat flux at the reattachment point and general correlation of the heat transfer coefficient with the 0.8 power of velocity. Seban and Fox (Ref 12) measured the heat transfer on the bottom of a rectangular slot and again found a dependence on the 0.8 power of velocity. Haugen (Ref 13) and Dhanak (Refs 14, 15) studied the heat transfer and momentum transfer in the separated flow region over a cavity facing an oncoming turbulent boundary layer of varying thickness. Also, Maull and East (Ref 16) note the presence of three-dimensional vortex flow in rectangular slots, with the number of cellular structures depending on the slot geometry, and an unstable condition resulting when the geometrical configuration does not produce a cellular structure. Finally, Snedeker and Donaldson (Ref 17) observed that flow over hemispherical cavities is bistable, with the vortex axis considerably skewed to the flow direction.

There is likewise only a small amount of experimental work directly concerned with heat transfer in the resonator regions, although Pratt & Whitney has observed more severe erosion in ablative chambers in areas aft of large apertures than aft of small ones (Ref 18) and has designed regeneratively cooled units for a variety of propellants, chamber pressures and coolant channel configuration (Ref 19) without apparently paying much heed to the local heat transfer considerations around the resonators. Aerojet-General has measured the temperature of the gas in the resonator cavities and found temperature levels equal to 30 to 60% of the combustion temperature, depending on the number of orifices per cavity (Ref 20), and increasing with the area of

IV, C, Heat Transfer (cont.)

the resonator apertures (Ref 21). Nonetheless, until the ALFP program, there has not been a concerted effort to determine the effect of the resonator aperture on the gas-side heat transfer or the heat transfer within the orifice or resonator cavity.

b. Gas-Side Heat Transfer Coefficients

The analytical methods of Spalding and Patanker (Ref 22) and Hangen (Ref 13) were used in an attempt to describe heat transfer coefficient downstream of an orifice. The resulting solution was not verified experimentally during the ALFP program and hence is not discussed further.

In the place of the above mentioned extensive heat transfer, analyses, which were predicated on the assumption that heat transfer coefficients would be two and three times the Bartz value calculated for an unlined chamber, a much simpler analytical technique is proposed. The substitute analytical technique consists of simply using the nominal unlined heat transfer coefficient based on the usual Bartz coefficient relation evaluated at the core (combustion products) recovery temperature.

Such a result seems to be unconservative when first proposed; however, considerable experimental evidence exists that does not refute it. Experimental evidence that appears to refute it has been found upon further examination to be due to other causes, such as mean flow through the liner.

c. Experimental Acoustic Liner Thermal Data Evaluation

Uncooled cylindrical copper liner insert sections as shown in Figure 14 were used during the Acoustic Liner Feasibility Program

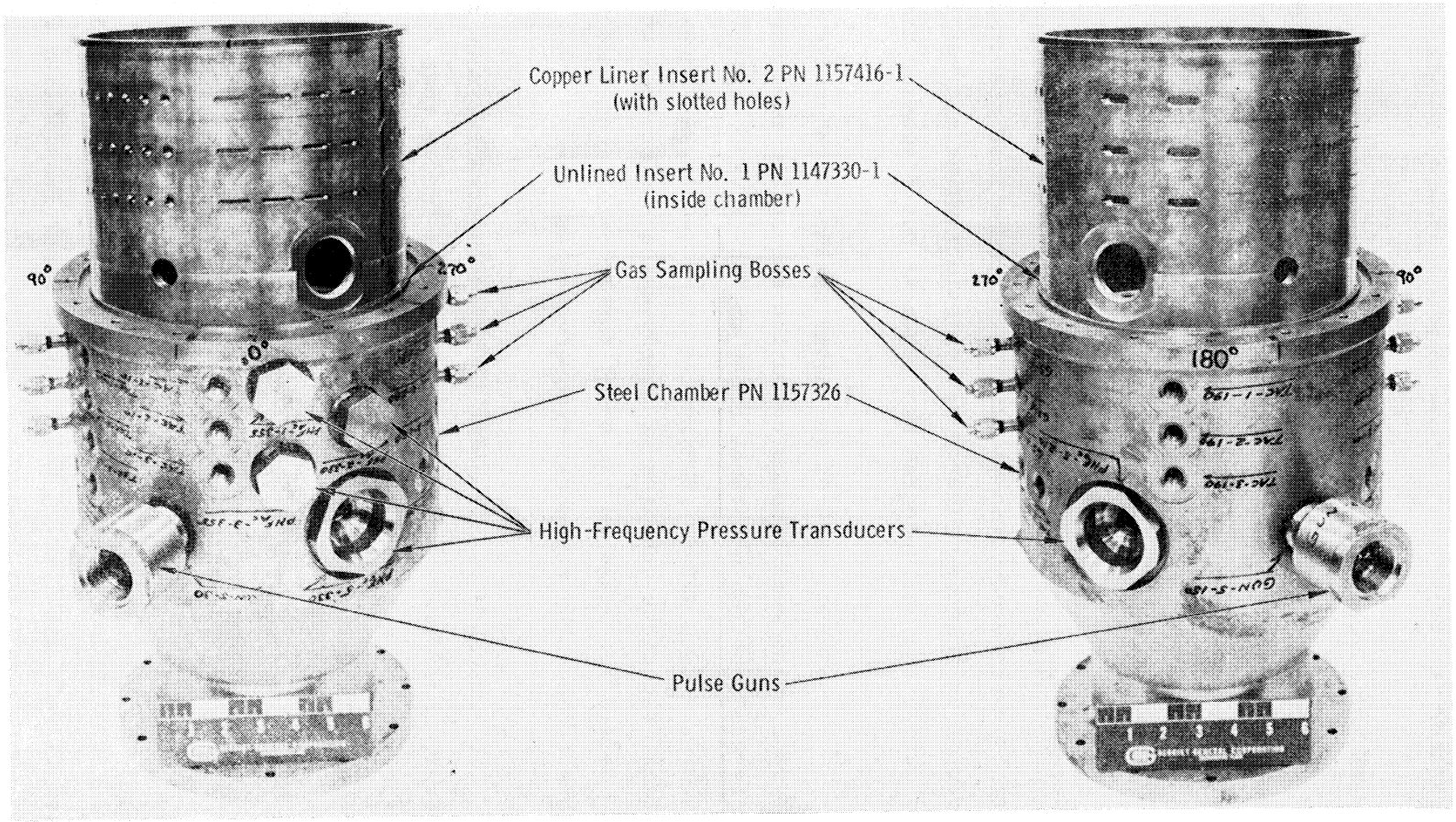

Figure 14. Uncooled Steel Thrust Chamber with Copper Acoustic Liner Insert

IV, C, Heat Transfer (cont.)

(ALFP), which were heavily instrumented with gas-side thermocouples, to provide a basis for studying the effect of acoustic liner orifices on gas-side heat transfer. Two chamber cylindrical insert sections were utilized: the first of these was "unlined", that is, had no orifices or resonators; the other was acoustically "lined", or had orifices and gas cavity volumes. Thermocouples on the "lined" chamber were placed downstream of orifices of several configurations - round holes of varying diameter, and slots of different widths as shown in Figure 15. Similar locations were instrumented on the "unlined" chamber. There were some thirty thermocouples on each chamber, but not all of these were monitored in every test or in all of the tests because of insufficient recording channels. A total of four unlined chamber tests and ten lined chamber tests were analyzed.

The effect of acoustic liner orifices on the gas-side heat transfer coefficient does not verify the analytical models proposed in the Phase I portion of the program. The film coolant and/or barrier cooling mixture ratio and temperature which vary with axial distance, are apparently perturbed by the orifices; the effect thereof cannot be isolated from the effect on the heat transfer coefficient. Nonetheless, the test data show heat fluxes with and without the liner to be somewhat less than would be predicted using the conventional Bartz coefficient and the core recovery temperature. At the present the Bartz coefficient is the recommended design standard.

Each valid thermocouple response was analyzed by means of an iterative computer program to determine the combination of heat transfer coefficient, hg, and recovery temperature, T_r, which yielded the indicated thermal response. The indicated temperature is typically matched within a few percent throughout the whole response, using a criterion wherein the variation in hg and T_r with time is minimized. About 120 thermocouple responses were so analyzed, although not all of these could be correlated.

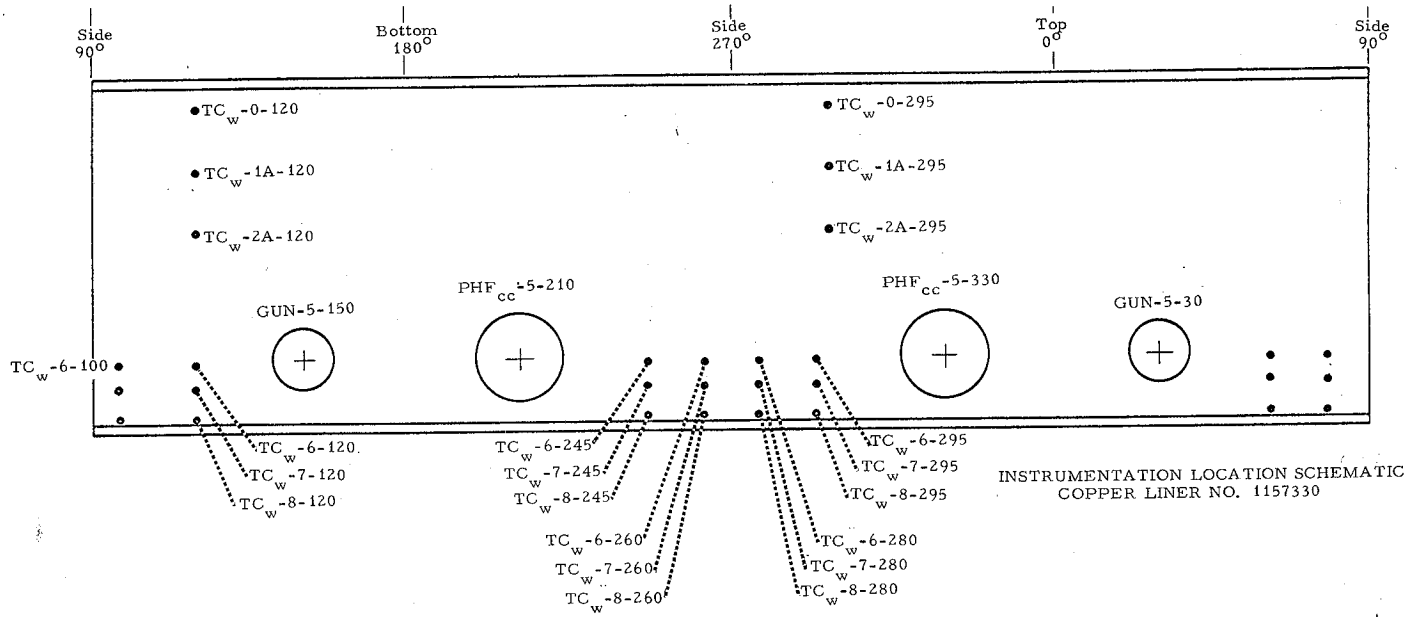

INSTRUMENTATION LOCATION SCHEMATIC
COPPER LINER NO. 1157330

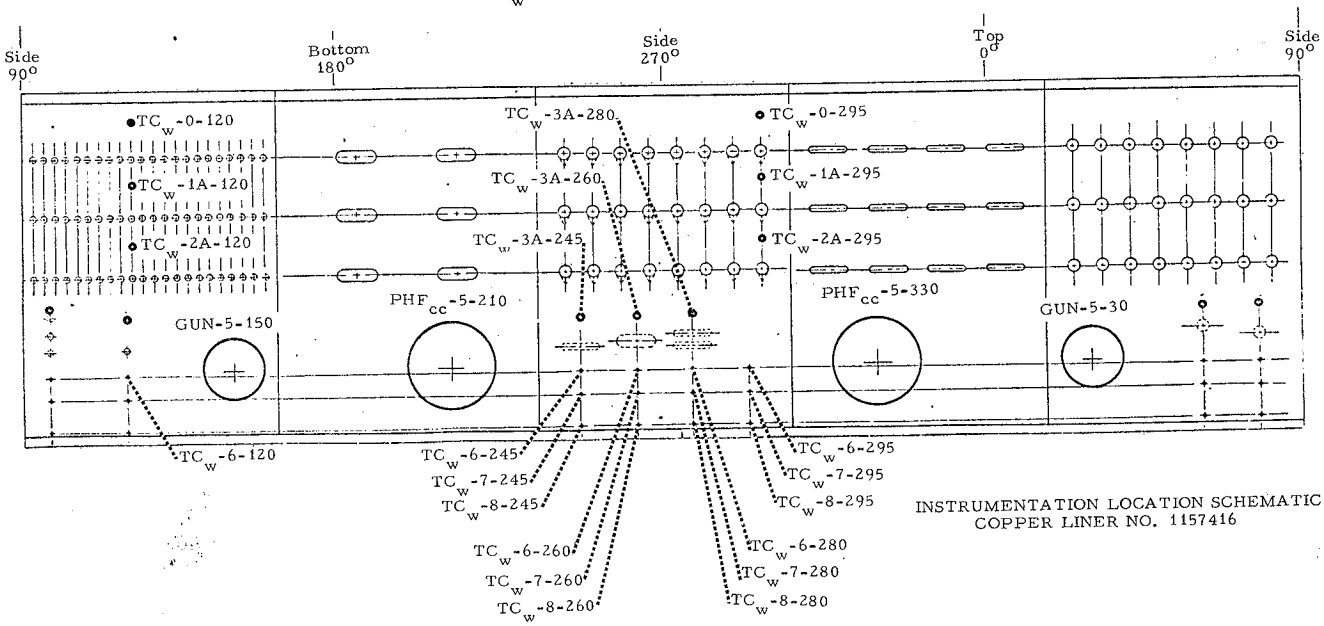

INSTRUMENTATION LOCATION SCHEMATIC
COPPER LINER NO. 1157416

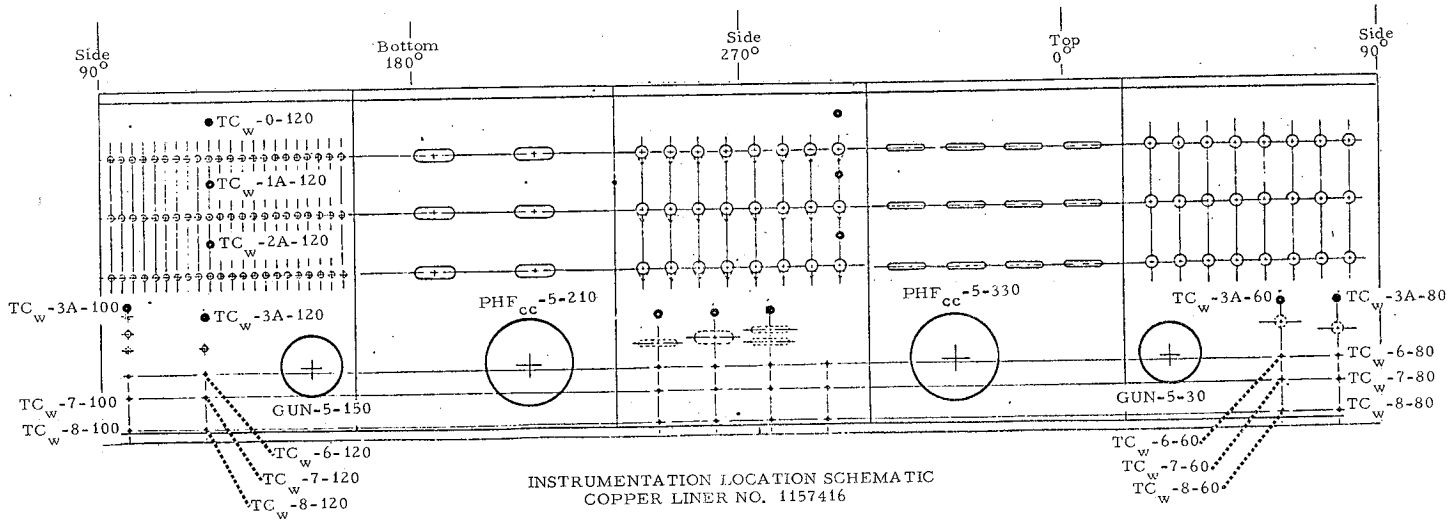

INSTRUMENTATION LOCATION SCHEMATIC
COPPER LINER NO. 1157416

*NOTE: View is from inside surface looking aft.

Figure 15. Thermocouple Locations for Uncooled Copper Liner

IV, C, Heat Transfer (cont.)

Some of the data combined very high heat transfer coefficients with recovery temperatures less than the monopropellant combustion temperature, which indicates that the fuel film coolant and/or barrier fuel has vaporized but not combusted. The low temperature Hg and Tr combinations are plotted, in terms of hg versus Tr, in Figure 16a. Data from both the acoustically lined chamber and the unlined chamber are shown. For the most part, a smooth trend is noted for the unlined chamber data, while the data from the lined chamber are somewhat scattered over a range of higher temperatures. The lowest temperatures are about 400°F, or 80°F more than the boiling point of the coolant. Apparently, these data signify the presence of a fuel vapor environment, with temperatures higher than the boiling point but lower than the monopropellant combustion temperature of the fuel film coolant.

The high temperature hg and Tr combinations are similarly plotted on Figure 16b for those data with Tr above the monopropellant point. Here again the data fall on a smooth trend, going from high coefficients and low temperatures to low coefficients and high temperatures. Data from both the acoustically lined chamber and the unlined chamber are pretty well interspersed throughout the range of data points, in contrast to the pattern of Figure 16a.

The high temperature data are replotted in Figure 17a in terms of the heat transfer coefficient vs mixture ratio, MR, where the mixture ratio corresponds to the combustion temperature which is taken equal to the inferred recovery temperature, a good approximation in the cylindrical chamber section. Also shown on the figure is a theoretical line for hg as a function of MR, based on the usual relationship:

$$hg = 0.026 \left(\frac{4}{\pi}\right)^{0.8} \frac{\dot{w}^{0.8}}{D^{1.8}} \left(\frac{T}{T_f}\right)^{0.8} \left(\frac{MW_f}{MW_\infty}\right)^{0.8} \frac{\mu_f^{0.2} C_{Pf}}{Pr_f^{0.6}}$$

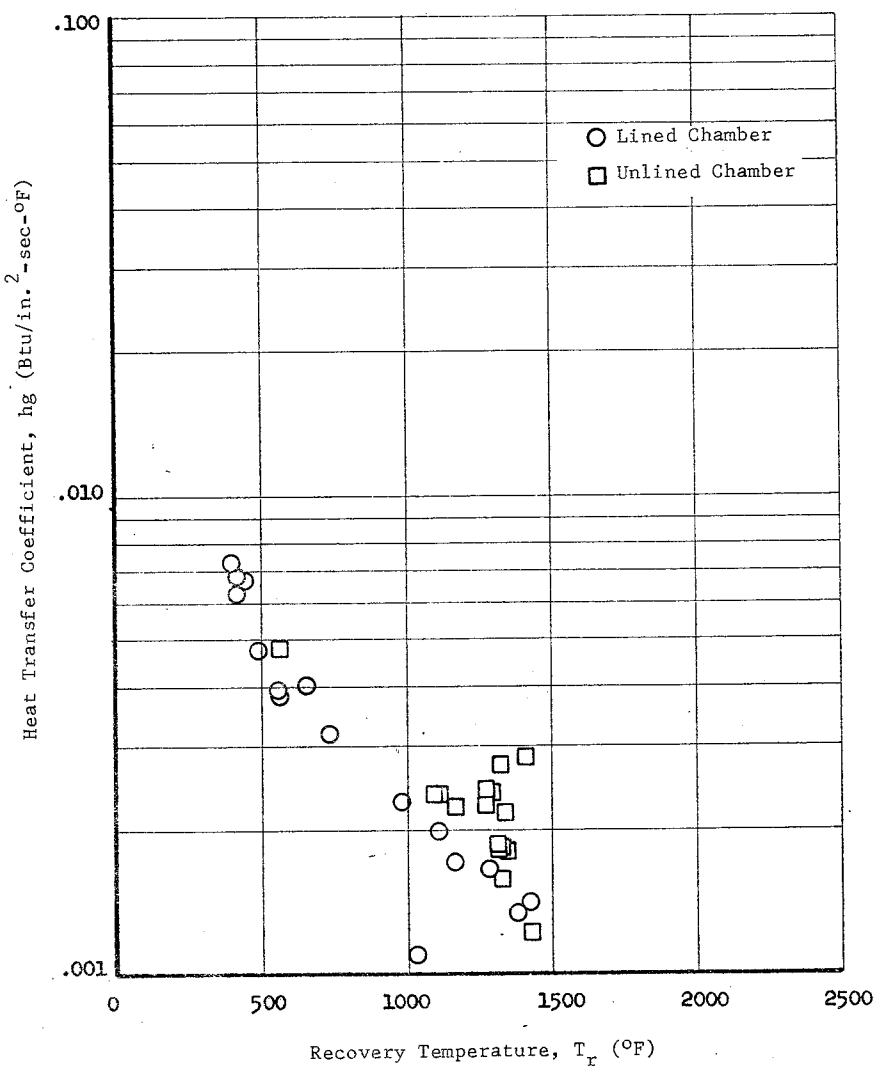

HEAT TRANSFER COEFFICIENT VS RECOVERY TEMPERATURE FOR RECOVERY TEMPERATURES LESS THAN MONOPROPELLANT COMBUSTION TEMPERATURE

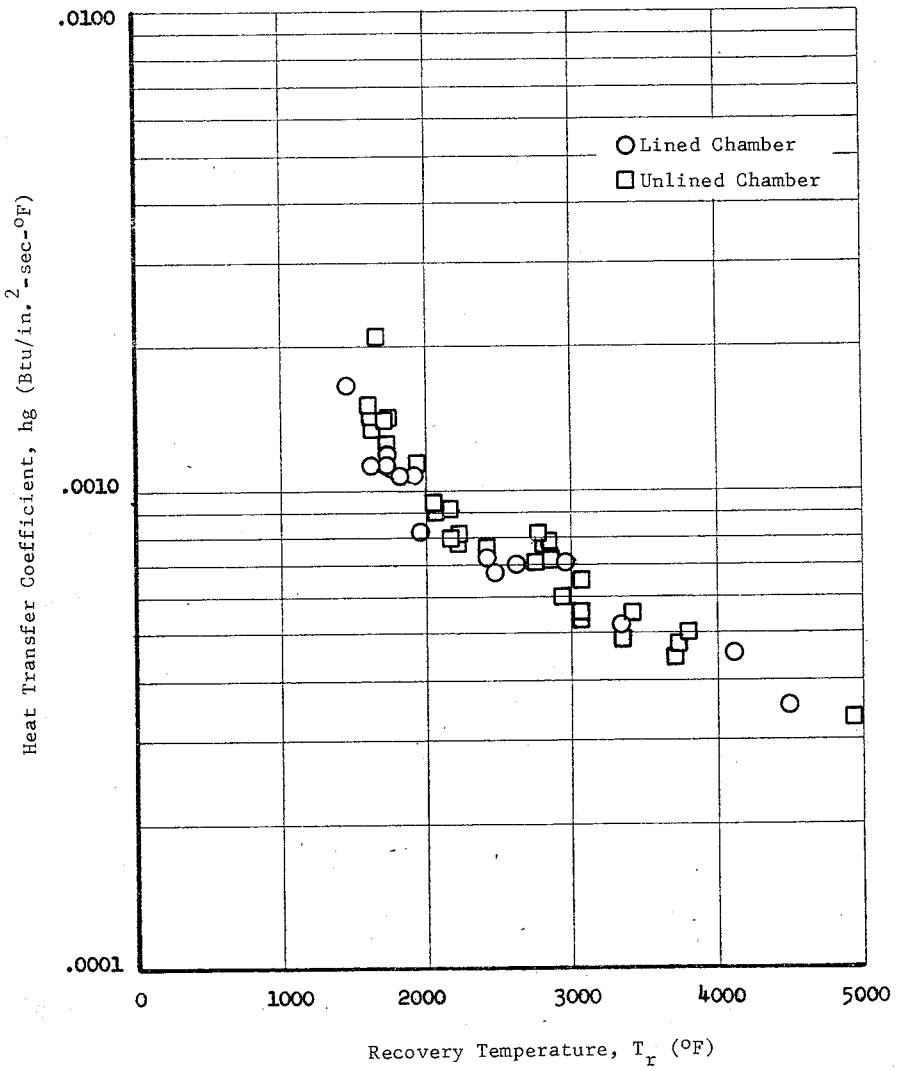

HEAT TRANSFER COEFFICIENT VS RECOVERY TEMPERATURE FOR RECOVERY TEMPERATURES GREATER THAN THE MONOPROPELLANT COMBUSTION TEMPERATURE

Figure 16. Heat Transfer Coefficient Data Groupings vs Recovery Temperatures

IV, C, Heat Transfer (cont.)

where the film temperature, T_f, is the mean of the combustion temperature at a given MR and an assumed 400°F wall temperature. The film properties, MW_f, μ_f, Cp_f, and Pr_f--molecular weight, viscosity, specific heat, and Prandtl number, respectively--are evaluated at the film temperature for that MR. The specific heat is determined on an enthalpy basis to account for chemical reactions. T_∞ is the core combustion temperature, $\dot{w}$ the weight flow, and D the chamber diameter. The theoretical line shows the correct trend and is within 25% of all but a few data points; it is however low at low MR's and high at high MR's.

Since one of the original objects of the ALFP program was to study the effect of orifices on gas-side heat transfer, it was pertinent to examine more closely some of the hg and Tr combinations from various axial positions along the same circumferential location. No clear trend emerged from such an examination. Points downstream of acoustic liner orifices were not typified by high coefficients, as earlier (Phase I) analytical studies had predicted on the basis of boundary layer tripping, nor were the acoustically lined chamber data indicative of a more severe heat transfer environment in general, as was expected.

Drawing conclusions about the gas side heat transfer coefficient, hg, from experimental data is complicated by the presence of variations in the recovery temperature T_r. First, the method of determining the hg, T_r combinations must be evaluated. With low heat transfer coefficient boundary conditions that were typical of the high temperature (T_r) data, long response times are necessary to correctly infer the (hg) coefficient and driving temperature. Ideally, the gas-side wall thermocouple response should "knee over", or show a sharp reduction in rate of change of temperature with time. This knee over was not possible during a five second test in the high temperature data, and hence the inferred boundary conditions were uncertain.

IV, C, Heat Transfer (cont.)

Thus, widely different hg, Tr combinations can yield the same wall temperature response. A high (hg) coefficient combined with a low (T_r) temperature produces almost the same response as a low (hg) coefficient combined with a high (T_r) temperature. Hence, it may be that the well-defined trend of hg vs T_r shown in Figure 16b is nothing more than the unfortunate result of insufficient response times. This is quite apart from the uncertainties arising from the accuracy of the thermocouple itself, the exactness of its position on the gas-side surface, and the assumption of constant gas-side boundary conditions necessary for data reduction.

For design purposes the exact formulation of the film coefficient downstream of a resonator orifice may not be necessary knowledge. More pertinent in the design of regeneratively cooled liners, is the anticipated gas-side heat flux. Figure 18 shows the predicted heat flux for all the hg and T_r combinations, including both the high and low temperature data, for a 400°F wall. Of some 45 high temperature data points, 90% fall within 1.65 $\pm$ 15% Btu/in.^{2}-sec; all but one data point fall within 20%, and that one is some 60% high. The average value of the high temperature points is 1.58 Btu/in.^{2}-sec, or 1.55 Btu/in.^{2}-sec if the single high value is discarded. The low temperature data are more scattered, yielding in some instances fluxes of 2.0 Btu/in.^{2}-sec. The predicted flux based on the core temperature and nominal Bartz coefficient is 2.03 Btu/in.^{2}-sec. All but the one high data point fall below this value. Hence, those conditions represent reasonable design values.

d. Orifice Heat Transfer

The flow in the orifice is probably composed of a series of a series of counterrotating vortices, the number of such vortices depending on the height-to-diameter ratio of the cavity. The axes of the vortices may

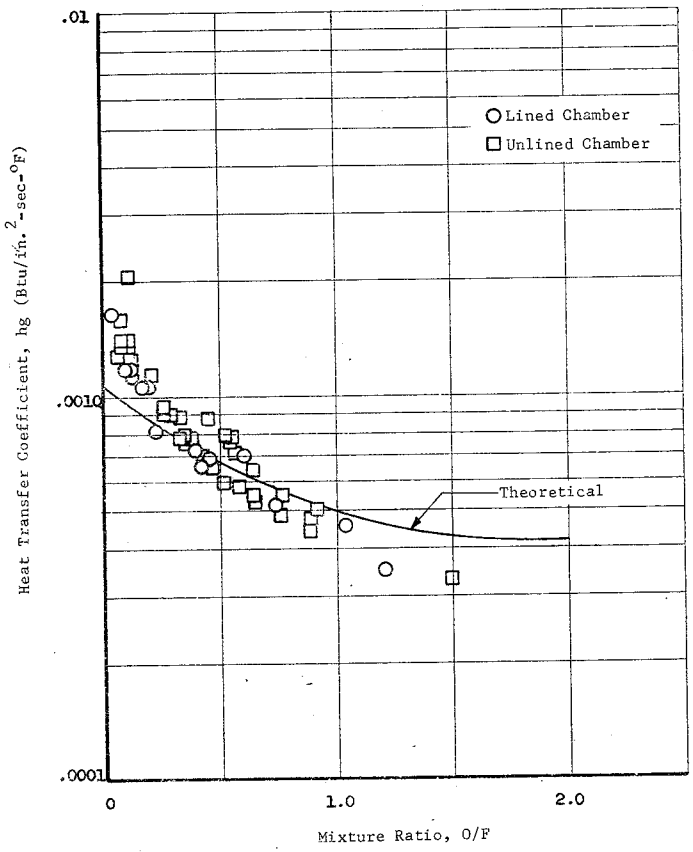

Figure 17. Heat Transfer Coefficient vs Mixture Ratio

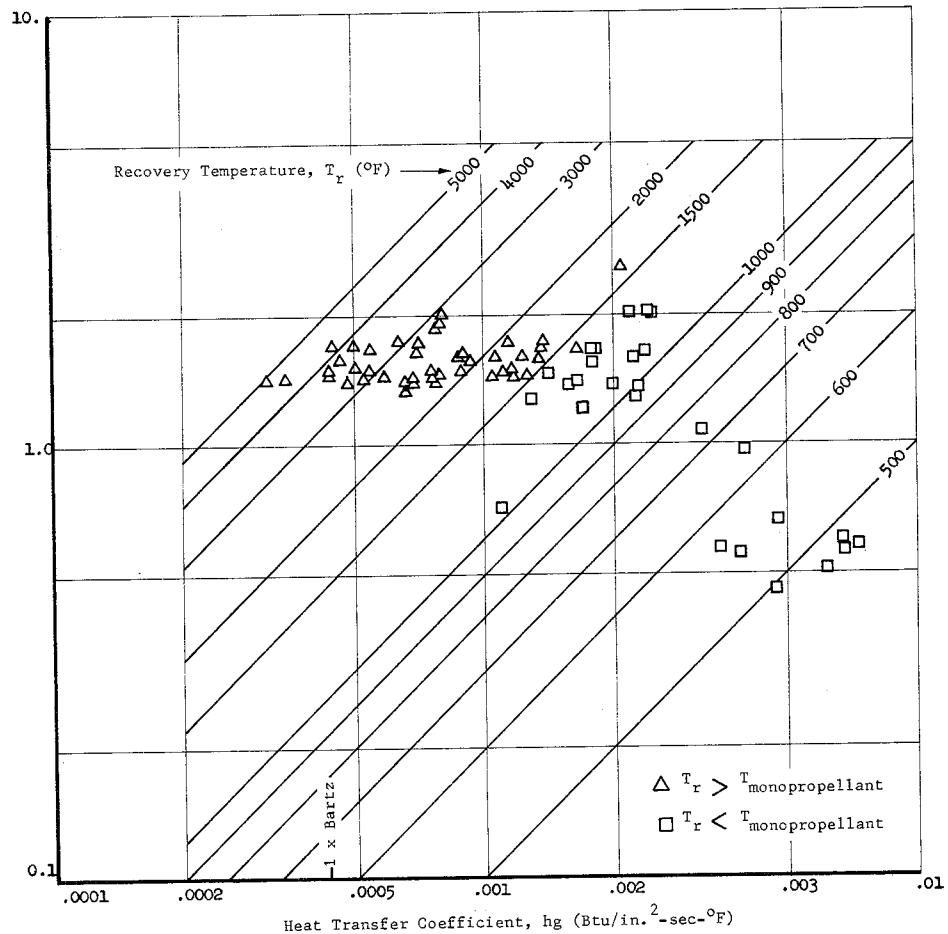

Figure 18. Heat Transfer Coefficient vs Heat Flux

IV, C, Heat Transfer (cont.)

be skewed to the mainstream flow, as noted in Ref 17. In any event, high velocities are not unexpected in the orifice and, as a consequence, the convective heat transfer coefficient may be quite high.

Haugen gives an expression for the Stanton number:

$$N_{St} = \frac{h}{\rho\, u_\infty\, c_p} = 0.0365\ (\delta/b)^{-0.1367} \pm 15\%$$

for boundary layer thickness (δ) -to-slot width (b) ratios of 0.1 to 0.8, somewhat less than the value of present interest. The corresponding heat transfer coefficient 0.00205 Btu/in.^{2}-sec-°F, is about five times the chamber value and twice the throat coefficient.

On the basis of test firings to date, such high values seem improbable. At the least, erosion of cavity walls in ablative liners is usually not as severe as erosion on the gas-side surface, considering the course that erosion is related to both chemical and thermal effects. However for completeness the trade-off studies consider higher coefficient because it is not inconceivable that such would be the case with a different injector design.

e. Cavity Heat Transfer

The flow in the resonator cavity is likewise probably cellular in nature, barring any net flow in the azimuthal or axial directions. Axial flow is generally to be avoided because significant heat transfer may be developed in the high velocity regions brought about by the large axial pressure gradient due to combustion. Azimuthal flow would not seem to pose a comparable problem, however, since no large pressure gradients should exist. Individual rows of resonator cavities are recommended to prevent mean follow

IV, C, Heat Transfer (cont.)

through the cavity. Experimental evidence shows no significant cavity heat flux occurs in individual orifice rows, but that two or more rows of apertures opening into a single cavity have very high heat fluxes, that are in proportion to the axial pressure drop across the orifices.

2. Heat Transfer Problem Areas

Under this heading are included factors that have historically proven to be problems in thrust chamber design, as well as potential problems arising from the presence of the acoustic resonator which were not evaluated in the ALFP program.

a. Heat Soakback from Ablative Liner

Injector heat soakback refers to the postfire transfer of heat from the ablative liner to the injector and valves by both radiation to the injector face and conduction via the injector/chamber flange. High heat soakback may lead to excessive valve temperatures and concomitant deterioration of the seal material and to the danger of propellant detonation on restart. Duty cycle considerations are all-important, with short firings and long coast periods; for instance, soakback is generally not a problem. The concern with an acoustically lined ablative chamber is that because of the stagnant region formed by the resonators the chamber near the injector is much hotter than would be the case for an unlined chamber, thus aggravating the heat soakback. Typically, analysis of the soakback problem involves constructing a thermal model of the entire engine system, including the adjacent spacecraft hardware, with proper accounting for the environmental conditions introduced by the vehicle mission.

IV, C, Heat Transfer (cont.)

b. Local Orifice Heat Transfer

Chamber gas flow over and leakage through the resonator apertures are expected to induce a higher gas-side heat transfer coefficient than the nominal Bartz value, in the region immediately aft of the aperture with some injector designs, by virtue of boundary layer tripping and establishment of a new boundary layer. The coefficient may be a factor of 2 to 3 times the nominal figure. Thus, there is a local area of high heat flux surrounding each aperture, this high local flux which depends not only on the exterior flux but also the geometrical wall configuration ultimately determines the flux into the coolant or ablative wall. With ablative cooling, the concern is excessive surface erosion and with the regenerative or transpiration cooled liners local boiling and monopropellant decomposition can result in failure.

c. Regenerative Manifolding Design

Local high heat fluxes near the apertures result in regenerative systems which involve a multipass section in order to yield coolant velocities necessary to meet high burnout flux values. Providing manifolding for such a multipass system may prove difficult, at least within the constraints of reasonable pressure drop limits ($<10\%$ P_c).

d. Analytical Problem

One of the goals of the ALFP program was to find workable correlations for the heat transfer on the gas side aft of a resonator orifice, as well as in the orifice and cavity itself. These areas have not received much theoretical consideration, in spite of the higher heat transfer that may be expected. No theoretical correlations have yet been put forward,

IV, C, Heat Transfer (cont.)

nor has much experimental work been done to deduce empirical relationships. There has been, however, a great deal of analytical work on related flow situations, notably free-jet boundaries, flow across slots, flow across forward and backward facing steps, and so on. Most of these deal strictly with two-dimensional flow and thus are not altogether applicable to a cylindrical orifice, wherein the flow is probably three-dimensional. Nonetheless, they offered a starting point for the ALFP study. The results of the study showed that with the injector used local high heat fluxes were not a problem.

e. Inconsistent Experimental Results

Under inconsistent results are included the experimental data scatter arising from any and all sources -- variations in operating conditions from test to test, variations between supposedly similar chambers and locations within a particular chamber, etc. The thermal instrumentation is designed to be redundant, such that the configurations are duplicated either within the chamber or from one chamber to another so as to avoid drawing wrong conclusions from spurious data. The ALFP showed variations in local flux in the order of 2 times the nominal value apparently due to injector characteristics rather than the presence of the acoustic liner.

3. Heat Transfer Trade-Offs

Parametric studies have been made of different designs for acoustic liners in respect to their heat transfer characteristics. Each of the designs is based on the LMA engine, employing N_2O_4/A-50 propellants at 1.6 mixture ratio and 120 psia chamber pressure. Regeneratively cooled, film-cooled, transpiration-cooled, and ablative chamber liners were studied, based on a common cylindrical section 7.8 in. in diameter.

IV, C, Heat Transfer (cont.)

a. Regeneratively Cooled Chambers (Without Film Cooling)

The regeneratively cooled concepts are illustrated in Figure 19.

The high film coolant flow rate (say 12% of the fuel) has been shown to cause such a large reduction in gas-side heat transfer that regenerative cooling may be unnecessary for high temperature materials such as nickel or Hastelloy-X. However this amount of film cooling is unrealistic from a performance point of view.

In regenerative cooling without the assistance of film cooling, the gas-side heat transfer is usually assumed to be severe because of boundary layer tripping by the resonator apertures or more importantly mean gas flow from the chamber through the apertures. The tubular design without film cooling shown in Figure 19a requires a many-pass regenerative system unless small diameter tubes are used and excessive pressure drop rules out designs capable of the higher heat fluxes which might be expected. The concentric cylinder design with axial flow shown in Figure 19d requires a very narrow flow passage and may be impractical to fabricate. The same concept employing azimuthal flow is somewhat better, but still limited. The drilled copper cylinder shown in Figure 19c is suitable only if gas-side heat transfer is not increased significantly by the resonator apertures, and then only with a high temperature, high conductivity material such as copper. The grooved cylinder with axial flow shown in Figure 19b is restricted to small, closely-spaced flow passages; with azimuthal flow the restrictions are not quite so severe. Generally speaking, without film cooling regenerative cooling is a possible, but not very satisfactory approach to the design of an acoustic liner for this system, and only if orifice-induced boundary layer tripping does not cause significant increases in gas-side heat transfer and mean

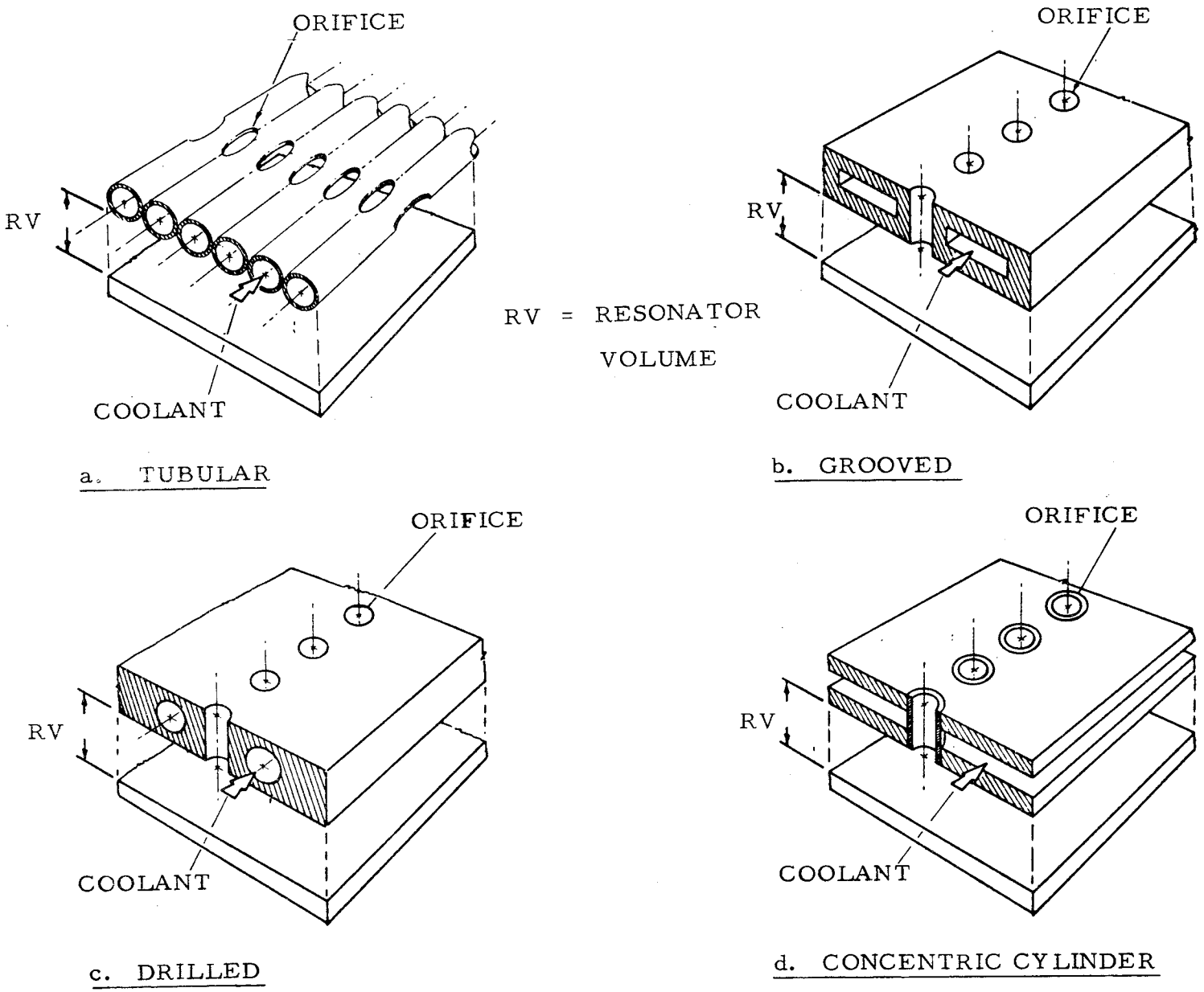

Figure 19. Regenerative Cooling Design Concepts

IV, C, Heat Transfer (cont.)

chamber gas flow through the apertures is minimized. Also, high temperatures in the solid-wall liner may delay restart after engine shutdown because of the danger of propellant detonation, thus limiting duty cycle capability.

The analysis treats the gas-side heat transfer coefficient as a parameter equal to one, two, and three times the Bartz coefficient ($h_{g_{Bartz}}$ = 0.000436 Btu/in.^{2} sec °F) in order to allow for the mean gas flow or flow tripping effect, the magnitude of which is presently unknown. Recovery temperature, T_r, is 5080°F, with no film cooling. The film coolant temperature profile is discussed in a subsequent section.

The heat transfer parameter that dictates the geometry for all four designs is the coolant burnout heat flux. The burnout heat flux is equated to the maximum gas-side heat flux, taking into account the flux concentration due to area differences between the gas-side and the coolant-side. Typical heat fluxes in the cylindrical portion of the chamber on the gas-side are of the order of 2 Btu/in.^{2} sec for the nominal Bartz coefficient. A design burnout ratio, (the ratio of the estimated heat flux to burnout heat flux) R_{Bo}, of 0.75 is employed, and the burnout heat flux of the fuel is given by Ref 23.

$$(q/A)_{BO} = 1.0 + 0.0007\ V\Delta T,\ V\Delta T < 8000, \text{ and}$$
$$= 4.4 + 0.000275\ V\Delta T,\ V\Delta T > 8000$$

where $(q/A)_{BO}$ is in Btu/in.^{2} sec, V is the coolant velocity in ft/sec, and ΔT is the subcooling in °F. A subcooling (the coolant saturation temperature minus the coolant bulk temperature) of 200°F is used throughout, reflecting a coolant bulk temperature rise of 100°F, which would be expected in a 4 in. long section for the nominal Bartz coefficient. The higher coefficients arising from boundary layer tripping are taken to be significant only locally

IV, C, Heat Transfer (cont.)

and not a cause of higher coolant bulk temperatures. Coolant bulk temperature rise does not appear as a heat transfer limitation except for unduly long liners; the rise is typically less than 25°F per inch of axial length.

Gas-side wall temperature does pose a limit for some designs, notably the grooved cylinder. The maximum gas-side temperature lies midway between adjacent cooling channels and is approximated by a one-dimensional conduction analysis. The maximum allowable temperature for both stainless steel and copper is taken to be 1500°F, for nickel 2000°F, and for aluminum 600°F.

Pressure drop poses a limit only for the tubular design at high Bartz multipliers. A friction factor of 0.015 is considered and only friction pressure drop is treated; turnaround and entrance or exit losses, which may be significant, are not accounted for. Velocities typically range from 10 to 50 ft/sec, and a maximum pressure drop of 50 psia is allowed.

(1) Tubular Design (Figure 19a)

The gas-side heat flux, $(q/A)_o$, is found from

$$(q/A)_o = \frac{T_r - T_{WL}}{\frac{1}{h_g} + \frac{t}{k}}$$

where t/k is the wall resistance (thickness-to-conductivity ratio), and T_{WL} is the wall temperature on the coolant-side, which is taken to be $T_{sat} + 40$ by virtue of the nucleate boiling condition. The coolant-side heat flux, $(q/A)_i$, is found from the gas-side flux and the ratio of outer-to-inner surface areas

IV, C, Heat Transfer (cont.)

$$(q/A)_i = (q/A)_o \frac{A_o}{A_i} = (q/A)_o \frac{\pi d_t}{\pi(d_t - 2t)}$$

where d_t is the tube outer diameter and t is the tube wall thickness. From the burnout heat flux expression, and accounting for the design burnout heat flux ratio, the necessary coolant velocity can be found. The required coolant flow areas, A_f, determined (by continuity) from

$$A_f = \frac{\dot{W}}{\rho V}$$

wherw $\dot{W}$ is the fuel flow rate, 4.4 lbm/sec, and ρ the fuel density, 0.0317 lbm/in.^{3}. This flow area equals the product of the number of tubes, N_t and the flow area per tube, divided by the number of passes, N_p.

Approximately

$$N_t = \frac{\pi D_c}{d_t}$$

where D_c is the chamber diameter. Thus,

$$A_f = \frac{1}{N_p} \frac{\pi D_c}{d_t} \frac{\pi}{4} (d_t - 2t)^2$$

The relationship between d_t, t, and N_p can be determined; Figure 20 shows this for stainless steel tubes, for the three Bartz coefficient multipliers. The dashed lines indicate friction pressure drops greater than 50 psia; it can be seen that to accommodate more than twice the Bartz coefficient leads to excessive pressure drops.

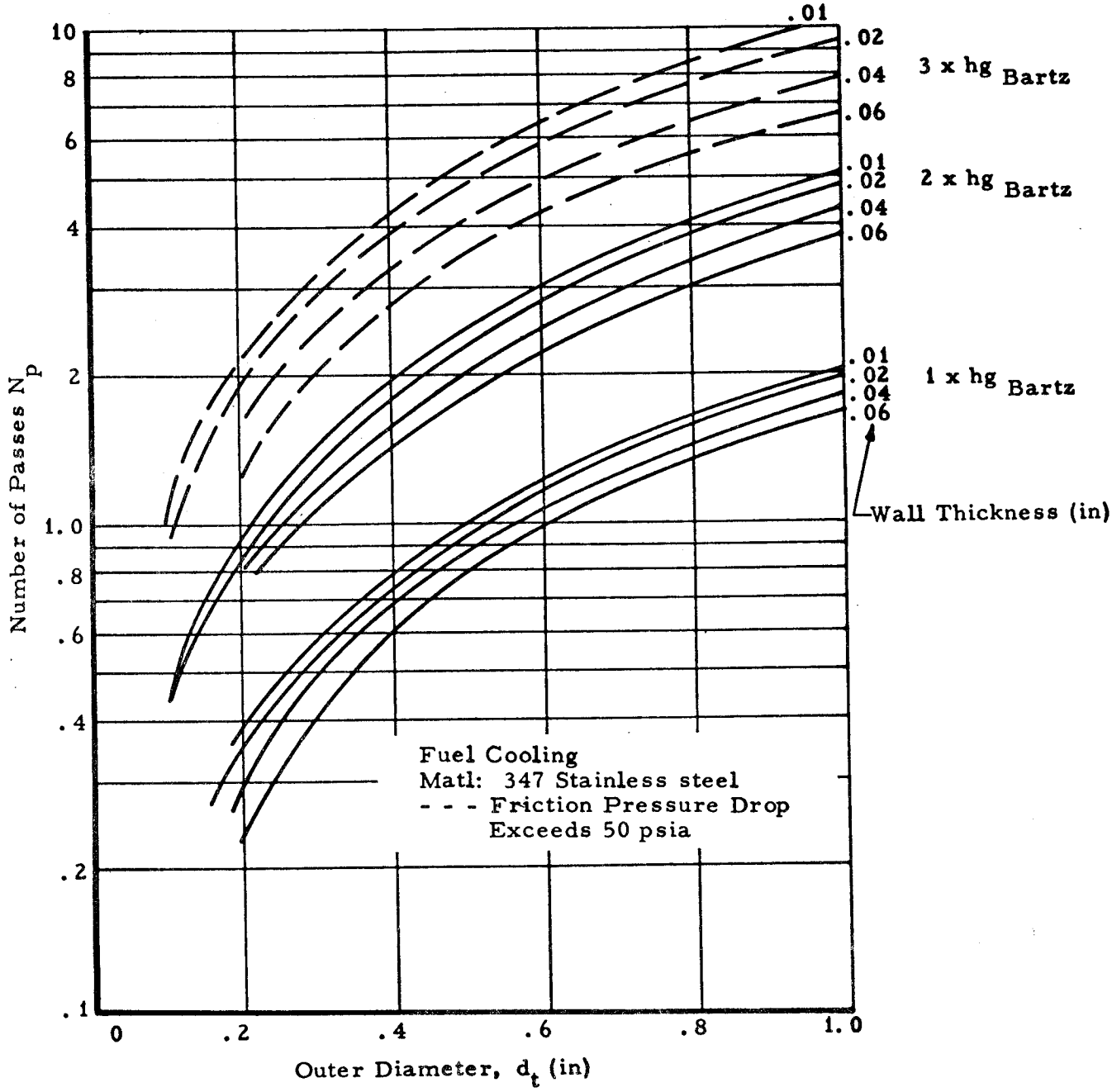

Figure 20. Required Geometry for Tubular Design

IV, C, Heat Transfer (cont.)

(2) Concentric Cylinder Design -- Axial Flow -- Figure 19d

The required coolant velocity and flow area are found as above. No area correction of the heat flux is required. The coolant flow area equals

$$A_f = \pi D_c d$$

d being the depth between concentric cylinders. Figure 21 presents the required coolant channel depth in terms of the wall resistance. Maximum wall thicknesses, to accommodate three times the Bartz coefficient, are 0.060 in. for stainless steel, 0.080 in. for aluminum, 0.25 in. for nickel, and about 1.0 in. for copper.

(3) Concentric Cylinder Design -- Azimuthal Flow

The calculational procedure for azimuthal flow is the same as for axial flow, except that the coolant flow area equals

$$A_f = d\ell$$

where ℓ is the axial length, taken to be 4.0 in. for this case. This assumes the coolant flow makes one complete revolution ("full circle"); for half a revolution ("half circle")

$$A_f = 2d\ell$$

and the depth must be halved to yield the necessary velocities. The required geometrical configurations are shown in Figure 22. Wall thicknesses are

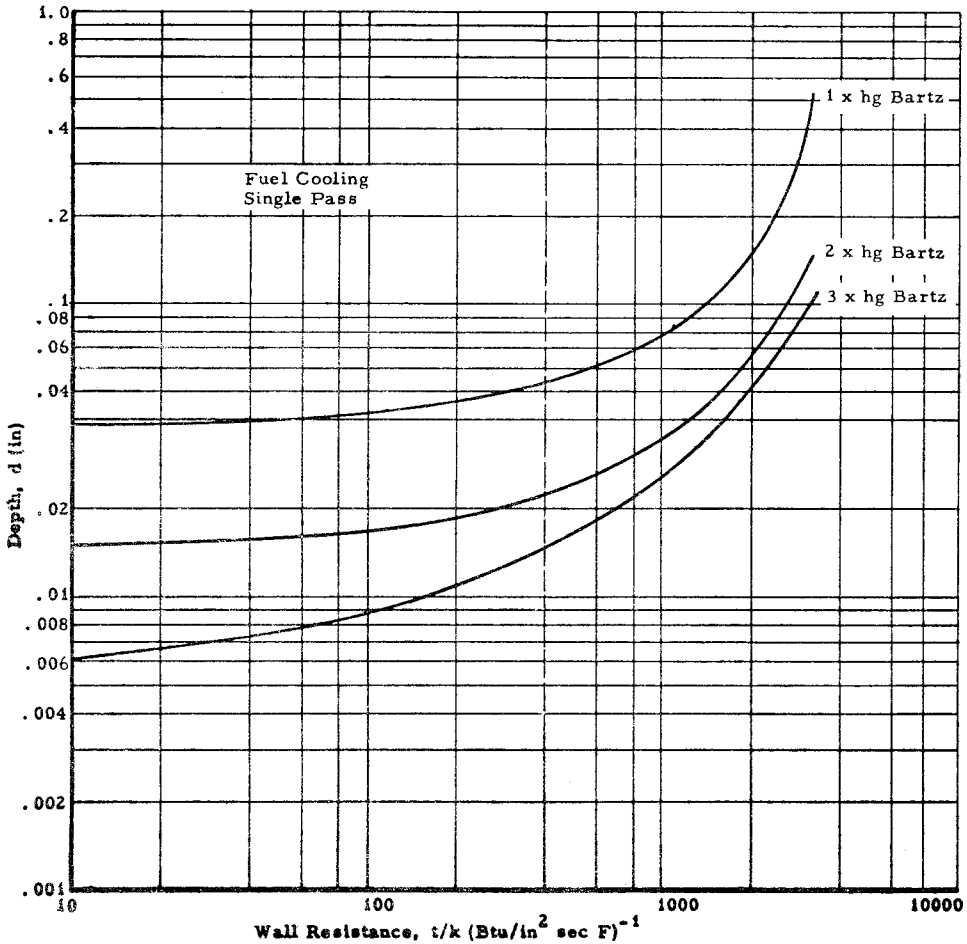

Figure 21. Required Geometry for Concentric Cylinder with Axial Flow

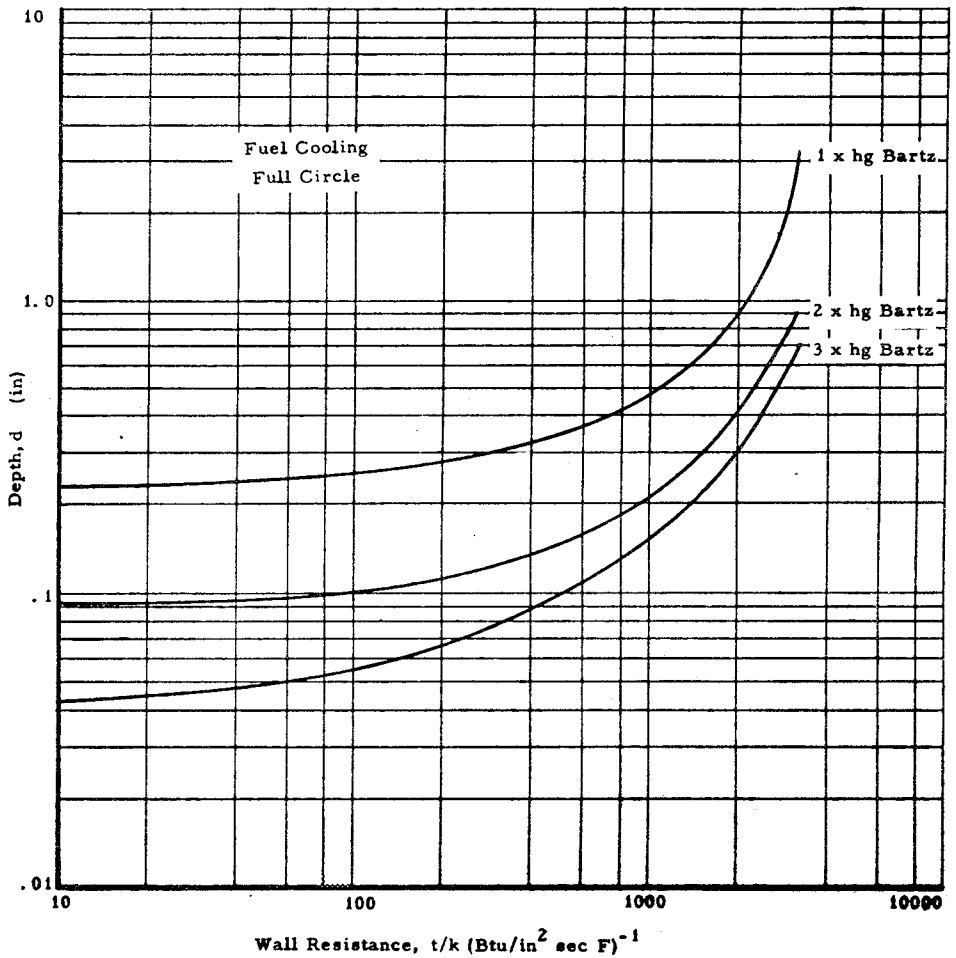

Figure 22. Required Geometry for Concentric Cylinder with Azimuthal Flow

IV, C, Heat Transfer (cont.)

limited to the values given above for the axial flow case. In general, at high Bartz multipliers, channel depths are inordinately small for the axial flow case and none-too-large for azimuthal flow.

(a) Pressure Drop Analysis

The concentric cylinder design requires a very narrow coolant passage for gas-side heat transfer coefficients much higher than the nominal Bartz value because of burnout heat flux considerations.

This requirement previously appeared so restrictive that the design seemed impractical or impossible because of fabrication difficulties. Recently, however, electroformed samples* have been obtained with small diameter channels between closely-spaced walls, and the concentric cylinder design thus appears more feasible than it did formerly. At two or more times the nominal Bartz coefficient the pressure drop is still found to be excessive because of the smaller flow area and higher coolant velocity necessary to accommodate the larger gas-side heat flux.

The coolant (fuel) flow through the concentric cylinders is azimuthal. Pressure drop is determined by drawing an analogy to flow through banks of tubes, as in crossflow heat exchangers. Staggered rows of tubes, and also a single row of in-line tubes, are considered.

*Fabricated by Dynatex Division of Republic Corp., Redwood City, Calif.

IV, C, Heat Transfer (cont.)

Pressure drop, ΔP, is given in psi by Ref 24 as

$$\Delta P = \frac{f' G_{max}^{2} N}{201.\rho} \left(\frac{\mu_s}{\mu_b} \right)^{0.14} ;$$

where G_{max} is the mass fluw at the minimum area between tubes in lbm/in.^{2} sec, ρ is the density in lbm/in.^{3}, N is the number of tubes, and μ_s and μ_b are the viscosities evaluated at the wall and bulk temperatures, respectively. The empirical friction factor, f', is evaluated for turbulent flow (Reynolds numbers above 1000, based on maximum mass flux and tube diameter) from

$$f' = 0.25 + \left[\frac{0.118}{\left(\frac{S_T}{D_o} - 1 \right)^{1.08}} \right] \cdot \left(\frac{G_{max} D_o}{b} \right)^{-0.16}$$

for staggered tube arrangements, and from

$$f' = 0.044 + \left[\frac{0.08\ S_L/D_o}{\left(\frac{S_T}{D_o} - 1 \right)^{0.43 + 1.13\ D_o/S_L}} \right] \cdot \left(\frac{G_{max} D_o}{\mu_b} \right)^{-0.15}$$

for in-line arrangements. Here D_o is the tube outer diameter, S_T is the transverse spacing between tubes and S_L is the lateral spacing. As a point of information, Ref 25 quotes the equations for f' erroneously.

Three gas-side heat transfer coefficients are considered: one, two, and three times the nominal Bartz value, the higher values representing the possible effect of boundary layer tripping by the

IV, C, Heat Transfer (cont.)

resonator apertures. To accommodate the larger heat fluxes, higher coolant velocities are required, or equivalently smaller flow areas, since the flow rate is fixed. According to Ref 26, the required flow areas are:

$$A_f = 0.932 \text{ in.}^2 \text{ at } 1 \times h_{g_{Bartz}}$$

$$= 0.368 \text{ in.}^2 \text{ at } 2 \times h_{g_{Bartz}}$$

$$= 0.172 \text{ in.}^2 \text{ at } 3 \times h_{g_{Bartz}}$$

The axial length of the channel is taken to be 2.0 in. for all cases involving the staggered tube bank; the channel depth is thus:

$$d = 0.466 \text{ in. at } 1 \times h_{g_{Bartz}}$$

$$= 0.184 \text{ in. at } 2 \times h_{g_{Bartz}}$$

$$= 0.086 \text{ in. at } 3 \times h_{g_{Bartz}}$$

The maximum mass flux, G_{max}, is based on the minimum flow area, e.g., the cross section through a transverse row of tubes. Only integral numbers of tubes are feasible in a transverse row and some flow area is obviously necessary between tubes.

The friction factor, f', is plotted in Figure 23 for flow through banks of staggered and in Figure 24 for in-line tubes. Figure 25 shows the predicted pressure drop in terms of the tube diameter and transverse spacing for flow through the staggered tube bank at 1, 2, and 3 times the Bartz coefficient respectively. As would be

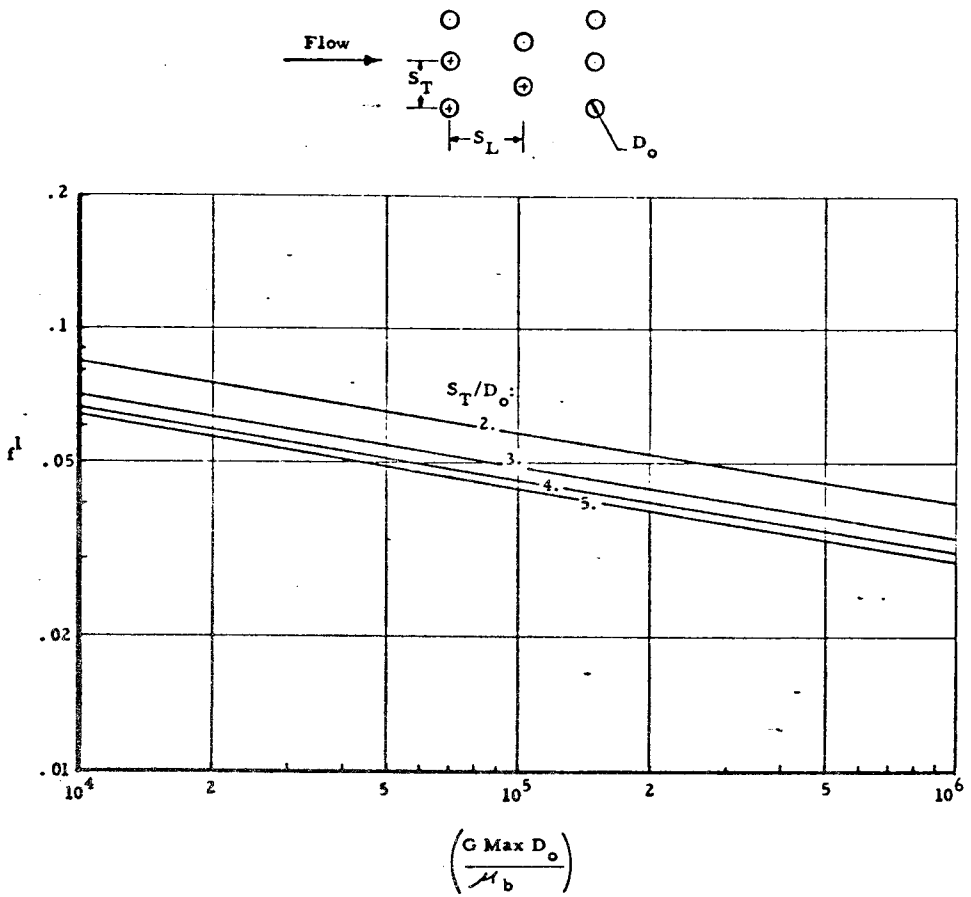

Figure 23. Friction Factor for Staggared Tube Bank

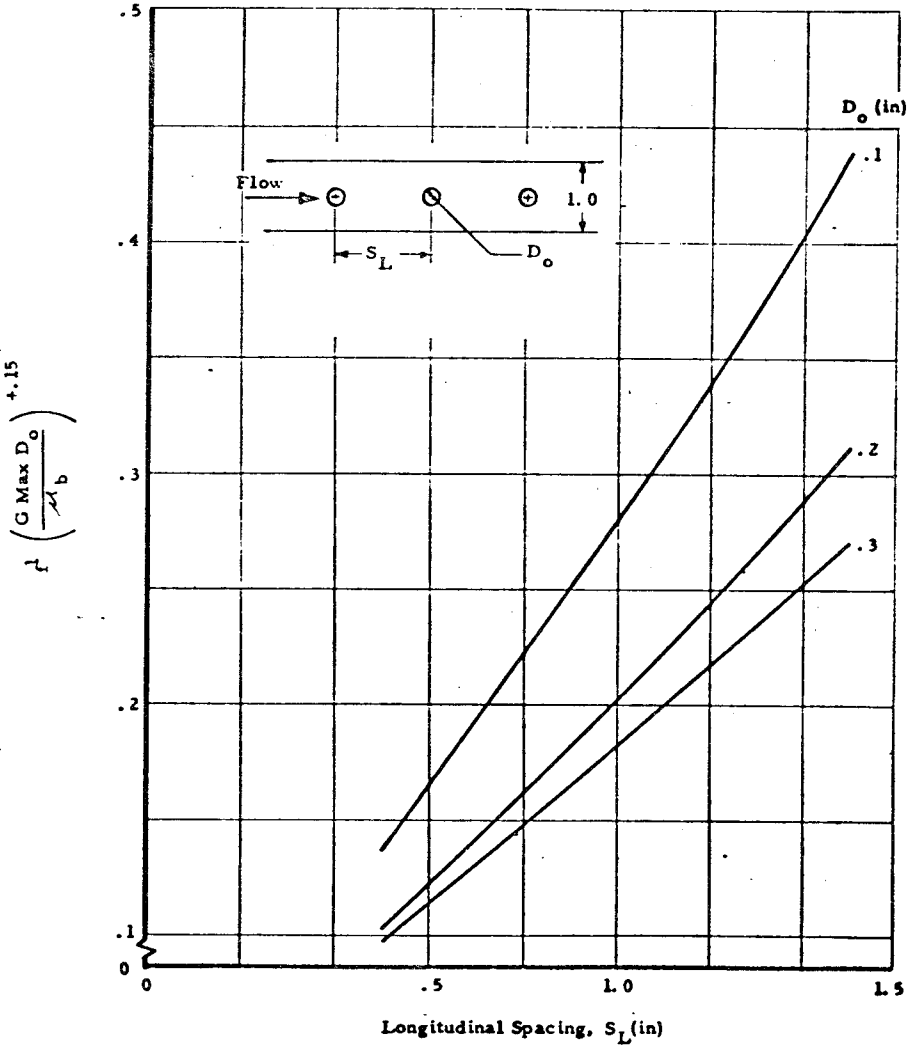

Figure 24. Friction Factor for Single Row of In-Line Tubes

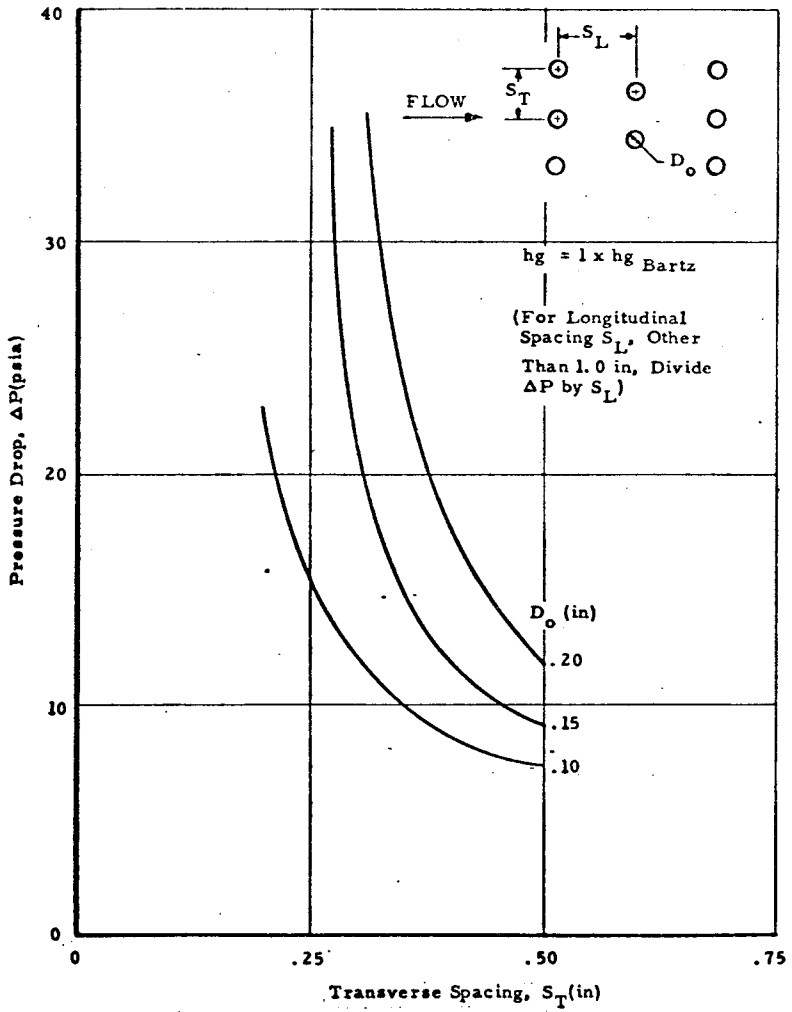

(a)

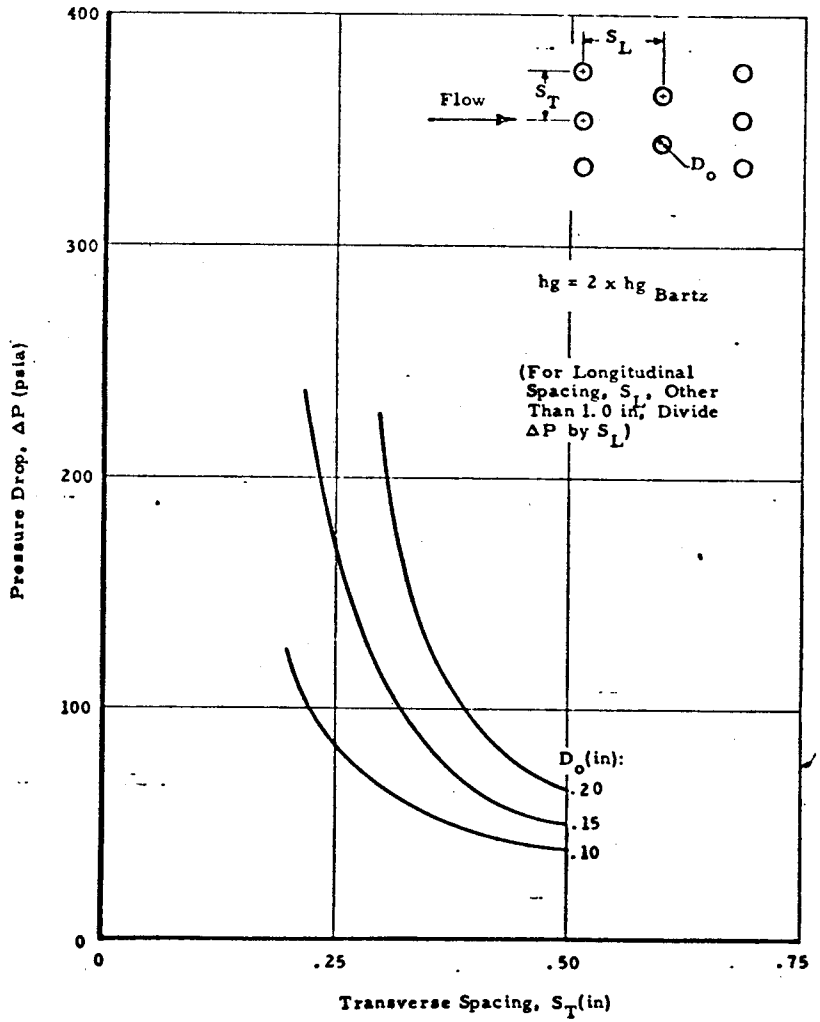

(b)

Figure 25. Predicted Pressure Drop for Cross Flow Through Staggard Channels

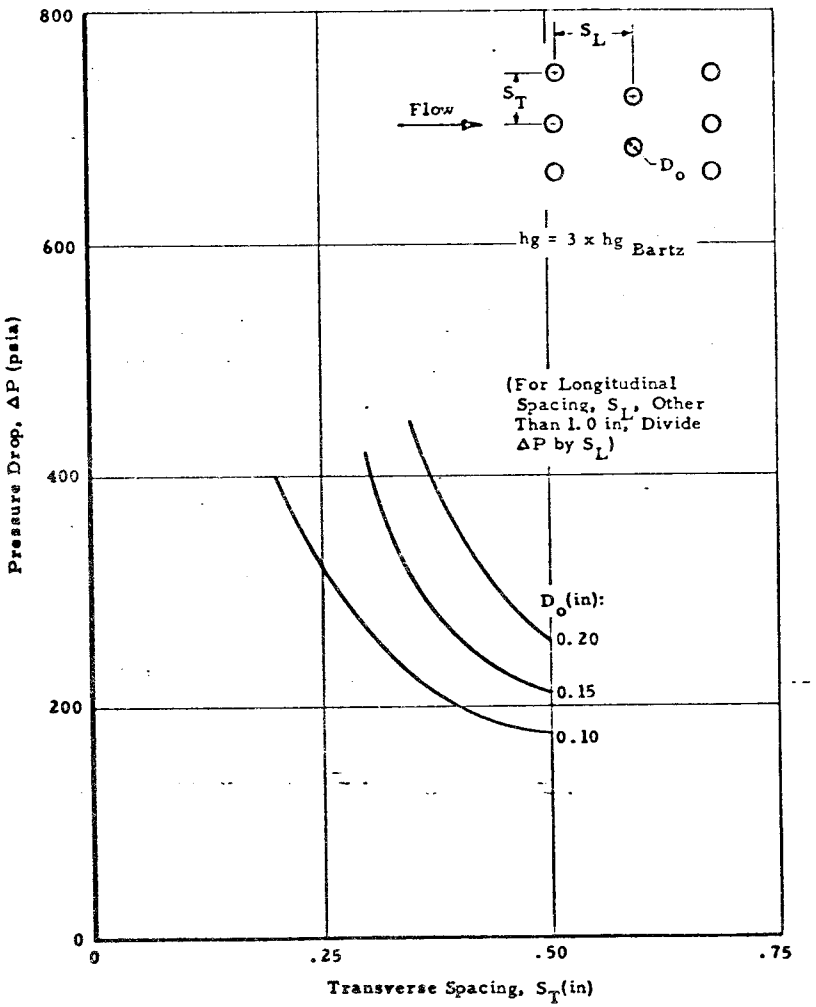

Figure 25(c). Predicted Pressure Drop for Cross Flow Through Staggard Channels

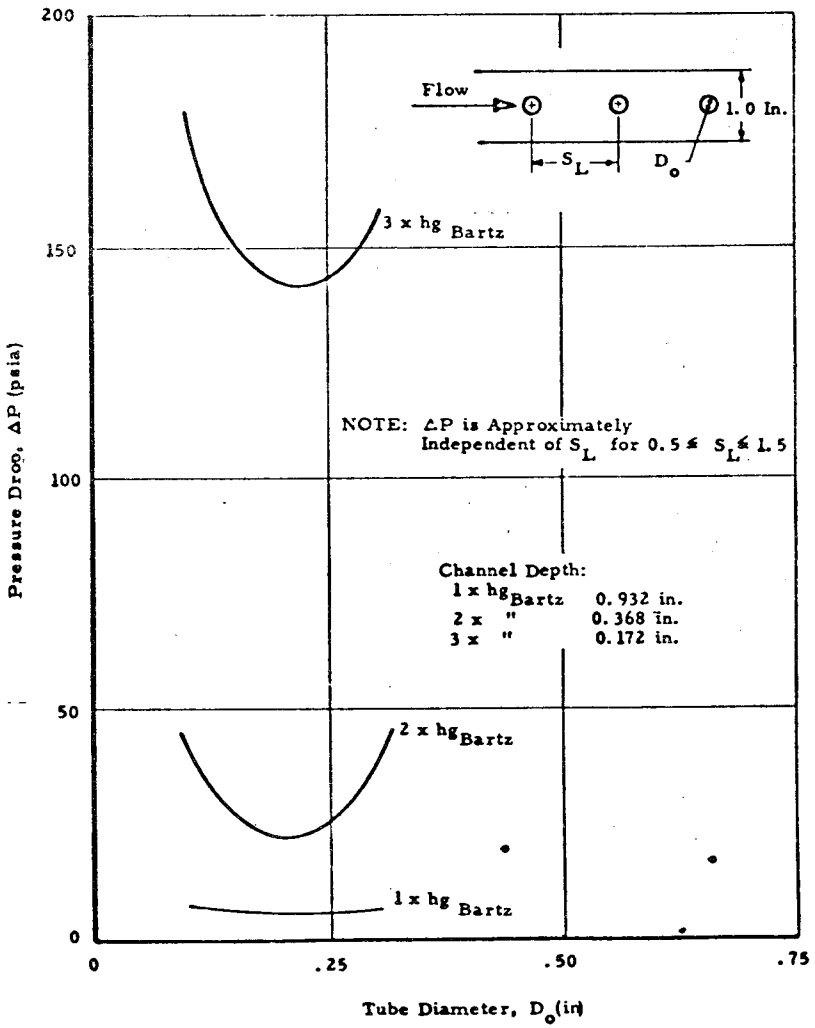

Figure 26. Predicted Pressure Drop for Flow Across Single Row of In-Line Tubes

IV, C, Heat Transfer (cont.)

expected, the pressure drop decreases as the tube diameter decreases and also as the lateral spacing increases. The figures are based on a longitudinal spacing of 1.0 in.; other values can be easily treated since pressure drop is inversely proportional to longitudinal spacing. Figure 26 shows the predicted pressure drop across a single longitudinal row of in-line tubes, for all three gas-side heat transfer coefficients. The axial length is taken to be 1.0 in. Here the longitudinal spacing is found to be unimportant, in that as the spacing increases the pressure drop per tube increases and the number of tubes decreases. The compensation thereof yields a 5% maximum variation in pressure drop as the longitudinal spacing varies from 0.5 to 1.5 in. The single row of tubes produces a considerably lower pressure drop than the staggered arrangement, as would be expected.

It should be noted that the expression for pressure drop across banks of tubes may lose validity as the channel depth becomes small because of the influence of wall friction. This possibility should be investigated further. Also, countersinking or chamfering the holes, which has been suggested as a way of shortening the acoustic length, may cause higher pressure drops than given here due to increased fluid velocity.

(b) Conclusions

The high pressure drops corresponding to three times the Bartz coefficient would seem to rule out that case completely. Even at two times the Bartz coefficient, small orifice diameters and large transverse and longitudinal spacings will be required to maintain moderate pressure drops. Thus sufficient open area for acoustic damping, within reasonable pressure drop limits, will be obtained only if the increase in gas-side heat transfer due to boundary layer tripping is not excessive.

IV, C, Heat Transfer (cont.)

(4) Drilled Cylinder -- Figure 19c

The procedure is similar to those for the preceding cases. The area correction on heat flux is taken to be ratio of the gas-side surface area to the total circumference of the coolant channel. The gas-side area, on a per-channel basis, equals the spacing, s, between channel center lines. Thus

$$(q/A)_i = (q/A)_o \frac{s}{\pi d_t}$$

The coolant flow area is

$$A_f = \frac{N_c}{N_p} \frac{\pi}{4} (d_t)^2$$

where N_p is the number of passes, and the number of channels, N_c is

$$N_c = \frac{\pi D_c}{s}$$

s being the channel spacing. Thus, d can be found in terms of s for a given flow area. Since the conductivity of copper is so high, the wall resistance is only a small part of the total resistance, $\frac{1}{h} + \frac{t}{k}$. The heat flux is, therefore, almost independent of wall thickness, and the required coolant velocity changes but little with wall thickness. Walls up to 0.4 in. between the gas-side and the coolant surface may be adequately cooled for the given spacing. The worst case (zero thickness) has been figured here, implying minimal flow area. Figure 27 presents the results. The double-valued nature of the curves arises from the form of the ultimate equation being solved

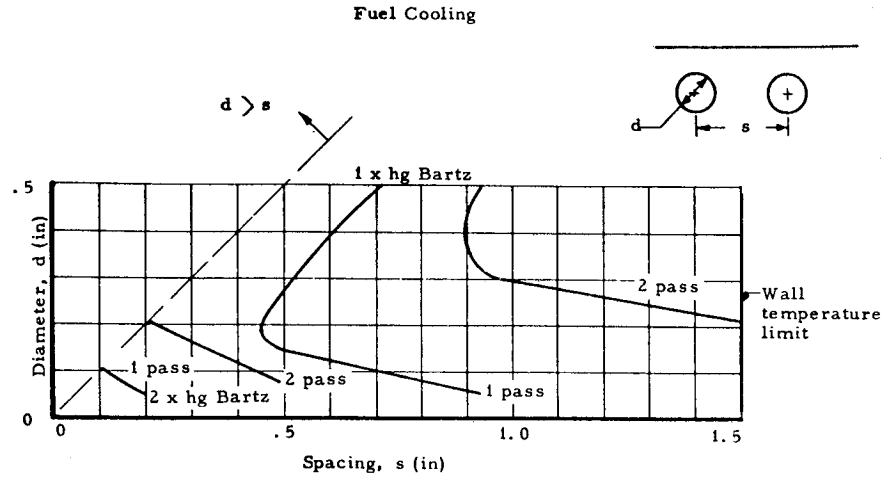

Figure 27. Required Geometry for Drilled Copper Cylinder with Axial Flow

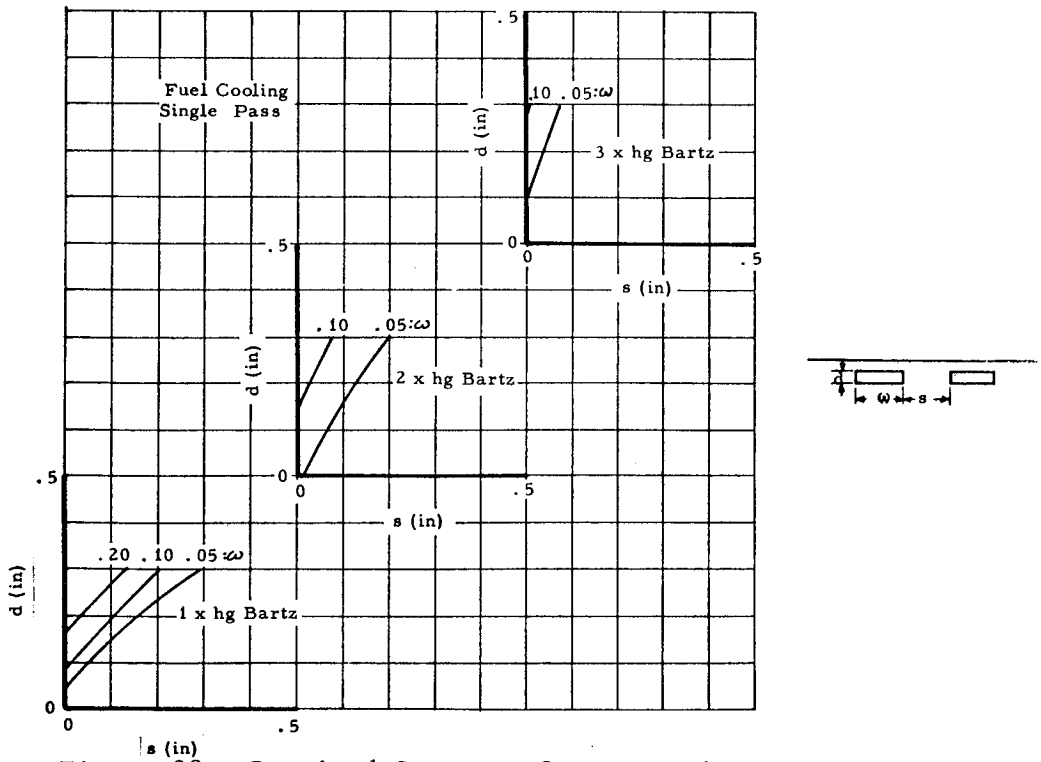

Figure 28. Required Geometry for Grooved Copper Cylinder with Axial Flow

IV, C, Heat Transfer (cont.)

$$K_1 = K_2 \, d_t - \frac{d_t^2}{s}$$

where K_1 and K_2 are numerical constants. Differentiation yields

$$\frac{ds}{d(d_t)} = \frac{K_2 s - 2d}{K_1 - K_2 d}$$

which indicates an inflection point at

$$d_t = \frac{K_2 s}{2}$$

Similar behavior is noted for the grooved cylinder as well. Solutions for which the channel diameter exceeds the spacing are obviously excluded, and consequently the twice-Bartz coefficient approximates an upper limit.

(5) Grooved Cylinder -- Axial Flow - Figure 19b

For grooved (rectangular) axial flow passages, the heat flux correction is taken to be

$$\frac{A_o}{A_i} = \frac{w + s}{w + 2d}$$

where w is the width and d the depth of the channels and s is the spacing between channels. Thus, only three surfaces are considered for the inner surface. With the drilled passage the whole circumference was treated. The flow area is

IV, C, Heat Transfer (cont.)

$$A_f = \frac{N_c}{N_p} (wd)$$

where the number of channels N_c is

$$N_c = \frac{\pi D_c}{w + s}$$

Again only the worst case, minimum coolant flow area, has been considered. Figure 28 presents the results for a single-pass system, and Figure 29 for a double-pass system. Single-pass systems are limited to the low Bartz coefficient and to small channel widths to yield spacings that will accommodate the resonator orifices. The double-pass system is not quite so limited to low Bartz coefficients, and higher-pass systems would be even better.

(6) Grooved Cylinder -- Azimuthal Flow

Azimuthal flow in a grooved cylinder offers considerable latitude in the geometrical design. The heat flux correction is the same as for axial flow. For full-circle flow, the flow area is

$$A_f = N_c (wd)$$

where the number of channels N_c is

$$N_c = \frac{\ell}{w + s}$$

For the results given in Figure 30, the cooled liner length, ℓ, has been taken equal to 4 in. Different values of ℓ may be treated by scaling the channel

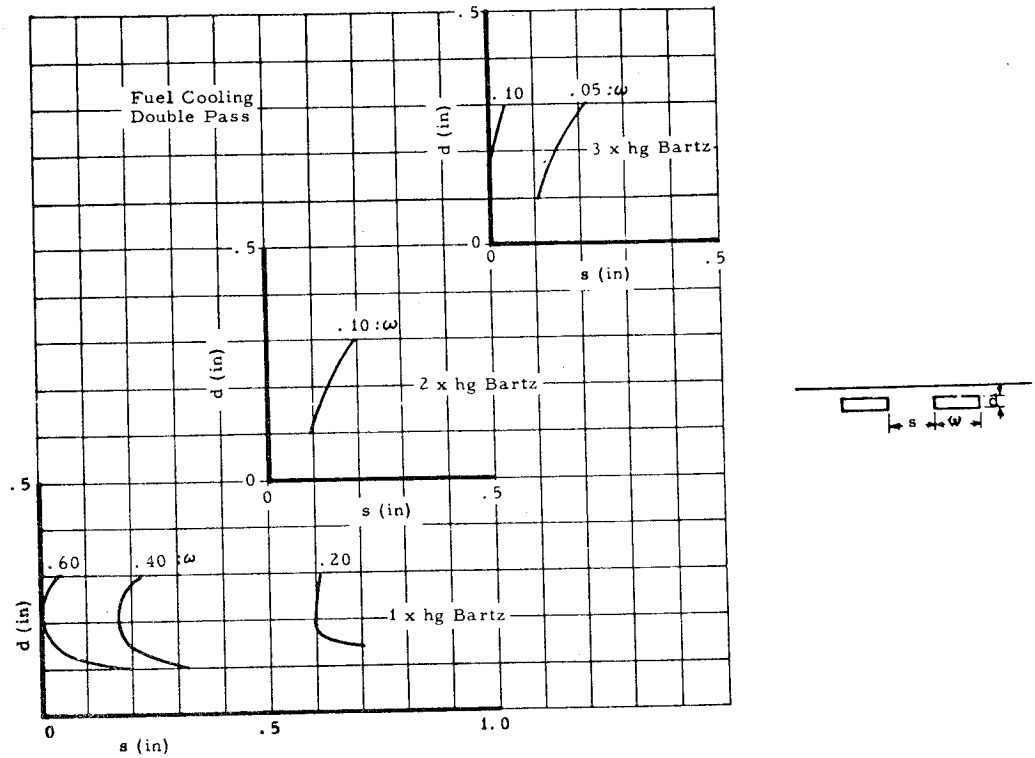

Figure 29. Required Geometry for Grooved Copper Cylinder with Axial Flow

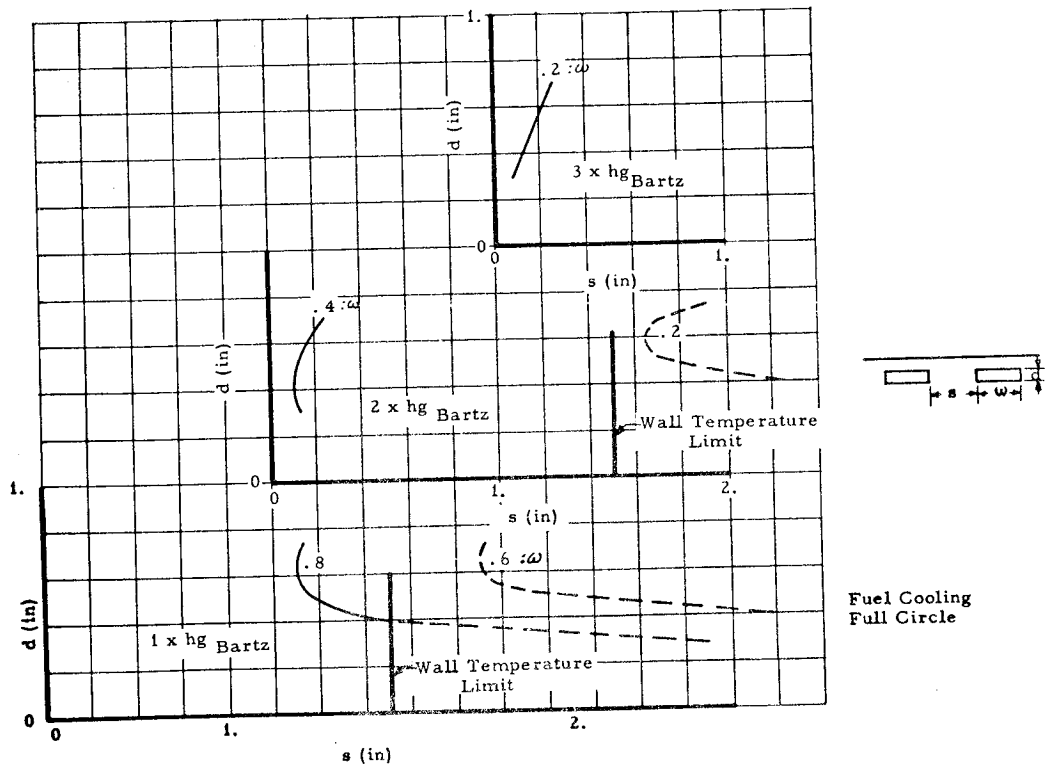

Figure 30. Required Geometry for Grooved Copper Cylinder with Azimuthal Flow

IV, C, Heat Transfer (cont.)

depth (d) in inverse proportion to ℓ. With azimuthal flow, relatively wide spacing can be maintained, even at the high Bartz multiplier. Of all the design concepts, this one offers the most leeway for placement of the resonator orifices.

b. Film-Cooled Designs (with Regenerative Cooling)

A high film coolant flow rate, say 12% of the fuel, considerably reduces the gas-side heat transfer. The film coolant temperature profile, starting at the point of monopropellant combustion, is shown in Figure 31 for two analytical models. The entrainment model represents mixing of the main stream gas and film coolant by means of a mixing parameter; the Seban model is a generalization of experimental data based on empirical correlations. Both models treat chemical equilibrium and nonreactive cases. The highest temperature within a 4.0-in. length is predicted by the nonreactive entrainment model to be 2150°F. That value has been taken as the recovery temperature in the following parameter studies; this is no doubt conservative since it ignores the existence of a liquid length. On the basis of a simple energy balance that considers no entrainment losses from the film and no increase in heat transfer due to roughness of the film, the liquid length is about 7.0 in. A more realistic treatment that accounts for entrainment losses and increased heat transfer yields a liquid length of 4.2 in. Test Nos. 1299-D01-OM-001, -002, -003, and -004, which yielded no erosion or charring of a 4.0-in. length below the injector, tend to corroborate this long liquid length. If the film coolant does in fact persist as a liquid for such a distance, the need for any additional cooling, e.g., regenerative, becomes questionable. However, that length may not exist on the acoustic liner, if the resonator apertures cause the liquid layer to break up.

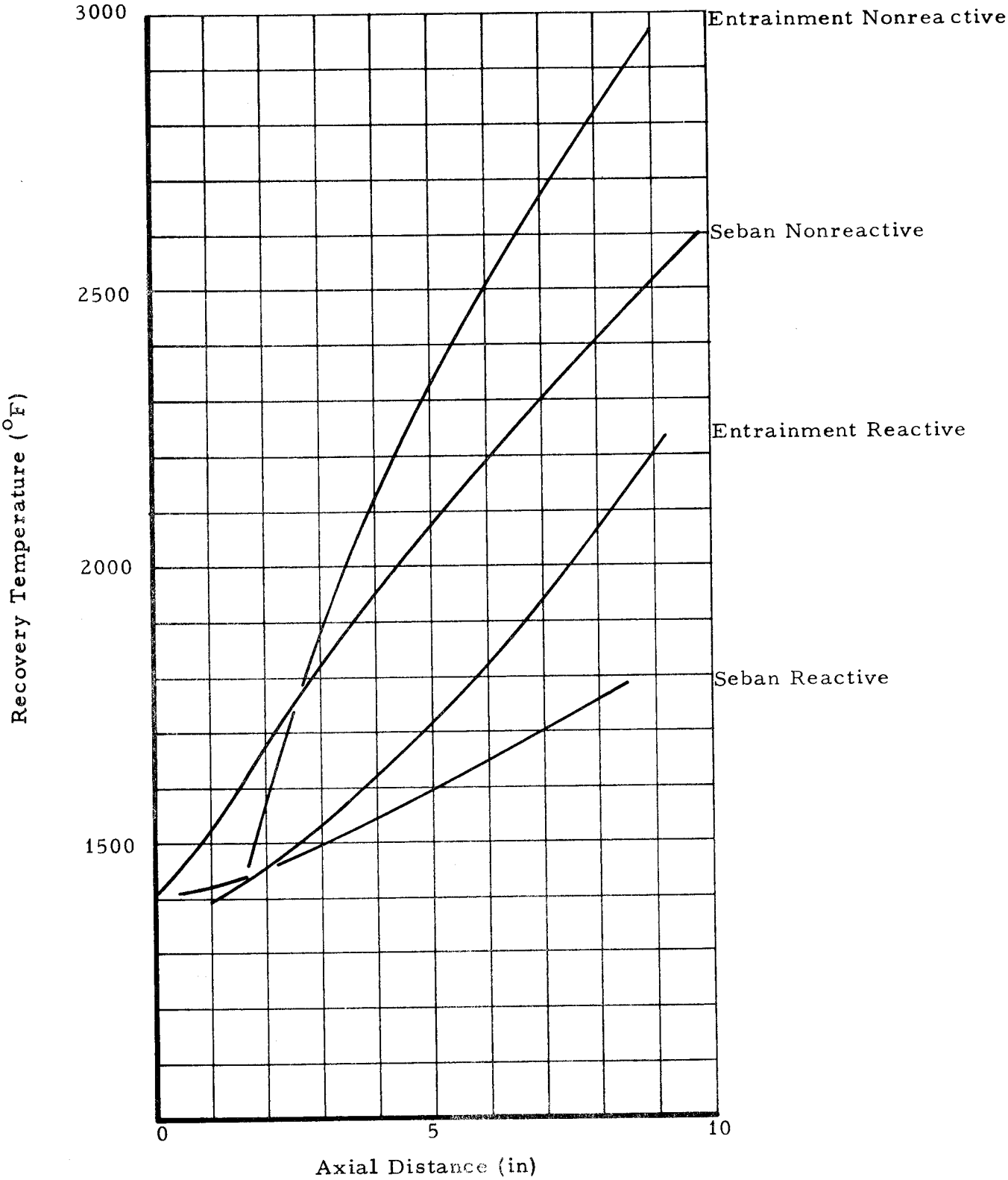

Figure 31. Predicted Film Coolant Temperature Profiles

IV, C, Heat Transfer (cont.)

Nonetheless, for illustrative purposes the required geometrical relationships have been calculated. Only the case of highest (3x) Bartz coefficient multiplier has been treated. The procedures are identical to those outlined earlier for the non-film-cooled designs.

Results are presented graphically in Figures 32, 33, 34 and 35 for the tubular, concentric cylinder, drilled cylinder, and grooved cylinder, respectively. All concepts yield workable designs and allow sufficient spacing for resonator orifices.

The tubular design offers relatively large diameters in combination with few required passes. The concentric cylinder in axial flow is still somewhat limited, although for azimuthal flow the channel depth is reasonably large. For wall resistances above 1000 $(Btu/in.^2\ sec\ °F)^{-1}$ the heat flux is less than the burnout value for pool boiling, and any channel depth (viz, coolant velocity) will suffice. With the drilled copper liner the coolant channels may be placed so far apart that wall temperature rather than burnout heat flux becomes the limiting factor. The grooved cylinder design also allows moderate channel widths and depths at relatively wide spacings.

c. Transpiration Cooling

Both fuel and oxidizer are considered for cooling purposes, and the required coolant mass fluxes for each are calculated as a function of wall temperature for various gas-side heat transfer coefficients. Coefficients of one, two and three times the Bartz coefficient are treated, reflecting the unknown effect of orifice-induced boundary layer tripping on the convective coefficient. No effort as yet has been made to arrive at a working design, with resonator cavities and orifices as integral parts of the transpiration-cooled wall.

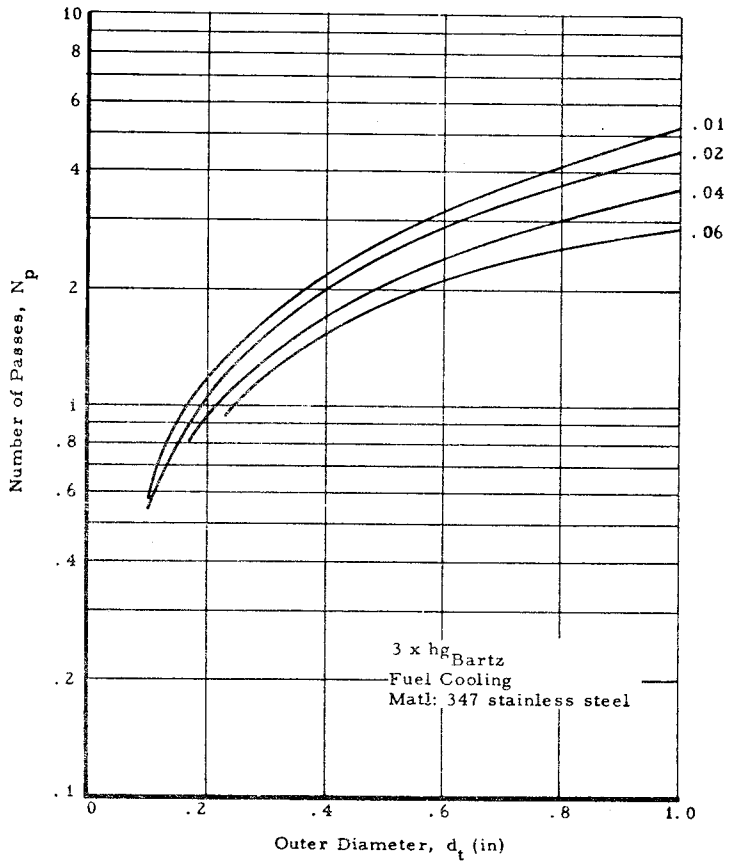

Figure 32. Required Geometry for Tubular Design with Film Cooling

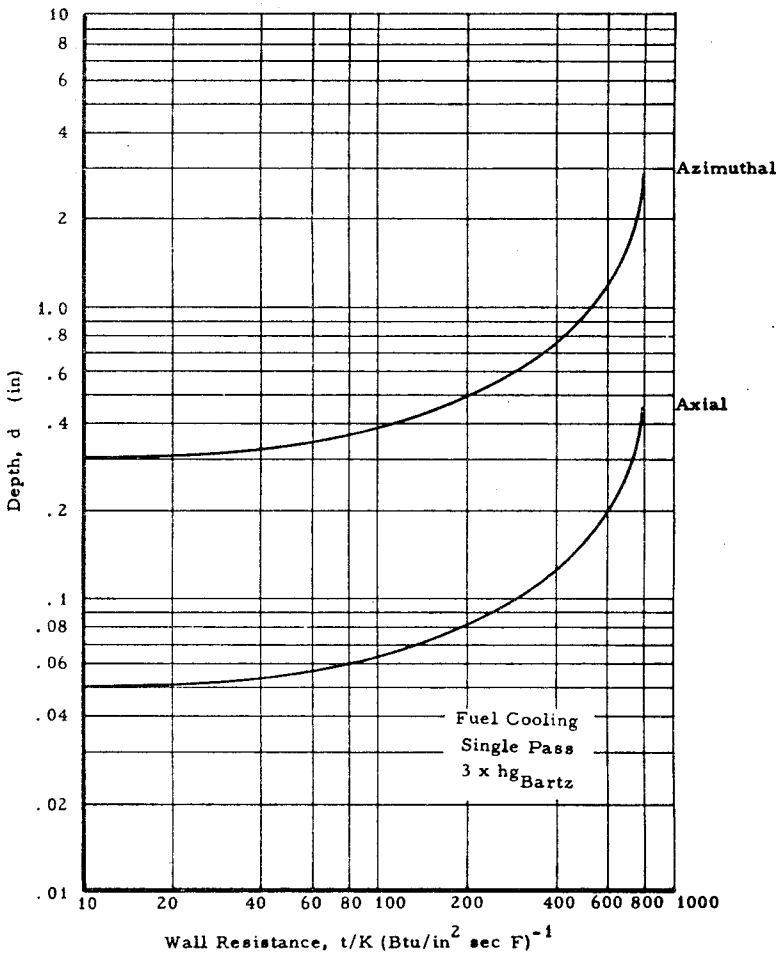

Figure 33. Required Geometry for Film Cooled Concentric Cylinder

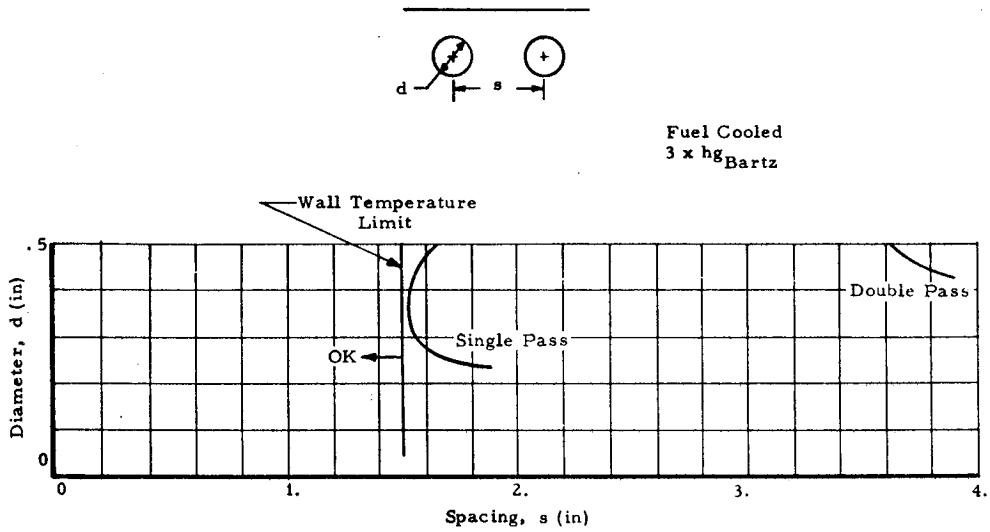

Figure 34. Required Geometry for Film Cooled Drilled Copper Cylinder

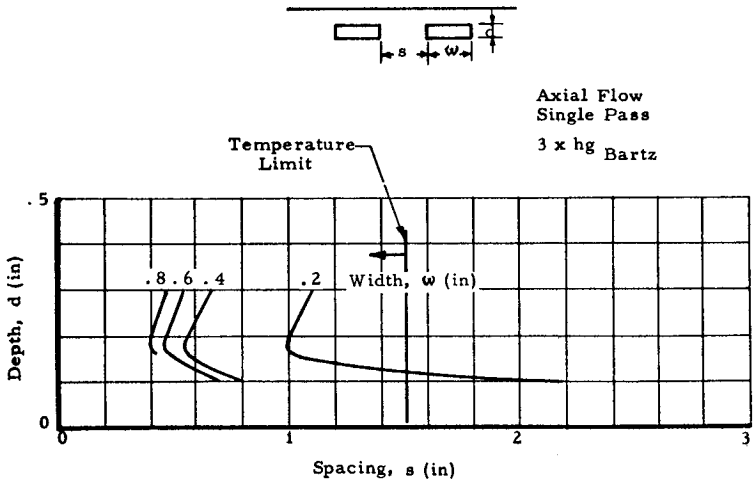

Figure 35. Required Geometry for Film Cooled Grooved Copper Cylinder

IV, C, Heat Transfer (cont.)

To maintain wall temperatures of 1000 to 1500°F, coolant mass fluxes typically range from 0.002 to 0.005 lbm/in.^{2} sec. The total surface area for a 4.0 in. long liner section approximates 100 in.^{2}, and thus the coolant flow rate is 0.2 to 0.5 lbm/sec. The fuel is somewhat better than the oxidizer as a coolant, although it is limited to lower temperatures because of the detonation danger. On the basis of availability, however, the oxidizer is the better choice, since a smaller percentage is required and higher temperatures are allowable.

(1) Analysis

The required coolant mass flux is found from a simple energy balance between the coolant temperature rise and the gas-side heat transfer

$$(\dot{W}/A)\ C_p\ (T_{wg} - T_B) = h_g\ (T_r - T_{wg})$$

The coolant is taken to have the same temperature as the wall at interior points, and any "film cooling effect" by the transpired fluid is ignored. The mass flux $(\dot{W}/A)$ is solved in terms of gas-side wall temperature for the different values of coefficient, h_g. Film coefficients of one, two and three times the Bartz coefficient ($h_{g_{Bartz}}$ = 0.000436 Btu/in.^{2} sec °F) are considered. The recovery temperature, T_r, is 5080°F, and no film cooling is considered. The heat of vaporization is included in the specific heat (Cp) term.

The energy balance approach has been found in AGC experience to yield good results at high heat fluxes and somewhat conservative results at the low heat fluxes typified by this study. A more rigorous heat exchange analysis could also have been undertaken, using a computer program developed for that purpose.

IV, C, Heat Transfer (cont.)

(2) Results and Conclusions

Figure 36 shows the required mass flux for oxidizer cooling, and Figure 37 the flux for fuel cooling. The percentage of the overall flow of each is also indicated, for a section 4.0 in. long.

Transpiration cooling offers reasonable performance, notwithstanding complexities in the design of resonator cavities and orifices. However, the required flow rates are equal to about half the present injected film coolant flow rate, for which satisfactory regenerative systems can be designed. As noted in Section IV,E,2, the film coolant is so effective that additional regenerative cooling may be unnecessary with high temperature materials. Thus, in view of the relative simplicity of regenerative cooling, transpiration would appear to be the less suitable.

d. Ablative Liner Cooling Analysis

A study was made of an ablative wall for acoustic liner applications on the LMA engine similar to previous studies which dealt with regenerative and transpiration cooling. Both film cooling and barrier cooling are considered here, with the film cooling percentage and the barrier mixture ratio treated as independent variables. The ablative wall is assumed to be 0.5 in. thick silica phenolic. Two gas-side heat transfer coefficients are considered: the Bartz coefficient (0.000436 Btu/in.^{2} sec °F) and three times the Bartz coefficient. The latter value corresponds to the largest coefficient that might be expected downstream of resonator orifices as a result of boundary layer tripping by the orifices, on the basis of analysis to date. The backside of the wall is considered to be adiabatic.

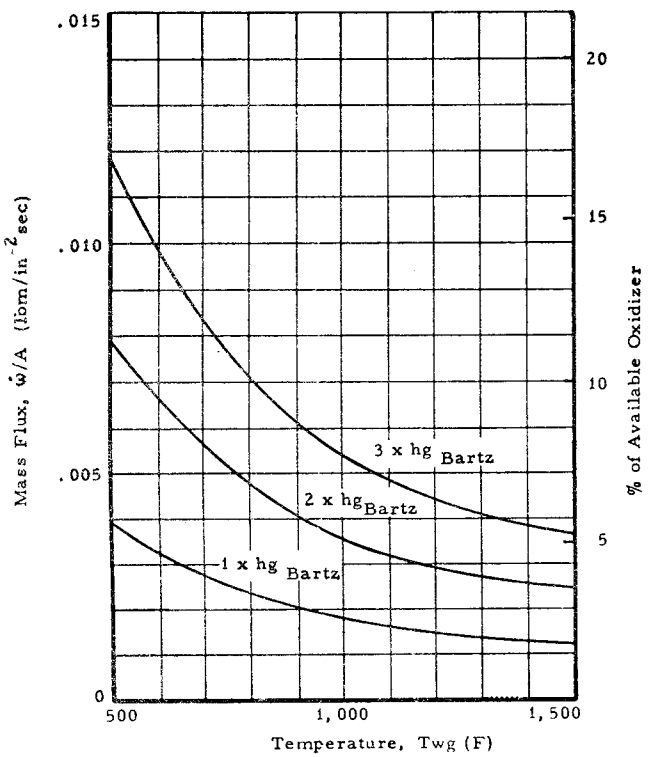

Figure 36. Required Transpiration Mass Flux Oxidizer Cooling

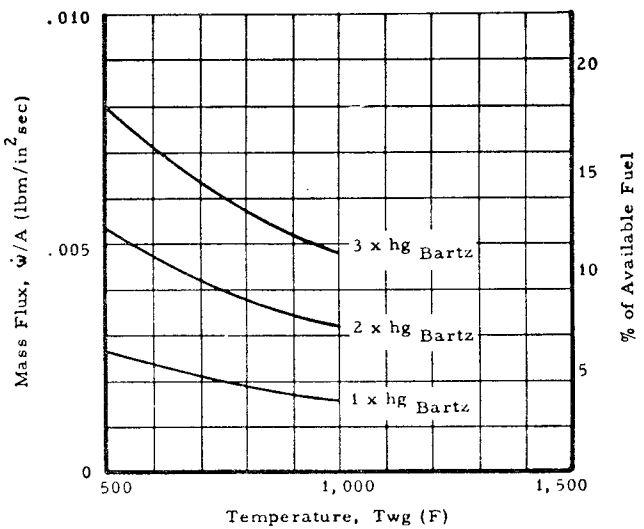

Figure 37. Required Transpiration Mass Flux Fuel Cooling

IV, C, Heat Transfer (cont.)

With fuel film cooling the predicted gas-side erosion, using either heat transfer coefficient, is negligible because of the long liquid length of the coolant. There is some in-depth pyrolysis throughout the material, for durations longer than 60 sec, however.

With barrier cooling, the predicted erosion rate varies exponentially with barrier mixture ratio, exceeding 1.0 mil/sec at either MR 1.10 and three times the Bartz coefficient or at MR 1.20 and one times the Bartz coefficient, for barrier flow equal to 20% of the total flow.

(1) Film Cooling

The liquid length, L, of the film coolant is calculated from the energy balance relationship:

$$L = \frac{W_c \left[\varepsilon(H_{SV} - H_{in}) + (1 - \varepsilon)\zeta\ (H_{SL} - H_{in})\right]}{f\ h_g\ (T_r - T_d)}$$

where W_c is the film coolant flow rate per unit circumference, ε is the fraction of the liquid that is vaporized, ζ is an entrained liquid enthalpy parameter which in this case is taken as zero, and H_{SV}, H_{SL}, and H_{in} are the enthalpies of the saturated vapor, saturated liquid, and inlet fluid, respectively; f is an enhancement factor to account for the increased nominal film coefficient, h_g, due to liquid roughness; T_r and T_d are the recovery and saturation temperatures, respectively. The ratio ε/f is evaluated from data of Graham (Ref 27) and is arbitrarily increased by a factor of 1.6 to yield agreement between the predicted liquid length and the estimated average virgin length in a series of ALFP ablative chamber compatibility tests. Figure 38 shows the predicted liquid length as a function of the percent (fuel) film cooling.

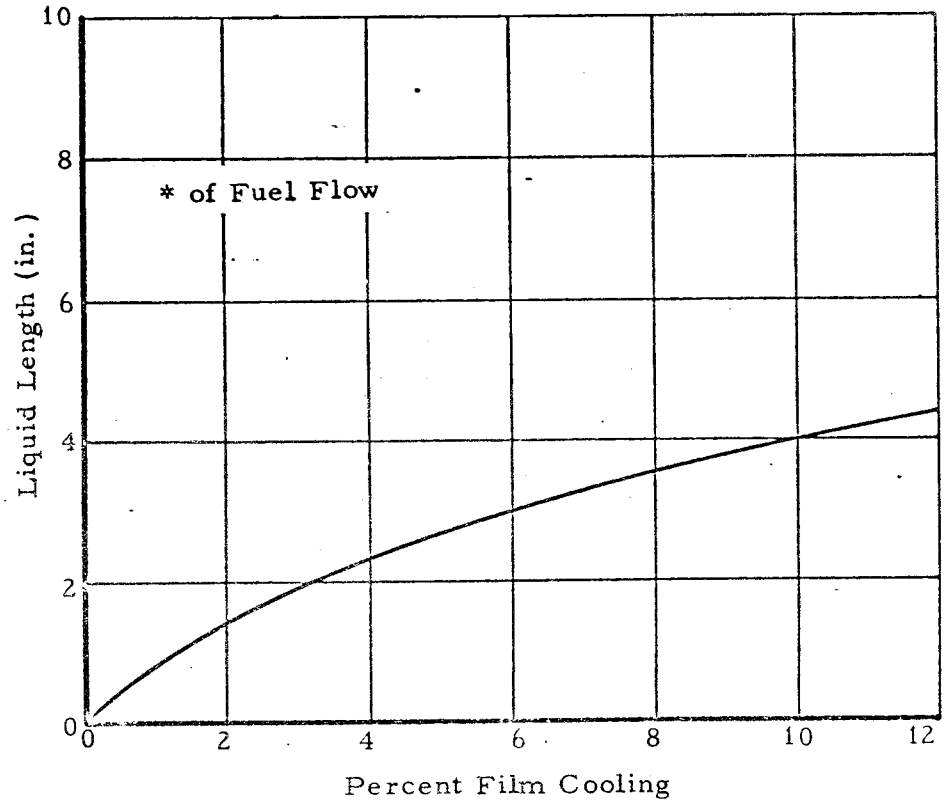

Figure 38. Predicted Liquid Length vs Percent Film Cooling

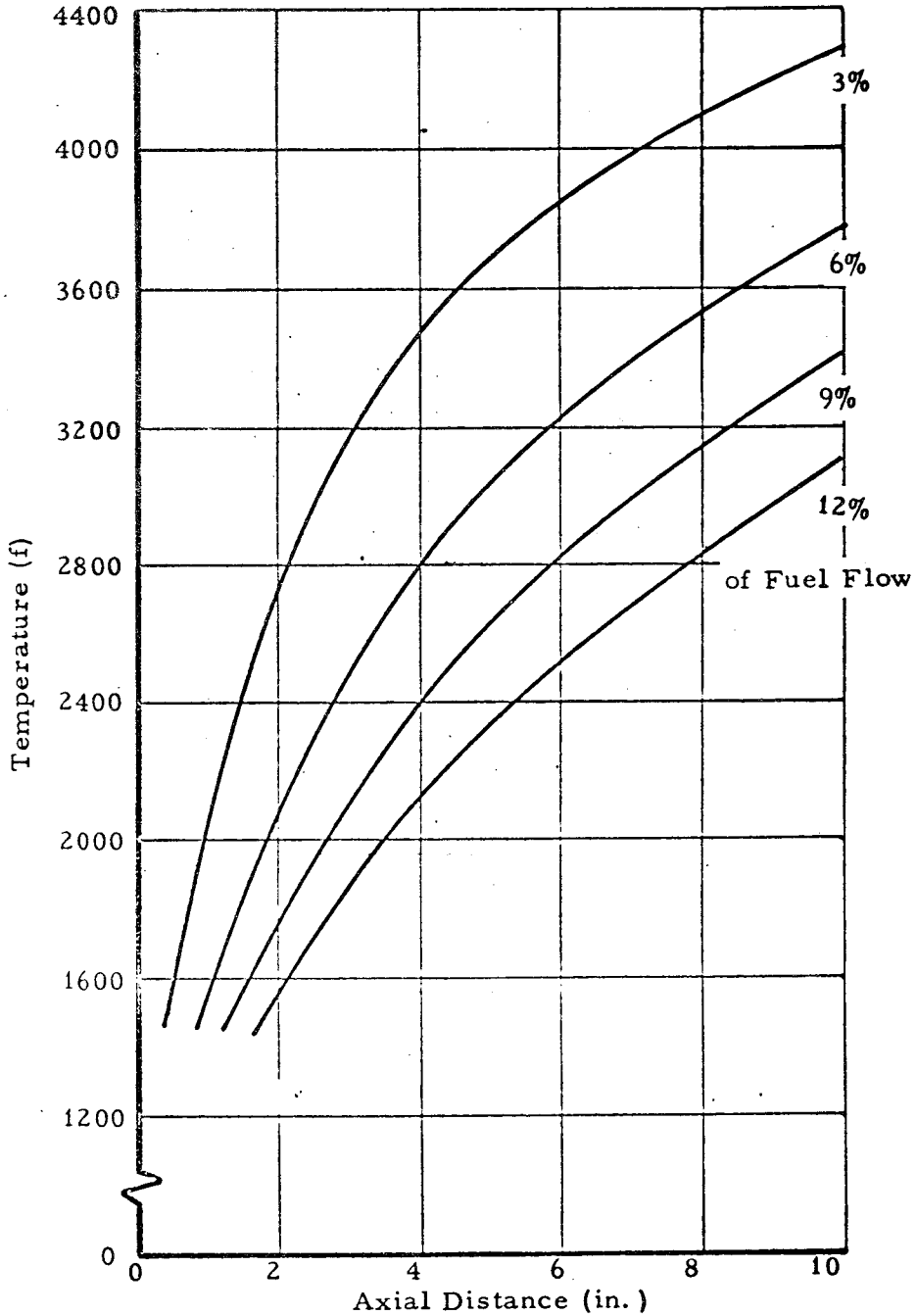

Figure 39. Film Coolant Temperature Profiles Based on Nonreactive Entrainment Model

IV, C, Heat Transfer (cont.)

The gaseous film coolant temperature and mixture ratio profiles, starting at the end of the liquid length, have been calculated from the Seban and entrainment models for both reactive and non-reactive flows. The entrainment model represents explicitly mixing of the mainstream gas with the film coolant, through the use of a mixing parameter and a shape factor for the mixing layer between the mainstream and the film. The Seban model is a generalization of Seban's empirical asymptotic correlations for plane, unaccelerated flow. The reactive models base the film temperature profile on the enthalpy-mixture ratio relationship, assuming equal enthalpy and elemental concentration effectivenesses. The non-reactive models base film temperature directly on mixture ratio, taking specific heats to be constant.

Figure 39 shows the predicted temperature profile for various film coolant flow rates based on the non-reactive entrainment model, which predicts the highest temperature profiles. Since the acoustic liner is restricted to the forward end of the chamber, which is cylindrical for 7.5 in., the various profiles are all started at zero axial distance and subsequently adjusted to the proper liquid length. A similar series of profiles can be drawn for the local mixture ratio at the wall surface.

From these data, crossplots can be made to find recovery temperature and mixture ratio as a function of percent film cooling at a given axial station. Figure 40 shows these relationships at an axial distance of 4.0 in., which is taken as the maximum likely distance from the injector for locating the resonator section.

As can be seen from this figure, with film coolant flow rates greater than 3-percent of the fuel the recovery temperature is less than 3000°F. Likewise for flow rates greater than 5.5-percent of the fuel the mixture ratio of the film at the wall is effectively zero.

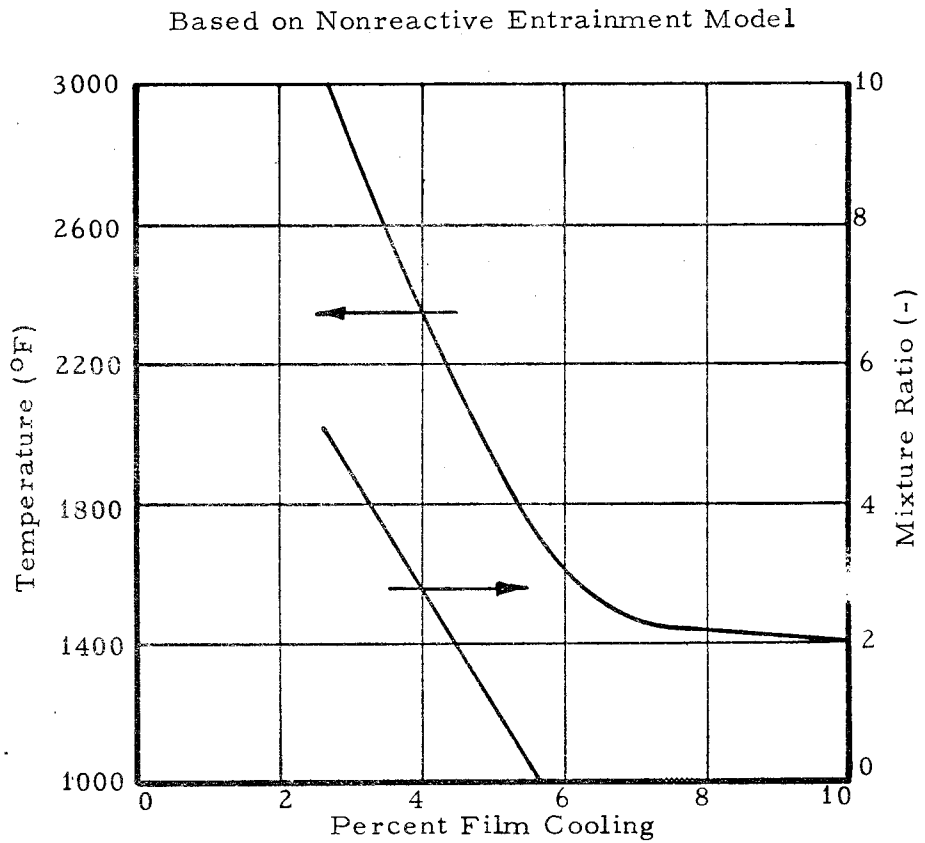

Figure 40. Predicted Recovery Temperature and Mixture Ratio at 4.0 in Axial Distance vs Percent Film Cooling

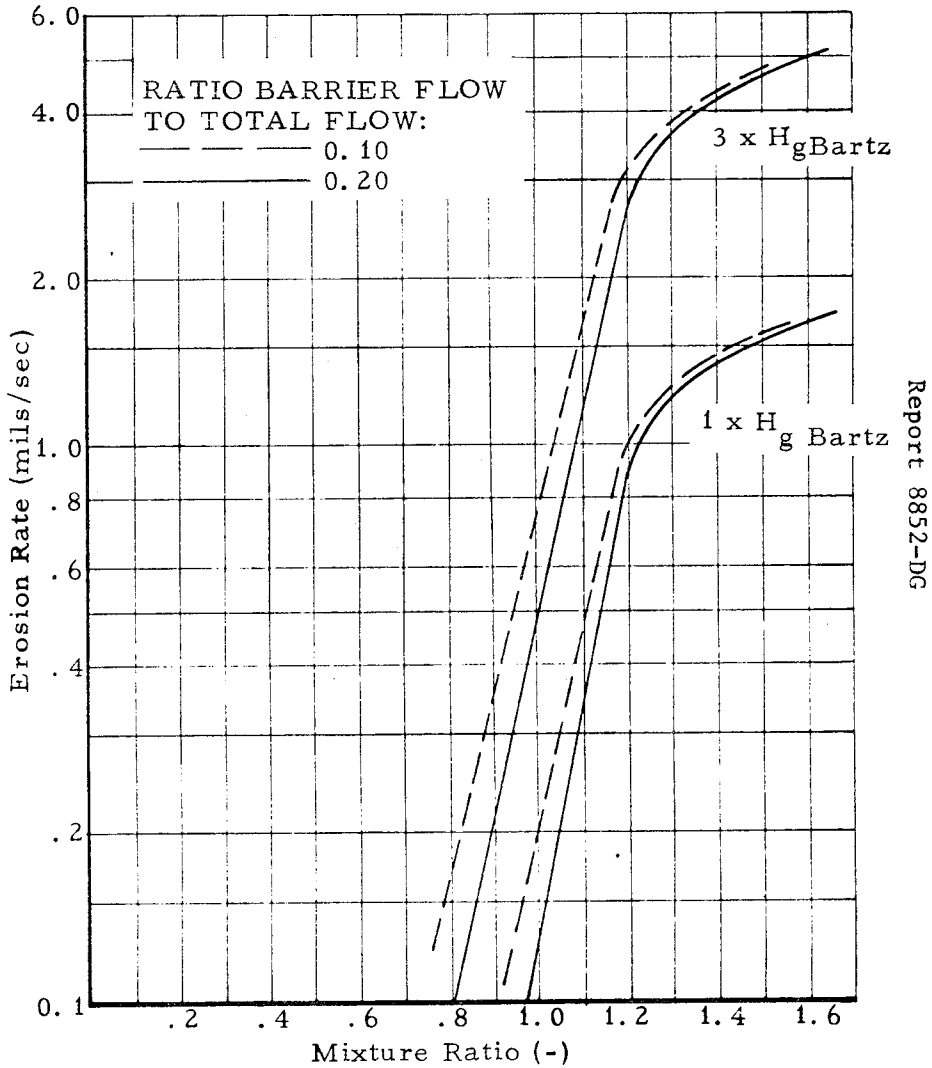

Figure 41. Predicted Average Erosion Rate vs Initial Mixture Ratio of Barrier Zone

IV, C, Heat Transfer (cont.)

Since liquid film cooling is such an effective mechanism, only a single case is considered here, and that mostly for illustration. This case corresponds to 3-percent film cooling, which is about the minimum value that gives adequate coverage to the entire periphery (Ref 28). The charring, erosion and thermal responses are calculated with the Vidya (Ref 29) computer programs, Equilibrium Surface Thermochemistry (EST) program, and Charring Material Thermal Response and Ablation (CMA) program. These programs treat chemical equilibrium on the gas-side surface and account for multiple pyrolysis reactions internally. A firing duration of 600 sec is considered, corresponding to the longest duration specified in the contract. Charring is fairly complete in the interior half of the wall in 600 sec, although the exterior half is only partially charred and a flow of pyrolysis gases exists for the whole duration. No erosion is predicted to occur, even at a heat transfer coefficient of three times the Bartz value.

(2) Barrier Cooling

The barrier-cooling analysis is similar to the film-cooling analysis, except that the liquid length is no longer a consideration since the flow near the wall consists of low mixture ratio combustion products. Barrier temperature and mixture ratio profiles are calculated from the Seban and entrainment models as before, and the charring, erosion and thermal responses are again found using the Vidya EST and CMA computer programs.

Figure 41 shows the predicted erosion rate as a function of initial barrier mixture ratio for a barrier flow equal to 10-percent and 20-percent of the total flow. The strong dependence of erosion rate on mixture ratio demonstrates that erosion in large part is due to chemical effects: a 20-percent change in mixture ratio yields an

IV, C, Heat Transfer (cont.)

order of magnitude change in erosion rate. In addition, the erosion rate is noted to be almost in direct proportion to the heat transfer coefficient.

For both the film cooling and barrier cooling studies, the assumption is made that the backside of the ablative wall is adiabatic, the rationale being that the gas in the resonator cavities has a relatively low temperature and that the heat transfer coefficient between it and the wall is small. This, of course, requires that there be no flow through the resonator, and that vortex effects in the resonator be not significant. Whether this is indeed the case, even for a well-baffled resonator volume, remains to be seen.

(3) Conclusions

Based on the indicated analytical approach, both film and barrier cooling appear to offer long-duration capability. Film cooling seems more advantageous, in view of the long liquid length and low initial film temperature. However, excessive amounts of film cooling may cause liquid fuel to flow into the resonators and thus provide the possibility of combustion inside the cavities.

4. Heat Transfer Design Criteria

The usual design criteria for ablative and regeneratively cooled chambers are well known and apply also to acoustic liner sections. The uncertainty of the gas-side boundary condition as a result of boundary layer tripping by the resonator orifice was thus the major design problem confronting the thermal analyst, along with the unknown magnitude of heat transfer from the resonator volume to the surrounding walls.

IV, C, Heat Transfer (cont.)

An analysis of gas-side heat transfer was made as mentioned in Section IV,C, involving a flow analysis of the orifice region coupled with a boundary layer analysis of the downstream wall, was perhaps enlightening but not necessarily accurate and, hence, of questionable value. In the interest of conservatism, a worst-case film coefficient equal to three times the Bartz value was presumed. However subsequent testing with a highly instrumented chamber indicate a film coefficient of one times Bartz is adequate.

Orifice heat transfer is not considered likely to be as great as that previously indicated by analysis. Cavity heat transfer is also expected not to be severe so long as axial flow between cavities is prevented. The effects of orifice and cavity heat transfer are probably treated adequately by the conservative assumption regarding gas-side heat transfer.

Regenerative Cooling. Regenerative cooling presents the greatest number of design considerations, namely:

1. Material wall temperature - must be satisfactory from the standpoint of strength of the material, as well as melting point.

2. Coolant burnout heat flux - must exceed the gas-side heat flux by a reasonable margin.

3. Coolant pressure drop - dictated by system requirements but is also a factor in burnout heat flux.

4. Coolant bulk temperature rise - primarily a factor in burnout heat flux characteristics but, if excessive, should be considered in light of bulk boiling or propellant detonation.

IV, C, Heat Transfer (cont.)

5. Compatibility - coolant must be compatible with wall material.

Ablative Cooling. Material integrity, viz. tolerable erosion rate for the design duty cycle, is the single most important design criterion with ablatives. Since material erosion is largely due to chemical attack, compatibility between the boundary layer gas (film coolant) and the wall material is of overriding importance. A second consideration, wall thickness, arises from backside temperature and heat soakback limitations.

IV, Design Mechanics (cont.)

D. MATERIALS (NON-METALICS)

1. Materials Selection Analysis

a. General Guide Lines

A materials analysis for an acoustic liner presents some unique and different requirements from those previously encountered in selecting ablative materials for liquid rocket chambers. Preliminary investigations indicated that modification of theoretical models or completely different theoretical models for performance prediction are required. Empirical data is not generally available in sufficient quantity to provide anything other than guidelines. Comparative analysis of potential materials required a qualitative evaluation based on known and estimated effects of acoustic liner orifices, injector orifice patterns, heat flux, film cooling, and chemical reaction. Variations in any of these parameters could significantly change the conditions of the test and thereby effect the design and material selection. Those parameters which can be ascertained by stress and heat transfer analyses are used as the primary criteria for selecting candidate materials for an acoustic liner.

The use of an "off the shelf system" is preferred and generally dictated by economic considerations. Many of the potential materials are not characterized and can not be easily scaled up to moderate size chambers (say an 8-in. diameter chamber) for demonstration purposes.

The objectives of the material analysis are:

(1) To select an ablative material which will perform as an acoustic liner based on the stress and heat transfer analyses that assume that the chamber conditions would not exceed the abilities of composite materials.

IV, D, Materials (Non-Metalics) (cont.)

(2) To select a material with restart capabilities.

(3) To select a material to withstand thermal shock of start transient.

(4) To select a back-up material or technique for separation of acoustical cavities.

(5) To select a material which can withstand the required duty cycle in an environment as yet somewhat undefined.

b. Review of Experience

Regression rate, char rate, and structural integrity are the primary criteria to be considered in evaluating the material to be used as an acoustic liner. A detailed review of previous experience by means of a comprehensive literature survey to ascertain quantitative data for ranking as to each criterion requires an exhaustive survey of materials test data. Furthermore, the individual testing vehicles produce different thermo-chemical environments which complicate and in most instances prohibit comparative analysis from more than one test vehicle. Even the conditions of full-scale development and production motors have changed when injectors are modified. On the other hand, many general and accepted conclusions have evolved related to types of materials, fabrication techniques, quality requirements, and overall performance for ablative materials. Because the criteria for ranking performance of ablative materials have been different for individual environments, only a limited range of materials and fabrication techniques has been used in liquid rocket engine thrust chamber components.

The following paragraphs summarize some of the specific knowledge gained from the materials references (Refs 30 through 36).

IV, D, Materials (Non-Metalics) (cont.)

Based on the performance of the acrylonitrile phenyl silane silica-fabric system in the Apollo Service Propulsion System (SPS), it is concluded that a silica-fabric-reinforced system could be utilized as an acoustic liner. A greater stiffness was needed and a stronger char than that provided by the rubberized system was also indicated. However, the basic silica-reinforced thermoset appeared to be a good candidate providing the wall temperature did not exceed the melt temperature of the silica reinforcement. Propellant compatibility had been demonstrated in the Apollo SPS engine.

Thirty-eight different materials combinations were tested during the Ablative Thrust Chamber Feasibility Program (Contract AF 04(647)-212/SA3). Thirty-six subscale thrust chamber firings were made at chamber pressures between 200 and 500 psi P_c. Based on conclusions drawn from the tests, five full-scale chambers were fabricated from silica and asbestos reinforced phenolics. Two of the chambers had ceramic throats: one of Pyrolytic Tantalum Carbide and the other of AT-J Graphite.

The best overall performance was obtained from the silica reinforced systems. The propellant was N_2O_4/A-50 and was severely oxidizing at the chamber wall as evidenced by the high regression rate of the AT-J graphite. The program further demonstrated the better structural capabilities of the broad goods reinforced systems over the chopped fabric molding compounds.

The comparative performance of the silica and quartz indicated that quartz should be evaluated while screening materials for the acoustic liner. Although polyimides (Ref 30) were not equivalent to the phenolics, the potential for greater strengths at elevated temperature made their evaluation desirable. Polyimides with varying properties and with fabrication processing other than those tested are also available. Other comparative tests have indicated polyimides are slightly superior to phenolics in ablative environments.

IV, D, Materials (Non-Metalics) (cont.)

Sixty-nine test specimens were exposed to plasma arc environments (Ref 31). Thirty-five specimens contained carbon, eleven contained graphite, and ten contained silica, two were of fused silica, three of boron, and the remaining eight were combinations of miscellaneous fabrics. Test results indicated the following related to the material selection for the acoustic liner:

(1) The silicon carbide heat of ablation was higher than that of silica. (The wool form was superior to the fiber.)

(2) Boron fibers had high ablation rates.

(3) Fillers had no significant effect on ablation and did not produce a change in total reflectance.

Seventy materials were tested in a simulated liquid exhaust (Ref 32). Resins included phenolics, polyimides, and PBI. Reinforcements included silica, silica and carbon, zirconia fiber, and oxidation resistant carbon. Reimpregnated pyrolized composites were also tested. The results indicated the following related to a material selection for the acoustic liner:

(1) Silica was better than the carbon/silica, zirconia fiber and oxidation resistant carbon.

(2) The phenolic systems had the least erosion and the polyimide was almost equivalent for the reimpregnated pyrolized systems.

(3) The PBI system test was slightly superior to phenolic.

A fourth program evaluated (Ref 33) was intended to develop an ablative composite which can withstand a highly oxidative liquid propellant environment at high temperatures and pressures. However, to date,

IV, D, Materials (Non-Metalics) (cont.)

only a test method for screening test specimens in a plasma test flame has been developed. Initial results indicate organic-metalic chemicals used in the fabrication of ablative composites have provided improvement over the unmodified silica-phenolic systems. The studies are continuing including evaluation of carbiding in-situ using tantalum, zirconium and hafnium.

The materials and preliminary test data did not appear complete enough to be of use. However, based on the preliminary recommendations, a silica reinforced phenolic with metalic fillers was selected as one of the candidates for evaluation.

Phenolic, polyimide, polyphenylene and other resin systems reinforced with carbon, graphite, silica, quartz and boron nitride fabrics were tested (Ref 34) using a plasma arc in steady state and transient environments. The application of the results to the selection of material for an acoustic liner was limited. For the conditions tested the following was shown:

(1) Polyimide resin was the best ablative material when used with silica and quartz reinforcement.

(2) Silica-reinforced systems were less sensitive to orientation in fabric lay-up during a high shear turbulent flow test.

(3) The polyimide and phenolic resins appeared to be equivalent.

Several hundred zirconium diboride composites were screened for oxidation resistance by plasma arc tests (Ref 35). Results indicate that additional silicon carbide whiskers reduce the rate of diboride oxidation. Addition of graphite detracted from the oxidation resistance. Further testing indicated that hafnium diboride is superior to zirconium

IV, D, Materials (Non-Metalics) (cont.)

diboride in oxidation resistance. Although the melting temperature and oxidation resistance of the diborides were attractive and improvement had been made in thermal shock resistance, it did not appear feasible to push toward development of a diboride acoustic liner until the concept had been demonstrated in a liquid rocket motor 8 in. in diameter or greater.

Quartz and silica reinforcements were compared by testing in an N_2O_4/AeroZINE 50 engine (Ref 36). Quartz reinforcements were slightly superior.

The reinforcements were tested at angles 0°, 30°, 60°, and 90° to the motor centerline. The 60° angle resulted in low erosion and low char depths for most materials.

Quartz was considered as a possible alternate or improvement over silica; however, the degree of superiority demonstrated did not appear significant in an acoustic liner. A preference for quartz could only be established if the silica were marginal in performance.

The use of orientation 60° to centerline did not appear to be the best orientation for an acoustic liner. Delaminations were more likely to occur at the high angle.

c. Methods for Preliminary Material Selection

Standard procedures are used for preliminary material selection including a literature survey, plasma arc screening, evaluation of "non-standard" materials, and consultation with material suppliers for possible candidates. Materials of a particular category are considered to be equivalent. For example, all silica-fabric reinforced phenolic materials are

IV, D, Materials (Non-Metalics) (cont.)

considered equivalent in potential performance and ease of fabrication, thereby eliminating the screening of many types of silica phenolic from material suppliers as well as of equivalents from each material supplier. This approach is taken because the performance of like ablative materials has been found not to vary significantly (Ref 37). Melt temperature of the silica systems is basically the same. Carbon yield of most of phenolic resins does not vary sufficiently wide enough to make resins a primary area for evaluation. Furthermore, it is usually not within the scope of a single rocket engine development program to accomplish an extensive comparative evaluation of similar materials.

The property variations of silica fabric/phenolic, which have the greatest influence on the regression rate, are melting temperature of the silica fiber, virgin plastic density, specific heat and activation energy (Ref 38). The melting temperature of the silica fabric is the most significant factor. Effects of char density, heat of gasification, heat of vaporization of reinforcing fibers, and thermal conductivity, should also be investigated. The melting temperatures and densities of silica-fabric phenolics do not vary significantly short of inducing out-of-the-ordinary processing. Therefore, silica phenolics in the virgin condition are considered as equivalent and detailed comparative screening is not necessary. The literature concerning actual and simulated test conditions for composite materials was reviewed to ascertain what materials have been tested which might become candidates for an acoustic liner.

Suppliers of ablative and composite materials should be contacted for recommendations and test samples of selected candidate materials to be screened in the plasma arc.

The plasma arc testing is selected as an inexpensive screening test using gaseous oxygen to simulate the effect of the oxidizer.

IV, D, Materials (Non-Metalics) (cont.)

A cold wall heat flux can be determined by heat transfer analysis. However, motor pressure, actual gas composition, and shear forces are not usually simulated.

d. Material Screening Methods

Material screening methods for selection of a material and/or materials for an acoustic liner consist primarily of plasma arc, plug module, and full scale sectioned liner.

(1) Plasma Arc

Figure 42 shows a typical "plasma arc" test setup. The plasma arc screening test is used to preselect materials for further evaluation by plug module and full scale sectioned liner tests. The plasma arc tests at nominal chamber heat fluxes may not show a significant difference. Some of the materials were selected because of their endurance at testing durations equal to the duty cycle at the nominal heat flux. Further evaluation of selected materials should be made by testing at higher cold wall heat fluxes. The high heat flux tests are made to ascertain the limits for the materials in relation to their melting temperature and viscosity after melting. Temperatures produced at the specimen surface by four times the nominal heat flux may be greater than the melt temperature of the materials tested. The data obtained may indicate that environmental conditions are severe enough to melt some otherwise acceptable material.

(2) Subscale Tests

It may not be feasible to test materials in subscale chambers on all programs. Funding may not be available, and the schedule

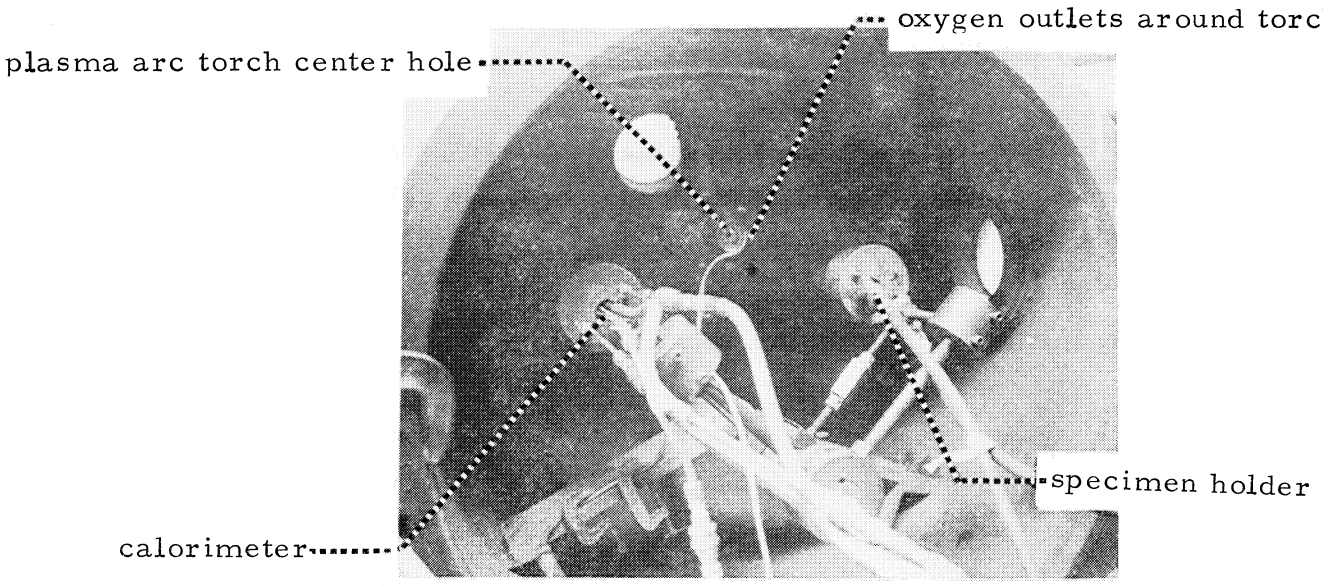

Figure 42. Plasma Arc Apparatus

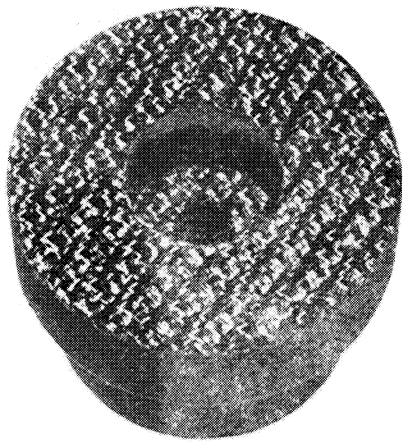

Figure 43. Plug Module

IV, D, Materials (Non-Metalics) (cont.)

may not allow time to complete subscale testing before the fabrication of full scale chambers. Therefore, subscale tests can only be recommended for very large engine programs.

(3) Full Scale Module Tests

The plasma arc data can only be used for rough screening because chamber pressure, propellant gas chemistry flow and shear forces can not be simulated and the material response which affects regression in the chamber may be an insignificant factor in plasma arc testing. Materials are selected for testing plug modules in the full scale chamber. The plug has an acoustic hole and cavity as shown in Figure 43. The effects of the surrounding material on the performance of the plugs can not generally be eliminated as was the location in the chamber as related to injector pattern. However, this test apparatus appears to be the best screening method available within the economic and schedule limitations.

(4) Segmented Full Scale Liners

A segmented liner composed of three to four different materials has been utilized in both liquid chamber and solid rocket motors to evaluate materials as well as variables associated with processing (Ref 39). No deep gouges or non-uniform erosion has occurred at the longitudinal segments. Epoxy and elastomeric adhesives have been used and close tolerances are maintained at the joints. With one exception, the segmented liner provides the best method for screening material candidates: an erratic injector pattern which produces one or two severe streaks makes it impossible to maintain an identical thermo-chemical environment for each segment. However, if the injector pattern has already been established there is the possibility of some selection of segments in relation to streaks prior to test.

IV, D, Materials (Non-Metalics) (cont.)

The interaction between materials because of melting or high regression is minimized by the use of longitudinal segments. Longitudinal segments are generally preferred to circumferential segments because of reduced interaction between various combinations of materials (Ref 40).

e. Comparative Tests

The screening methods discussed are only measures of comparative ablation; however, the performance criteria for an acoustic liner material are resistance to regression and structural integrity for extended firing duration. Structural integrity is simply resistance to degradation, delamination or cracking throughout the test. It was assumed that the materials retained their mechanical properties at the thermal and environmental conditions of use if they were intact at the end of the test. It is not feasible to characterize all candidate materials at the temperatures of use and data with few exceptions are unavailable.

Those materials are eliminated from further consideration if delamination occurs during plasma arc testing, laboratory carbonization, or if high regression rates occur in the plasma arc or plug module test. No chemical or physical analysis is generally made to ascertain the cause for poor performance except where obvious discrepancies are noted. For example, the Pyrocarb and Pyrolarex silicon-impregnated systems both are promising candidates although incomplete impregnation would produce non-uniform regression. Both materials when properly processed offer a combination of high strength at elevated temperature together with resistance to regression because of the infiltration of silicon and silicon carbide.

IV, D, Materials (Non-Metalics) (cont.)

f. Materials Characterization

Selection of alternative materials for an acoustic liner can best be accomplished by characterizing each in terms of the planned application and would necessarily include the measurement of thermal and physical properties at the extremes of the expected environment. This evaluation should be completed prior to ablative testing. Economic considerations usually place limitations on preliminary screening; therefore, it is necessary to reduce in number the materials submitted to a full characterization. This screening can be accomplished at a small portion of the cost required to characterize a material. Some data on physical properties, usually supplied by the vendor, are available for most materials. Further data can be acquired by categorizing similar type materials. The curves shown in Figures 44 through 48 represent the typical properties of silica reinforced phenolic. These and additional thermal data are used for preliminary stress and thermal analysis of the silica-reinforced materials. The data are too limited to accomplish a complete analysis because the high temperature data must be extrapolated.

Characterization requires measurement of raw material properties, documentation of critical processing parameters, and measurement of cured component properties for use in thermal and stress analyses. The raw material properties of silica reinforced phenolic that are minimal for evaluation are: breaking strength, type of weave, and percent purity of the reinforcement; resin viscosity, percent filler and percent resin solids; and the percent flow, percent volatile content, degree of resin advancement, degree of polymerization of tack strength and tack temperature, percent resin content of the pre-impregnated (Prepreg) material. These parameters should be measured and a usable range established for production components. For components of which there are two grades, these properties should be documented. The data are useful in evaluating in-process discrepancies and for detecting

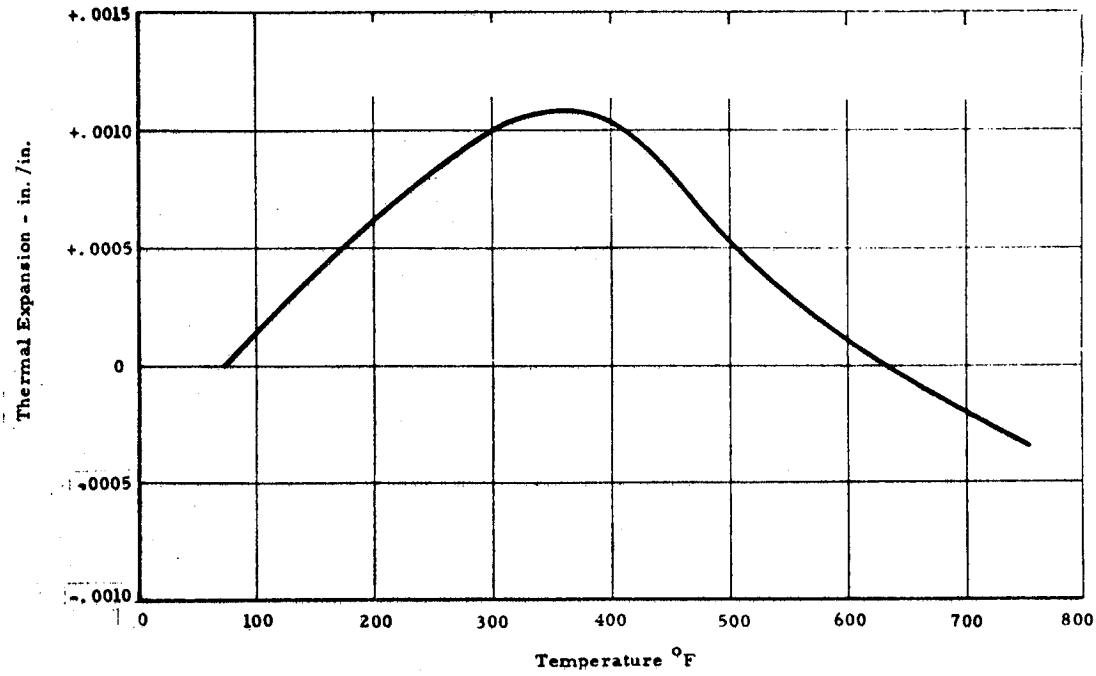

Figure 44a. Thermal Expansion vs Temperature for Silica Reinforced Phenolic in the Fill Direction

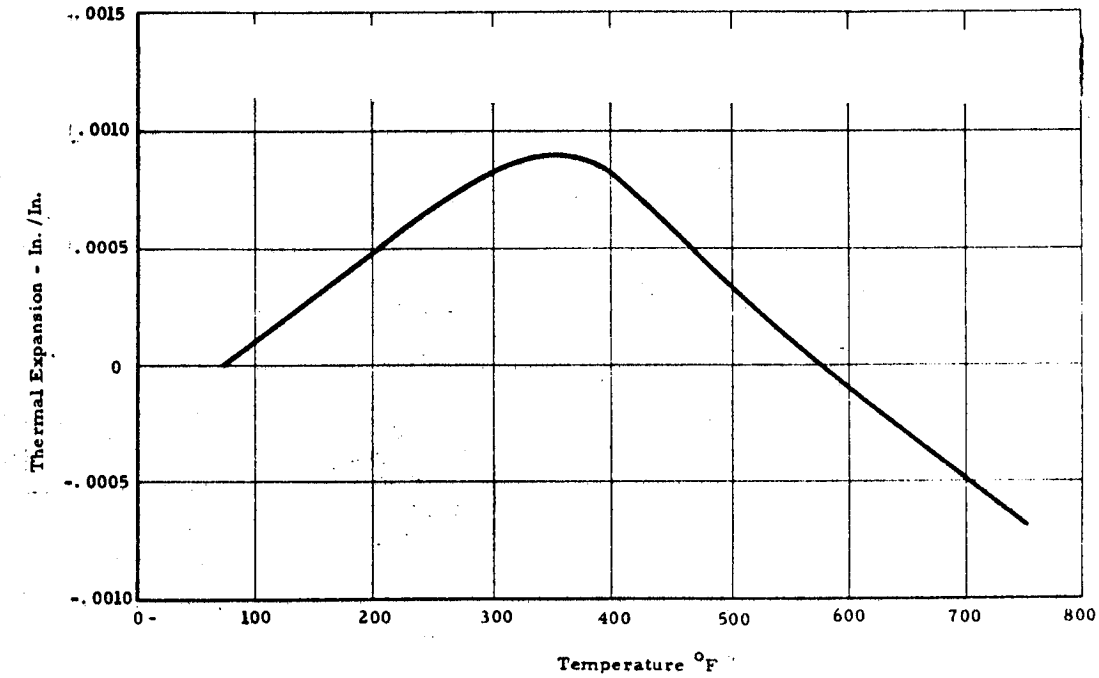

Figure 44b. Thermal Expansion vs Temperature for Silica Reinforced Phenolic in the Warp Direction

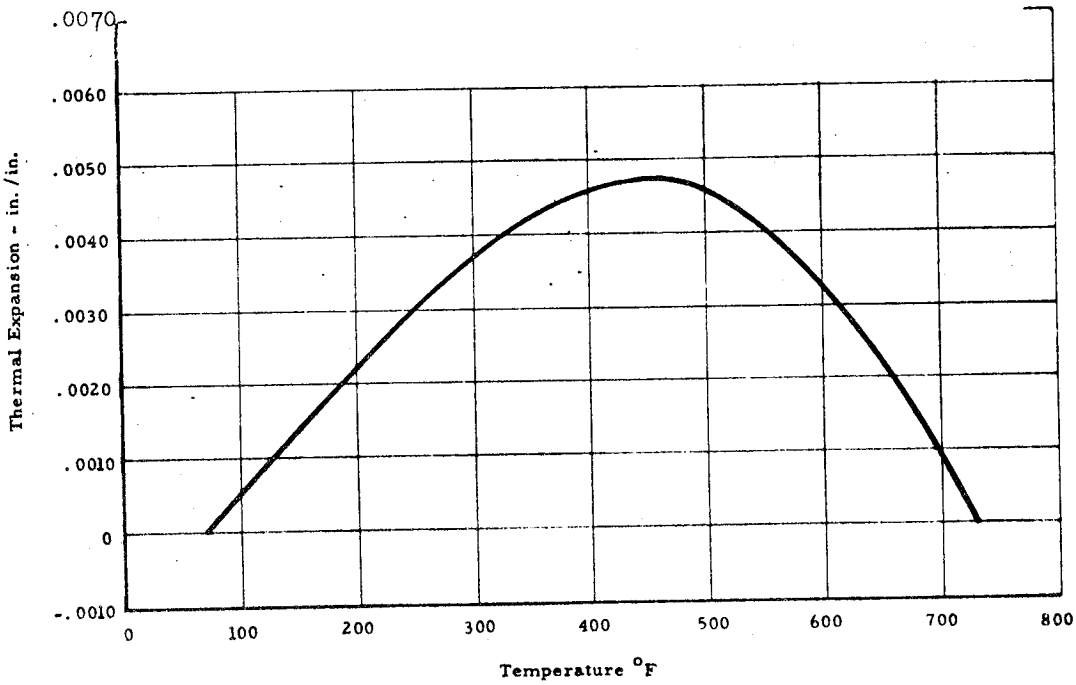

Figure 44c. Thermal Expansion vs Temperature for Silica Reinforced Phenolic Across Lamina Direction

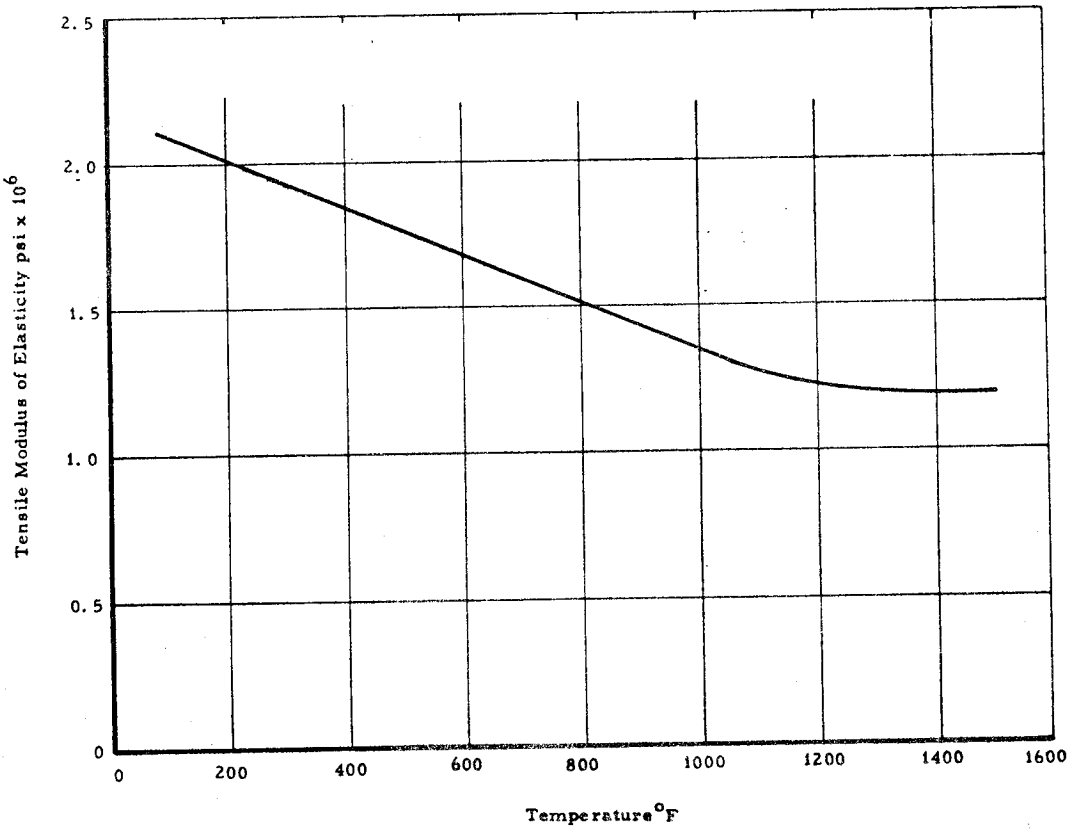

Figure 45. Tensile Modulus of Elasticity vs Temperature for Silica Reinforced Phenolic

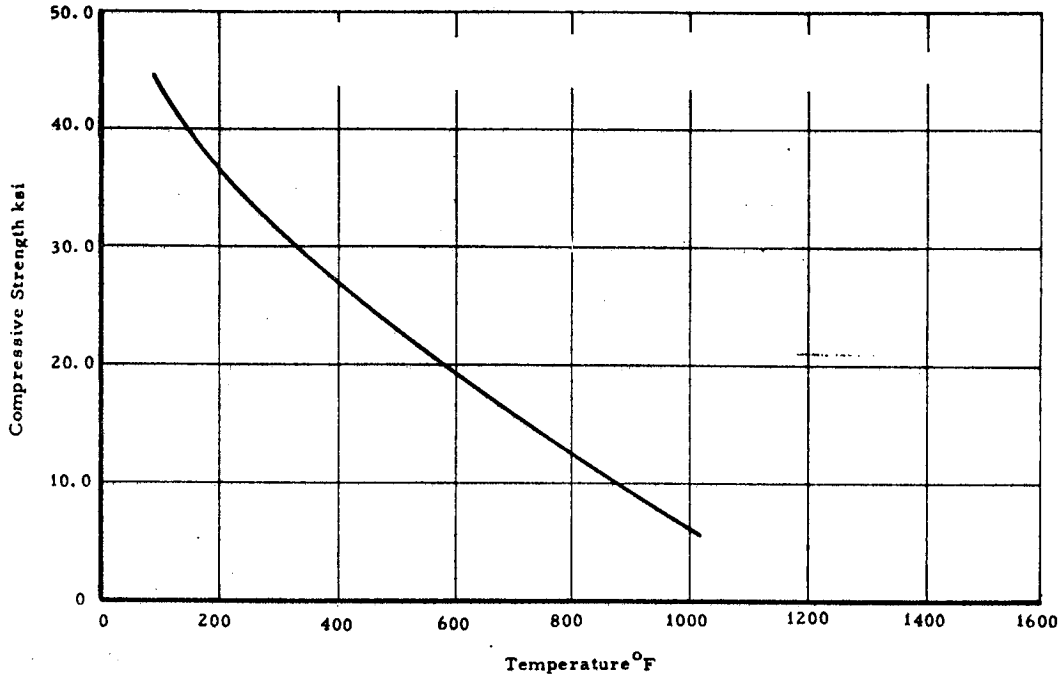

Figure 46a. Flatwise Compressive Strength vs Temperature of Silica Reinforced Phenolic

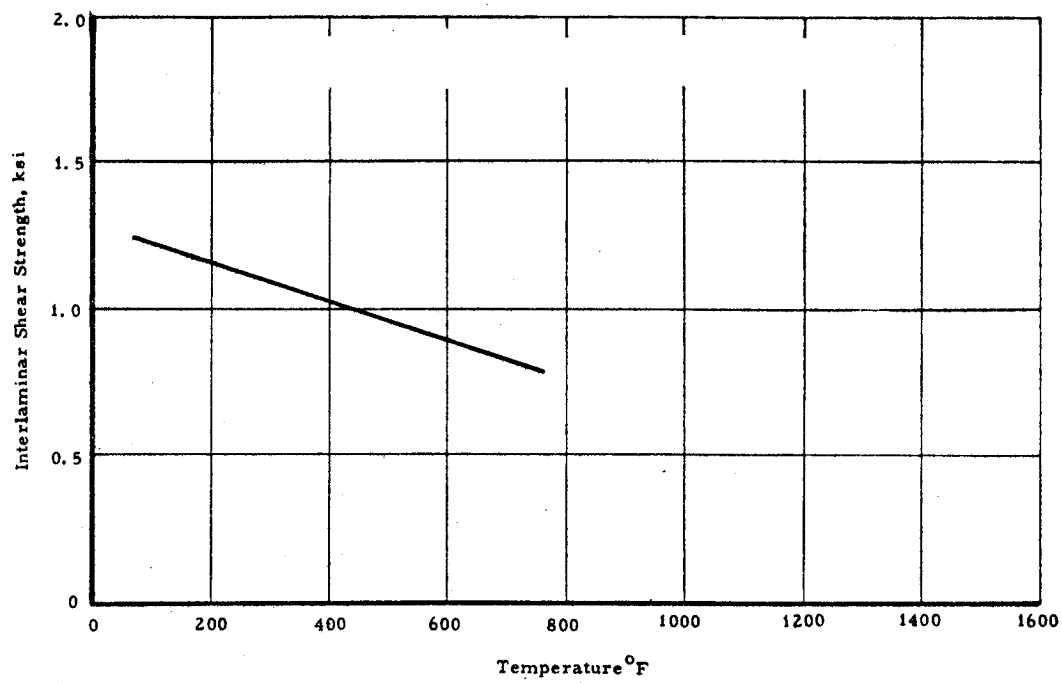

Figure 46b. Interlaminar Shear Strength vs Temperature of Silica Reinforced Phenolic

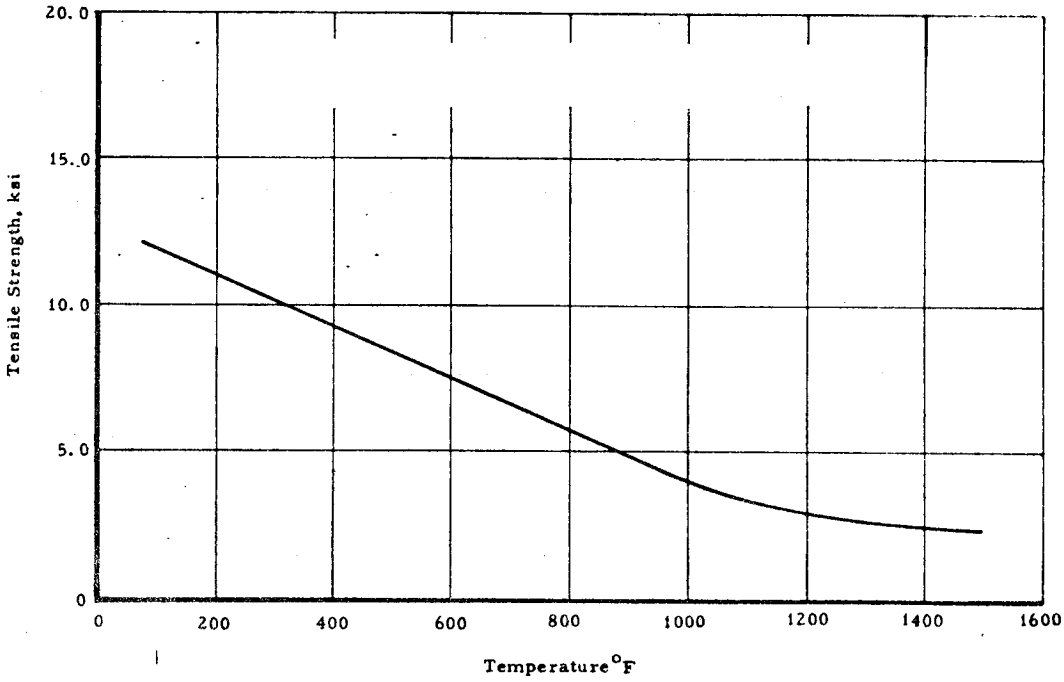

Figure 46c. Tensile Strength vs Temperature of Silica Reinforced Phenolics

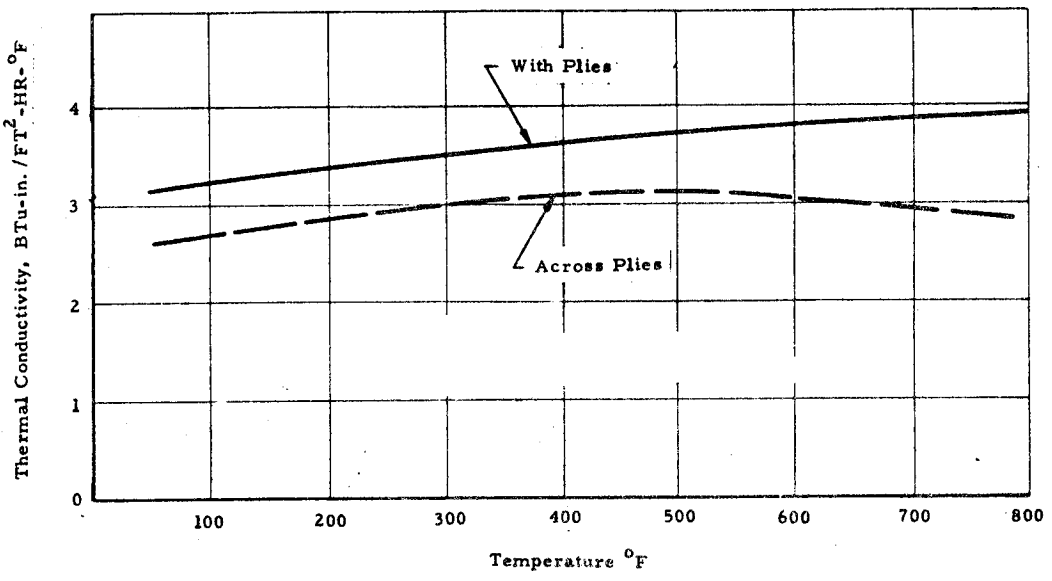

Figure 47. Thermal Conductivity for Silica Reinforced Phenolic

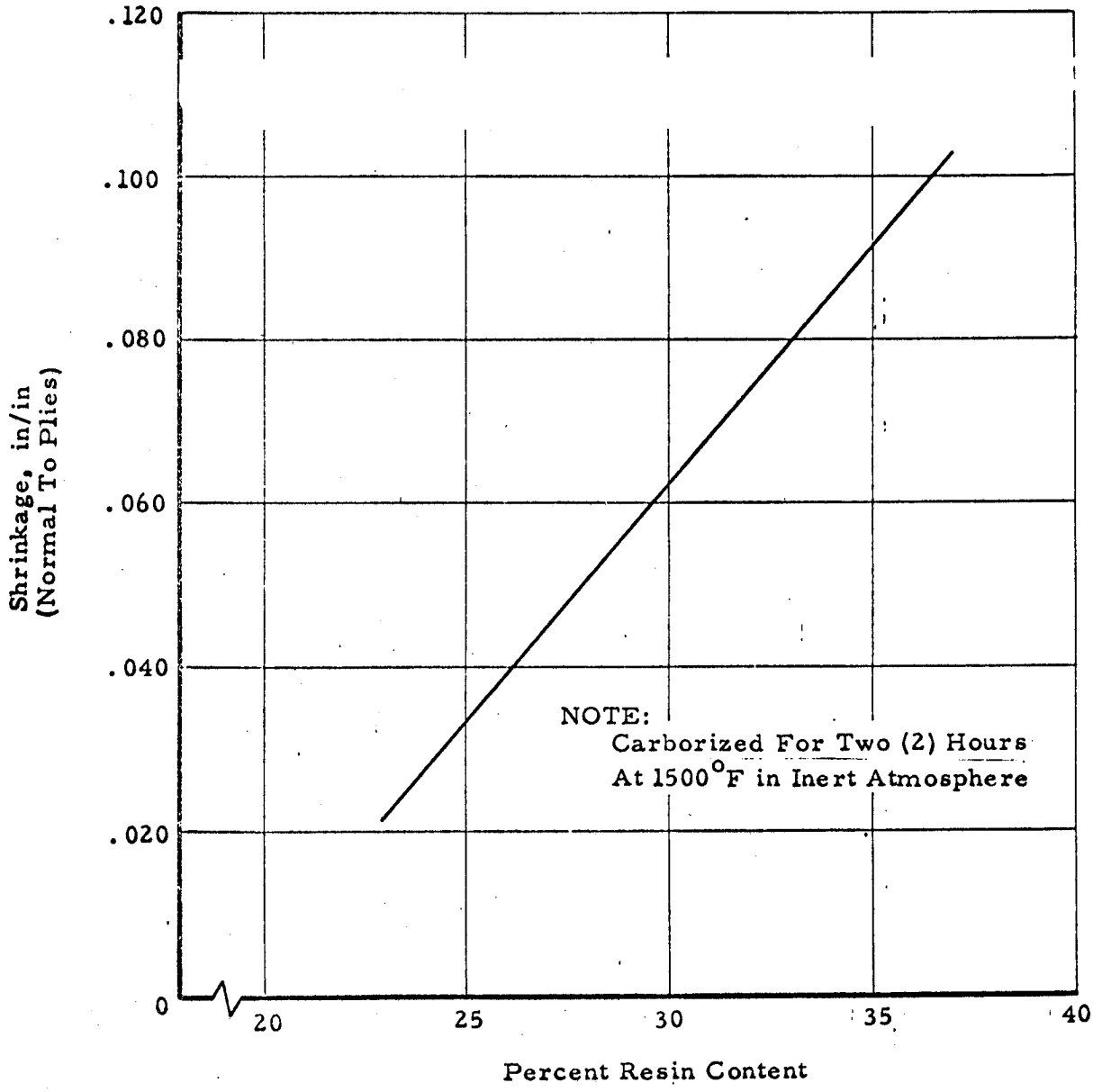

Figure 48. Shrinkage of a Typical Silica Reinforced Phenolic Composite as Affected by Resin Content

IV, D, Materials (Non-Metalics) (cont.)

ambiguities in the properties of the components subsequent to curing. The in-process requirements are discussed below under fabrication considerations.

The properties of the cured components complete characterization are listed below. These properties include those needed for thermal and stress considerations as well as for quality and reliability.

(1) Tensile and Compressive Strength at 2500°F
(2) Tensile and Compressive Modulus at 2500°F
(3) Thermal Expansion to 1500°F
(4) Impact Strength
(5) Density
(6) Thermal Diffusivity
(7) Specific Heat
(8) Thermal Conductivity

Some difficulty is expected in obtaining properties at 2500°F. However, measurements have been made on fibrous graphite composites at these and higher temperatures.

g. Fabrication Considerations

(1) Ablatives

(a) Fabric Orientation

The use of a preimpregnated flexible fabric which is formable prior to cure allows several choices for orientation of the fabric in relation to the gas flow (centerline of the chamber). An example of possible choices is shown in Figure 49. The most common is a fabric angle

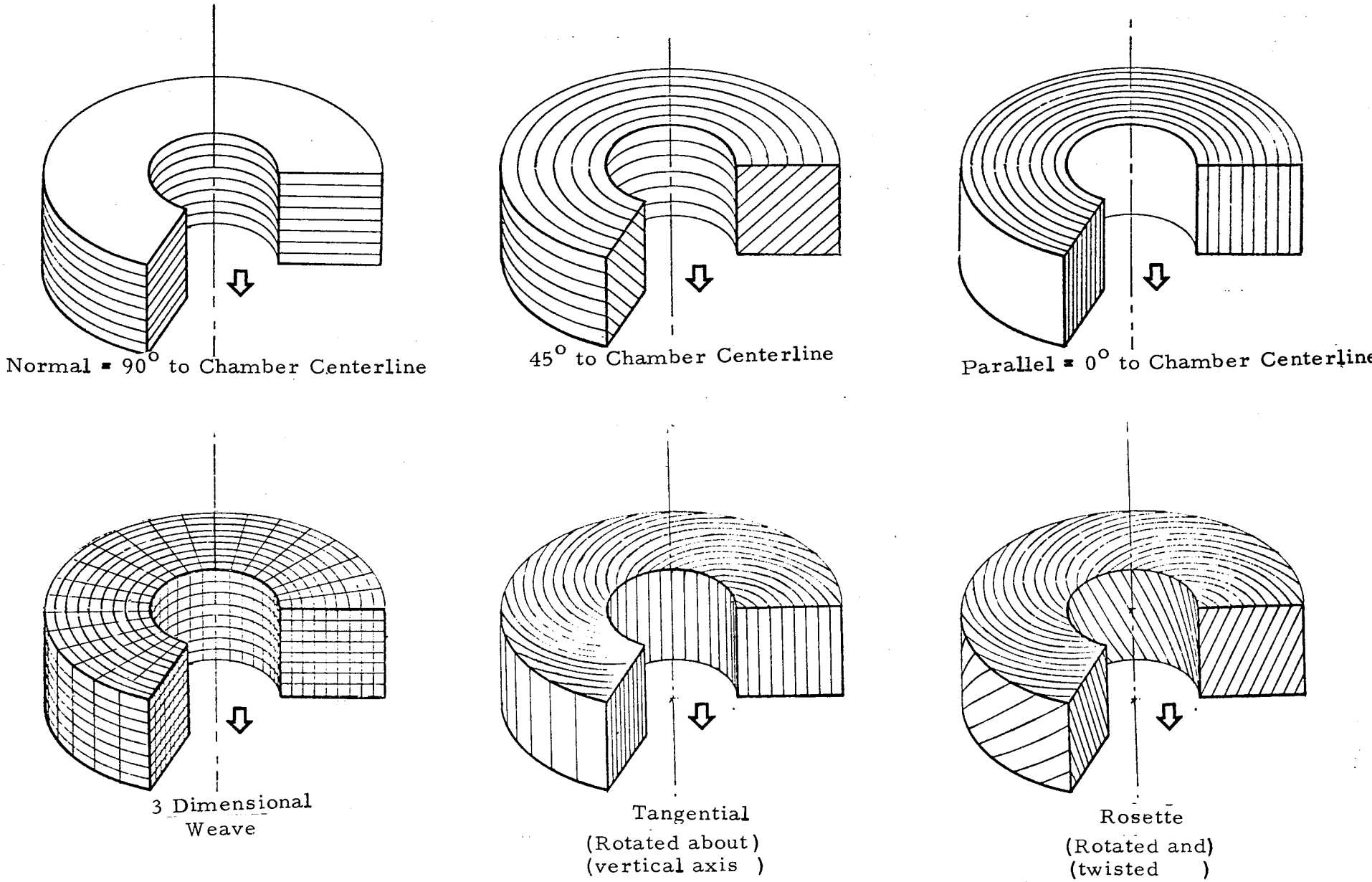

Figure 49. Typical Ablative Chamber Fabric Configurations

IV, D, Materials (Non-Metalics) (cont.)

between 90° and 0° to the gas flow in a cone or cylinder. This orientation may be achieved by the tape wrap or a cut pattern layup. The 3D is a woven fabric with yarns parallel perpendicular and circumferential to the centerline. In the "tangential" layup the ply is exposed to the interior surface parallel to the centerline and the rosette has three angles that can be varied to produce a variety of orientations.

The initial analysis indicated that a low angle (5° to 15°) would be best for an acoustic liner. A higher density can be attained during wrapping resulting in smaller wrinkles. Low-angle wraps had been successfully carbonized. There is less opportunity for delamination through the wall because of the long path between plies. The low-angle wrap is also a better structure to accommodate the orifices required in the acoustic liner.

Tape wrapping at fabric angles of 5° to 15° has not proven to be entirely satisfactory and therefore other fabric orientations and lay-up techniques were investigated. Two basic problems occurred with the low angle wrap. Delaminations occurred in fabrication during the carbonization process and there was some mechanical loss of fabric just aft of the acoustic holes during test firing. A higher angle (45°) or a rosette orientation eliminated both discrepancies.

(b) Cure Pressure

The effects of pressure variations during tape wrapping and curing on the properties of components fabricated from carbon-reinforced phenolics have been evaluated over the normal range used in fabrication of ablative plastic components (Ref 39). The findings in most instances are applicable to silica-reinforced phenolics because of the similarities in

IV, D, Materials (Non-Metalics) (cont.)

the preimpregnated raw materials. It has also been established that the virgin ablative and charred densities affect the surface regression rate of silica phenolic (Ref 38). Processing factors which affect the density of silica phenolic are basically the same regardless of material system. Percent-resin content, the pressure applied by the tape-wrapping roller, and the cure pressure are perhaps the most significant. These parameters not only affect density and thereby surface regression but also affect the mechanical and thermal properties. For example, a low wrapping pressure produces a low as-wrapped density. Application of cure pressure produces wrinkles which significantly decrease hoop tensile strengths and change the transient thermal expansion profile as the temperature rises in the inner wall.

Applications of cure pressure and carbonization are also fabrication processes which can vary significantly, thereby affecting the performance of the ablative component. In addition, there are lay-up/molding processes other than tape-wrapping/hydroclave-cure which should be considered for the acoustic liner fabrication. The primary method that can be considered is a 3D weave of the silica reinforcement. This and alternative techniques have many of the same process variables plus some individual variables which must be controlled to ensure quality and reproducibility.

(c) Tape Wrapping Methods

The tape wrapping method basically consists of wrapping a warp or bias cut tape of a specified width onto a mandrel. An example of the wrap and bias weave direction is shown in Figure 50. The tape width is dictated by the fabric angle, tape elongation with resultant change in the width of the tape, requirements for final wall thickness, and as-wrapped density. The as-wrapped density is a function of (1) degree of advancement of the prepreg, (2) roller pressure, (3) wrapping rate (mandrel

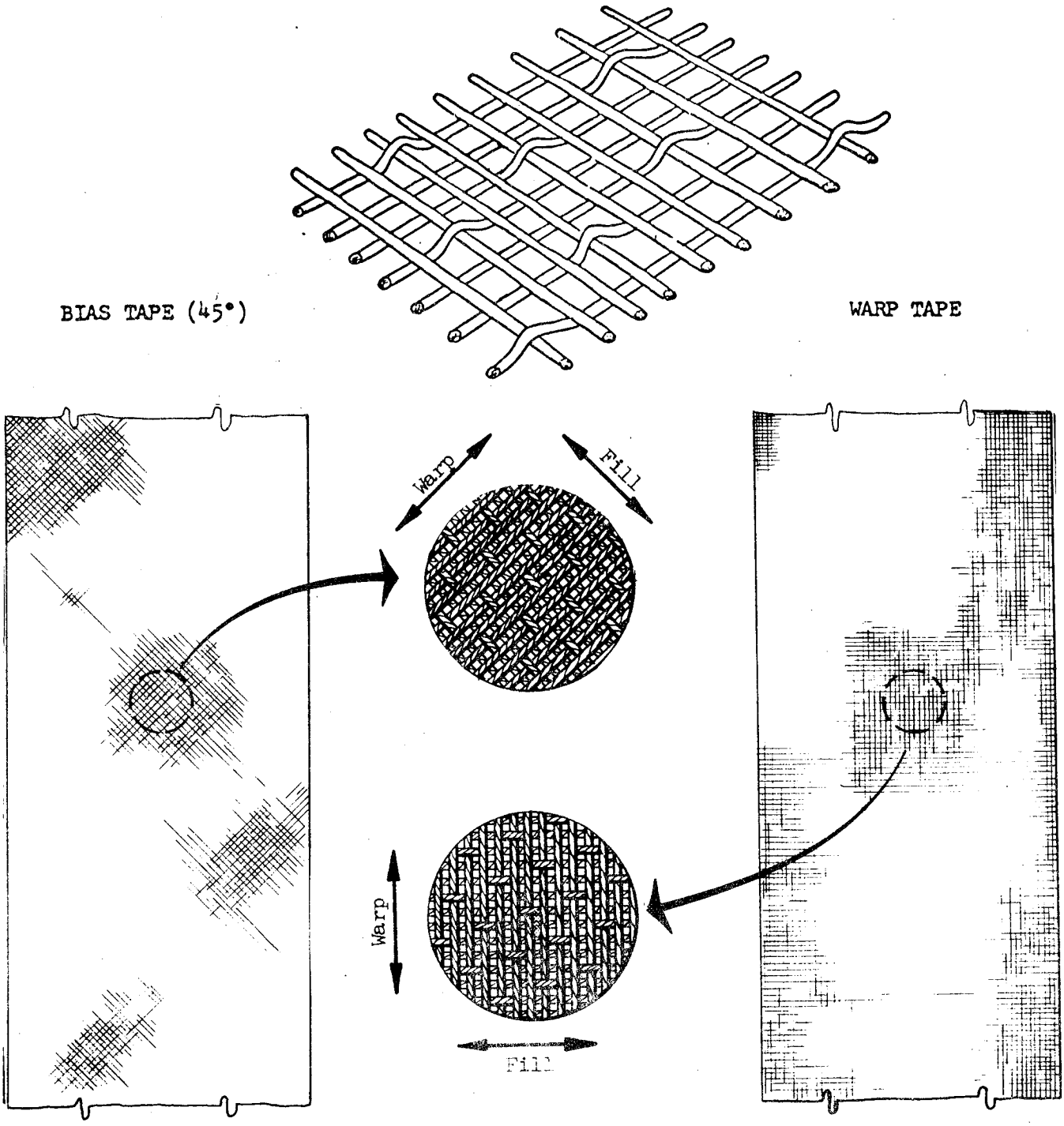

Figure Illustration of Fabric Tapes Showing Direction of Warp and Fill Fibers (Weave Shown is an 8 Harness Satin)

speed in rpm), (4) mass temperature, and (5) tape temperature (Ref 39). The criteria for establishing the limits for these process parameters are to achieve as high debulk as possible without damaging the reinforcement and to obtain a wrapped billet which is knitted together by the cohesive bonding of the resin at the reinforcement interfaces. The significance of the roller pressure and tape temperature on the physical interlocking and the resultant effect on interlaminar shear have not been ascertained. However, it is feasible to fabricate with extreme roller pressure and tape temperature which could significantly reduce the interlaminar shear strength of the cured composite. Over advancement of the resin could reduce the cross linking of phenolic at the interface and excessive pressure could reduce the physical nesting of the fabric.

Two literature sources are used primarily to establish the tape wrapping methods for the segmented liners. They are described in References 38 and 39.

(d) Molding Methods and Curing

The most economical and reliable technique for fabrication of ablative cylinders or cones for rocket nozzle components has been tape wrapping followed by an autoclave or hydroclave cure. However, requirements for each component must be analyzed in order to select the best technique. The molding pressure required to achieve the desired density is the primary parameter to be selected. The cure cycle including heating rate, maximum time at temperature and time at temperatures below the final cure temperature should be ascertained. It has been demonstrated that cure pressures between the limits of 200 and 1000 psi have only minor effects on the resultant composite density when the as-wrapped density was 90% or higher (Ref 39). A system with a highly advanced low resin content is very sensitive

IV, D, Materials (Non-Metallics) (cont.)

to pressure application and requires pressures of 1000 psi or more for good densification. The thickness of the component is also a factor which affects the cure pressure required. In general, two hours of curing at 300°F are adequate for most phenolic systems.

A minimum pressure of 200 psi and a cure cycle of two hours at 300°F (part temperature) is selected for the silica-reinforced acoustic liner candidates. Those components which are to be carbonized are also post cured (after removal from the mandrel) for five days up to 500°F to relieve stress and further devolatilize the components. Some decomposition of the resin also occurs during extended exposure to 500°F.

(e) Carbonization

Carbonization (decomposition or pyrolysis) occurs as the phenolic resin is heated above 500°F (Ref 41). The decomposition of the phenolic molecule produces a residual carbon (approximately 50 percent by weight) and various gas constituents including methane and water vapor (Ref 42) accompanied by shrinkage (Ref 39) primarily across the plies of the laminate, microscopic cracks of varying dimensions are produced in the residual carbon matrix. In many instances, delaminations and micro cracks occur, particularly if the heating rate is very high, as in a rocket nozzle environment; however, slow heating in an oven (in an inert atmosphere) reduces the tendency of the composite to delaminate. Many components made of carbon and graphite-reinforced phenolics have been carbonized by a slow cycle, varying from 48 hours to two weeks, without delamination. Silica-reinforced test specimens also have been carbonized in the laboratory up to 1500°F without delaminations. Demonstration of the carbonizing of an acoustic liner configuration made of silica-reinforced phenolic as shown in Figure 51 has been accomplished during the ALFP program. The carbonization cycle previously used for a graphite reinforced phenolic, AGCarb-101, was chosen for the ALFP ablative acoustic liner.

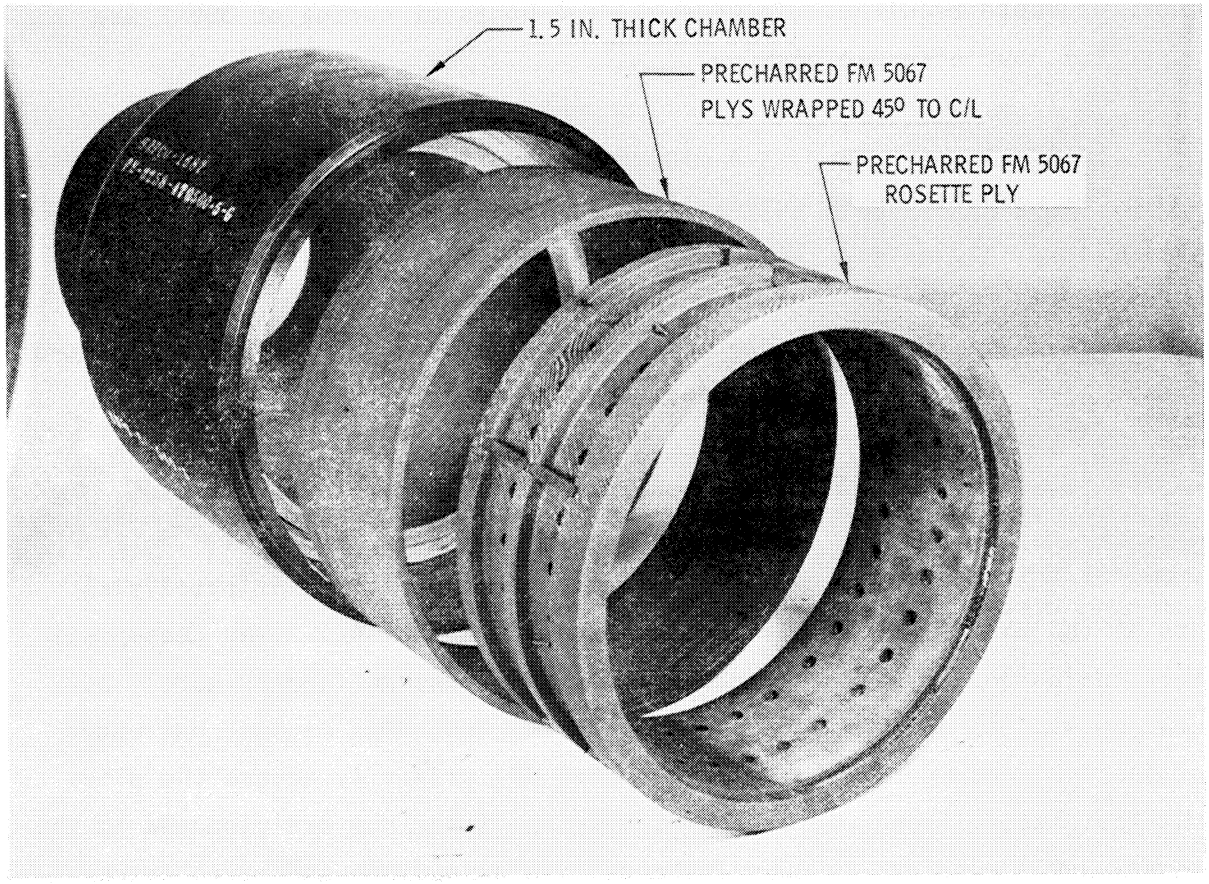

Figure 51. Carbonized Acoustic Liner

IV, D, Materials (Non-Metalics) (cont.)

Composite systems with a reinforcing fabric or fiber in a carbonized resin or pitch have been demonstrated to retain enough structural integrity to be utilized as rocket nozzle components.

Comparisons of mechanical properties of carbonized carbon, graphite and silica-reinforced phenolic, show the silica-reinforced systems decrease in strength rapidly above 2500°F and the carbonaceous systems retain strength above 4500°F. The latter system retains compressive strengths of 300 psi after a 10 minute soak of 2500°F. The compressive specimens are tested with plies of reinforcement parallel to load; therefore retention of bond and shear strength between plies is also indicated at 2500°F. Complete characterization has not been accomplished for charred silica-reinforced systems. The carbonized or precharred systems are preferred for candidate materials over virgin systems for the following reasons:

1 Shrinkage across the plies is less than 1 percent for carbonized silica reinforced phenolic (as against greater than 5 percent for the same material in an initially uncarbonized condition).

2 Delaminations almost always occur during pyrolysis of a virgin ablative liner, but do not with carbonized ablatives, or if delaminations do occur they can be corrected by reimpregnation with resin.

3 Design is less complicated if adjacent components can be fitted to a stabilized system.

4 The contribution of outgassing toward extending the life of a silica reinforced composite is negligible based on heat transfer analysis.

IV, D, Materials (Non-Metalics) (cont.)

5 A virgin material is usually charred (and possibly delaminated) early in a test firing and therefore offers no significant advantage.

6 The retention of strength at elevated temperatures, thermal shock resistance, and dimensional stability of carbonized composites indicates their suitability for an acoustic liner.

(2) Composites

(a) Material Layup

The composite systems considered were reinforced zirconia. Zirconia fibers are produced in several forms including woven fabric, needled felt, and bulk fibers. The zirconia fiber or fabric, like other standard reinforcements, can be impregnated with organic resin; however, composites can also be made by using a zirconia cement as the matrix to hold the fibers and/or fabric. The wet layup fiberglass-resin procedure is presently utilized. The fabric is precut to the dimensions needed, impregnated with the zirconia cement and laid-up to the configuration required. The basic considerations are the same as for any fiberglass resin lay-up -- the percentage of matrix material, wet-out in individual fiber bundles, shelf life (time from impregnation to lay-up), removal of excess matrix material or volatiles, etc., must be considered. Exacting control limits for these processing parameters have not been established and the resulting laminates therefore contain voids. Accordingly, some effects of processing on performance may be erroneously attributed to an inherent characteristic of the material. Documentation of the processing steps is required to assist in evaluating the performance of test samples of composite systems.

IV, D, Materials (Non-Metalics) (cont.)

(b) Molding and Curing

The molding and curing technique is dictated by the composite material and the configuration being fabricated. Most of the composite systems are in the developmental stage; therefore, each step of the molding and curing procedure should be documented. Control limits should be used if they can be ascertained.

(c) Sintering

A reinforced-zirconia system requires an additional processing step of sintering after curing. Trade-off studies as to the best temperature, time and atmosphere are not conclusive, and the best cycle for mechanical properties does not appear to be the best for performance as an acoustic liner in a liquid chamber environment. A higher sintering temperature reduces the shrinkage and, therefore, reduces the tendency to delaminate and distort. The best sintering temperature for thermal shock resistance has not been established. Documentation of individual steps is normally required and limits established if there is sufficient fabrication history available.

2. Materials Trade-Offs

It is not possible to make a satisfactory systematic, quantitative comparison of the various materials studied, their properties, or their compatibility in liquid rocket motor environments. However, there are sufficient data from the background experience and the literature survey to perform qualitative trade-off studies. The factors which received the most weight were necessarily durability, reliability, and economics, with allowance for the amount of available information related to performance in similar

IV, D, Materials (Non-Metalics) (cont.)

test conditions. Basically the comparisons were made between ablatives, other composite systems, and coatings. In addition, trade-offs are made within each of these categories.

a. Ablatives

(1) Charred vs Uncharred

The ablative materials considered include reinforced phenolic materials both in the virgin and charred condition. The former are most often used for liquid rocket nozzle components. In the (virgin) uncharred condition the initial heat penetration is slower and the fabricated components are less expensive than precharred materials which require additional processing. Virgin materials char during the motor firing, delaminate, and shrink upon exposure to the combustion gases; a slow precharring cycle generally reduces the delamination and separations. It therefore appears feasible to fabricate an acoustic liner and prechar it before installation. The retention of strength at elevated temperatures, thermal shock resistance, and the dimensional stability of charred (carbonized) materials indicate the suitability of a carbonized component as an acoustic liner.

The precharred liner would be more dimensionally stable during testing and be less prone to delamination, enhancing both the durability and reliability of the liner. The additional cost would be less than 10 percent higher than an ablative liner made from virgin material. The precharring would not change the compatibility with the combustion gases. The conversion of the resin to char would occur in the same way as during testing but would take place under controlled conditions.

IV, D, Materials (Non-Metalics) (cont.)

(2) Reinforcement Trade-Offs

Several types of fibers are utilized as reinforcements for resins to make ablative rocket nozzle components. Those most frequently used are carbon, graphite, silica and asbestos, but Nylon, carbon-silica and quartz are also used in special applications. Zirconia fabric, silicon carbide fibers, cellulose fabrics and papers and many organic reinforcements are also available.

Silica reinforced phenolics are generally used in liquid rocket motors operating at low- or intermediate-pressures where oxygen or an oxygen compound is the oxidizer. Both carbon and graphite are readily oxidized by the combustion gases where oxygen or its reactive compounds (H_2O, CO_2, N_2O_4) is present. Silica is limited primarily by its melting temperature, approximately 3000°F. Therefore, a silica reinforced phenolic, with wall temperatures exceeding 3000°F, will regress as it melts.

Higher melt temperature reinforcements as well as resistance to oxidation are needed in the more severe environments. Zirconia cloth with a reported melt temperature of 4700°F appeared to have the needed melt temperature and oxidation resistance and appeared to be superior to silica. However, the cost of the raw material is 20 to 40 times that of silica, the fabrication technique is not fully developed, and the stability and reliability are unknown (Ref 37). Silicon carbide whiskers or fibers, with melting temperature of 4100°F, cannot be fabricated by conventional techniques; impregnation, bonding and distribution technology is still in the development stage and costs are high ($100 to $200 per lb). Carbon silica (avceram) is a unique combination, 70% silica and 30% carbon, with the possibility of combining the best in each reinforcement. The cost is intermediate between silica and carbon fabric; therefore, it appears to be a prime candidate.

IV, D, Materials (Non-Metalics) (cont.)

(3) Resins

The primary requisite for a resin system is the carbon yield after decomposition, when it should provide a carbon matrix to retain the reinforcement and produce an integral composite. Phenolics have hitherto been the primary resins used in rocket nozzle components. Charring of a phenolic consists in the coalescing of a 6-member benzene ring after the loss of hydrogen and pendant groups. The carbon yield for the many varied resin systems classified as phenolics is generally 50 $\pm$ 5 percent (Ref 38). There are other resin systems which offer potentially as great or greater carbon yields: polyphenylenes, polyimides, and epoxy novolacs. Costs of these resins range up to $500/lb. The lower cost polyphenylene and polyimides have not demonstrated a significant improvement over the "standard" phenolics either in carbon yield or ablative performance.

(4) Fillers

Phenolics used as ablatives are classified as filled and unfilled. The filled resins contain small particles, generally microscopic, of inorganic fillers. Differences in ablative performance have been negligible, and therefore the presence or lack of filler was not a criterion for evaluation of the resin systems. Oxidation-resistant fillers were considered; however, the data available do not support a conclusive judgement concerning their performance in liquid rocket nozzle environments.

(5) Density

The performance of ablatives, whether virgin or charred, is related to density. However, all of the virgin silica-reinforced systems that were considered had minimum densities of 1.70 gms/cc. On the

other hand, densities of the precharred systems can be increased by a reimpregnation process after carbonizing. Since the additional improvement in mechanical properties and firing performance was unknown, the initial testing was accomplished without attempting to increase density of the carbonized composites.

(6) Sources of Raw Material

There are several silica-reinforced phenolic materials from the various "prepreg" material suppliers which are basically the same; the differences include type of phenolic resin, ease of fabrication, cure cycle required, fillers, and small variations in price. Because of the high cost of testing and screening, not all of the available silica phenolics were evaluated; however, with few exceptions, those with a cured density of 1.70 gms/cc and a resin system which yields 50 $\pm$ 5 percent carbon char were considered equivalent. The silica reinforced phenolics that were used were selected because of characteristics demonstrated during other test programs. Sufficient comparisons could not be made during the laboratory test phase of this program to establish their superiority for use as acoustic liners over the other silica-reinforced phenolic systems that are known.

b. Composite Systems

The other composite systems considered were in general much more costly than the ablative systems, but those systems such as silicon carbide and silicon-infiltrated fibrous graphite would be significantly more durable than the silica-reinforced ablatives. Unfortunately, the processing has not been demonstrated sufficiently reliable and performance ranged from very good (no regression) to almost total failure. Therefore, these composite systems were not used as acoustic liners because of the high cost and doubtful reliability.

IV, D, Materials (Non-Metalics) (cont.)

The thermal shock resistance of ZrO_2/ZrO_2, SiO_2/ZrO_2, (fabric material/resin) Pyrocarb and Pyrolarex (silicon infiltrated) was not known for a liner configuration. Therefore, reliable performance of the acoustic liner could not be assured for the multiple start application. In addition, the costs were high because of the special tooling and facilities needed as well as of the raw material.

c. Coatings

For coatings to provide protection to the liner substrate, the requirements were: a material with a high melting temperature (above 3000°F), thermal shock resistance, resistance to oxidation and adhesion to the substrate. The amount that a coating can extend the useful life of the liner substrate depends on its compatibility with the propellant exhaust gases. The oxides of aluminum and hafnium appear to be best adapted for high melting temperature and resistance to oxidation. The resistance to thermal shock and the degree of adherence to a substrate are unknown. The cost for applying the coating is rather low (less than 10 percent of the cost of the substrate); however, the durability is questionable until the coatings can be retained on the substrate. Coatings can be applied to a silica-reinforced liner after charring without detriment to the liner material; therefore, the evaluation of such coatings can be combined with an evaluation of charred silica-reinforced phenolic.

3. Materials Problem Areas

a. Conventional Problems

There are certain criteria which affect any material system used in a liquid rocket nozzle, and they also apply to the design and

IV, D, Materials (Non-Metalics) (cont.)

fabrication of an acoustic liner. These are: compatibility with the propellant combustion gas environment, processing and quality control of the hardware, and capability of surviving a multiple start test schedule.

(1) Compatibility

The materials used for an acoustic liner must be chemically compatible with the combustion products in the chamber. Fuel film cooling is frequently used to maintain a boundary layer which does not react with the liner materials. However, streaking from the impingement of oxidizer or mixed propellants on the liner wall produces localized regression of materials of silica-reinforced phenolic which might eliminate them from use for acoustic liners operating for extended (greater than 100 seconds) duration.

A recommended solution to the problem of material compatibility is the use of higher melting reinforcements, other composite systems, or ceramic coatings. However, the component cost will be increased and there will be a sacrifice of reliability. The problem of compatibility must be further evaluated for each injector or injector modification. Empirical trade-off studies of hardware in a full scale design are needed to resolve problems of compatibility and durability in those applications where silica-reinforced systems are not sufficiently compatible to assure serviceability for an extended duration.

(2) Processing

Designs should be developed for full scale hardware made of either composite systems or ceramics. Demonstration on a full scale would be needed of the fabrication and processing technique. Some material and process development would be required for most systems. In addition to

the processing of ceramics and other composite systems, there are problems associated with the fabrication of ablatives. The variables and their effects on cured components properties are discussed in detail in Reference 38. Additional problems of shrinkage, distortion and delamination are inherent to the carbonizing step for fabricating precharred materials. The effects of fabric orientation, resin system, reimpregnation, and carbonizing cycles on silica-reinforced ablatives have not been ascertained. Development is required to obtain optimum gain from each variable, and until then informed judgement must be applied in the selection of the fabric orientation, resin system and process cycles. Results of related material and process studies should be used where available.

(3) Quality Control

A definition of acceptable quality control and of the quality level of silica-reinforced phenolic in the uncharred condition has been established (see Refs 38 and 39). However, the quality control requirements for charred silica-reinforced phenolics and other composite systems with and without coatings have not as yet been established. Processing steps must be documented and end products characterized to assure identification of significant variables which could affect the performance of these materials in an acoustic liner. The reliability level of these components cannot be satisfactorily established without complete documentation and characterization. The cost of characterization for all candidates is prohibitive and furthermore some systems have proprietary processing which is not available for analyses. Therefore, the necessary quality control cannot be fully defined in these cases.

IV, D, Materials (Non-Metalics) (cont.)

(4) Restart

The endurance of a material after multiple start-stop cycles requires a low sensitivity to extreme temperature changes (ΔT to 3000°F or ΔT to 5000°F). Silica-reinforced phenolics in the charred condition have demonstrated this quality up to 3000°R. The capability of other composites, ceramics and coatings to withstand repeat heat-up and cool-down cycles has not yet been demonstrated.

b. Acoustic Damper Problems

(1) Lack of Industry-Wide Liner Experience

There are unique problems related to the acoustic apertures which extend through the liner and to the gas cavities behind. There is no wide industrial experience of the effect on silica-reinforced phenolic when its strength and ply-integrity have been compromised by cutting apertures through the reinforcing fabric, as is done in fabricating an acoustic liner. There is concern because the cavity area is unsupported. Also there is no history to show effects of gas flow through the apertures; composite systems or coatings which are brittle and sensitive to thermal shock will be more prone to crack or break-up where there are apertures. Localized areas of support between cavities will also produce mechanical and thermal stress concentrations, as discussed under IV,D, Structures.

(2) Lack of Durable Materials

Perhaps the most significant problem is obtaining a material capable of performing through multiple stop-start cycles for extended duration without fuel film cooling or barrier cooling. Materials which retain strength at high temperatures are sensitive to oxidation.

IV, D, Materials (Non-Metalics) (cont.)

Those which are resistant to oxidation have low melting temperatures or are brittle and sensitive to thermal shock. Those composites which appear to provide the best combination of properties for continuous operation without film cooling are comparatively high in cost and require additional development of fabrication processes.

IV, Design Mechanics (cont.)

E. STRUCTURAL CONSIDERATIONS

1. Structural Analysis

Considerable design, analytical, and testing experience has been amassed concerning problems inherent in high temperature applications of anisotropic non-metallic materials. Further experience has been collected on metallic isotropic structures subject to high heat fluxes as the outgrowth of the successful design and testing of ablative, radiation-cooled, and regeneratively cooled chambers. Of particular interest in an acoustic liner structural analysis is the previous experience acquired from the results of the use of acoustic liners to damp combustion instabilities on other programs.

a. Review of Experience

Several acoustically damped thrust chambers have been built and successfully tested; one configuration, in particular, is directly related to the design of successful acoustic liner structures. Under the LF_2/N_2H_4 (BA-1014) Ablative Thrust Chamber Program (Contract F04611-67-C-003) (Ref 20) an AGCarb-101 acoustic liner was built and tested. This anisotropic non-metallic material exhibits properties which are very directionally sensitive. While no structural failure of the resonator occurred during testing, it was analyzed in light of a structural failure of the chamber throat, attributable to a poorly manufactured part and excessive radial restraint. Using the chamber experience, the stresses in the acoustic resonator were reduced by making the liner thinner, thus reducing the thermal gradient, and making allowances for both radial and longitudinal expansion, thus reducing the compressive loads induced by external restraints. Successful testing of the liner verified the analytical approach.

IV, E, Structural Considerations (cont.)

b. Environmental Considerations

Experience in the analysis of thrust chamber components has shown that, while pressure distributions are an important design consideration, temperature gradients pose the most severe structural problems.

The acoustic liner is exposed to a severe thermal environment and to pressure gradients resulting from combustion instability and detonations from pulse charges. The thermally induced stresses are the more significant and because the thermal gradients are often steep an understanding of their magnitude is very important, especially when brittle materials are used or when the chamber is subjected to a large number of temperature cycles.

Finite element computer programs presently used in structural analysis can readily handle these thermal gradients and pressure perturbations.

c. Material Properties

The mechanical characteristics of the materials employed are most important for stress analysis. Metals are generally well covered by the standard references such as MIL-Halbk-5,"Aerospace Structural Materials Handbook" and supplier data sheets. Non-metallics, such as the materials used for ablative chambers, do not presently have the structural characterizations necessary for sophisticated analysis (as indicated by the limited data in Figures 44 through 48). It is difficult to acquire sufficient additional data concerning laminated materials, which exhibit vastly different material properties in the warp, fill, and cross-ply directions and are very sensitive to fabrication and testing techniques.

IV, E, Structural Considerations (cont.)

The material properties necessary to a structural analysis are:

(a) Young's modulus
(b) Ultimate tensile and compressive strength
(c) Coefficient of thermal expansion
(d) Shear strength
(e) Poisson's Ratio

The above properties should be defined for the warp, fill, and cross-ply directions and in the full temperature range of the operating environment.

d. Method of Analysis

The analytical tools are conventional stress analysis techniques and several computer programs which have been used reliably for a number of years in the industry literature as evidenced by test correlations on all solid and liquid rocket programs. Finite element computer programs are employed in the analyses:

(1) Finite Element Computer Programs

The finite element method is applied to the determination of displacements and stresses within plane or axisymmetric solids with linear or nonlinear material properties. The continuous body is replaced by a system of elements of triangular or quadrilateral cross-section. Since the elements are of arbitrary shapes and material properties, the procedure may be applied to structures comprised of many materials and configurations.

IV, E, Structural Considerations (cont.)

In the finite element approximation of solids, the continuous structure is replaced by a system of elements which are interconnected at joints or nodal points. Equilibrium equations, in terms of unknown displacement of the nodal point, are developed at each joint. Solution of this set of equations constitutes solution of the system.

The advantages of the finite element method, as compared to other numerical approaches, are numerous. The method is completely general with respect to shape and material properties. Complex bodies and anisotropic material, and filament structures are readily handled.

(2) Finite Element Analysis for Thin Shells

The finite element analysis is also applicable to elastic isotropic shells of arbitrary shapes and is ideally suited for axisymmetrical or non-axisymmetrical thrust chambers provided the "R/t" ratio is not too low. A plate element shell analysis is formulated by: 1) approximately representing the shell as a series of flat plate elements; 2) expressing the membrane and bending characteristics of a plate element by combining a plate-bending element with a plane-stress element, and 3) insuring the compatible response of the adjacent elements.

e. Basic Assumptions and Limitations

Stress analysis is based on Hook's law where all elements of the structure remain elastic and linear. In structures whose loading is very complex, as where there are thermal gradients, and whose physical properties are non-linear, as in the case of laminated structures, the stress and strain relation is not always linear. For this reason it is

IV, E, Structural Considerations (cont.)

extremely important to have complete knowledge of the material behavior. The accuracy of the analysis is established by the accuracy of the data concerning material properties and the exactness of the knowledge as to temperature distributions.

f. Boundary Conditions

The acoustic liner will be unrestrained after assembly and therefore in the initial phases of chamber operation, the liner will be considered a free cylinder. However, as the temperature in the liner rises (and it will heat much faster than the surrounding structure) the liner will expand radially and the resonator spacer rings will contact the outer structure. At this point the liner will be analyzed as a supported cylinder.

g. Identification of Failure Modes

There are several modes in which the liner can fail structurally. Aside from material delaminations the liner can fail in hoop compression if sufficient radial clearance is not allowed at the points where the liner contacts the backup structure. This is one of the reasons why it is important to have an accurate assessment of the temperature distribution with respect to time. For the same reason it is important to have an accurate set of expansion characteristics for the material.

The liner can fail in axial compression if the liner is not allowed to grow freely in the axial direction. Again it is important to have complete thermal and material data to establish the axial gaps.

If brittle materials such as zirconia are used the temperature gradient through the liner will be enough to cause cracks at the

IV, E, Structural Considerations (cont.)

ports both axially and circumferentially. The cracks will start on the backside of the liner and propagate to the inside.

The pressure differential across the liner can reach the point where the liner can fail in hoop tension. This can only happen early in chamber operation since the liner gains support from the rest of the chamber when the liner heats.

(1) Steady State Loads

Under steady state operating conditions there is no pressure differential between the chamber and the acoustic cavity. However, the chamber must be capable of withstanding the chamber pressure loads without excessive radial deflections. If the chamber expands too far in the hoop direction, the liner will become loose and subject to vibration as well as hot gas leaks through the liner cavity.

(2) Dynamic Loads

The mechanical response of the acoustic liner is related to the hoop natural frequency of the chamber. Resonance may develop between the acoustic input from the combustion and the natural frequency of the chamber-liner system. The resulting amplitude is

$$A = \frac{F}{2k} \omega_n t \text{ Sin } (\omega_n t),$$

where: A = amplitude, f = the driving force, ω_n = natural frequency, k = spring constant, and t = time.

IV, E, Structural Considerations (cont.)

The relationship between absolute amplitude, A, and the driving force F is:

$$F = A\ (k - m\omega^2)$$

which is plotted in Figure 52 to show the large response at the natural frequency ω_n.

In order to assess the capability of a structure to withstand pulse type loads the magnification factor of the load must first be determined. The magnification factor is dependent of the pulse shape, duration, and the dynamic response of the structure. Following is a general method of evaluating the magnification factor with respect to the acoustic liner.

The absolute maximum displacement as a function of duration of the half-cycle sine pulse is shown in Figure 53.

It can be seen that as the ratio τ/T increases the absolute displacement ratio approaches 1.0. There would be no amplification and the pressure perturbation would be fully effective.

In the case of the unsupported acoustic liner considered here (Figure 54), $\tau = 0.01$ and $T = 0.00316$. The ratio τ/T is then equal to 3.16 and the amplification is approximately 1.2. When the liner is supported by the chamber the τ/T ratio becomes 26.7 and the amplification becomes 1.0.

The hoop natural period, T, for the liner is determined in the following analysis (see Figure 54).

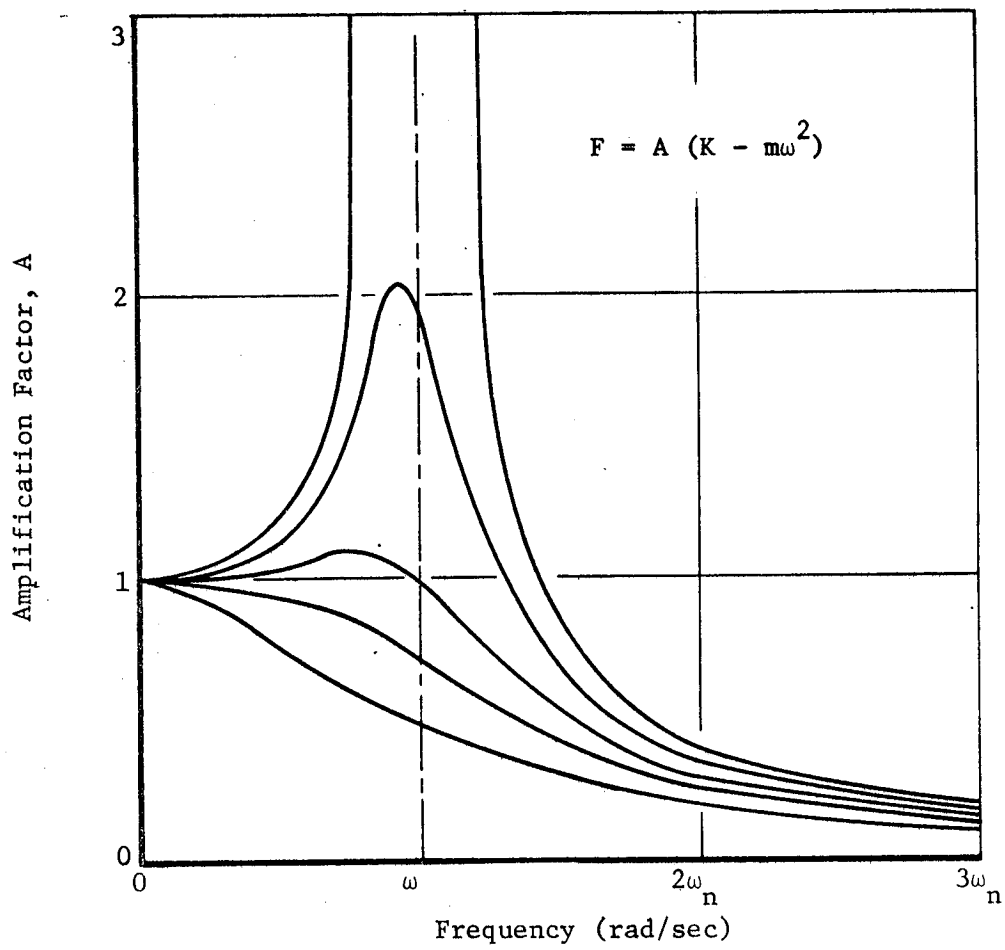

Figure 52. Structural Frequency Response of Combustion Chamber

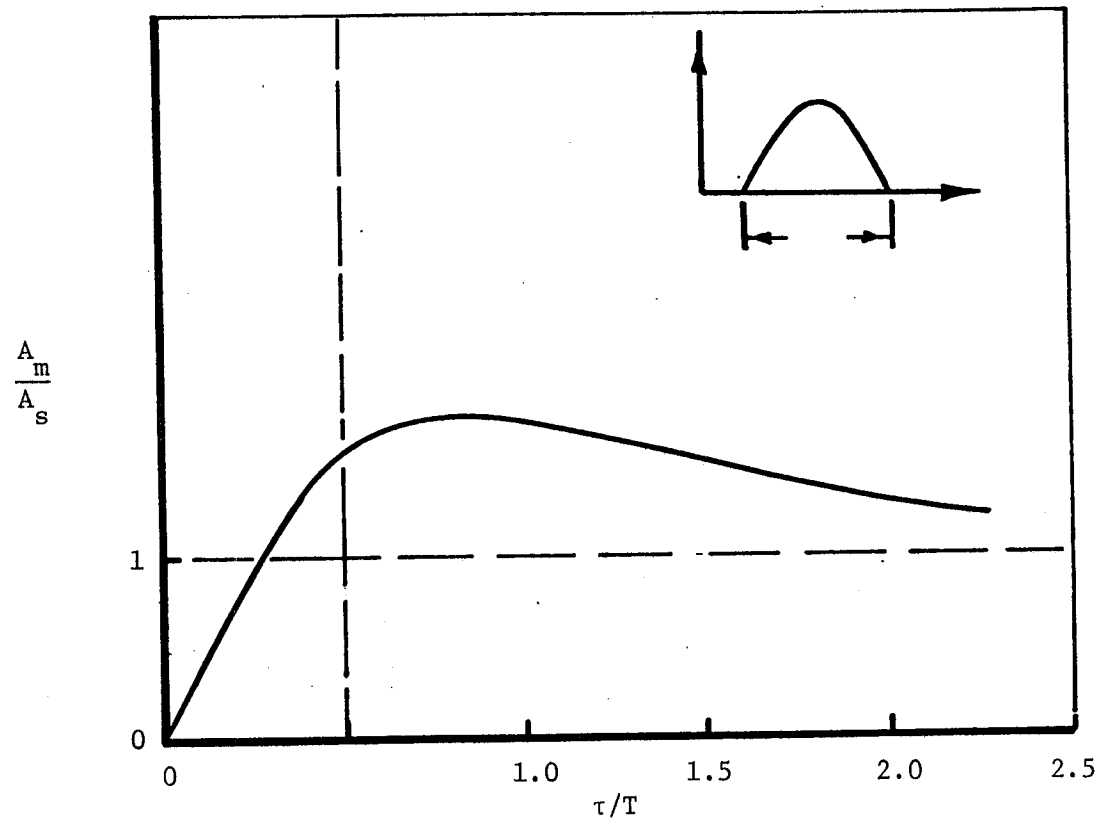

Figure 53. Amplification of the Acoustic Liner Response

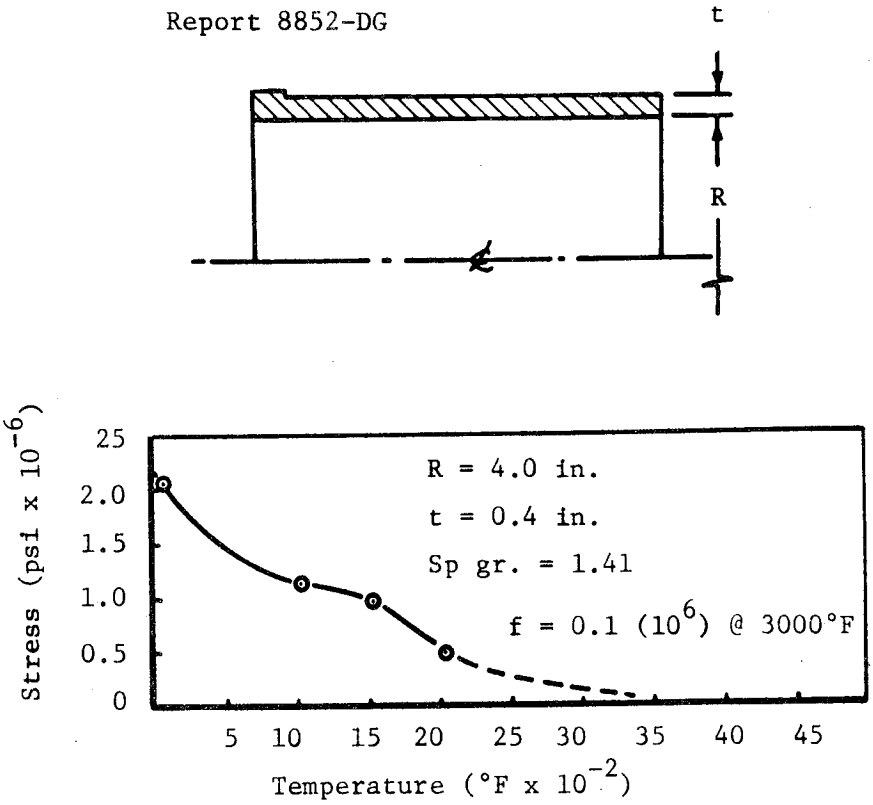

Figure 54. Natural Frequency of Liner Under Hoop Stress

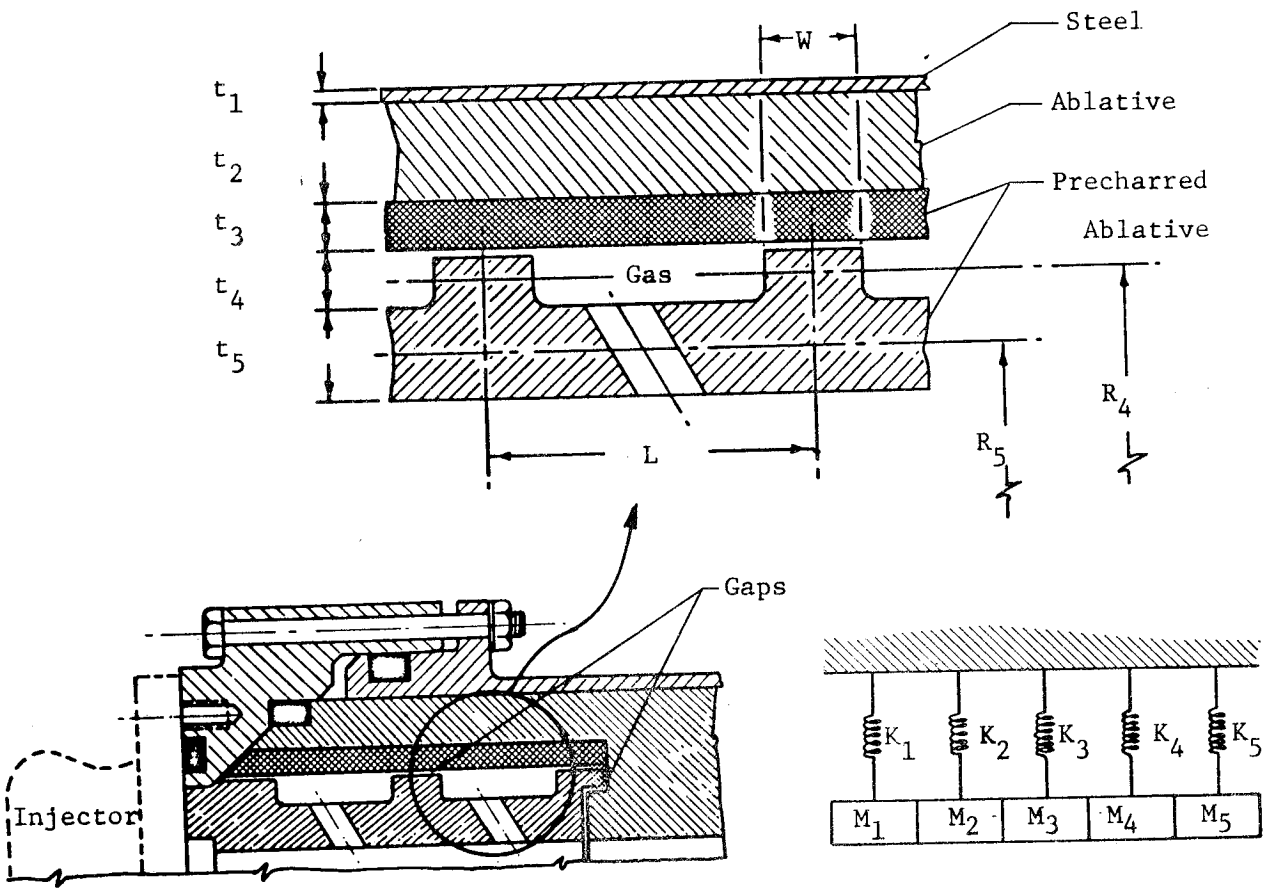

Figure 55. Ablative Chamber and Acoustic Liner with Steel Outer Case Structural Schematic

IV, E, Structural Considerations (cont.)

Then the hoop spring rate is

$$K = \frac{Et}{R^2} = \frac{0.1(10^6)\ (0.4)}{16} = 2500 \text{ lb/in.}$$

The hoop natural frequency is

$$f = \frac{1}{2\pi}\sqrt{\frac{k}{m}}$$

$$w = \frac{1.41(62.4)\ (0.40)}{1728}$$

$$= 2.035(10^{-2}) \text{ lb/in.}^2$$

$$m = \frac{2.035(10^{-2})}{32.2}$$

$$= 0.0633(10^{-2})$$

$$= \frac{1}{2\pi}\sqrt{\frac{2500}{0.000633}} = 317 \text{ cps}$$

$$T = \frac{1}{317} = 0.00316 \text{ sec}$$

For a composite structure such as shown in Figure 55 the procedure is much the same except that an effective spring constant must be determined in the manner shown below:

$$K_1 = \frac{E_1\ L\ t_1}{R_1^2} \qquad K_2 = \frac{E_2\ L\ t_2}{R_2^2}$$

$$K_3 = \frac{E_3\ L\ t_3}{R_3^2} \qquad K_4 = \frac{E_4\ W\ t_4}{(R_4)^2} \qquad K_5 = \frac{E_5\ L\ t_5}{R_5^2}$$

and the mass is given by $M_n = (L_n\ 2\pi r_n\ t_n)\ \frac{\rho_n}{g}$

IV, E, Structural Considerations (cont.)

The effect spring constant for the composite structure is given by

$$K = K_1 + K_2 + K_3 + K_4 + K_5$$

and

$$M = M_1 + M_2 + M_3 + M_4 + M_5$$

and the natural frequency is given by

$$f = \frac{1}{2\pi} \sqrt{\frac{K}{M}}$$

where M = total mass of the composite structure in the length L.

(3) Temperature Loads, Shock and Fatigue

The temperature environment within which the acoustic liner must operate introduces several structural problems. Some of the problem areas are:

(1) Loads or stresses due to thermal expansion of dissimilar materials or due to temperature differences of like materials;

(2) Loss of material strength at elevated temperature;

(3) Effect of thermal shock on brittle materials (composites and ceramics); and

(4) Low-cycle fatigue of metal parts such as regeneratively cooled liners.

IV, E, Structural Considerations (cont.)

Restraints on the liner should be limited so that loads due to thermal interferences will not develop. This can be done if the temperature distribution with respect to time is available. The liner should be held locally (to maintain its position) but allowed to grow radially and longitudinally. Judicious use of gaps is advisable as shown in Figure 55. Ideally all the components should just fit at steady state temperature distribution.

The mechanical properties of all structural materials are degraded as temperature increases. Many ablatives exhibit erratic thermal expansion characteristics when exposed to temperatures above their curing temperature and behave differently with each heating cycle. These material characteristics must be considered in any structural analysis, especially of a chamber that is subject to restarts.

In selecting a material for the acoustic liner some attention has to be directed at the materials resistance to thermal shock. During the start transient very sharp thermal gradients may be encountered. A thermal shock parameter has been formulated and can be used to weight the material selection. The thermal shock parameter (Ref 43) is:

$$R = \frac{C_t \, S_u}{E_t \, \alpha}$$

where C_t = thermal conductivity

S_u = ultimate tensile strength

E_t = Young's Modulus

α = Linear Coefficient of Expansion

IV, E, Structural Considerations (cont.)

It can be seen that for resistance to thermal shock a low coefficient of expansion is important which in effect reduces the thermal strain. A high thermal conductivity is also important in reducing the temperature gradient. Charred materials do not seem to be susceptible to thermal shock.

When evaluating the resistance of a material as to thermal shock, the ply orientation and direction of thermal gradient have to be considered. Non-isotropic materials, such as laminated structures, are very sensitive to the direction of the plies. Generally the conductivity is much higher parallel to the plies than it is across the plies, while the expansion rates are greater across the plies. Strength is also greatest parallel to the plies. From this it is apparent that for materials subject to high thermal gradients it is more advantageous to lay up the structure so that the thermal gradient is across the plies. The value of the conductivity chosen should be that which corresponds to the direction of the gradient while the values of Young's modulus, and coefficient of expansion should correspond to the direction perpendicular to the thermal gradient.

Material yielding will almost invariably occur whenever metals are exposed to an environment of high heat flux. In applications such as regeneratively cooled liners which are subject to repeated firings the structure may need be reviewed for possible low-cycle fatigue failure. From this analysis, a cyclic life for the critical region of the liner could be determined and a comparison made to the required duty cycle of the chamber. For an approximate evaluation of the allowable cyclic strain the following formula may be used (Ref 44):

$$\varepsilon_t = \frac{2 F_{ty}}{E} + \frac{e}{z} (\bar{N})^{1/2}$$

IV, E, Structural Considerations (cont.)

where ε_t = allowable cyclic strain range

F_{ty} = 0.2% offset yield strength at the maximum temperature of the cycle

E = modulus of elasticity

e = fracture elongation

N = average cyclic life which should be taken as 10 times the number of engine firings

For more detailed fatigue predictions the methods and test data described in References 45, 46, 47, and 48 would be helpful.

For steady state temperature conditions, the thermal stresses can be approximated using (Ref 49):

$$\sigma_x = \sigma_\psi = \pm \frac{E\alpha\ (\Delta T)}{2(1-\mu)} \quad (F)$$

Where: σ_x = meridional stress

σ_ψ = hoop stress

E = modulus of elasticity

μ = Poisson's Ratio

α = coefficient of thermal expansion

ΔT = temperature gradient across thickness

F = geometry factor 1.25 near edge; 1.0 elsewhere

and the sign indicates cold side and hot side stresses.

During the startup or shutdown transients, the peak transient thermal stress can be approximated by (Refs 47 and 50).

IV, E, Structural Considerations (cont.)

$$\sigma_x = \sigma_\psi = \frac{E\alpha T_o}{(1-\mu)(1.5 + \frac{3.25}{\beta})}$$

where T_o = Suddenly imposed surface temperature

β = Biot's number = $\frac{h\ L}{K}$

h = heat transfer coefficient

L = half the wall thickness = $\frac{t}{2}$

K = material conductivity

The liner should be supported in such a manner that it will be capable of withstanding a radial pressure differential caused by detonation without itself becoming excessively loaded. Basically the material behind the liner is the structure and as such should be designed to carry all of the loads developed during engine firing. The liner support should be so designed that the liner is just in contact with the chamber separators. Since the unsupported spans are short and the liner thickness fairly large the loads applied to the liner will pass directly into the chamber structure. The acoustic liner will develop bending type of stresses at the supports.

Locations of the spacers behind the acoustic liner should be based on the thickness of the liner. Spacing should be such that λL remains less than 1.0. In this way the liner hoop loads will be minimized with most of the loads reacted by the structural shell.

$$\lambda = \sqrt[4]{\frac{3\ (1-\mu^2)}{R_2^2 t^2}}$$

IV, E, Structural Considerations (cont.)

where: L = Span Length
μ = Poisson's Ratio
R = Radius
t = Thickness

2. Structural Problems

The structural integrity of the acoustically lined thrust chamber is largely dependent on the capability of the liner and external casing to support the mechanical loads due to pressure and thrust and to withstand the thermal loads. It is difficult to accurately evaluate stresses introduced by temperature gradients and differential thermal expansion of adjacent parts, due to their time dependent nature. The liner could fail due to start or shutdown transients, pressure transients induced by explosive devices, thermal shocks, or, after a few firings, due to low-cycle fatigue. The aim of the structural design should be to relieve thermal and mechanical stresses by minimizing constraints and using a floating construction, providing compatibility for expansion, and temperature control through compensating for differential thermal expansion.

In order to account for the interaction of loads it is necessary to analyze the composite liner-and-chamber structure as a unit as described in Section IV,E,1,g. The properties of the structure, can be made to be orthotropic in behavior by appropriate consideration of their material properties.

3. Structural Criteria

1. The liner should be unrestrained thermally so that loads do not develop from interferences, caused by thermal expansion. This

IV, E, Structural Considerations (cont.)

can be achieved if the temperature distribution vs time is available. The liner should be held locally (to maintain its position) but allowed to grow radially and longitudinally. Judicious use of gaps is advisable. Ideally all the components should just fit when thermal equilibrium is reached.

2. The liner should be supported in such a manner that it will be capable of withstanding a radial pressure differential due to a detonation without becoming excessively loaded. The material behind the liner is the basic structure and as such should be designed to carry all of the loads developed during engine firing. The liner support should be so designed that the liner is just in contact with the chamber separators. Since the unsupported spans are short and the liner thickness fairly large the loads applied to the liner will pass directly into the chamber; however, the liner will develop bending stresses at the supports.

3. In selecting a material for the liner attention must be directed to resistance to thermal shock. During the start transient very sharp thermal gradients may be encountered. A thermal shock parameter that has been formulated and can be used to weight the material selection is:

$$R = \frac{C_t \, S_u}{E_t \, \alpha} \; ;$$

where C_t = thermal conductivity
S_u = ultimate tensile strength
E_t = Young's Modulus
α = linear coefficient of expansion

It can be seen that for best resistance to thermal shock a low coefficient of expansion is important which in effect reduces the induced thermal strain.

IV, E, Structural Considerations (cont.)

A high thermal conductivity is also important in that good conductivity reduces the temperature gradient. Charred materials do not seem to be susceptible to thermal shock.

Non-isotropic materials, such as laminated structures, are very sensitive to the direction of the plies. Usually the conductivity is much higher parallel to the plys than it is across the plies, as is the material strength. On the other hand the expansion rate is greater across the plies. It is apparent that for materials subject to high thermal gradients it is most advantageous to lay up the structure so that the thermal gradient is across the plies. The ply orientation and direction of thermal gradient therefore have to be considered when evaluating the resistance of the material to thermal shock. The value for conductivity should be used which corresponds to the direction of the gradient while the value of Young's modulus, coefficient of expansion, and coefficient of expansion should correspond to the material direction perpendicular to the thermal gradient.

4. The stress concentration factor can be reduced and thus reduce the likelihood of fracture by chamfering the holes in the acoustic liner.

5. The locations of the spacers behind the acoustic liner should be based on the thickness of the liner. The spacing should be such that the value of λ L remains less than 1.0. In this way the liner hoop loads will be minimized with most of the loads reacted by the structural shell.

IV, E, Structural Considerations (cont.)

$$\lambda = \sqrt[4]{\frac{3\ (1-\nu^2)}{R_2^2 t^2}}\ ,$$

where L = Span Length
μ = Poisson's Ratio
R = Radius
t = Thickness

6. The dynamic response of the liner is related to the natural frequency of the chamber material under hoop stress. If this frequency is not close to the frequency of the combustion response, there will be no amplification.

7. When selecting the materials for a regeneratively cooled acoustic liner, the selection should consider resistance to low-cycle fatigue.

Whenever metals are used in an environment of high heat flux there will almost invariably be local yielding. Since the yield strains mainly result from temperature gradients and their magnitudes are fixed by the temperature, ultimate type failures will not occur.

REFERENCES

1. Reardon, F.H., "Correlation of Sensitive-Time-Lag-Theory Combustion Parameters with Thrust Chamber Design and Operating Variables," ICRPG Fifth Combustion Conference, CPIA Publication No. 183, December 1968, p. 237.

2. Crocco, L., "Aspects of Combustion Instability in Liquid Propellant Rockets," J. Amer. Rocket Soc., Part I: vol. 21, November 1951, Part II: vol. 22, January 1952.

3. Anonymous, "Gemini Stability Improvement Program," (GEMSIP), Aerojet-General Corp: Report GEMSIP FR-1, 31 August 1965, Contract AF 04(695)-517.

4. Anonymous, "A Study of the Suppression of Combustion Oscillations with Mechanical Damping Devices," Phase II Summary Report, Pratt and Whitney Aircraft Report PWA FR-1922 July 1966 (Appendix A).

5. Hunsaker, J.C. and Rightmire, B.G., Engineering Applications of Fluid Mechanics, McGraw-Hill Book Co., New York, 1947, p. 452.

6. Fox, J., "Surface Pressure and Turbulent Airflow in Transverse Rectangular Notches," NASA Technical Note D-2501, 1964.

7. Charwat, A.F., et al., "An Investigation of Separated Flows--Part I: The Pressure Field," Journal of the Aerospace Sciences, Vol. 28, pp. 457-470, 1961.

8. Charwat, A.F., et al., "An Investigation of Separated Flows--Part II: Flow in the Cavity and Heat Transfer," Journal of the Aerospace Sciences, Vol. 28, pp. 513-527, 1961.

9. Larson, H.K., "Heat Transfer in Separated Flows," Journal of the Aerospace Sciences, Vol. 26, No. 11, pp. 731-738, 1959.

10. Roshko, A., "Some Measurements of Flow in a Rectangular Cutout," NASA Technical Note 3488, 1955.

11. Seban, R.A., Emery, A., and Levy, A., "Heat Transfer to Separated and Reattached Subsonic Turbulent Flows Obtained Downstream of a Surface Step," Journal of the Aerospace Sciences, Vol. 26, No.12, pp.809-814, 1959.

12. Seban, R.A. and Fox, J., "Heat Transfer to the Air Flow in a Surface Cavity," Proceedings of the 1961 International Heat Transfer Conference, ASME, p. 426.

REFERENCES (cont.)

13. Haugen, R.L., "An Analytical and Experimental Study of Heat and Momentum Transfer in Turbulent Separated Flow Past a Rectangular Cavity," Ph.D. Thesis, Michigan State University, 1966.

14. Haugen, R.L. and Dhanak, A.M., "Heat Transfer in Turbulent Boundary Layer Separation over a Surface Cavity," Journal of Heat Transfer, pp. 335-340, November 1967.

15. Haugen, R.L. and Dhanak, A.M., "Momentum Transfer in Turbulent Separated Flow Past a Rectangular Cavity," Journal of Heat Transfer, pp. 641-646, September 1966.

16. Maull, D.J. and East, L.F., "Three-Dimensional Flow in Cavities," Journal of Fluid Mechanics, Vol. 16, pp. 620-632, 1963.

17. Snedeker, R.S. and Donaldson, C.DuP., "Observation of Bistable Flow in a Hemispherical Cavity," AIAA, Vol. 4, No. 2, p. 735, 1966.

18. A Study of the Suppression of Combustion Oscillations with Mechanical Damping Devices, Pratt & Whitney Report PWA FR-1922, July 1966.

19. A Study of the Suppression of Combustion Oscillations with Mechanical Damping Devices, "Summary of Results for Tasks III through VI," Pratt & Whitney Report PWA FR-1330, November 1964.

20. Schindler, R.C. and Kiser, H.V., Development and Demonstration of Ablative Thrust Chamber Assemblies Using LF_2/N_2H_4 Blend Propellants, Aerojet-General Final Report, Contract F04611-67-C-0003, AFRPL-TR-69-2, January 1969, Confidential.

21. Kobayashi, A.C., "Improved Transtage Injector Program," AGC Memo 9648:0487, March 1969.

22. Spalding, D.B. and Patankar, S.V., Heat and Mass Transfer in Boundary Layers, CRC Press: Cleveland, 1958.

23. Rousar, D.C., "Heat Transfer Characteristics of AeroZINE 50 at High Velocities and High Subcoolings," AGC, TCER 9648-003, 11 November 1966.

24. Jakob, M., "Heat Transfer and Flow Resistance in Crossflow of Gases Over Tube Banks," Trans. ASME, Vol. 60, 1938, pp. 381-386.

25. Kreith, F., Principles of Heat Transfer, International Textbook Company, Scranton, 1961, pp. 389-390.

REFERENCES (cont.)

26. Memo 9648:0488, R.W. Michel to R.A. Hewitt, dtd 28 March 1969, Subj: "Parametric Heat Transfer Study of Regeneratively-Cooled Acoustic Liner".

27. Graham, A.R., "Film Cooling of Rocket Motors," Ph.D. Thesis, Purdue University, 1958.

28. Van Huff, N.E., "Design Criterion Monograph," to be published.

29. McCuen, P.A., et al., "A Study of Solid-Propellant Rocket Motor Exposed Materials Behavior," AFRPL-TR-65-33, 1965.

30. Pauli, A.J., "Experimental Evaluation of Several Advanced Ablative Materials as Nozzle Sections of a Storable-Propellant Rocket Engine," NASA Technical Memorandum - NASA TM X-1559 April 1968.

31. Mitchell, B.J., et al., "Part II - Critical Environments and Additional Arc Heater Screening, June 1966 AFML-TR-65-156.

32. Mayo, C.S., "Part/Ablative Plastic Characterization in Simulated Motor Exhaust," AFML-TR-65-245, July 1968.

33. Speyer, F.B., "Development of Advanced Composites Pressure Liquid Environments," Part I Materials Development, AFML-TR-68-243, September 1968.

34. Mitchell, B.J. and Tempesta, F.L., "Additional Arc Heater Screening and Trajectory Simulation," Part II, AFML-TR-67-175, October 1968.

35. Clougherty, E.V., "Research and Development of Refractory Oxidation Resistant Diborides," AFML-TR-68-190, October 1968.

36. Peterson, D.A., et al., "Rocket Engine Evaluation of Erosion and Char as Functions of Fabric Orientation for Silica Reinforced Nozzle Materials," NASA TMX-1721, January 1969.

37. Warga, J.J., et al., "Evaluation of Low-Cost Materials and Manufacturing Processes for Large Solid Rocket Nozzles," AFRPL-TR-67-310, Dec. 1967.

38. Cline, P.B. and Scultz, T.E., "Investigation of the Effect of Material Properties on Composite Ablative Matrrial Behavior," NASA CR-72142, April 1967.

39. Davis, H.O., et al., "Evaluation of Characteristics Affecting Attainment of Optimum Properties of Ablative Plastics," AFRPL-TR-68-29, Vol. I.

REFERENCES (cont.)

40. Dickson, J.C. and Howard, W.S., "Nonregeneratively Cooled Thrust Chamber Development Program," AFRPL-TR-65-138, Sept. 1965.

41. Farmer, R.W., "Thermogravimetry of Phenol-Formaldehyde Polycondensate Part II," AFML-TR-65-246, March 1967.

42. Ladacki, Michael, et al., "Heat of Pyrolysis of Resin in Silica-Phenolic Ablator," AIAA Vol. 4, No. 10, October 1966.

43. Dorn, John E., Mechanical Behavior of Materials at Elevated Temperatures, McGraw-Hill, New York, 1961.

44. Harvey, John F., Pressure Vessel Design, D. Oan Norstrand Co., Inc., New York, 1963.

45. Avery, L.R., Carayanis, G.S., and Michky, G.L., "Thermal-Fatigue Tests of Restrained Combustor Cooling Tubes," Experimental Mechanics, Journal of SESA, June 1967, pp. 256-264.

46. Kuyper, D.J. and Barge, H.L., "Simplified Thermal Fatigue Analysis for Liquid Rocket Combustion Chambers," Journal of Spacecraft, AIAA, January 1967, pp. 126-128.

47. Manson, S.S., Thermal Stress and Low Cycle Fatigue, McGraw-Hill Book Co., 1966.

48. Manson, S.S. and Gary Halford, "A Method of Estimating High Temperature Low Cycle Fatigue Behavior of Metals," NASA TM X-52270, June 1967.

49. Timoshenko, S. and Woinowski-Frieger, S., Theory of Plates and Shells - McGraw-Hill Book Co., Second Edition, 1959, pp. 497-501.

50. Baley, B.A. and Weiner, H.J., Theory of Thermal Stresses, John Wiley & Sons, 1960, p. 284.

APPENDIX I

ACOUSTIC LINER DESIGN APPROACHES

TABLE OF CONTENTS

FIGURE LIST

A. INTRODUCTION

No comprehensive study of acoustic dampers can be made without consideration of the acoustics, combustion, and gas dynamics of a hot firing rocket engine. Many useful experiments have been made using combustion chambers at ambient conditions without flow, and others have been made using ambient air with mean flow, but the proof of any theory can only be verified by full scale rocket test firings. This is especially true of the evaluation of acoustic resonators in combustion chambers due to the presence of: (1) thermal gradients, (2) gas composition gradients, (3) static pressure gradients, (4) mean gas velocity gradients, (5) combustion gradients, (6) acoustic pressure gradients, (7) acoustic nozzle losses, and (8) non-linear high amplitude acoustic losses. All of these factors are present in a rocket chamber but their importance as design considerations is exaggerated by the presence of an acoustic resonator.

The following analyses are included to show the advantages and disadvantages of each. The major shortcomings of the absorption coefficient approach were eliminated by two major modifications: (1) an acoustic liner size weighting factor consisting of the total orifice area divided by the cross-sectional area of the chamber (injector area), and (2) using the combustion chambers characteristic impedance (product of chamber gas speed of sound and density) to normalize the liner impedance.

B. CLASSICAL ACOUSTIC DAMPER ANALYSIS

The simplified analysis of an air resonator made by Helmholtz about a century ago still is used as a starting point for the evaluation of an acoustic liner design for a rocket engine. The common textbook method for describing this simplified analysis is with a mechanical or electrical analogy. A word of caution at this point: the classical analysis alone is not sufficient for evaluation of acoustic liners for rocket engines.

B, Classical Acoustic Damper Analysis (cont.)

The mechanical analogy consists of a spring mass system as shown in Figure I-1. The differential equation of the mechanical system with a periodic forcing function is:

$$m\ddot{x} + r\dot{x} + kx = F_o e^{j\omega t} \qquad \text{Eq. I-1}$$

The damped natural frequency of such a system is given by

$$\omega_d = \sqrt{\frac{k}{m} - \left(\frac{r_1}{2m}\right)^2} \qquad \text{Eq. I-2}$$

or if the damping is small, so that

$$\left(\frac{k}{m}\right) >> \left(\frac{r_1}{2M}\right)^2$$

then, the undamped natural frequency is given by:

$$\omega_n = \sqrt{\frac{k}{m}} \qquad \text{Eq. I-3}$$

The natural frequency of the acoustic system can be related to the mechanical system just described by the following substitutions:

$$\text{mass} = m = \rho V_o = \rho\, A_o\, \ell_e$$

$$\text{spring constant} = K = A_o \frac{dp}{dx}$$

$$= -A_o^2 \frac{dp}{dV}$$

$$= c^2 \rho\, A_o^2 / V$$

$$\text{forcing function} = F_o e^{j\omega t} = PA_o e^{j\omega t}$$

$$\text{damping constant} = r_1 = \rho\omega^2\, A_o^2 / c2\pi$$

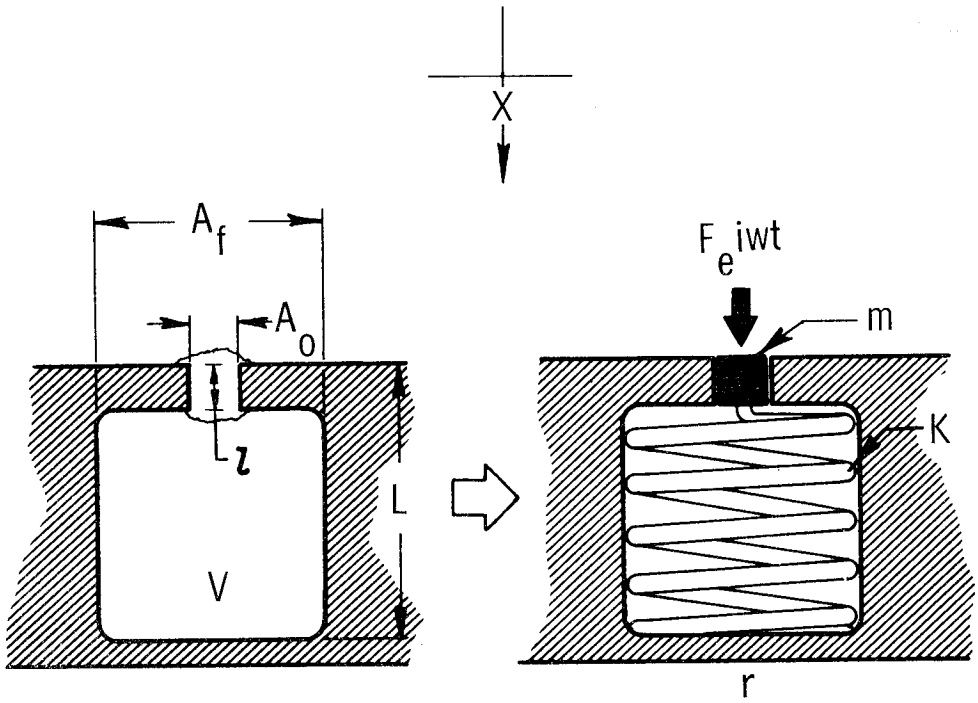

A_f = AREA OF FACE

A_o = AREA OF ORIFICE

V = VOLUME CAVITY

L = BACKING LENGTH

ℓ = EFFECTIVE LENGTH OF ORIFICE VOLUME

F = FORCE FUNCTION

m = MASS

r = DAMPING CONSTANT

K = SPRING CONSTANT

ρ = GAS DENSITY

P = GAS PRESSURE

c = SPEED OF SOUND

Figure I-1. Mechanical Analogy of Acoustic Resonator

B, Classical Acoustic Damper Analysis (cont.)

This then gives the natural frequency of the acoustic resonator as

$$f = \frac{c}{2\pi}\sqrt{\frac{A_o}{V\,\ell_e}} \qquad \text{Eq. I-4}$$

where A_o represents the area of the orifice, and unsubscripted V represents the volume of the cavity. This formula is often re-written in terms of open area ratio, σ, (defined as the orifice area divided by the resonator backing area as A_o/A_b and the backing distance, L (as shown in Figure A-1) as follows:

$$f = \frac{C}{2\pi}\sqrt{\frac{\sigma}{L\,\ell_e}}$$

Either method is valid since they are equivalent.

Many assumptions were made to arrive at this simple formula for the resonant frequency; therefore, it is useful only for broad approximations of the resonant frequency of a given design. A correction that can be applied to improve the estimate relates to the relationship of the effective length of the orifice to its actual length. There are numerous versions of this length correction; however, typically, the values approximate three-fourths of the diameter of the orifice. A necessary assumption is that all dimensions of the resonator are less than one sixteenth of a wave length for the tune frequency.

C. EARLY ROCKET ENGINE CORRECTIONS TO ABSORPTION COEFFICIENT APPROACH

In the preceding discussion it was assumed that the viscous losses in the orifice are small compared to the acoustic radiation losses. This assumption probably is the least realistic aspect of the preceding analysis for use in rocket engine applications. Actually, at high sound pressure levels and with small orifices, the viscous losses are quite high and the radiation losses are no longer described by the equation for the acoustic resistance of an orifice opening into free space (see Refs I-1, I-2, and I-3). This acoustic

C, Early Rocket Engine Corrections to Absorption Coefficient Approach (cont.)

resistance is better explained by incompressible gas dynamic parameters associated with turbulent incompressible gas flow caused by either direct or alternating air flow (Ref I-4, I-5, I-6, and I-7).

As a result, it is recognized that the sound energy dissipating quality of a Helmholtz resonator is determined predominantly by the previously-ignored viscous losses and by turbulence losses associated with high sound pressure levels. This loss mechanism is best described with a nonlinear acoustic resistance and has been empirically curve fitted for single resonators (Ref I-5) and multiple resonators (Ref I-8). An attempt also has been made to model the nonlinear acoustic resistance losses theoretically (Ref I-9). The model assumes that the nonlinear losses result from the jet formation at the exit of the orifice (viz., while the resonator is expelling gas) and that all of the kinetic energy of this gas jet is lost by conversion to turbulence. This represents a nonlinear loss mechanism, because kinetic energy is proportional to the square of the velocity of the jet. The model very closely correlates the data obtained empirically. It deviates most at the very high sound pressure levels where little experimental data are available. This is to be expected because very high sound pressure levels are known to be highly nonlinear with respect to many acoustic loss mechanisms. The results obtained by using this relatively simple theory also indicate that the empirical results used for previous rocket liner design applications are in error because the experiments have been performed using air at ambient conditions and were not corrected for viscosity, density, and frequency to the hot environment of an operating combustion chamber.

Having once resolved what the nonlinear losses are for an operating combustion chamber resulting from high sound levels, it is necessary to correct for the effects of high sound level, and mean gas flows past or through the liner. As indicated, this has been accomplished empirically (Ref I-7, I-10,

C, Early Rocket Engine Corrections to Absorption Coefficient Approach (cont.)

I-11, I-12, and I-13). These effects are manifested as a decrease in the effective mass of the orifice and result in a significant increase in the resonant frequency of the resonator. The maximum shift observed for a specific resonator is reported to be 63% of the resonant frequency obtained in a static environment. Some question still exists concerning the results obtained (Ref I-12) because of the effect of flow past the resonator orifice and a saturation effect of the acoustic resistance resulting from mean flow turbulence effects as a function of frequency and velocity. Mechel (Ref I-11) defined an acoustic resistance ratio which was experimentally shown to vary between 1.0 and 3.5 for a frequency of 400 Hertz. Currently, some absorption coefficients are evaluated using 3.5 as an upper limit or using a simple curve-fit formula that has no upper limit. However, the absorption coefficients obtained using these two methods clearly are not in agreement at high velocities of flow.

D. ANOMALIES OF ABSORPTION COEFFICIENT ANALYSIS

The evaluation of a particular acoustic liner design now can be made using the knowledge obtained from the empirical data of both theoretical models and a correct gas property scaling technique founded in theoretical model. The best method for evaluating an acoustic liner design in a particular chamber is not necessarily by the absorption coefficient method, which is emphasized in the technical literature (Ref I-8 and I-14). This method does not consider the system as a whole. Rather, it is based upon designing a liner independently of the combustion chamber and then incorporating it into the chamber wall. If the liner is truly a large array of resonators making up a significant portion of the total chamber wall area, then it definitely should be evaluated as a complete system because its effect upon the chamber modes cannot be ignored. Conversely, if the liner is limited to a small area (i.e., just around the injector) the absorption coefficient method does not give good design comparisons. A good example of the misleading results that

D, Anomalies of Absorption Coefficient Analysis (cont.)

can be obtained using the absorption coefficient method is shown with the following two designs:

	$\frac{\sigma}{ND}$	$\frac{L}{in.}$	$\frac{d}{in.}$	$\frac{t_1}{in.}$	$\frac{SPL}{DB}$	$\frac{f_o}{H_3}$	$\frac{\alpha}{ND}$
Design 1	0.25	0.625	0.2	0.0625	190	8000	0.34
Design 2	0.16	0.40	0.2	0.0625	190	8000	0.57

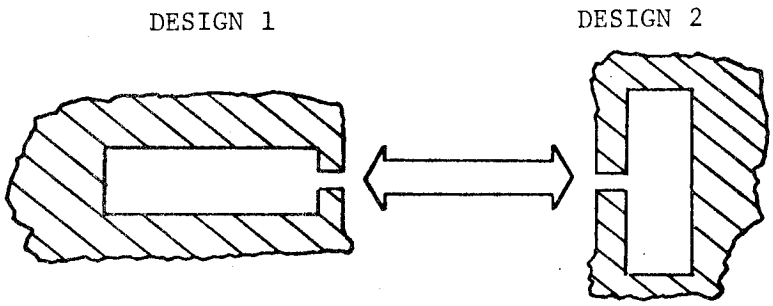

Note that the resonant frequencies, f_o, of the two designs are equal; the orifice thickness, t_1, diameter, d, and volume V, of the resonator also are the same. The open area ratio, σ (ratio of orifice area to backing area), and backing distance, L, are simply ratioed so as to yield the same resonant frequency. The sound pressure level, SPL, of the incident pressure oscillation is taken to be equal for the two designs as are all of the gas properties.

If the analytical assumptions are obeyed, then, the use of only one row array of such an acoustic liner in a rocket chamber would result in identical absorption, but the calculated absorption coefficients differ by a factor of approximately two at resonance. Therefore, a more meaningful method for comparing two acoustic liner designs is needed.

E. RECENT MODIFICATION OF THE ABSORPTION COEFFICIENT ANALYSIS

It is necessary to determine the acoustic resistance and reactance of the Helmholtz resonator in the system in order to determine its relative damping ability. A typical approach for measuring the damping ability of a resonator is by means of a standing-wave impedance tube measurement. The apparatus for such an experiment is available commercially from Bruel and Kjaer*. The analytical justification for such a device is well founded and provides as an end result the absorption coefficient as a function of frequency of a resonator placed at the end of the standing-wave tube. The only measurement required is the amplitudes of the maximum and minimum acoustic pressure oscillations at two respective points along the tube. If the incident acoustic pressure is defined as P_i and the reflected acoustic pressure is P_r, then the maximum pressure measured is seen to be the sum of the incident and reflected pressures while the minimum pressure is the difference. An absorption coefficient, α is defined as the ratio of the energy absorbed by the resonator to the total energy striking the resonator. Since the acoustic energy is proportional to the square of the acoustic pressure the absorption coefficient is defined as:

$$\alpha = 1 - \frac{P_r^2}{P_i^2} \qquad \text{Eq. I-5}$$

It can be shown that the characteristic impedance of the gaseous medium is, $Z_i = \rho c$, the product of its density, and its speed of sound. A complex acoustic impedance nondimensionalized by the characteristic impedance, Z*, is defined as follows:

$$Z^* = \bar{\theta} + iX \qquad \text{Eq. I-6}$$

$$= \left(\frac{p'}{Q'/A}\right) \Big/ \left(\rho c\right)$$

*Manufacturer

E, Recent Modification of the Absorption Coefficient Analysis (cont.)

Further Z*, can be defined in terms of the incident and reflected acoustic pressures as:

$$Z^* = (1 + P_r/P_i) \; / \; (1 - P_r/P_i) \qquad \text{Eq. I-7}$$

or conversely

$$P_r/P_i = (Z^* - 1) \; / \; (Z^* + 1)$$

Substituting this equation into the absorption coefficient equation (Eq. I-5) gives

$$\alpha = 1 - [(Z^* - 1) \; / \; (Z^* + 1)]^2 \qquad \text{Eq. I-8}$$

or with further substitution for Z*:

$$\alpha = 1 - [(\theta + iX - 1) \; / \; (\theta + iX + 1)]^2 \qquad \text{Eq. I-9}$$

By algebraic manipulation this equation can be reduced to:

$$\alpha = \frac{4\theta}{(\theta + 1)^2 + X^2} \qquad \text{Eq. I-10}$$

By the ideal application of this formula to a standing-wave tube the resonator array uniformly covers the entire end of the tube and only axial pressure waves are present, such that the resonator array is exposed to a uniform acoustic pressure over the sample surface. This formula can still be used even if these criteria are not satisfied. For example, if the resonator array does not cover the entire end of the tube but only a portion of it and a perfect reflector covers the remaining portion, then the resistance and reactance terms of the absorption equation can be corrected by multiplying them by the ratio of the

E, Recent Modification of the Absorption Coefficient Analysis (cont.)

total area of the end of the tube, A_t, covered by the resonator array, A_r. This results in the following equation for absorption coefficient:

$$\alpha = \frac{4\theta\ (A_t/A_r)}{[\theta\ (A_t/A_r) + 1]^2 + [X\ (A_t/A_r)]^2} \qquad \text{Eq. I-11}$$

and

$$Z^*_Q = (\theta + iX)\ A_t/A_r \qquad \text{Eq. I-12}$$

where Z^*_Q is the impedance corrected to the condition where the resonator array covers less area than the entire end of the tube cross-sectional area.

The acoustic resistance ratio θ is defined by the acoustic resistance R divided by the characteristic tube acoustic impedance, $\rho_t c_t$. The acoustic resistance term was defined for a resonator wall surface by Rayleigh (Ref I-1) as:

$$R_s = \sqrt{(\mu_r\ \rho_r\ \pi f)} \qquad \text{Eq. I-13}$$

The orifice resistance was approximated by Ingard (Ref I-5) to be equal to the product of the surface resistance R_s and the orifice length to diameter ratio, t/d, and an experimentally determined aperture resistance end correction was found to be approximately equal to the aperture diameter. This resulted in a total Helmholtz resonator resistance made up of the sum of the inside and outside wall surfaces of the resonator aperture plate, of the empirical end correction resistance and the orifice resistance as follows:

E, Recent Modification of the Absorption Coefficient Analysis (cont.)

$$R_{total} = R_{walls} + R_{aperture} + R_{ends}$$

$$= 2R_s + 4R_s\,(t/d) + 2R_s$$

$$= 4R_s\,(1 + t/d)$$

$$R_t = 4\,(\mu_r\,\rho_r\,\pi f)^{1/2}\,(1 + t/d) \qquad \text{Eq. I-14}$$

Therefore the total resonator acoustic resistance ratio of a single resonator is:

$$\theta_1 = \frac{R_t}{\rho_t\,c_t} = \frac{4\,(\mu_r\,\rho_r\,\pi f)^{1/2}\cdot(1 + t/d)}{\rho_t\,c_t} \qquad \text{Eq. I-15}$$

Note that the tube characteristic impedance, ρc, is based on tube conditions, not resonator conditions. To adjust this resistance ratio formula to account for the resistance of an array of resonators it is necessary to multiply θ_1 by the ratio of the total resonator face area, A_r, of the array to the total aperture area, A_o. This is done to account for conservation of the acoustic volume flow rate perturbation Q'.

Therefore: $\theta = \theta_1 \cdot (A_r/A_o) = \theta_1/\sigma$

$$= \frac{4\,(\mu_r\,\rho_r\,\pi f)^{1/2}}{\rho_t\,c_t\,\sigma}\cdot(1 + t/d) \qquad \text{Eq. I-16}$$

where $\sigma = A_o/A_r$.

Note that correcting this formula by the term (A_t/A_r) shown in Equation I-11 for absorption coefficient results in θ being a function only of the total tube area A_t and of the aperture area A_o, since the area of the resonator face (or backing area), A_r, cancelled out of the resistance term.

E, Recent Modification of the Absorption Coefficient Analysis (cont.)

The nondimensional reactance term, X, is based on the assumption that the resonator is an oscillatory system of the second order. Under such an assumption and comparing the mechanical analogy used earlier for the spring constant, mass, and re-defining the damping constant as R_t, it can be shown that the reactance can be approximated by:

$$X_1 = \frac{2\pi f_o \ell_e \rho_r}{\rho_t c_t} \left(\frac{f}{f_o} - \frac{f_o}{f} \right) \qquad \text{Eq. I-17}$$

where f_o is the resonator tuned frequency.

Again the correction for conservation of acoustic volume flow rate perturbation requires that X_1 be divided by the open area ratio term, $\sigma = A_o/A_r$, for a resonator array that covers the entire end of the tube area. If the resonator array is smaller or larger than the end area of the tube the expression for reactance, X, must be further corrected by multiplying by the A_t/A_r term shown in Equation I-11. This again results in the significant parameters being only the aperture area, A_o, and the tube cross-sectional area, A_t:

$$X_V = \frac{2\pi f_o A_t \rho_t}{\rho_t c_t \sigma A_r} \left[\frac{f}{f_o} - \frac{f_o}{f} \right]$$

or

$$X_Q = \frac{2\pi f_o A_t \rho_r}{\rho_t c_t A_o} \left[\frac{f}{f_o} - \frac{f_o}{f} \right] \qquad \text{Eq. I-18}$$

The correction to area ratio, A_t/A_r or A_t/A_o, has much significance since it eliminates an anomaly. Consider an example of two resonators that have the same volume, V, and same aperture area, A_o, but one resonator twice as long and half as wide as the other. Clearly these two resonators would have the same acoustic impedance, and therefore the same absorption if placed in the end of a standing-wave tube (SWT) and evaluated without reference to

E, Recent Modification of the Absorption Coefficient Analysis (cont.)

any resonator areas. However, if the absorption coefficient is determined using the ratio of aperture area to resonator backing area, A_o/A_b, then the absorption coefficients for the two resonators will differ by a factor of two. This difference is due to the erroneous use of the resonator backing area, A_b, as a parameter instead of the cross-sectional area, A_t, of the SWT.

Since the general use of resonators in rocket chambers is limited to the chamber walls and the best placement is usually around the perimeter of the injector, it seems appropriate to use the injector area, A_t, (or tube cross-sectional area) as the appropriate cross-sectional area of the SWT, and the sum of resonator array aperture areas as the area, A_o. By this approach it is clear that any array of resonators tuned to the same frequency and placed at the end of a SWT (or at a rocket injector perimeter) and having the same total aperture area and total volume will have the same impedance and absorption. To illustrate this best the absorption coefficient equation is written:

$$\alpha = \frac{4\Phi}{(\Phi + 1)^2 + \Psi^2} \qquad \text{(Ref Eq. I-10)}$$

with Φ and Ψ defined:

$$\Phi = \frac{A_t}{A_o}\left[\frac{4\,(\mu_r\,\rho_r\,\pi f)^{1/2}\,(1 + t/d)}{\rho_t\,c_t}\right] \qquad \text{Eq. I-19}$$

and

$$\Psi = \left[\frac{2\,\pi f_o\,\ell_e\,\rho_r}{\rho_t\,c_t}\right]\left[\frac{A_t}{A_o}\right]\left[\frac{f}{f_o} - \frac{f_o}{f}\right] \qquad \text{Eq. I-20}$$

or

$$\Psi = A_t\left[\frac{\ell_e}{VA_o}\right]^{1/2}\left[\frac{f}{f_o} - \frac{f_o}{f}\right]\left[\frac{c_r\,\rho_r}{c_t\,\rho_t}\right] \qquad \text{Eq. I-21}$$

E, Recent Modification of the Absorption Coefficient Analysis (cont.)

where A_t = Cross-sectional area of tube, (injector area)

A_o = Aperture or orifice area

ℓ_e = Effective aperture length

V = Resonator volume

f_o = Resonator tuned frequency, $f_o = \frac{c_r}{2\pi} \sqrt{A_o/V\,\ell_e}$

An evaluation of the absorption coefficient formula shows that the maximum absorption is obtained when the acoustic resistance ratio, Φ, is unity and the acoustic reactance ratio, Ψ, is zero. This corresponds to the tuned frequency. If Φ were greater than unity it can be seen that adding more resonators, and thereby increasing the total aperture area, A_o, would improve the absorption coefficient. Conversely if Φ is less than unity, then adding more resonators and increasing the total aperture area, A_o, would decrease the absorption coefficient. This is not unexpected when it is realized that total absorption occurs when the impedance of the resonator at the end of a SWT is exactly equal to the characteristic impedance of the SWT. This means any impedance that is greater or less than the characteristic impedance will reflect some percent of the incident acoustic energy. This results in the conclusion that too many resonators can provide as poor an absorption coefficient as too few. If this result is not empirically verified then it is possible that the absorption coefficient in any of its many forms is not the parameter that should be optimized.

F. EFFECT OF SOUND PRESSURE LEVEL AND MEAN GAS FLOW

The discussion up to now has not considered the complications introduced when a Helmholtz resonator array is used as a damping device in a rocket engine combustion chamber. The present corrections to the absorption coefficient approach or any other analytical approach must include the effects of: (1) very high amplitude sound on the aperture impedance, (2) mean gas flow velocities past or through apertures on the aperture impedance, and (3) variable gas temperature and composition on the speed of sound, density and viscosity.

1. Nonlinear SPL Acoustic Resistance Effects

Many attempts have been made to determine and define a nonlinear resistance parameter for Helmholtz resonator subject to high sound pressure levels (SPL's). Refs I-4, I-8, I-14, I-15, and I-16 all show empirical curves for the nonlinear resistance parameter. As shown in Figure I-2, all the curves show the same trend. The most recent data appear to substantiate the theoretical model proposed by Sirignano, et al, (Ref I-9) in 1966 for predicting the nonlinear resistance of a Helmholtz resonator as a function of aperture particle velocities. The range of nonlinear resistance given by the various reference sources in Figure I-2 leaves much to be desired. The highest to lowest value of nonlinear resistance at any given sound pressure level differs by an order-of-magnitude, so a compromise curve drawn through all of the various data would result in a value that could be in error by a factor of about five if either of the limit curves are correct. A similar situation occurs if the nonlinear resistance data are plotted as a function of the gas particle displacement in the aperture divided by the aperture thickness as shown in Ref I-14. In that case the highest and lowest data differ by two orders of magnitude. Sirignano's analytical model for the nonlinear resistance term simply assumes that the kinetic energy of the jet of gas flowing through a resonator aperture is totally lost, and that the nonlinear resistance term $\Delta_{n\ell}$ can be represented by an additional orifice length which would produce the same energy loss as the gas jet.

F, Effect of Sound Pressure Level and Mean Gas Flow (cont.)

The Aerojet-General theory curve for the nonlinear acoustic resistance, ϵ, shown in Figure I-2 is obtained by combining the theory of Sirignano, et al, (Ref 1966), Ingard (Ref I-5), and Ingard and Ising (Ref I-7). The ϵ curve labled as "Ingard" in Figure I-2 is from Ref I-5 and was calculated by Ingard for a very specific set of circumstances that should not be interpreted as representing typical rocket engine acoustic liner design conditions. For example Ingard's data were for a single resonator, tuned to 224 cps, with air at ambient conditions. Since frequency is a significant factor in determining ϵ in Ingard's earlier calculations, it can be seen that his curve would have been closer to the other estimated ϵ curves if the resonator tune frequency had been greater, say 2000 cps or more. Ingard (Ref I-5) provided the equations and assumptions necessary for converting ϵ from a function of aperture particle velocity to a function of sound pressure level (SPL). This is accomplished by considering the impedance relation as follows:

$$Z = p'u' = 2R_t \quad \left\{\begin{array}{l}\text{for a resonator in a wall, at} \\ \text{its resonance frequency}\end{array}\right\} \qquad \text{(Ref Eq. I-6)}$$

solving for p' gives

$$p' = 2R_t.(u') = 2\,u' \left[4\,(\mu\rho\pi f)^{1/2}\,(1 + t/d + \Delta_{n\ell}/d)\right] \qquad \text{Eq. I-22}$$

This relationship for p' can then be converted to an rms acoustic pressure amplitude and evaluated as in terms of the SPL equation as follows:

$$SPL = 20 \log_{10} \frac{p'\ (rms)}{P_r} \qquad \text{Eq. I-23}$$

where $P_r = 2 \times 10^{-4}$ (dynes/cm^2) (rms)

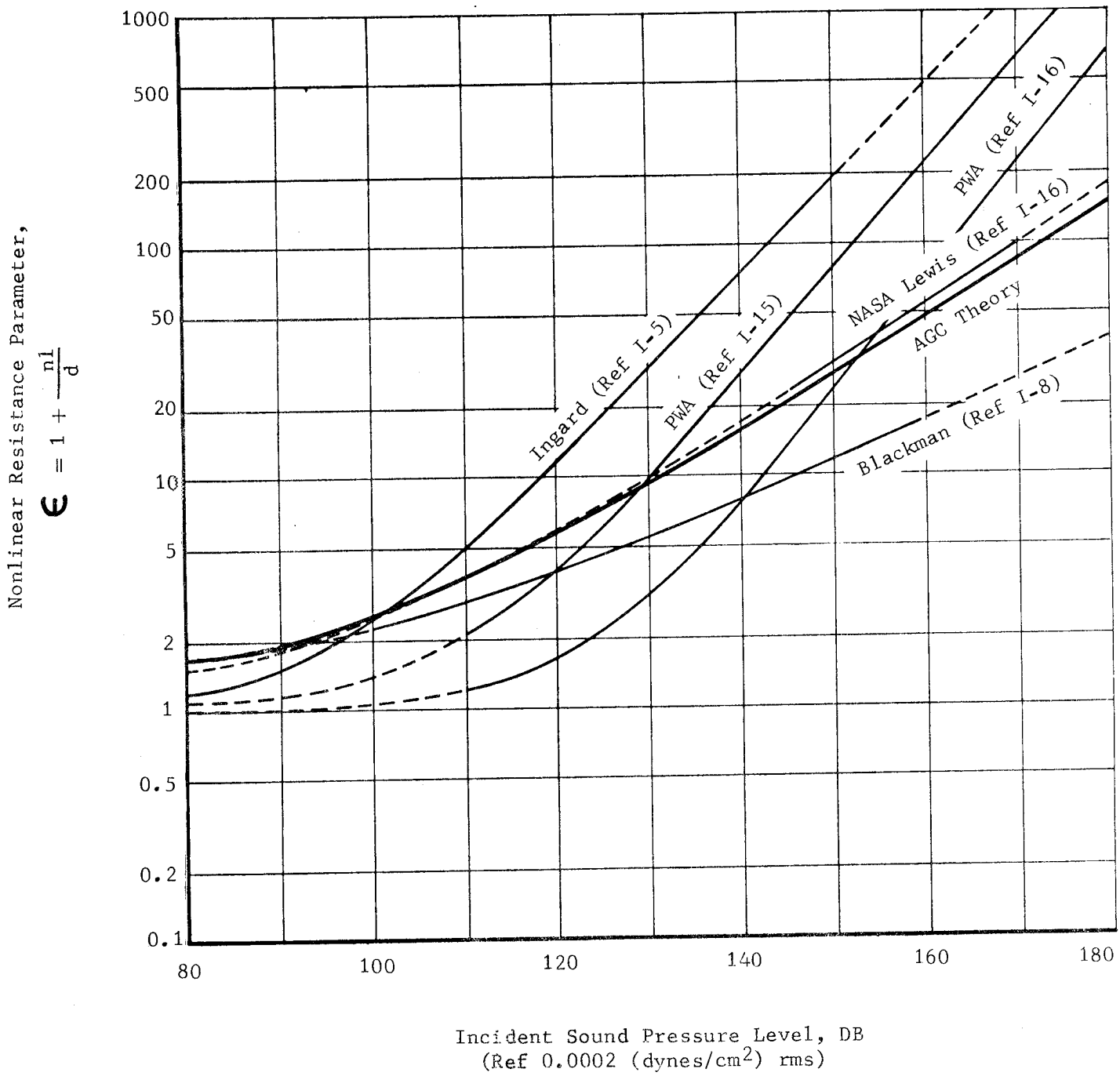

Figure I-2. Comparison of Nonlinear Resistance Versus Sound Pressure Level Curves

F, Effect of Sound Pressure Level and Mean Gas Flow (cont.)

What remains to be evaluated is the term $\Delta_{n\ell}/d$ which Ingard (Ref 25) obtained for a particular resonator as:

$$\Delta_{n\ell}/d = 0.7\ (u'/100)^{1.7} \qquad \text{Eq. I-24}$$

Later Sirignano, et al, (Ref I-9) presented a theoretical curve that superimposed on one of Ingard's original empirically obtained curves which suggest that:

$$\Delta_{n\ell}/d = 1.0\ (u'/100)^{1.0} \qquad \text{Eq. I-25}$$

Using this relationship it is possible to plot the AGC theory curve shown in Figure I-2 which assumes Ingard's (Ref 25) resonator and Sirignano's relationship for $\Delta_{n\ell}/d$, or ε, as a function of SPL.

Care should be taken when using these curves to realize they are functions of many parameters. For example, if the environment of the resonator is not ambient air but that of a rocket chamber the parameters of the resistance term R_t must be corrected in a manner described by Sirignano (Ref I-4). Another correction is suggested by Ingard's more recent work (Ref I-7) showing the acoustic resistance at high sound levels is correlated by the following simple equation involving the resonator gas density, ρ_r, and resonator aperture velocity, u'_r:

$$R = \rho_r\ u'_r \qquad \text{(Ref Eq. I-14)} \qquad \text{Eq. I-26}$$

This implies that the earlier equation for $\Delta_{n\ell}/d$ should have included a gas density correction term, composed of the ratio of the design density, ρ_d, to empirical density, ρ_a, such that Ingard's earlier equation (Eq. A-I-22) for p' would be more generally written as follows:

F, Effect of Sound Pressure Level and Mean Gas Flow (cont.)

$$p' = 8\ (\mu_r\ \rho_r\ \pi f)^{1/2}\ \left[1 + t/d + (\rho_d/\rho_a) * (\Delta_{n\ell}/d)\right]\ u' \qquad \text{Eq. I-27}$$

This density ratio correction has the effect of making the nonlinear resistance term smaller for a given p' (rms) in very high pressure rocket engines. Equation I-27 is used to define the AGC theory curve in Figure I-2. One other correction appears to be in order since Equation I-26 is independent of frequency. This implies that the linear portion of Equation I-27 is correct, and that the nonlinear portion should be separated from the frequency term as follows:

$$p' = u'_r\ \ 8\ (\mu_r\ \rho_r\ \pi f)^{1/2}\ .\ (1 + t/d) + \rho_r\ u'_r \qquad \text{Eq. I-28}$$

Note that ρ for ambient air is approximately 1.2×10^{-3} gm/cm^3 which is very close to the value obtained by the previous formula using Ingard's (Ref 1953) earlier data for nonlinear resistance as follows:

$$8\ (\mu_r\ \rho_r\ \pi f)^{1/2}\ \left(\frac{u'_r}{100}\right) \approx \rho_r\ u'_r\ (\text{gm/cm}^3)\ (\text{cm/sec})$$

$$8\ (0.83 \times 10^{-3})\ (224)^{1/2}\ (u'_r/100) \approx (1.2 \times 10^{-3})\ u'_r$$

$$(1.0 \times 10^{-3})\ u'_r \approx (1.2 \times 10^{-3})\ u'_r$$

Thus it can be seen that Equation I-28 will produce a curve almost identical to Equation I-27 for Ingard's (Ref I-5) data, but that higher resonant frequencies will have more effect at high sound levels using Equation I-27. Ingard's more recent data (Ref I-7) indicates that Equation I-28 should be used to evaluate the acoustic resistance of an aperture at high sound levels.

F, Effect of Sound Pressure Level and Mean Gas Flow (cont.)

Using Ingard's simple high sound level acoustic resistance relation, $\rho\, u'$, to determine the power dissipated by a resonator leads to some interesting results. For example if an electrical analogy is used for the perturbation pressure, and velocity as follows:

Electrical	Acoustic
Voltage, E	Perturbation pressure, p'
Current, I	Perturbation velocity, u'
Resistance, R	Acoustic Resistance, R
$P = IE$	Power dissipation, $P = u' \cdot p'$
$= I^2R$	$= (u')^2 \cdot R$
$= E^2/R$	$= (p')^2/R$

If the power dissipated is the important resonator parameter then it is necessary to use the term u'.p' as large as possible. If a high sound pressure level is assumed in a typical rocket engine application, then the resonator resistance at resonance can be written as

$$Z_{res} = R = p'u'_r = \rho_r\, u'_r$$

Solving for u' gives

$$u' = (p'/\rho_r)^{1/2} = \sqrt{\frac{p'}{p_r} R_r\, T_r} \qquad \text{Eq. I-29}$$

where R_r = gas constant of the resonator gas

T_r = gas temperature of the resonator gas

F, Effect of Sound Pressure Level and Mean Gas Flow (cont.)

Now the power dissipated by the resonator is:

$$P = p' u'_r = (p') \cdot (p'/\rho_r)^{1/2} = (p')^{3/2} \sqrt{\frac{R_r T_r}{P_r}} \qquad \text{Eq. I-30}$$

The subscript, r, stands for the resonator gas condition as opposed to the chamber gas subscript, c.

The implication of Equation I-30 is that for a given sound pressure level input the resonator will have a greater acoustic power dissipation if the ambient pressure, P_r, is low, and the cavity gas molecular weight is low, and the cavity temperature is high. Also it should be noted that if the power dissipation equation were written in terms of E^2/R instead of I.E the need to minimize R becomes apparent:

$$P = (p')^2/R, \text{ where } R = p'/u'_r = \rho_r u'_r; \qquad \text{Eq. I-31}$$

thus the optimum resonator design for a given SPL is obtained by minimizing the acoustic resistance of the resonator. However since the resistance of the resonator at high SPL's is only a function of $\rho_r u'_r$ and u'_r is determined by p' then ρ_r is the only remaining variable, thus ρ_r should be minimized as stated above.

Another implication of Equation I-30 is that the power dissipated by the resonator increases nonlinearly as the SPL increases, implying that a resonator may cause a rocket engine instability to limit cycle. This result assumes that the power dissipation per resonator is the best parameter to optimize. It was previously shown that if the absorption coefficient is to be optimized then the specific acoustic resistance ratio, Φ, should be optimized at unity for a resonator array that covers the end of the standing-wave tube. These two methods of optimizing can be reconciled by noting that

F, Effect of Sound Pressure Level and Mean Gas Flow (cont.)

fewer optimized resonators are required to match the tube impedance for a maximum absorption coefficient. Rewriting Equation I-19 (and being careful to note when resonator and chamber gas properties are used) with the nonlinear resistance term, $\rho u'$, added gives:

$$\Phi = \frac{A_t}{A_o \rho_c c_c} \left[4 (\mu_r \rho_r \pi f)^{1/2} (1 + t/d) \right] + \rho_r u'_r \quad . \qquad \text{Eq. I-32}$$

at high SPLs this equation resolves to

$$\Phi = (\rho_r u' A_t) / (A_o \rho_c C_c)$$

or more clearly

$$\Phi = (\rho_r/\rho_c) \cdot (u'_r/C_c) \cdot (A_t/A_o) \qquad \text{Eq. I-33}$$

Since the absorption coefficient is maximized when $\Phi = 1.0$, and the other parameter ratios have values of $\rho_r/\rho_c > 1.0$, $u'/c << 1.0$, and $A_t/A_o >> 1.0$, it can be seen that for a given u'/c' and ρ_r/ρ_c there is an optimum A_t/A_o. If the density in the resonator cavity is decreased then the total amount of resonator aperture area, A_o, required can be decreased to obtain the optimum design. This criterion is compatible with both methods of design optimization.

2. Acoustic Reactance Saturation with SPL

High SPL not only changes the resonator resistance, it also affects its reactance. The reactance of the resonator can be written as the sum of two parts; namely an inertance (mass) and a compliance (spring) as follows:

F, Effect of Sound Pressure Level and Mean Gas Flow (cont.)

$$X_r = X_m + X_s,$$

where the electrical analogies are inductance and capacitance, respectively. The inertance and compliance terms are defined as:

$$X_m = 2\pi fm = 2\pi f\ (\rho_r\ A_o\ \ell_e)$$

and

$$X_s = 2\pi fK = 2\pi f\ (\rho_r\ C_r^2\ A_o^2/V)$$

The term X_m represents the reactance due to the mass of the gas in the resonator aperture, and the X_s term represents the reactance due to the spring constant of the gas volume in the resonator cavity. A change in the aperture reactance as a function of SPL or aperture particle velocity was first observed by R. H. Bolt, et al, (Ref I-17) and has later been substantiated by many other sources using both direct and indirect means (Refs I-6, I-7, and I-12). The change appears to be due to a reduction in the acoustic mass of the aperture gas, due to a reduction in its effective length, t_e. This results in an increase in the resonant frequency of the resonator as the incident SPL is increased (neglecting resistance changes). There are several ways of presenting experimental data showing this effect. They consist primarily of plotting one of the following parameters: (1) aperture reactance, (2) aperture mass, (3) effective aperture thickness, (4) resonant frequency or (5) changes in any of the above quantities as a function of aperture particle velocity. The relationship between these quantities is as follows:

F, Effect of Sound Pressure Level and Mean Gas Flow (cont.)

Aperture Reactance, $X_m = 2\pi f\ (\rho_r\ A_o\ \ell_e)$

Effective Aperture Thickness; $\ell_e = t + \delta$ where $\delta \leq 0.8d$

Aperture mass, $m_o = \rho_r\ A_o\ \ell_e = \rho_r\ A_o\ (t + \delta)$

Resonant Frequency, $f_o = \frac{C_r}{2\pi}\ \sqrt{\frac{A_o}{V\ (t + \delta)}}$

Thus X_m, t_e, m_o and f_o are all functions of the aperture thickness and diameter. Aperture reactance is the most difficult to use due to the frequency being variable whereas the gas properties and resonator geometry are usually constant for a given system. The relationship between the change in resonant frequency of a resonator and the change in its acoustic mass can be obtained as follows:

If: $f_o = \left[K/m\right]^{1/2}$,

$\log f_o = (1/2)\log K - (1/2)\log m.$

Differentiating both sides (K remaining constant) gives:

$\Delta f_o/f_o = -1/2\ (\Delta m/m).$

Since the aperture mass is directly proportional to the aperture thickness, the incremental ratios of mass, aperture thickness, reactance, and frequency have the relationship

$$(\Delta m/m) = (\Delta\ \ell_e/\ell_e) = (\Delta\ X_m/X_m) = -2\Delta f_o/f_o \qquad \text{Eq. I-34}$$

where the change in reactance occurs at constant frequency.

F, Effect of Sound Pressure Level and Mean Gas Flow (cont.)

If the aperture reactance is measured at two different frequencies then the following relation is required.

$$X_m = 2\pi fm$$

or

$$\log X_m = \log 2\pi + \log f + \log m.$$

Differentiating gives

$$\Delta X_m/X_m = \Delta f/f + \Delta m/m,$$

or substituting from Equation I-34

$$\Delta X_m/X_m = \Delta f/f - 2\Delta f/f$$

$$= - \Delta f/f \qquad \text{Eq. I-35}$$

The result of the many experimental attempts to show the effect of high SPL or aperture velocity is that it leads to a decrease in the aperture reactance, the aperture mass, or the effective aperture thickness. Of the few references that show experimental data for aperture reactance as a function of aperture particle velocity however, none clearly show the saturation effect as with mean flow which will be discussed later. Refs I-7, I-17, and I-18, show data indicating changes in reactance as a function of aperture particle velocity. Care should be taken to correct the units of the various data presentations since some employ rms velocities instead of peak amplitude and some define velocity instead of volume flow impedances (reactances); otherwise they are all very similar in content. It is suggested, however

F, Effect of Sound Pressure Level and Mean Gas Flow (cont.)

(Ref I-7) that the aperture reactance reaches a minimum value (saturates) after attaining a critical value of aperture particle velocity, i.e., the saturation value appears to correlate with one-half the effective length. This result is compatible with the result obtained for mean flow past or through the aperture as summarized in Ref I-19. However, after considering all references, the best correlation for determining the resonant frequency of a resonator or its reactance at any frequency and at high sound levels appears to be the following:

$$f_o = \frac{C_r}{2\pi} \sqrt{\frac{A_o}{V}(t + \frac{\delta}{5})} \qquad \text{Eq. I-36}$$

and

$$X_m = 2\pi f \left[\rho_r A_o (t + \delta/5)\right] \qquad \text{Eq. I-37}$$

where $\delta = 0.8d$

This assumes that the saturated effective length of the aperture is

$$(t_e)_{sat} = t + 0.2\delta \cong t + (0.2)(0.8)d = t + 0.16d,$$

which suggests that aperture diameter has very little effect on the aperture's effective length at high SPLs relative to that at low SPL. However, if the aperture thickness is small compared to the orifice diameter, then the diameter determines the aperture's effective length.

F, Effect of Sound Pressure Level and Mean Gas Flow (cont.)

3. Mean Gas Flow Effects

The second consideration complicating the evaluation of resonators is the mean gas flow through or past the resonator aperture. Ingard (Ref I-7), Mechel, et al, (Refs I-10, I-11, and I-12), and McAuliffe (Ref I-6), provided most of the early analytical and empirical correlations that account for the effect of mean flow on acoustic resonator parameters. Ingard (Ref 28) subsequently clarified earlier acoustic experiments by showing the analytical relationship and empirical correlation between the acoustic nonlinearities of an orifice caused by oscillatory gas velocities and mean gas flows through an orifice. Ingard's (Refs I-7 and I-17) and McAuliffe's (Ref I-6) work shows that the increased acoustic resistance of an aperture due to high incident sound pressure levels and that due to flow through the aperture are proportional to the product of the gas density, ρ, and the maximum gas velocity through the aperture, u, where the gas velocity can be either the oscillatory velocity, u', or the mean gas velocity $\bar{u}$. The acoustic effect of mean gas flow past a resonator aperture has been found (Refs I-6 and I-7) to be similar to mean gas flow rates through the aperture except that much greater flow rates past the aperture are required to produce the same acoustic impedance change as either oscillatory or mean gas flow rates through the orifice. These effects are shown in Figure I-3.

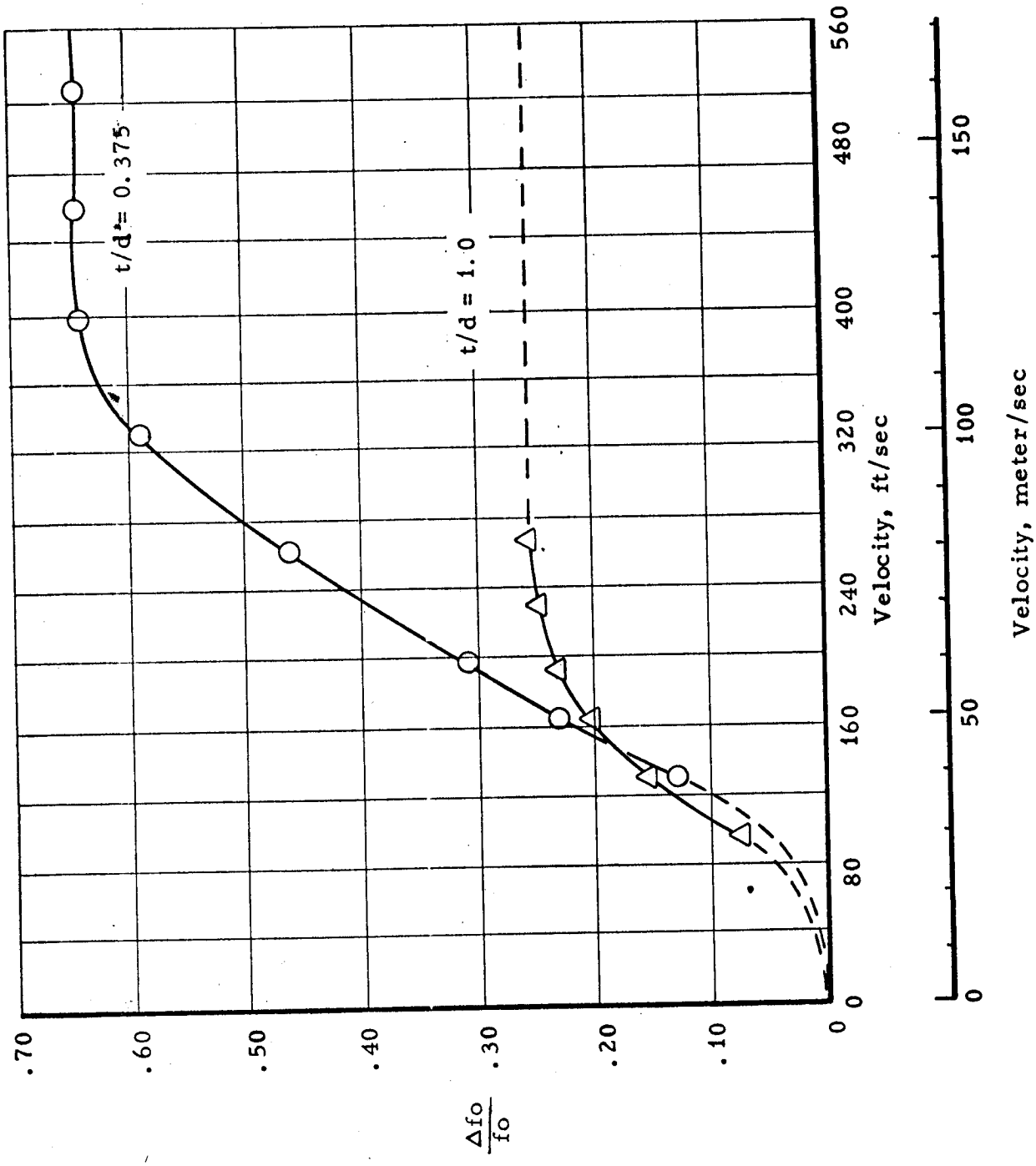

Figure I-3. Effect of Gas Flow Past Orifice on Response Frequency for Various Orifice Thickness-to-Diameter Ratios

G. GENERALIZED ACOUSTIC LINER ANALYSIS

This analysis (which utilizes Refs I-19 through I-24) is one of the approaches considered for overcoming the indicated shortcomings of the one-dimension array resonator analysis. It specifically related to transverse modes rather than the analysis of a separate one-dimensional resonator array.

The governing equations are written in cylindrical coordinates for both regions 1 and 2 as shown on Figure I-4. Assuming radial flow through the liner holes, the one-dimensional wave equation can be written to relate the two regions. The acoustic equation in cylindrical coordinates was written for two regions; the region between the outer chamber wall and the liner as well as the region between the centerline of the chamber and the liner:

$$\frac{\partial^2 P}{\partial r^2} + \frac{1}{r}\frac{\partial P}{\partial r} + \frac{1}{r^2}\frac{\partial P^2}{\partial \theta^2} + \frac{\omega^2}{c^2} P = 0 \qquad \text{Eq. I-38}$$

If it is assumed the variables can be separated, the solution has the form $P = R(r)\Theta(\theta)$. Substituting this solution into Equation 26, the following ordinary differential equations are obtained:

$$\Theta'' + \nu\Theta = 0 \qquad \text{Eq. I-39}$$

$$r^2 R'' + rR' + \left(\frac{\omega^2}{c^2} r^2 - \nu^2 \right) R = 0 \qquad \text{Eq. I-40}$$

The solutions to these equations are, respectively

$$\Theta = A \sin(\nu\theta) + B \cos(\nu\theta) \qquad \text{Eq. I-41}$$

$$R = D J_\nu \left(\frac{\omega}{c} r\right) + E Y_\nu \left(\frac{\omega}{c} r\right) \qquad \text{Eq. I-42}$$

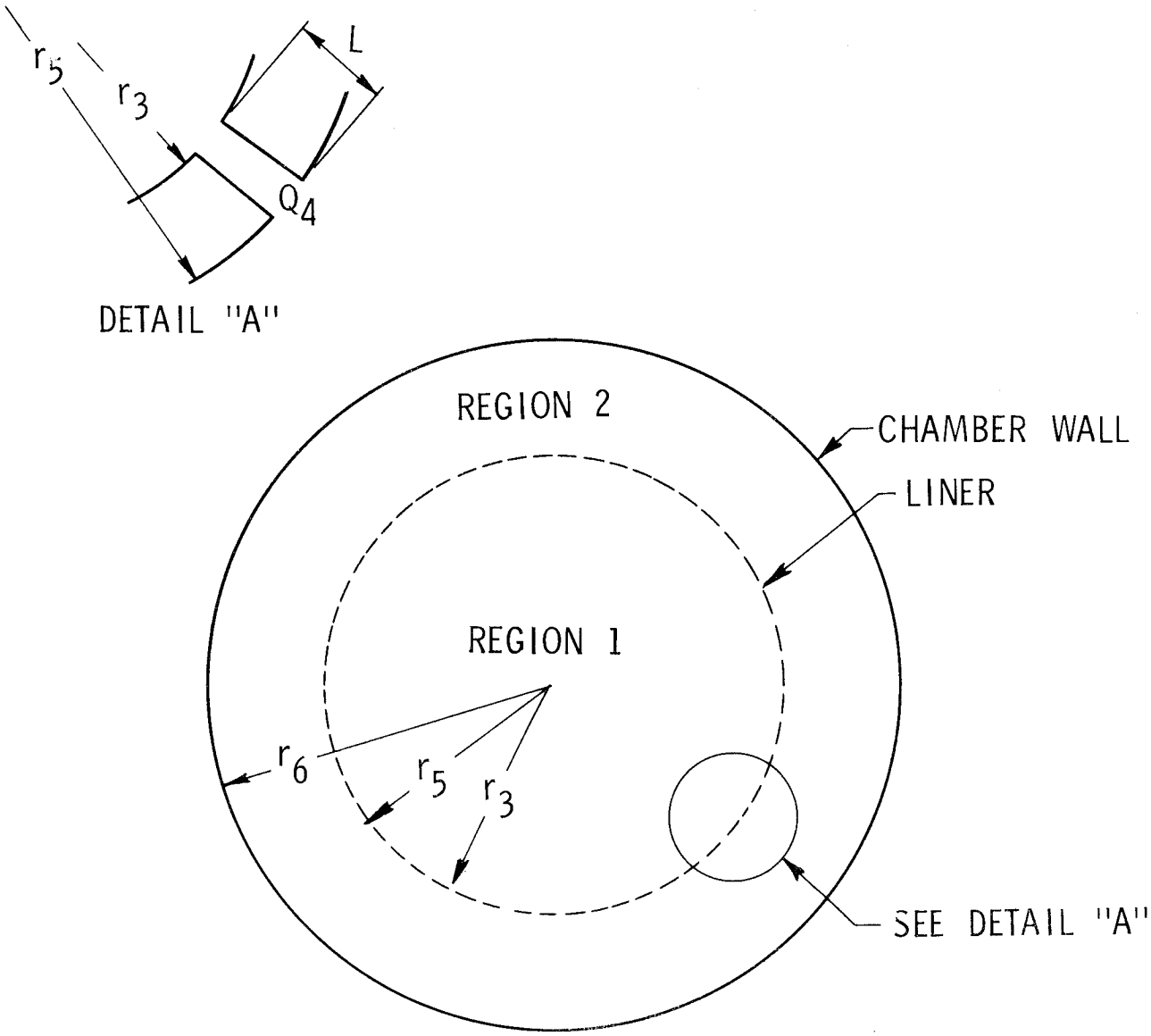

Figure I-4. Liner Model

G, Generalized Acoustic Liner Analysis (cont.)

The orifices between these two regions can be treated using the one-dimensional wave equation and a resistance connecting the orifices to the interior region. Radial volume flow and pressure must be matched at the interface. The same conditions must apply to connect the orifices to the outer region. In addition, the radial velocity at the outer wall is zero and the pressure at the center of the chamber is finite.

The equations across the three regions as well as the matching and boundary conditions form a set of nine homogeneous algebraic equations. The characteristic equation of this system is obtained by equating the determinant of the matrix formed by the nine equations to zero. Integrating the differential equations by separation of variables and applying the boundary conditions lead to a set of simultaneous homogenous equations, the coefficient determinant of which must vanish for a non-trivial solution to exist. The coefficients are transcendental functions; therefore, it is impractical to solve for the eigenvalues directly. The damping rate is obtained by plotting the amplitude of the inverse of the determinant as a function of frequency in the area of the characteristic equation zeros. Based upon these considerations, a computer program was developed to evaluate the determinant as a function of frequency. From the output of the program, it then is possible to determine the damping resulting from the liner by the frequency bandwidth at the half power point by using the following relationship:

$$\text{damping rate } (\delta_r) = 8.7\ \pi\Delta f \ \text{(db/sec)}$$

where Δf is the half-power frequency bandwidth of the response function.

The new resonant frequencies of the chamber cavity are determined by plotting the inverted matrix with the resonant frequencies being at the maximum values of the inverted matrix viz, the zeros of the characteristic equation.

G, Generalized Acoustic Liner Analysis (cont.)

Examples of the resulting output from the analysis are shown on Figures I-5 and I-6. The effect of incorporating an acoustic resonator in the chamber wall is illustrated on Figure I-6. The resonator has a resonant frequency of 2800 hz and the chamber without the liner had a first tangential mode resonant frequency at approximately 3400 hz. With the addition of the resonators, the chamber cavity assembly resonant frequency is reduced to 2015 hz. The first tangential mode frequency depression observed here was investigated further and it was found to be primarily a function of cavity temperature for a fixed geometry. The frequency depression of both the first and second tangential modes as a function of cavity temperature is shown on Figure I-7. Figure I-6 shows the analytical results for the same 8.0-in. diameter chamber with a rough chamber wall which had a resistance equivalent to that used for the resonator design discussed above. The results show only a small shift from the 3400 cps resonant frequency of the combustion chamber without a liner and a damping rate which is in the order of 20 db/sec lower than the resonant liner. These results should be used for comparison purposes only because the computing technique applied to obtain them has not been verified against the simplified model results as yet.

It appears that the results obtained from the simplified analysis shown on Figure I-8 are more reliable. The advantage of an analytical approach that treats the acoustic liner as an integral part of the combustion chamber is that it will predict the effect of the liner upon damping rate for each of the transverse modes and the change in the resonant frequencies of the system resulting from the introduction of the liner.

Because of the individual treatment of the backside cavity and the chamber cavity as well as the general treatment of the resonator neck, this analysis also can be used for what is generally referred to as a non-resonant liner. A modification of the Crocco-developed time-lag stability

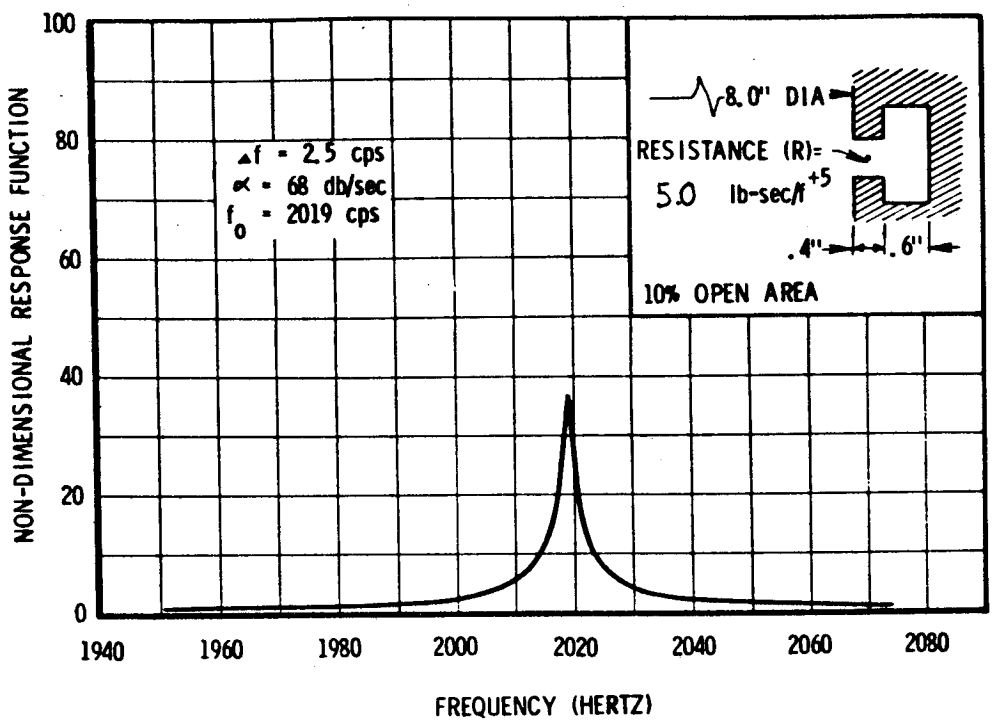

Figure I-5. Nondimensional Chamber Response Function Versus Frequency for a 2800 hz Liner in an 8-in. Chamber

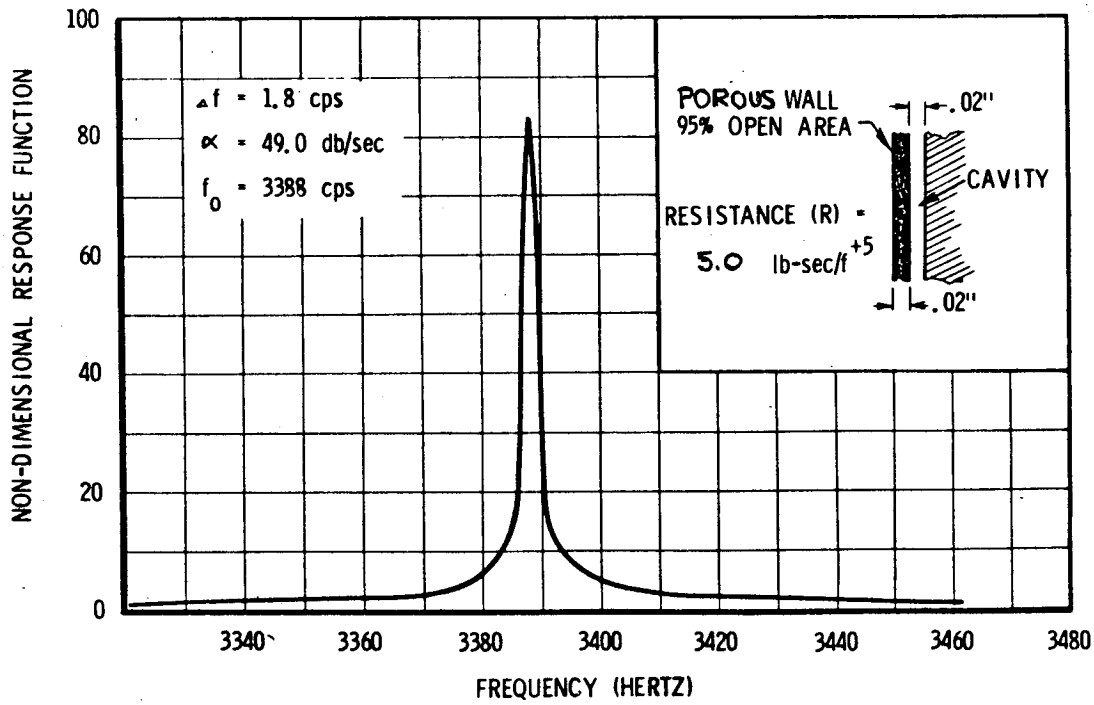

Figure I-6. Nondimensional Chamber Response Function for a Nonresonant Liner in an 8-in. Chamber

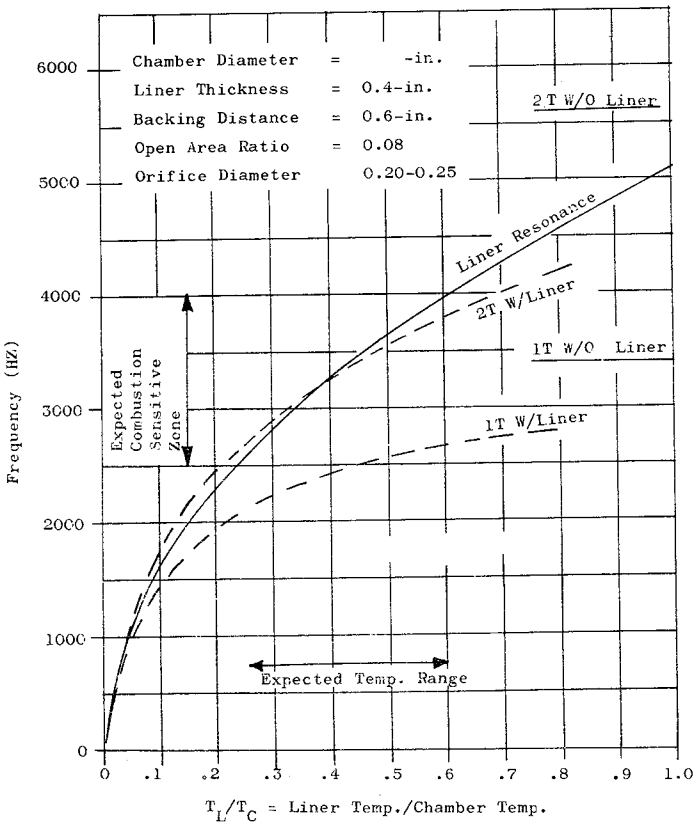

Figure I-7. Frequency Depression of First and Second Tangential Modes

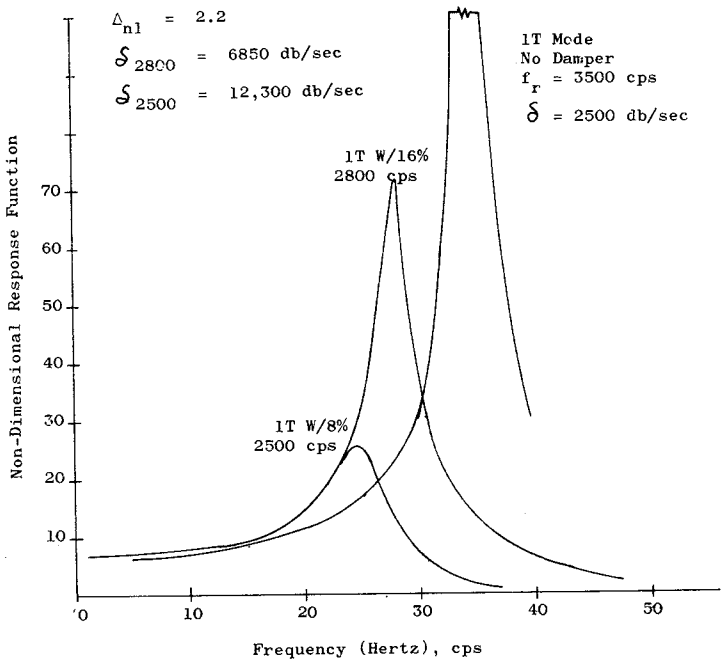

Figure I-8. Cylindrical Acoustic Analysis

G, Generalized Acoustic Liner Analysis (cont.)

model (Refs I-25, I-26, I-27) is used in the previously discussed analyses. The modification consists of introducing the liner as a boundary condition at the chamber wall. The analysis is a linearized treatment of the combustion process using the small perturbation technique, which results in a prediction of the zones of instability as a function of two parameters (n and τ), where n is a gain parameter and τ is a phase parameter.

The expected result of adding the liner is a shift in the stability zone to the right and upward as was shown on Figure I-9, which means that the system would move from unstable to stable combustion. The injector operating point was determined from empirical correlations of the type shown in Refs I-28 and I-29 which have been determined from an accumulation of experimental data.

H. INJECTOR FACE RESONATOR ANALYSIS

In this analysis, it is assumed that the combustion is concentrated at the injector face. The acoustics of the chamber are described by the nozzle admittance, which is the relationship between perturbations in the axial and transverse velocity and nozzle contour, the frequency, and the mode being analyzed. The analysis is an extension of the linear n-τ theory developed by Crocco and others. This particular analysis is taken from Reardon (Ref I-30) who deals with the problem of non-uniform injection (i.e., injection density varies over the face of the injector). The same mathematical technique is applied in this analysis where the admittance of the face varies with position. In this case, the injection density is uniform, but at the outer edge of the injector there is a resonator which produces a different admittance in this region. The admittance of the resonator (Y_r) was obtained from the literature (Ref I-8), except for the quarter wave tube which was obtained from another source (Ref I-31).

H, Injector Face Resonator Analysis (cont.)

A similar analysis was accomplished to include the coupling of feed system oscillations with transverse mode acoustic oscillations in the combustion chamber (Ref I-32). After writing all dependent variables as a mean plus a perturbation ($p = \bar{p} + p'$), the problem is reduced to solving the acoustic equation for a cylinder (in this case, with zero length) with a nozzle at one end and an admittance that depends upon position on the other (injector) end.

For a cylinder, the most general expression for the solution of the acoustic equation

$$\nabla^2 p' + \Omega^2 p' = 0 \qquad \text{Eq. I-43}$$

is

$$p' = \sum_{h=1}^{\infty} \sum_{\nu=0}^{\infty} A_{\nu h} P_{\nu h}(Z) R_{\nu h}(r) \Theta_{\nu}(\theta) \qquad \text{Eq. I-44}$$

where $P(Z) = A_{\nu h} \cosh \left[(S_{\nu h}^2 - \Omega^2)^{1/2} Z \right] + B_{\nu h} \sinh \left[(S_{\nu h}^2 - \Omega^2)^{1/2} Z \right]$

$R_{\nu h}(r) = J_{\nu}(S_{\nu h} r)$

$\Theta_{\nu}(\theta) = \text{Cos } \nu\, \theta$

$A_{\nu h}$ = constants to be determined by the boundary conditions

p' = the perturbation in pressure

J_{ν} = Bessel function of order ν

$S_{\nu h}$ and ν = separation constants

Ω = the nondimensional angular frequency, $\omega r_c / C$

H, Injector Face Resonator Analysis (cont.)

The axial velocity in the chamber is given by:

$$u' = -\frac{1}{\gamma j\Omega} \sum_{h=1}^{\infty} \sum_{\nu=0}^{\infty} A_{\nu h} \frac{d P_{\nu h}(Z)}{dZ} R_{\nu h}(r)\, \Theta_{\nu}(\theta) \qquad \text{Eq. I-45}$$

where γ is the ratio of specific heats.

The boundary condition at the injector is the sum of the generation rate of burned gas and the flow from the resonator matching the gas flow in the chamber.

$$(Y_r + Y_{n\tau})\, p' = \bar{\rho} u' + \bar{u} \rho' \qquad \text{Eq. I-46}$$

The symbol, $\bar{u}$ is the chamber gas mean velocity near the injector and $Y_{n\tau}$ is the combustion admittance. Using the momentum equation in the z direction and the isentropic relation between ρ' and p', the above equation becomes

$$(Y_r + Y_{n\tau} - \frac{\bar{u}}{\gamma}) p' = -\frac{1}{\gamma j\Omega} \frac{dp'}{dZ} \qquad \text{Eq. I-47}$$

All of the variables are non-dimensionalized (Ref I-30). Using these non-dimensional variables

$$\frac{p'}{\rho'} = \gamma \text{ and } \bar{\rho} = 1.$$

Then, using the assumed solution for R and θ above, the equation becomes:

$$(Y_r + Y_{n\tau} - \frac{\bar{u}}{\gamma}) \sum_{h=1}^{\infty} \sum_{\nu=0}^{\infty} A_{\nu h} P_{\nu h} R_{\nu h} \Theta_{\nu} = \frac{j}{\gamma\Omega} \sum_{h=1}^{\infty} \sum_{\nu=0}^{\infty} A_{\nu h} \frac{dP_{\nu h}}{dZ} R_{\nu h} \Theta_{\nu}$$

Eq. I-48

H, Injector Face Resonator Analysis (cont.)

The functions R and Θ are orthogonal which allows solution for the coefficients $A_{\nu h}$ in Equation I-48.

$$\int_0^1 \int_0^{2\pi} R_{\nu h} H_\nu R_{pq} \Theta_q \, r \, dr \, d\theta \begin{cases} = 0 \text{ if } \nu \neq q, \; h \neq p \\ = H_{pq} \text{ if } \nu = q, \; h = p \end{cases}$$

If both sides of Equation I-48 are multiplied by $P_{pq} \Theta_p$ and integrated, separate equations (q times p) without summations result. For a 1T mode, $\nu = 1$ and $h = 1$. For a 2T mode, $\nu = 2$ and $h = 1$. These are the only modes considered in this analysis; therefore, only two of these equations need be retained: Using the solutions for R and Θ given previously and recalling that the injector is at $z = 0$, for the 1T mode, Equation I-48 becomes:

$$\frac{j}{\gamma\omega} (S_{11}^2 - \Omega^2)^{1/2} B_{11} H_{11} = A_{11} \int \int Y_b R_{11}^2 \Theta_1^2 \, r \, dr \, d\theta + A_{11} \left(Y_{n\tau} - \frac{\bar{u}}{\gamma}\right) H_{11}$$

Eq. I-49

A similar equation can be obtained for the 2T mode.

For a given mode of oscillation, the boundary condition at the nozzle is determined by the nozzle admittance relation

$$\gamma U + \frac{Ts_{\nu h}}{\Omega} P = 0$$

where U is the z-dependent factor in the axial velocity,

$$u' = U(z) R_{\nu h}(r) \Theta_\nu (\theta)$$

and T is an admittance coefficient which is obtained from an existing computer program (Ref I-28).

H, Injector Face Resonator Analysis (cont.)

From the momentum equations in the z-direction, it is found that

$$U = -\frac{1}{\gamma j\Omega}\frac{dP}{dZ}$$

The nozzle admittance equation for the 1T mode then becomes

$$\frac{j}{\Omega}(S_{11}^2 - \Omega^2)^{1/2} B_{11} = -\frac{S_{11}T}{\Omega} A_{11} \qquad \text{Eq. I-50}$$

Equations I-49 and I-50 are two homogeneous equations in A_{11} and B_{11}. For these equations to have a solution, their determinant must be zero. The equation thus formed is the system characteristic equation, which characterizes the dynamics of the system and can be used to determine its stability. A n-τ plot can be obtained from this equation.

To obtain the n-τ plot, the factor $\int\int Y_r R^2\Theta_r^2 \, dr d\theta$ must be evaluated. Y_r is zero in the center of the injector and is a function describing the resonator at the edge of the injector. The impedance of a Helmholtz resonator is given by $\bar{\theta} + j\bar{\chi}$, (Ref I-8, cf Eq . I-6, Supra).

$$\bar{\theta} = \frac{4}{\sigma\rho_t c_t}\left(\frac{\pi u_r \rho_r f}{g}\right)^{1/2}\left(1 + \frac{t_1}{d} + \frac{\Delta n\ell}{d}\right) \qquad \text{(cf Eq. I-16)}$$

$$\bar{\chi} = \frac{2\pi\rho_r f_o \ell_e}{\rho_t c\sigma}\left(\frac{f}{f_o} - \frac{f_o}{f}\right) \qquad \text{(cf Eq. I-17)}$$

H, Injector Face Resonator Analysis (cont.)

where

σ = ratio of acoustic resonator orifice area to face area
ρ = gas density, lb-sec^2/ft^4
c = velocity of sound, fps
f = frequency, sec^{-1}
μ = gas viscosity, lb/sec-ft
g = gravitational constant, 32.2 fps^2
t_1 = acoustic resonator orifice thickness, ft
d = orifice diameter, ft
$\Delta_{n\ell}$ = nonlinear correction factor, ft
f_o = resonant frequency, sec^{-1}
ℓ_e = effective length of orifice mass, ft

Subscripts

t = tube (chamber) conditions
r = resonator conditions

To obtain an expression for Y_r, the above expression is nondimensionalized in a manner consistent with the chamber non-dimensionalization. In addition, Y_r is an admittance per unit area. The area selected is somewhat arbitrary, except that it must be the same area used in the integral.

The impedance of the quarter wave tube also is $\overline{\theta} + j\overline{\chi}$, where

H, Injector Face Resonator Analysis (cont.)

$$\overline{\chi} = -j \cos \left(\frac{2\pi\ fL\rho_r}{\rho_t\ c_t}\right) Q$$

$$\overline{\theta} = 0$$

L_Q = length of tube

A sample calculation using the IFAR computer program and the nozzle admittance program (Refs I-28 and I-33) resulted in the curves shown in Figure I-9. The effect of the acoustic liner tuned to primarily damp the first tangential mode is qualitatively indicated. It is clear that the second tangential combined with the first longitudinal acoustic mode is the least damped.

Identification of combined modes in hot firing chambers is very difficult even when an acoustic liner is not present. With an acoustic liner present it is nearly impossible in chambers with L/D's of one or greater.

Assumed Chamber Condition

Chamber pressure, psia	100
Velocity Past liner, ft/sec	0
Sound level, dB	190
Speed of sound, ft/sec	3600

Assumed Liner Condition

Temperature, ^{o}R	2640
Speed of sound, ft/sec	2605
Density, lb/ft^3	8.35×10^{-2}
Viscosity, lb/ft-sec	3.53×16^{-5}

ACOUSTIC LINER DIMENSIONS

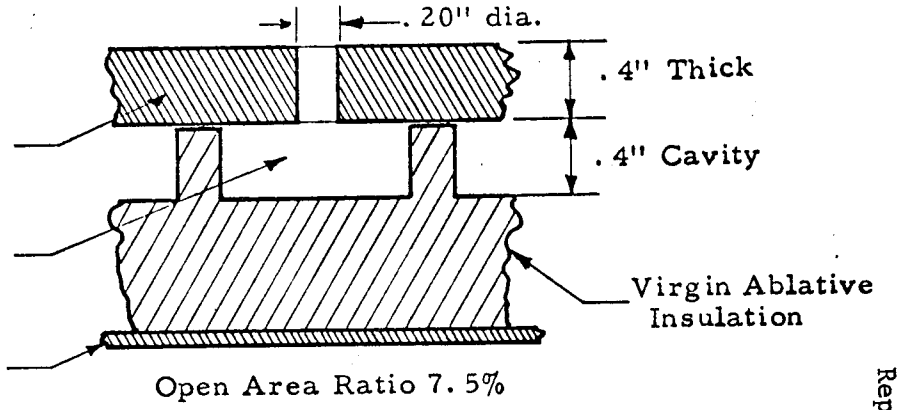

Open Area Ratio 7.5%

Note:

1. Resonator tuned to a frequency of 3045, cps.
2. Total cavity volume, 15.80 in^3
3. Total area of resonator holes, 2.51 in^2

——— Without liner

– – – – With liner

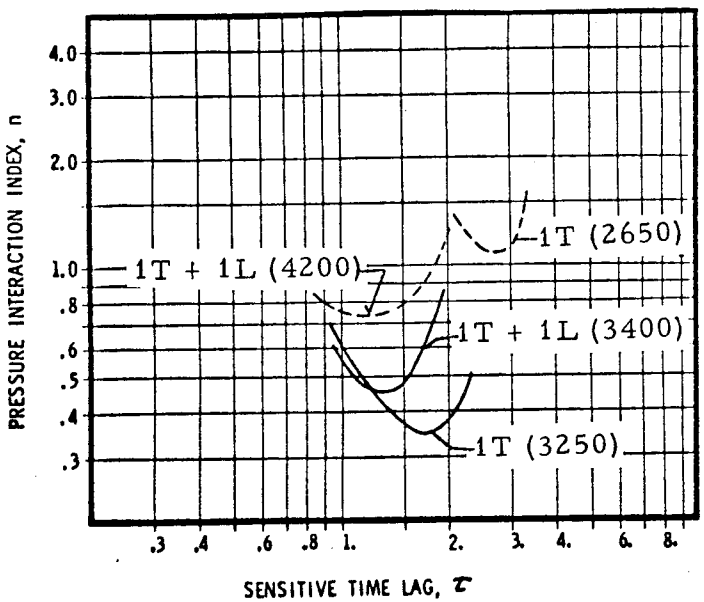

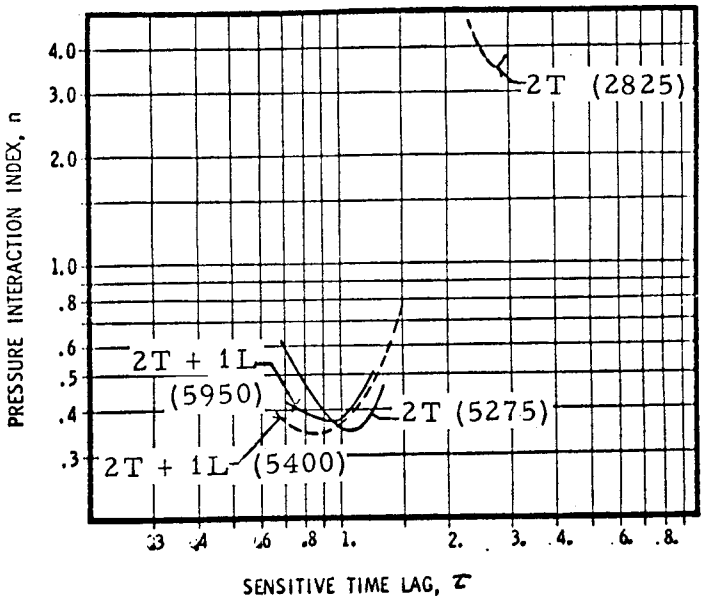

Figure I-9. First Tangential Mode Damper, n & τ Plots

REFERENCES

I-1 Rayleigh, Lord, J.W.S., The Theory of Sound Vol. II, Dover Publications, pp 172f and p 192f.

I-2 Morse, P.M., Vibration and Sound, 2nd Edition, McGraw-Hill Book Co., Inc., N.Y., 1948, p 235f.

I-3 Wood, Alexander, Acoustics, Dover Publications, New York, 1966, 3 ed., p 103.

I-4 Ingard, Uno, "On the Theory and Design of Acoustic Resonators", J. Acoust. Soc. Amer., Vol. 25, No. 6, Nov 1953, pp 1037-1061.

I-5 Ingard, U. and Labate, S., "Acoustic Circulation Effects and the Non-Linear Impedance of Orifices," Journal of the Acoustical Society of America, Vol. 22, March 1950.

I-6 McAuliffe, C.E., "The Influence of High Speed Air Flow on the Behavior of Acoustical Elements", M. Sc. Thesis, Massachusetts Institute of Technology, 1950.

I-7 Ingard, Uno; and Hartmut, Ising; "Acoustic Nonlinearity of an Orifice", J. Acoust. Soc. Am; Vol. 42, No. 1, July 1967, pp 6-17.

I-8 Blackman, A.W., "Effect of Nonlinear Losses on the Design of Absorbers for Combustion Instabilities." ARSJ, Vol. 30, No. 11, Nov 1960, pp 1022-1028.

I-9 Sirigano, W.A., et al, "Acoustic Liner Studies," ICRPG Third Combustion Conference, Vol. I, 17-21 October 1966.

I-10 Mechel, F., "Research on Sound Propagation in Sound-Absorbent Ducts with Superimposed Air Stresses", Vol. I, Report No. AMRD-TDR-62-140 (I) USAF Aerospace Medical Division, Wright Patterson Air Base, Ohio, December 1962.

I-11 Mechel, F.; and Schlitz, W.; "Research on Sound Propagation in Sound Absorbent Ducts with Superimposed Air Streams" Vol. II: Report No. AMRL-TDR-62-140 (II), USAF Aerospace Medical Division, Wright Patterson Air Force Base, Ohio, December 1962.

I-12 Mechel, F.; Mertens, P.; and Schlitz, W.; "Research on Sound Propagation in Sound-Absorbent Ducts with Superimposed Air Streams", Vol III; Report No. AMRL-TDR-62-140 (III), USAF Aerospace Medical Division, Wright Patterson Air Force Base, Ohio, December 1962.

REFERENCES (cont.)

I-13 Meyer, Erwin; Mechel, Fridolin; and Kurtze, Gunther; "Experiments on the Influence of Flow on Sound Attenuation in Absorbing Ducts", J. Acoust. Soc. Am., Vol. 30, No. 3, March 1958, pp 165-174.

I-14 Bailey, Curtis R.; An Investigation of the Use of Acoustic Energy Absorbers to Damp LOX/RP-1 Combustion Oscillations. NASA TN D-4210, November 1967.

I-15 Marino, Jr., P.A.; Bohn, N; and Garrison, G.D.; "Measurement of Acoustic Resistance at Sound-Pressure Levels to 17 1dB." J. Acoust. Soc. Am., Vol. 41, No. 5, May 1967, pp 1325-1327.

I-16 Phillips, Bert; Effects of High-Wave Amplitude and Mean Flow on a Helmholtz Resonator, NASA TM X-1582.

I-17 Bolt, R.H.; Labate, -- and Ingard, Uno, "The Acoustic Reactance of Small Circular Orifices," JASA Vol. 21, No. 2, March 1949, pp 94-97.

I-18 Bies, David A; and Wilson, O.B., Jr. "Acoustic Impedance of a Helmholtz Resonator at Very High Amplitude", JASA, Vol. 29, No. 6, June 1957, pp 711-714.

I-19 Phillips, Bert; On the Design of Acoustic Liners for Rocket Engines: Maximum Damping as a Design Objective. NASA TM X-1720, January 1969.

I-20 Phillips, Bert; and Morgan, Joe C.; Mechanical Absorption of Acoustic Oscillations in Simulated Rocket Combustion Chambers, NASA TN D-3792., January 1967.

I-21 Priem, Richard J. and Rice, Edward J.; Combustion Instability with Finite Mach Number Flow and Acoustic Liners, NASA TM X-52412, May 1968.

I-22 Bucher, R.E., "A Mathematical Analysis of the Suppression of High Frequency Combustion Instabilities by a Sound Absorbing Liner", AIAA 2nd Aerospace Sciences Meeting, Paper No. 65-107, New York, N.Y., January 1965.

I-23 Anonymous, "A Study of the Suppression of Combustion Oscillations with Mechanical Damping Devices", Pratt and Whitney Aircraft Report FR-1007, September 1964 (Appendix G).

I-24 Phillips, Bert; Hannum, Ned P.; Russell, Louis M.; On the Design of Acoustic Liners for Rocket Engines: Helmholtz Resonators Evaluated with a Rocket Combustor, NASA TN D-5171, April 1967.

REFERENCES (cont.)

I-25 Crocco, L. and Chang, S. I., Theory of Combustion Instability in Liquid Propellant Rocket Motors, AGARDograph No. 8, Butterworth's Scientific Publications, Ltd., London, 1956.

I-26 Crocco, L., Grey, J., and Harrje, D.T., "Theory of Liquid Propellant Rocket Instability of Its Experimental Verification, ARS Journal, Vol. 30, No. 2, February 1960.

I-27 Crocco, L., Harrje, D.T., and Reardon, F.H., "Transverse Combustion Instability in Liquid Propellant Rocket Motors," ARS Journal, Vol. 32, No. 3, March 1963.

I-28 Smith, A.J., Jr., Reardon, F. H., et al, "The Sensitive Time Log Theory and Its Application to Liquid Rocket Combustion Instability Problems", Vol I Engineers Manual, Aerojet-General Corporation, March 1968, AFRPL TR-67-314.

I-29 Reardon, F. H., "Correlation of Sensitive Time Lab Theory Combustion Parameters with Thrust Chamber Design and Operating Variables", ICRPG Fifth Combustion Conference, CPIA Publication No. 183, December 1968, pp 237-243.

I-30 Reardon, F.H., An Investigation of Transverse Mode Combustion Instabilities in Liquid Propellant Rocket Motors, Princeton University Aeronautical Engineering Report No. 550, 1 June 1963.

I-31 Beranek, L.L., Acoustics, McGraw-Hill Book Co., Inc., New York, 1954.

I-32 Waugh, R.C., et al, "A Mathematical Model for Transverse Mode Instability with Feed System Coupling for Titan IIIM", Presented at the Fifth ICRPG Combustion Conference, 1 October 1968.

I-33 Anonymous, "Stability Characterization of Advanced Injectors" Design Guide Volume 2 Aerojet-General Corp., Report 20672-P2D (Contract NAS 8-20672), January 1970.

APPENDIX II

ANNOTATED BIBLIOGRAPHY

A. ACOUSTIC RESONATORS

1. Combs, L. P.; Hoehn, F. W.; Webb, S. R.; et al; Combustion Stability Rating Techniques, Final Report AFRPL-TR-66-229, Sept. 1966.

   This report presents an investigation of nondirected explosive bombs, directed explosive pulse guns, and directed flows of inert gases. Propellants used were N_2O_4/50% N_2H_4 and 50% UDMH or with 100% UDMH at a chamber pressure of 150 psia and a mixture ratio of 1.6. A combination of nondirected bombs and pulse guns are the recommended stability rating methods for the above propellants and conditions.

2. Phillips, Bert; Hannum, Ned P.; Russell, Louis M.; On the Design of Acoustic Liners for Rocket Engines: Helmholtz Resonators Evaluated with a Rocket Combustor. NASA TN D-5171, April 1967.

   This document presents an analytical evaluation of Helmholtz resonators, especially aperture effective lengths and nonlinear characteristics. Experiments were carried out using variable cavity depth resonators in a hydrogen-oxygen rocket engine. Theoretically calculated acoustic resistances were correlated by an empirical function of the mean and oscillatory gas flows.

3. Phillips, Bert; On the Design of Acoustic Liners for Rocket Engines: Maximum Damping as a Design Objective. NASA TM X-1720, January 1969.

   A theoretical evaluation of the wave equation for transverse acoustic modes of a closed end cylindrical cavity without mean gas flow is presented. The analysis determined that the absorption coefficient can be used to design acoustic liners if the real part of the impedance is greater than unity. The shifting of acoustic mode frequencies is discussed.

4. Conrad, E. William; Bloomer, Harry E.; Wanhainer, John P., and Vincent, David D.; Interim Summary of Liquid Rocket Acoustic-Mode-Instability Studies at a Nominal Thrust of 20,000 Pounds. NASA-TN-D-4968, December 1968.

   Experimental results which relate to combustion instability in liquid rockets using hydrogen/oxygen and earth storable N_2O_4/A-50 propellants are discussed. Nonfiring acoustics tests, acoustic liner and injector baffle hot fire test results are evaluated. A discussion of problems associated with flow past acoustic liner apertures and the properties of the resonator gas are examined. This reference has data in common with reference: NASA TN D-3822 which was written earlier.

A, Acoustic Resonators (cont.)

5. Phillips, Bert; Effects of High-Wave Amplitude and Mean Flow on a Helmholtz Resonator, NASA TM X-1582.

   This document presents the results of an experimental investigation of the effects of mean flow and high-wave amplitude on the impedance of a Helmholtz resonator. Results indicated that for rocket engines the aperture effective length is approximately equal to the aperture thickness, and the acoustic resistance at high-wave amplitude is a turbulent-jet loss defined by the product of the gas density and particle velocity. An excellent theoretical section is presented for correlation with the empirical results.

6. Vincent, David W.; Phillips, Bert; and Wanhainen, John P.; Experimental Investigation of Acoustic Liners to Suppress Screech in Storable Propellant Rocket Motors. NASA TN D-4442, March 1968.

   This document presents an experimental and theoretical evaluation of acoustic liners in a rocket engine using N_2O_4/A-50 propellants at a chamber pressure of 100 psia and a thrust of 6700 pounds. Liner design variables included aperture size and shape, line percent open area and length. Bombs were used for stability rating. Longitudinal slots adaptable to regeneratively cooled configurations were found to be effective.

7. Bailey, Curtis R.; An Investigation of the Use of Acoustic Energy Absorbers to Damp LOX/RP-1 Combustion Oscillations. NASA TN D-4210, November 1967.

   This document presents an experimental evaluation of acoustic liners in both cooled and uncooled 4000-pound thrust combustion chambers operating at 1000 psia chamber pressures. A sample acoustic liner absorption coefficient calculation is presented based on the results of a NASA sponsored program NAS 8-11038 "A Study of the Suppression of Combustion Oscillations with Mechanical Damping Devices which was conducted by Pratt and Whitney Aircraft.

8. Wanhainen, John P.; Bloomer, Harry E.; Vincent, David W.; and Curley, Jerome K.; Experimental Investigation of Acoustic Liners to Suppress Screech in Hydrogen-Oxygen Rockets. NASA TN D-3822, February 1967.

   This document presents an experimental investigation of the use of acoustic liners in an engine using hydrogen/oxygen propellants, a chamber pressure of 300 psia, a mixture ratio of 4.0 to 6.0, and a thrust of 20,000 pounds. This document has some data in common with NASA TN D-4968 which is written later. Resonator cavity gas temperatures were found to be 600 to 1000°R during stable operation and 2000°R during stable operation and 2000°R during instabilities.

A, Acoustic Resonators (cont.)

9. Phillips, Bert; and Morgan, Joe C.; Mechanical Absorption of Acoustic Oscillations in Simulated Rocket Combustion Chambers, NASA TN D-3792.

   This document presents a nonfiring cold flow acoustics evaluation of single Helmholtz resonators and perforated liners in a cylindrical chamber. First tangential standing and spinning acoustic modes were excited as well as standing second tangential and first radial. It was indicated that a liner could be effective over a wide frequency range if a range of hole sizes were used. Angled resonator holes were evaluated and found to have no effect on absorption.

10. Wieber, Paul R.; Acoustic Decay Coefficients of Simulated Rocket Combustors. NASA TN D-3425, May 1966.

    This document presents a nonfiring cold acoustic bench test experiment using cylindrical chambers without mean gas flow. Decay rate measurements were made to indicate damping trends with chamber length, nozzle angle and injector baffle shapes. Baffled chambers had much higher damping than unbaffled chambers but no correlations were found.

11. Priem, Richard J. and Rice, Edward J.; Combustion Instability with Finite Mach Number Flow and Acoustic Liners. NASA TM X-52412, May 1968.

    This document presents a theoretical analysis of three dimensional small amplitude (linear) pressure oscillations in a combustion chamber with axial gas velocities. Combustion is assumed to be concentrated near the injector face and the equations solved for specific boundary conditions at the nozzle, combustion and acoustic linerwall. Axial acoustic mode pressure profiles for various chamber Mach numbers and length to diameter ratios are presented that show significant differences.

12. Blackman, A. W.; "Effect of Nonlinear Losses on the Design of Absorbers for Combustion Instabilities." ARSJ., Vol. 30, No. 11, November 1960. 11 1022-1028.

    This paper presents a discussion of the theoretical and empirical status of the nonlinear acoustic resistance of an orifice as of 1960. No mean flow through or past orifices is considered. Absorption coefficient equations are presented which take account of the nonlinear resistance term.

A, Acoustic Resonators (cont.)

13. Ingard, Uno; and Hartmut, Ising; "Acoustic Nonlinearity of an Orifice." J. Acoust. Soc. Am.; Vol. 42, No. 1, July 1967, pp. 6-17.

    This paper presents the test results from acoustic laboratory experiments and their interpretation. The tests involved the evaluation of nonlinear acoustic resistance and reactance as a function of sound level alone, or of sound level and mean gas flows through orifices. Hot wire measurements were made to evaluate orifice flow characteristics.

14. Phillips, Bert; Experimental Investigation of an Acoustic Liner with Variable Cavity Depth. NASA TN D-4492.

    This document presents the results of an experimental evaluation of a rocket engine using hydrogen-oxygen propellants at 300 psia chamber pressure, at 20,000 pounds thrust. The chamber wall was made up of individual Helmholtz resonators with adjustable cavity depths. Cavity gas temperature measurements and cavity gas samples were taken. The effect of liner length and position were evaluated.

15. Marino, Jr., P. A.; Bohn, N.; and Garrison, G. D.; "Measurement of Acoustic Resistance at Sound-Pressure Levels to 171dB." J. Acoust. Soc. Am., Vol. 41, No. 5, May 1967, pp. 1325-1327.

    This paper presents the results of impedance tube acoustic tests at high sound levels. The results appear to be an improvement over the results presented by Blackman in 1960 for the nonlinear resistance ratio as a function of sound pressure level. The method for obtaining data was different than Blackmans, and the plate thicknesses considered were generally greater.

16. Tabata, William K.; Antl, Robert J.; and Vincent, David W.; Storable Propellant Combustion Instability Program at Lewis Research Center, Paper No. 66-602, AIAA June 1966.

    This paper presents the results of rocket engine testing using N_2O_4/ 50% N_2H_4 and 50% UDMH at chamber pressures of 100 and 300 psia and thrust levels of 6700 and 20,000 pounds. Stability rating was accomplished with RDX explosive (MIL-R-398) charges ranging in size from 1.6 to 45.2 grains in tangential pulse guns. Acoustic liners were evaluated with a marginally stable and a spontaneously unstable injector. All liners were effective with the marginally stable injector.

A, Acoustic Resonators (cont.)

17. Rayleigh, Lord; J. W. S., The Theory of Sound, Vol. II, Dover Publications, P-172f and P192f.

    This is a classical theoretical treatment of Helmholtz resonators at low sound levels and without mean flow effects. Only acoustic losses considered are radiation losses at the resonator aperture. The kinetic energy of aperture gas oscillations is derived for an incompressible fluid.

18. Morse, P. M., Vibration and Sound, 2nd edition, McGraw-Hill Book Co. Inc., N.Y., 1948, P-235f.

    This portion of the text shows the resonant frequency formula derivations for a Helmholtz resonator with electrical analogies. High and low pass acoustical filters are discussed.

19. Wood, Alexander, Acoustics, Dover Publications, P-103.

    This text is similar in content to Rayleighs Theory of Sound and Morses Vibration and Sound; however, differences in approach, notation, and emphasis help in the understanding of the fundamentals of acoustic resonators and filters.

20. Morse, Philip M. and Ingard, Uno K.; Theoretical Acoustic, McGraw-Hill, Inc., New York, 1968. P-467.

    This text supersedes Morse's Vibration and Sound text in many acoustic areas; however, it does not necessarily repeat the information of the earlier work. Helmholtz resonator theory is limited, but the fundamental building blocks of acoustic theory are presented. Definitions for acoustical terms are excellent.

21. Beranek, L. L., Acoustics, McGraw-Hill, Inc., New York, 1952. P.

    This text is a very practical source of acoustic fundamentals which are required for understanding the more advanced texts.

22. Morse, P. M. and Feshbach, H., Methods of Theoretical Physics, Part I and II, McGraw-Hill, Inc., 1953.

    An advanced text on mathematical methods in physics including extensive acoustical analysis.

A, Acoustic Resonators (cont.)

23. Schindler, R. C. and Kiser, H. V., "Development and Demonstration of Ablative Thrust Chamber Assemblies Using LF_2/N_2H_4 Blend Propellants, Confidential, Aerojet-General Final Report AFRPL-TR-69-2, January 1969.

This is a confidential program, Contract No. F04611-67-C-003 using a 9.45 inch diameter, 7000 lbf thrust, 100 psia, LF_2/BA1014 thrust chamber assembly which evaluated one ablative acoustic liner and three steel acoustic liners.

24. Bucher, R. E., "A Mathematical Analysis of the Suppression of High Frequency Combustion Instabilities by a Sound Absorbing Liner". AIAA 2nd Aerospace Sciences Meeting, Paper No. 65-107, New York, N. Y., January 1965.

This paper presents an analysis for determining the best acoustic liner for a cylindrical rocket chamber by evaluating the damping coefficient of the chamber with and without an acoustic liner. This analysis predicts changes in the transverse acoustic mode frequencies, but disregards the presence of longitudinal modes or combinations of transverse and longitudinal modes.

25. Ingard, Uno, "On the Theory and Design of Acoustic Resonators", J. Acoust. Soc. Amer., Vol. 25, No. 6, Nov 1953, PP 1037-1061.

This paper presents basic theory and terminology for the absorption and scattering of sound from acoustic resonators in a free-field as well as in walls. The optimum resonator design for maximum absorption at liner sound levels without mean gas flow effects.

26. Gordon, Colin; and Smith, P. W. Jr.; "Acoustic Losses of a Resonator with Steady Gas Flow", J. Acoust. Soc. Am. Vol. 37, No. 2, Feb 1965, PP. 257-267.

This paper presents the results of cold flowing air in one end of a "T-burner" apparatus at atmospheric pressure, and varying the subsonic nozzle location, shape and Mach number. The results indicate significant nozzle loss changes as a function of these variables.

27. Smith, P. W.; and Feldman, B.; "Influence of Vent Design on Flow Dependent Acoustic Losses of a Resonator with Steady Gas Flow", Bolt Beranek and Newman, Inc., Final Technical Report for Ballistics Research Laboratories, Contract No. DA-19-020-AMC-00527(X), April 1966.

This document presents essentially the same results given in Gordon and Smith's J. Acoustic Soc. Am. paper, Vol 37, No. 2, Feb. 1965 PP. 257-267.

A, Acoustic Resonators (cont.)

28. Meyer, Erwin; Mechel, Fridolin; and Kurtze, Gunther; "Experiments on the Influence of Flow on Sound Attenuation in Absorbing Ducts", J. Acoust. Soc. Am. Vol. 30, No. 3, March 1958, PP. 165-174.

    This paper presents some of the experimental results obtained from a duct lined with individual Helmholtz resonators. A turbulent air stream with flow velocities varying from 0 to 266 feet/second was used in the duct to evaluate the attenuation of the resonators as a function of flow velocity past the resonator orifices. A gain in sound amplitude was observed at frequencies slightly above the Helmholtz resonance frequency due to the uniform spacing of the resonators down the duct. All the tests were made using air at ambient conditions. A small increase in resonant frequency was observed with increasing flow velocity.

29. McAuliffe, C. E., "The Influence of High Speed Air Flow on the Behavior of Acoustical Elements", M. Sc. Thesis, Massachusetts Institute of Technology, 1950.

    This thesis presents orifice impedance results for air flow through and past an orifice. Changes in both resistance and reactance of the orifice were measured. Some high sound level data was obtained with air flow.

30. Mechel, F., "Research on Sound Propagation in Sound-Absorbent Ducts with Superimposed Air Stresses", Vol. I, Report No. AMRL-TDR-62-140 (I) USAF Aerospace Medical Division, Wright Patterson Air Base, Ohio, December 1962.

    This report is similar to the J. Acoustic Soc. Am. paper, Vol. 30, No. 3 of March 1958, but gives more experimental and analytical details. Data is presented for both damped and undamped Helmholtz resonators as well as for quarter wave tubes. Flow past the resonators is considered, flow through is not. This document is one of three volumes.

31. Mechel, F.; and Schlitz, W.; "Research on Sound Propagation in Sound Absorbent Ducts with Superimposed Air Streams", Vol. II; Report No. AMRL-TDR-62-140 (II), USAF Aerospace Medical Division, Wright Patterson Air Force Base, Ohio, December 1962.

    This document is the second of three volumes. This volume presents a correlation for change of acoustic resistance as a function of flow velocity past the orifices.

A, Acoustic Resonators (cont.)

32. Mechel, F.; Mertens, P.; and Schlitz, W.; "Research on Sound Propagation in Sound-Absorbent Ducts with Superimposed Air Streams", Vol. III; Report No. AMRL-TDR-62-140 (III), USAF Aerospace Medical Division, Wright Patterson Air Force Base, Ohio, December 1962.

This document is the third of three volumes. This volume presents the results of periodically spacing Helmholtz resonators and determining the frequency of amplification. Again the effect of mean flow past the resonator orifices is emphasized.

33. Culick, Fred E., "Stability of High Frequency Oscillations in Gas and Liquid Rocket Combustion Chambers," TR 480, Massachusetts Institute of Technology Aerophysic Laboratory. June 1961.

This document presents a comprehensive stability analysis of rocket combustion in three dimensions with energy addition by combustion, standing acoustic pressure waves, on a converging nozzle with a sonic throat. No acoustic liner is considered in this analysis.

34. Anonymous, "A Study of the Suppression of Combustion Oscillations with Mechanical Damping Devices" Pratt and Whitney Aircraft Report FR-1007, Sept. 1964.

This document summarizes much of the Helmholtz acoustic resonator work prior to 1964. Emphasis is placed on the absorption coefficient approach to acoustic resonator array design method with acoustic resistance and reactance corrections for flow past or through the resonator orifices. Appendix G of this report presents an analysis by F. E. Culick which includes the chamber acoustic mode with an acoustic liner, a nozzle, and combustion effects, this analysis is similar to R. E. Bucher's analysis which is presented in AIAA paper number 65-107 in January 1965.

B. HEAT TRANSFER

1. Fox, J., "Surface Pressure and Turbulent Airflow in Transverse Rectangular Notches," NASA Technical Note D-2501, 1964.

   Surface pressure coefficients and airflow measurements in rectangular notches of length-to-height ratio 1/4 to 1-3/4 are presented for freestream velocities of 160 to 600 ft/sec.

2. Charwat, A. F., et al, "An Investigation of Separated Flows -- Part I: The Pressure Field," Journal of the Aerospace Sciences, Vol. 28, pp 457-470, 1961.

   Several types of separated regions such as blunt-base wakes, steps, and cavities, for subsonic and supersonic flow, are described, with regard to the existence, geometry and pressure distribution.

3. Charwat, A. F., et al, "An Investigation of Separated Flow -- Part II: Flow in the Cavity and Heat Transfer," Journal of the Aerospace Sciences, Vol. 28, pp 513-527, 1961.

   Part II describes local wall heat transfer for flow over a cavity, in terms of external Mach number, length-to-depth ratio of the cavity, ratio of boundary layer thickness to notch depth, etc.

4. Larson, H. K., "Heat Transfer in Separated Flows," Journal of the Aerospace Sciences, Vol. 26, pp 731-738, 1959.

   Heat transfer in separated flows was found to be about half that for attached flows, for both laminar and turbulent flow. The effect of transition on heat transfer in the separated laminar boundary layer is described.

5. Roshko, A., "Some Measurements of Flow in a Rectangular Cutout," NASA TN-3488, 1955.

   The pressure, velocity and skin friction for flow over a rectangular slot are described.

6. Seban, R. A., Emery, A., and Levy, A., "Heat Transfer to Separated and Reattached Subsonic Turbulent Flows Obtained Downstream of a Surface Step," Journal of the Aerospace Sciences, Vol. 26, pp 809-814, 1959.

   Reduced heat transfer was noted in the separated region immediately aft of the step; at the reattachment point a maximum in heat transfer occurs, and throughout most of the region the heat transfer coefficient depends on velocity to the 0.8 power.

B, Heat Transfer (cont.)

7. Seban, R. A. and Fox, J., "Heat Transfer to the Airflow in a Surface Cavity," proceedings of the 1961 International Heat Transfer Conference, ASME, pp 426-431.

   Heat transfer in the rectangular cavity was found to vary approximately as the 0.8 power of velocity.

8. Haugen, R. L., "An Analytical and Experimental Study of Heat and Momentum Transfer in Turbulent Separated Flow Past a Rectangular Cavity," PhD Thesis, Michigan State University, 1966.

   An analytical model is developed for the turbulent heat and momentum transfer in the separated flow region of a transverse rectangular cavity. Good correlation is achieved with experimental data.

9. Haugen, R. L., and Dhanak, A. M., "Heat Transfer in Turbulent Boundary Layer Separation Over a Surface Cavity," Journal of Heat Transfer, pp 335-340, November 1967.

   The heat transfer aspects of the Haugen thesis (No. 8 above) are described.

10. Haugen, R. L., and Dhanak, A. M., "Momentum Transfer in Turbulent Separated Flow Past a Rectangular Cavity," Journal of Heat Transfer, pp 641-646, September 1966.

    The momentum transfer aspects of the Haugen thesis (No. 8 above) are described.

11. Maull, D. J., and East, L. F., "Three-Dimensional Flow in Cavities," Journal of Fluid Mechanics, Vol. 16, pp 620-632, 1963.

    The vortex nature of flow in cavities with large span-to-chord ratios is described. Two orientations are possible for any series of vortex cells--the second being the reverse of the first--and unsteady flow usually results if the span/chord combination doesn't produce a cellular structure.

12. Snedeker, R. S., and Donaldson, C.duP., "Observation of Bistable Flow in a Hemispherical Cavity," AIAA, Vol. 4, p 735, 1966.

    A bistable vortex was found in the cavity, with the vortex axis considerably skewed to the direction of flow.

B, Heat Transfer (cont.)

13. Spalding, D. B. and Pantankar, S. V.; "Heat and Mass Transfer in Boundary Layers," CRC Press: Cleveland, 1968.

A computer program is developed for solution of the boundary layer equations for two-dimensional flows, not necessarily near walls. Couette flow is assumed near the boundaries, and slip or "false" values of physical parameters are utilized, for solution of internal nodal point parameters.

14. Boldman, D. R., et al, "Turbulence, Heat Transfer, and Boundary Layer Measurements in a Conical Nozzle with Controlled Inlet Velocity Profile," NASA TN D-3221, 1966.

Experimental determination of the boundary layer velocity profile, displacement thickness, momentum thickness, etc., showed a 1/30 power relationship for the velocity.

C. MATERIALS AND FABRICATION

The primary information utilized for application to selection and analysis of materials for an ablative acoustic liner is briefly summarized under each reference. The summary is not intended to place limitations upon the usefulness of the reports, but to emphasize a point of utility for the acoustic liner program.

1. Warga, J. J., et al, "Evaluation of Low-Cost Materials and Manufacturing Processes for Large Solid Rocket Nozzles", AFRPL-TR-67-310, Dec 1967.

   The "Standard" ablatives including silica reinforced phenolics were tested comparatively in a solid rocket nozzle. The difference in performance for a specific type of material was insignificant regardless of supplier. Control of the condition of the prepreg appeared to be more significant than source of the material. Based on this data (as well as other empirical tests) it appeared that a screening of silica reinforced phenolics from many sources was not necessary.

2. Cline, P. B. and Schultz, T. E., "Investigation of the Effect of Material Properties on Composite Ablative Materials Behavior", NASA CR-72142, April 1967.

   Correlation of performance (Recession Rate) with property variations of silica phenolic indicated silica fiber melting temperature and virgin plastic density were the most significant. These tests demonstrated that the control of the purity of the silica fabric (melt temperature) and fabrication technique of lay-up and cure/pressure were the most important for making an acoustic liner from a silica reinforced phenolic.

3. Davis, H. O., "Properties of Six Charred Reinforced Phenolic Materials", AGC Report No. 505, AF 04(694)-258, July 1963.

   Mechanical property measurements at 1500°F demonstrated the integrity of a charred silica phenolic; however, the upper temperature limit was not established in this study. Some indication was shown in the measurement of charred silica/phenolic compressive strength at 2500°F, Reference 1 above.

   A precharred silica phenolic appeared to be a potential integral structure up to at least 2500°F; therefore, it was a candidate for an acoustic liner in the less severe environments.

C, Materials and Fabrication (cont.)

4. Warga, J. J., et al, "The Effects of Material and Process Variables on the Properties of Three Carbon Fabric Reinforced Plastic Composites", AGC Report No. 561, February 1965.

The property measurements of precharred versus uncharred measurements of ablative materials demonstrated the better structural properties of material that had been carbonized at a relatively slow rate. The data (plus observation of post test ablative chambers) indicated better structure of a silica phenolic liner could be obtained by precharring the liner.

5. Dickson, J. C. and Howard, W. S., "Nonregeneratively Cooled Thrust Chamber Development Program", AFRPL-TR-65-138, Sept. 1965.

Precharred carbonaceous reinforced phenolic systems were utilized as chamber liners and performance was superior to the uncharred ablative systems. For those environments where thermal conductivity of the material is not the controlling limitation, the precharred (thermally stable) materials offer characteristics better suited to stop-start conditions. Problems related to high thermal dilation and outgassing can be eliminated by using precharred systems.

6. Davis, H. O., et al, "Evaluation of Characteristics Affecting Attainment of Optimum Properties of Ablative Plastics", AFRPL-TR-68-29, Vol I and II, February 1968.

Effects of material and processing variation were studied to ascertain their effects on properties and performance in a solid rocket motor. The measurements and limits necessary to control raw material, tape wrapping and cure/pressure variations were established for standard materials. The results of this study was utilized in selecting fabrication techniques and raw material properties for an acoustic liner.

7. Farmer, R. W., "Thermogravimetry of Phenol-Formaldehyde Polycondensate, Part II, AFML-TR-65-246, March 1967.

The behavior of phenolic resins when exposed to heat is measured. Of particular significance to use of phenolic in an acoustic liner is the approximate 50 percent carbon yield of the resin when pyrolyzed in a vacuum or inert atmosphere.

C, Materials and Fabrication (cont.)

8. Ladacki, Michael, et al, "Heat of Pyrolysis of Resin in Silica Phenolic Ablator", AIAA, Vol. 4, No. 10, October 1966

The gases evolved during decomposition of a phenolic resin were identified. Of particular significance were the large amounts of water vapor (potentially oxidizing the the carbon residue) and the hydrocarbons (potentially fuel).

9. Pauli, A. J., "Experimental Evaluation of Several Advanced Ablative Materials and Nozzle Sections of a Storable-Propellant Rocket Engine", NASA Technical Memorandum - NASA TM X-1559, April 1968.

Seven materials which were potential candidates for the acoustic liner were evaluated. Of these, the quartz and carbon/silica reinforcements and the polyimide resin were selected for screening tests.

10. Mitchell, B. J., et al, "Part II - Critical Environments and Additional Arc Heater Screening", AFML-TR-65-156, June 1966.

Sixty-nine test specimens were exposed to plasma arc environments for screening of materials. Results related to the acoustic liner program were: (1) silicon carbide had a higher heat of ablation than silica and (2) fillers had no effect on ablation.

11. Mayo, C. S., "Part I - Ablative Plastic Characterization in Simulated Motor Exhaust", AFML-TR-65-245, July 1965.

Seventy materials were tested in simulated liquid exhaust including phenolic, PBI and polyimide resins and silica, carbon/silica and zirconia fiber reinforcement. The findings of the study were used to assist in the selection of potential candidate systems for an ablative acoustic liner. Of particular significance was the performance of the silica, zirconia and carbon/silica reinforcements.

12. Speyer, F. B., "Development of Advanced Composites for High Pressure Liquid Environments", Part I, Materials Development, AFML-TR-68-243, Sept. 1968.

The program is directed toward the development of an ablative composite to withstand highly oxidative liquid propellant environments at high temperatures and pressures. Initial results indicate organic-metallic chemicals used in the fabrication of ablative composites provide improvement over the unmodified silica-phenolic systems. The studies are still in process and not complete for utilization on the acoustic liner program.

C, Materials and Fabrication (cont.)

13. Mitchel, B. J. and Tempesta, F. L., "Additional Arc Heater Screening and Trajectory Simulation, Part II", AFML-TR-67-176, October 1968.

    Phenolic, polyimide, polyphenylene and other resin systems reinforced with carbon graphite, silica, quartz and boron nitride fabrics were tested in plasma arc steady state and transient environments. Relation to the acoustic liner material selection included the ranking of polyimide and phenolic resins on silica and quartz reinforcement. The polyimide resin was the best.

14. Clougherty, E. V., "Research and Development of Refractory Oxidation Resistant Diborides", AFML-TR-68-190, October 1968.

    Several hundred zirconium diboride composites were screened for oxidation resistance by plasma arc tests. The melt temperatures and oxidation resistance of the diborides make them attractive as acoustic liner materials; however, it appeared that additional development would be required.

15. Peterson, D. A., et al, "Rocket Engine Evaluation of Erosion and Char as Functions of Fabric Orientations for Silica Reinforced Nozzle Materials", NASA TMX-1721, January 1969.

    Both quartz and silica reinforced phenolic were comparatively tested in N_2O_4/Aerozine 50 engine. Quartz was slightly better in erosion resistance; therefore, it was considered a candidate for the acoustic liner. Reinforcement angles of 0°, 30°, 60° and 90° to motor centerline were tested. The 60° angle resulted in low erosion and low char depths; however, a 60° angle did not appear the best for the acoustic liner.

16. "Apollo Lunar Module Descent Engine Ablative Chamber - Injector Compatibility Improvement Study", Contract NAS 9-8229, April 1969.

    The program objective is to develop a chamber throat material with little or no erosion in the LMDE chamber. The screening of materials has been conducted using a torch test which simulates the thermal and reactive gas environment. Results indicate materials (hard) such as JTA, SiC, W-reinforced zirconia, zirconia and coated carbonaceous materials such as SiC coated Carbone graphite and Pyrocarb 751 are needed to withstand the simulated environment. Possible thermal shock problems prohibited the use of any of these materials for the acoustic liner; however, the Pyrocarb-751 and zirconia reinforced zirconia were and are considered candidates for an acoustic liner.

C, Materials and Fabrication (cont.)

17. "Apollo Lunar Module Descent Engine Ablative Chamber - Injector Compatibility Improvement Study", Contract NAS 9-8229, March 1969.

An extensive survey of ablative and hard throat materials was conducted to develop an improved throat material for the Lunar Module Descent Engine. The final results of this program should be directly related to materials application for an acoustic liner because of the similarity in chamber design and the combustion environment. Preliminary results are discussed in Reference 16.

18. Pears, C. D., "The Thermal and Mechanical Properties of Five Ablative Plastics from Room Temperature to 750°F", AFML-TR-65-133, April 1965.

Two of the five ablative materials characterized were silica reinforced phenolics. The properties reported plus those of References 1, 3 and 6 were used to establish the typical properties for silica reinforced phenolics.